A Comparison Study Between Different Social Interaction in Multi-User Brain-Computer Interface (BCI) Gaming: Competitive vs. Collaborative

Finda Dwi Putri

SUBMITTED IN FULFILMENT OF THE REQUIRMENTS FOR THE DEGREE OF
Doctor of Philosophy

James Watt School of Engineering
University of Glasgow
September 2020

A Comparison Study between Different Social Interaction in Multi-User Brain-Computer Interface (BCI) gaming: Competitive vs. Collaborative

The growing interest in BCI gaming has initiated the possibility of multi-user BCI games, which require the involvement of two or more players with integrated brain signals to a BCI application. Multi-user BCI is a complex process, with challenges surrounding the technical aspects and the behavioural aspects all should be carefully considered. Several studies have tested multi-user BCI games based on different types of control paradigms. However, most of the studies focused on the technical aspects of the game and the information related to the neurological changes caused by the BCI gaming interaction is still relatively limited. The aim of this thesis is to investigate the electrophysiological changes that occur in the brain, due to interactive multi-user BCI gaming, where the BCI paradigm used is based on the alpha band non-verbalised operant conditioning.

Forty able-bodied healthy participants were involved in the multi-user BCI gaming experiments that were divided into two main experiments i.e. competitive and collaborative gaming. The BCI game was presented as two bars on each side of the screen with a seesaw placed in between. The bars are controlled by the changes of relative alpha power (RA) of each player, recorded from Pz. When one bar is higher than the other, the seesaw will be tilted down towards the side with a higher bar. A pair of players were asked to control their assigned bar to achieve a different goal for each gaming interaction. In competitive gaming, the players were asked to compete by upregulating their RA (which consequently increases their bar) and the goal was to increase the bar 10% above their opponent's bar for at least 1s to gain one score. In collaborative gaming, the players were asked to collaborate in balancing the seesaw (thus, balancing their bars) and the goal was to reach a similar bar level within the range of ±5% from each other for at least 0.5 s in order to score. Offline analyses were performed on the EEG data, including power spectral density, signal complexity, source localisation, and brain connectivity analyses. Brain connectivity analysis was performed by using Granger Causality (GC) and Directed Transfer Function (DTF). GC was performed to estimate both intra- and inter-brain connectivity in the time domain, and DTF was performed to estimate intra-brain connectivity in the frequency domain. Additionally, qualitative data analysis was performed via the NASA-TLX workload questionnaire.

The results revealed that different types of interaction produced a different kind of response in the brain activity of the players. These responses include the different fluctuation and the different spatial distribution of alpha power, the changing source localisation pattern, and the changes in intra- and inter-brain connectivity. It was found that the level of dominance between players also produced different brain activity responses, in both gaming interactions. Additionally, it was revealed that the level of posterior alpha power and intra-brain connectivity during resting state can be used to predict the gaming performance. Overall, the thesis has contributed to providing the information regarding the brain's cortical activity changes during different kinds of multi-user BCI gaming interaction, which is expected to benefit the development of multi-user BCI games and for other methodological considerations in designing multi-user BCI application.

Table of Content

Abstract ..... **i**

Table of Content ..... **ii**

List of Tables ..... **vi**

List of Figures ..... **viii**

Publication ..... **xx**

Acknowledgement ..... **xxi**

Declaration ..... **xxiii**

Abbreviation ..... **xxiv**

Chapter I Introduction **1**

1.1 The Nervous System 1

1.1.1 The Central Nervous System (CNS) and the Peripheral Nervous System (PNS) 1

1.1.2 Structural and functional organisation of the brain 2

1.2 Electroencephalography (EEG) 5

1.2.1 EEG waves generation 5

1.2.2 EEG frequency bands 6

1.3 EEG Biofeedback (Neurofeedback) 6

1.4 Brain-Computer Interface (BCI) 8

1.4.1 BCI gaming 10

1.5 Multi-user BCI gaming and Social Interaction 12

1.6 Aim and Objectives 13

Chapter II Literature Review **15**

2.1 Multi-user BCI gaming applications 15

2.2 Hyperscanning technology to study social behaviour 17

2.3 Summary 20

Chapter III Methods **21**

3.1 The BCI paradigm 21

3.1.1 The gaming interface 22

3.2 EEG recording 25

3.3 Data Analysis 27

3.3.1 Data Pre-processing 28

3.3.2 Power Spectral Analysis 28

3.3.3 Higuchi Fractal Dimension 29

3.3.4 Source Localisation Analysis 30

3.3.5 Brain Connectivity Analysis 32

3.3.6 Statistical Analysis 34

3.3.7 Post-experimental Questionnaire 36

Chapter IV Competitive Multi-user BCI: Part I- Electrophysiological Features 38

4.1 Introduction 38

4.2 Methods 39

4.2.1 EEG experiments 39

4.2.2 Data analysis 40

4.3 Results 42

4.3.1 RA, scoring performance, and individual alpha peak frequency 42

4.3.2 Spatial power spectral density 49

4.3.3 Higuchi Fractal Dimension 59

4.3.4 sLORETA source localisation analysis 63

4.3.5 NASA-TLX questionnaire 70

4.4 Discussion 73

4.5 Conclusion 79

Chapter V Competitive Multi-user BCI: Part II- Connectivity 80

5.1 Introduction 80

5.2 Methods 81

5.2.1 Connectivity Analysis 81

5.2.2 Statistical Analysis 82

5.3 Results 82

5.3.1 Intra-brain Granger Causality 82

5.3.2 Directed Transfer Function 91

5.3.3 Inter-brain Granger Causality 107

5.4 Discussion 109

5.5 Conclusion 114

Chapter VI Collaborative Multi-user BCI: Part I- Electrophysiological Features 115

6.1 Introduction 115

6.2 Methods 116

6.2.1 EEG experiments 116

6.2.2 Data analysis 117

6.3 Results 119

6.3.1 RA, scoring performance, and individual alpha peak frequency 119

6.3.2 Spatial power spectral density 125

6.3.3 Higuchi Fractal Dimension 136

6.3.4 sLORETA source localisation analysis 139

6.3.5 NASA-TLX questionnaire 146

6.4 Discussion 149

6.5 Conclusion 155

Chapter VII Competitive Multi-user BCI: Part II- Connectivity 156

7.1 Introduction 156

7.2 Methods 157

7.2.1 Connectivity Analysis 157

7.2.2 Statistical Analysis 158
7.3 Results 158
7.3.1 Intra-brain Granger Causality 158
7.3.2 Directed Transfer Function 168
7.3.3 Inter-brain Granger Causality 183
7.4 Discussion 185
7.5 Conclusion 189
Chapter VIII General Discussion 190
8.1 Discussion of the main findings 191
8.2 Limitations 198
8.3 Suggestion for future work 198
8.4 Conclusion 199
References 200
Appendix I 210
Appendix II 214

List of Tables

Table 4.1 The mean ± std of gaming RA from channel Pz and gaming scores from all participants averaged over all sub-sessions on each experimental day 44

Table 4.2 The median and interquartile range of gaming RA from channel Pz, and gaming scores from all participants averaged over all sub-sessions on each experimental day 45

Table 4.3 Table of *p*-values and H scores obtained from Kruskal-Wallis H test ($p<0.05$) of gaming RA (of each group) and gaming scores, across all sessions 45

Table 4.4 Table of *p*-values and Z scores obtained from Wilcoxon signed rank test ($p<0.05$) of gaming RA (of each group) and gaming scores between sessions 46

Table 4.5 The mean ± std of IA peak (Hz) from each participant in each session 48

Table 4.6 Table of F and *p*-values obtained from two-way ANOVA analysis ($p<0.05$) of IA peak frequency 48

Table 4.7 The location of the maximum and minimum source activity obtained from paired t-test analysis in sLORETA between gaming condition (BSD/SSD) and Baseline. 68

Table 4.8 The location of the maximum and minimum source activity obtained from paired t-test analysis in sLORETA between BSD and SSD 69

Table 4.9 The brain structures with the highest counts of source activity, found after paired t-test analysis in sLORETA between gaming condition (BSD/SSD) and Baseline. 69

Table 4.10 The brain structures with the highest counts of source activity, found after paired t-test analysis in sLORETA between BSD and SSD 70

Table 4.11 Table of statistical results of NASA-TLX scores for each category and for the overall score 72

Table 6.1 The mean ± std of gaming RA from channel Pz and gaming scores from all pairs averaged over all sub-sessions on each experimental day 121

Table 6.2 The median and interquartile range of gaming RA from channel Pz, and gaming scores from all pairs averaged over all sub-sessions on each experimental day 122

Table 6.3 Table of *p*-values and H scores obtained from Kruskal-Wallis H test ($p<0.05$) of gaming RA (of each group) and gaming scores, across all sessions. 122

Table 6.4 Table of *p*-values and *Z* scores obtained from Wilcoxon signed rank test ($p<0.05$) of gaming RA (of each group) and gaming scores between sessions 123

Table 6.5 The mean ± std of IA peak frequency (Hz) from each participant in each session 125

Table 6.6 Table of F and *p*-values obtained from two-way ANOVA analysis ($p<0.05$) of IA peak frequency 125

Table 6.7 The location of the maximum and minimum voxel values obtained from paired t-test analysis in sLORETA between gaming condition (BE/WO) and Baseline 144

Table 6.8 The location of the maximum and minimum voxel values obtained from paired t-test analysis in sLORETA between BE and WO gaming conditions 145

Table 6.9 The brain structures with the highest counts of source activity, found after paired t-test analysis in sLORETA between gaming condition (BE/WO) and Baseline 145

Table 6.10 The brain structures with the highest counts of source activity, found after paired t-test analysis in sLORETA between BE and WO. 146

Table 6.11 Table of statistical results of NASA-TLX scores for each category and for the overall score 148

List of Figures

Figure 1.1 Central Nervous System (left) and Peripheral Nervous System (right)..... 3

Figure 1.2 The topography of the cerebral hemispheres (top) and the Brodmann's area map 4

Figure 1.3 The general BCI scheme..... 8

Figure 3.1 The general BCI design. 21

Figure 3.2 The diagram of the BCI GUIs. 22

Figure 3.3 The illustration of the before (left) and after (right) effect of NC application on the control signal of a player with naturally higher alpha power, which is expected to balance the average RA of the two players during multi-user gaming experiment. 25

Figure 3.4 The diagram of experimental session: (a) the gaming interaction modes division and (b) the stages of each experimental session 26

Figure 3.5 EEG electrodes arrangement based on 10-20 system. The used electrodes are marked with red circles, (a) for 32 electrodes set up and (b) for 16 electrodes set up. 27

Figure 3.6 The subjects' position relative to the screen in multi-user BCI experiment. 27

Figure 3.7 Data analysis diagram (there is no specific order for each analysis step)..... 28

Figure 3.8 NASA-TLX questionnaire..... 37

Figure 4.1 The absolute alpha power spectral density at Pz, averaged from all baselines and all the highest-scoring sub-sessions, in (a) Session I, (b) Session II, and (c) Session III, for each group of players. 44

Figure 4.2. The individual pre-gaming RA (%) at Pz for all players in all three experimental sessions..... 46

Figure 4.3 (a-c) Mean ± std of individual gaming RA (%) at Pz and (d-f) gaming scores from all sub-sessions in each session -the bars with asterisks (a-c) indicate normalisation of RA during gaming. 47

Figure 4.4 Mean ± std of the real individual gaming RA (%) at Pz from all sub-sessions in all three experimental sessions, without any normalisation applied during gaming..... 48

Figure 4.5 Non-parametric permutation test ($p<0.05$) between the BSD condition and baseline for group D, in theta, alpha, lower beta, and higher beta frequency bands. FDR correction was applied for multiple comparison (FDR was not performed if the significant activation after

permutation only occur in one channel). White dot represents a significant difference before FDR correction (p<0.05) and no significant power changes were found after FDR was applied. 51

Figure 4.6 Non-parametric permutation test (p<0.05) between the BSD condition and baseline for group ND, in theta, alpha, lower beta, and higher beta frequency bands. FDR correction was applied for multiple comparison (FDR was not performed if the significant activation after permutation only occur in one channel). White dot represents a significant difference before FDR correction (p<0.05), and black dot represents a significant difference after FDR correction. 52

Figure 4.7 Non-parametric permutation test (p<0.05) between the SSD condition and baseline for group ND, in theta, alpha, lower beta, and higher beta frequency bands. FDR correction was applied for multiple comparison (FDR was not performed if the significant activation after permutation only occur in one channel). White dot represents a significant difference before FDR correction (p<0.05) and no significant power changes were found after FDR was applied. 53

Figure 4.8 Non-parametric permutation test (p<0.05) between BSD and SSD for group D, in theta, alpha, lower beta, and higher beta frequency bands. FDR correction (p<0.05) was applied for multiple comparison. White dot represents a significant difference before FDR correction and black dot represents a significant difference after FDR correction. 54

Figure 4.9 Non-parametric permutation test (p<0.05) between BSD and SSD for group ND, in theta, alpha, lower beta, and higher beta frequency bands. FDR correction (p<0.05) was applied for multiple comparison. White dot represents a significant difference before FDR correction and no significant power changes were found after FDR was applied. 55

Figure 4.10 Non-parametric permutation test (p<0.05) between groups in the Baseline condition, in theta, alpha, lower beta, and higher beta frequency bands. FDR correction was applied for multiple comparison (FDR was not performed if the significant activation after permutation only occur in one channel). Black dot represents a significant power difference after FDR correction (p<0.05). 56

Figure 4.11 Non-parametric permutation test (p<0.05) between groups in the BSD condition, in theta, alpha, lower beta, and higher beta frequency bands. FDR correction was applied for multiple comparison (FDR was not performed if the significant activation after permutation only occur in one channel). White dot represents a significant difference before FDR correction (p<0.05) and no significant power changes were found after FDR was applied. 57

Figure 4.12 Non-parametric permutation test (p<0.05) between groups in the SSD condition, in theta, alpha, lower beta, and higher beta frequency bands. FDR correction was applied for multiple comparison (FDR was not performed if the significant activation after permutation only

occur in one channel White dot represents a significant difference before FDR correction (p<0.05) and no significant power changes were found after FDR was applied. 58

Figure 4.13 Mean ± std of HFD in all channels during Baseline, BSD, and SSD condition for (a) group D (a) and (b) group ND. 61

Figure. 4.14 Mean ± std of HFD in all channels of both groups during (a) Baseline, (b) BSD, and (c) SSD. 62

Figure 4.15 Paired t-statistics (p<0.05) of the source localisation via sLORETA between the average BSD and the average Baseline over subjects in group D, in the frequency band of (a) theta, (b) alpha, (c) lower beta, and (d) higher beta. The figures inside the grey box is a 3D representation of the localisation map, and the boxes below it is the 3D slices representing the negative (left side) and the positive (right side) voxel values- blue for negative values and red to yellow for positive values. Voxel's coordinate positioning shown in the 3D slices figures is based on the Montreal Neurological Institute and Hospital (MNI) coordinate system. 65

Figure 4.16 Paired t-statistics (p<0.05) of the source localisation via sLORETA between the average SSD and the average Baseline over subjects in group D, in the frequency band of (a) theta, (b) alpha, (c) lower beta, and (d) higher beta. The figures inside the grey box is a 3D representation of the localisation map, and the boxes below it is the 3D slices representing the negative (left side) and the positive (right side) voxel values- blue for negative values and red to yellow for positive values. Voxel's coordinate positioning shown in the 3D slices figures is based on the Montreal Neurological Institute and Hospital (MNI) coordinate system. 66

Figure 4.17 Paired t-statistics (p<0.05) of the source localisation via sLORETA between the average BSD and the average SSD over subjects in group D, in the frequency band of (a) theta, (b) alpha, (c) lower beta, and (d) higher beta. The figures inside the grey box is a 3D representation of the localisation map, and the boxes below it is the 3D slices representing the negative (left side) and the positive (right side) voxel values- blue for negative values and red to yellow for positive values. Voxel's coordinate positioning shown in the 3D slices figures is based on the Montreal Neurological Institute and Hospital (MNI) coordinate system. 67

Figure 4.18 The mean ± std of NASA-TLX scores in each category, such as (a) mental, (b) physical, (c) temporal, (d) performance, (e) effort, and (f) frustration, for both groups of players in three different sessions. 71

Figure 4.19 The mean ± std of (a-b) NASA-TLX scores in each group, for each category in three sessions, and (c) the overall scores (summed up of the scores in all category) for each group in three sessions. 71

Figure 5.1 The networks zonation: FF (frontal-frontal), CC (central-central), PoPo (parieto-occipital – parieto-occipital), FC (frontal-central), FPo (frontal-parieto-ocipital), CF (central-frontal), CPo (central-parieto-occipital), PoF (parieto-occipital – frontal), and PoC (parieto-occipital – central). The first letter of the abbreviation indicates the source of the network, and the second letter indicates the sink. 83

Figure 5.2 (a-c) The average intra-brain GC matrices of group D for Baseline, BSD, and SSD. (d-f) The connectivity map for each condition- each map displays the average GC values above the 75th percentile of its corresponding matrix above them. (g-h) The matrices of *p*-values generated from a non-parametric paired permutation ($p<0.01$) of the intra-brain GC values from all trials between Baseline and each gaming condition, with FDR correction applied. The blue and red squares indicate the significant connections, blue indicates higher average GC value in Baseline and red indicates higher average GC value in gaming. 86

Figure 5.3 (a-c) The average intra-brain GC matrices of group ND for Baseline, BSD, and SSD. (d-f) The connectivity map for each condition- each map displays the average GC values above the 75th percentile of its corresponding matrix above them. (g-h) The matrices of *p*-values generated from a non-parametric paired permutation ($p<0.01$) of the intra-brain GC values from all trials between Baseline and each gaming condition, with FDR correction applied. The blue and red squares indicate the significant connections, blue indicates higher average GC value in Baseline and red indicates higher average GC value in gaming. 87

Figure 5.4 The bar graphs of the average GC values (mean ± standard error) in each zone for (a) group D, Baseline vs BSD, (b) group D, Baseline vs SSD, (c) group ND, Baseline vs BSD, and (d) group ND, Baseline vs SSD. A non-parametric paired permutation ($p<0.01$) was performed to compare the statistic between two conditions, with FDR correction applied. The blue bars indicate the average GC during Baseline and the red bars indicate the average GC during gaming experiment (BSD/SSD). 88

Figure 5.5 The matrices of *p*-values generated from a non-parametric paired permutation ($p<0.01$) of the intra-brain GC values from all trials between BSD and SSD for (a) group D and (b) group ND, with FDR correction applied. The blue and red squares indicate the significant connections, blue indicates higher average GC value in BSD and red indicates higher average GC value in SSD (c-d) The bar graphs of the average GC values (mean ± standard error) for BSD and SSD in each zone for (c) group D and (d) group ND. A non-parametric paired permutation ($p<0.01$) was performed to compare the statistic between two conditions, with FDR correction applied. The blue bars indicate the average GC during BSD and the red bars indicate the average GC during SSD 90

Figure 5.6 The matrices of *p*-values generated from a non-parametric paired permutation ($p<0.01$) of the intra-brain GC values from all trials between groups (D and ND) in (a) Baseline, (b) BSD, and (c) SSD, with FDR correction applied. The blue and red squares indicate the significant connections, blue indicates higher average GC value in group D and red indicates higher average GC value in group ND. 91

Figure 5.7 The average DTF matrices for group D for Baseline, BSD and SSD conditions, in each frequency band. 93

Figure 5.8 The connectivity maps display the average DTF values for group D above the 75th percentile of its corresponding matrix shown in Figure 5.7, for Baseline, BSD and SSD conditions, in each frequency band. 94

Figure 5.9 The matrices of *p*-values generated from a non-parametric paired permutation ($p<0.01$) of the DTF values from all trials between Baseline and each gaming condition (Baseline vs BSD and Baseline vs SSD) for group D in each frequency band with FDR correction applied. The blue and red squares indicate the significant connections, blue indicates higher average DTF value in Baseline (lower in gaming) and red indicates lower average DTF value in Baseline (higher in gaming). 95

Figure 5.10 The bar graphs of the average DTF values (mean ± standard error) in each zone between Baseline and each gaming condition (Baseline vs BSD, and Baseline vs SSD) for group D, in each frequency band. A non-parametric paired permutation ($p<0.01$) was performed to compare the statistic between two conditions, with FDR correction applied. The blue bars indicate the average DTF during Baseline and the red bars indicate the average DTF during gaming experiment (BSD/SSD). 96

Figure 5.11 The average DTF matrices for group ND for Baseline, BSD and SSD conditions, in each frequency band. 98

Figure 5.12 The connectivity maps display the average DTF values for group ND above the 75th percentile of its corresponding matrix shown in Figure 5.11, for Baseline, BSD and SSD conditions, in each frequency band. 99

Figure 5.13 The matrices of *p*-values generated from a non-parametric paired permutation ($p<0.01$) of the DTF values from all trials between Baseline and each gaming condition (Baseline vs BSD and Baseline vs SSD) for group ND in each frequency band with FDR correction applied. The blue and red squares indicate the significant connections, blue indicates higher average DTF value in Baseline (lower in gaming) and red indicates lower average DTF value in Baseline (higher in gaming) 100

Figure 5.14 The bar graphs of the average DTF values (mean ± standard error) in each zone between Baseline and each gaming condition (Baseline vs BSD, and Baseline vs SSD) for group ND, in each frequency band. A non-parametric paired permutation (p<0.01) was performed to compare the statistic between two conditions, with FDR correction applied. The blue bars indicate the average DTF during Baseline and the red bars indicate the average DTF during gaming experiment (BSD/SSD). 101

Figure 5.15 The matrices of p-values generated from a non-parametric paired permutation (p<0.01) of the DTF values from all trials between BSD and SSD for each group, in each frequency band with FDR correction applied. The blue and red squares indicate the significant connections, blue indicates higher average DTF value in BSD (lower in SSD) and red indicates lower average DTF value in BSD (higher in SSD). 103

Figure 5.16 The bar graphs of the average DTF values (mean ± standard error) in each zone between BSD and SSD for both groups, in each frequency band. A non-parametric paired permutation (p<0.01) was performed to compare the statistic between two conditions, with FDR correction applied. The blue bars indicate the average DTF during BSD and the red bars indicate the average DTF during SSD. 104

Figure 5.17 The matrices of p-values generated from a non-parametric paired permutation (p<0.01) of DTF values from all trials between groups (D and ND) for Baseline and each gaming condition (BSD and SSD), in each frequency band with FDR correction applied. The blue and red squares indicate the significant connections, blue indicates higher average DTF value in group D (lower in group ND) and red indicates lower average DTF value in group D (higher in group ND). 106

Figure 5.18 The matrices of the average inter-brain GC for each condition, i.e. Baseline, BSD, and SSD for each direction. 107

Figure 5.19 The matrices of p-values generated from a non-parametric single-sample permutation (p<0.001) with FDR correction applied, of the inter-brain GC from all trials. The white boxes represent the significant connections. 108

Figure 5.20 The significant inter-brain connectivity map based on the significant connections found in Figure 5.19, for both gaming conditions (BSD and SSD), in both directions 108

Figure 6.1 The absolute alpha power spectral density at Pz, averaged from all baselines and all the highest-scoring sub-sessions in, (a) Session I, (b) Session II, and (c) Session III, for each group of players. 121

Figure 6.2 (a-c) The individual pre-gaming RA (%) at Pz for all players in all three experimental sessions. (d-f) Mean ± std of individual gaming RA (%) at Pz during gaming and (g) the gaming scores, all taken from all sub-sessions in each session -the bars with asterisks (d-f) indicate normalisation of RA during gaming. 124

Figure 6.3 (a-c) Mean ± std of the real individual gaming RA (%) at Pz from all sub-sessions, without any normalisation applied during gaming..... 124

Figure 6.4 Non-parametric permutation test ($p<0.05$) between Baseline and BE for group D, in theta, alpha, lower beta, and higher beta frequency bands. FDR correction ($p<0.05$) was applied for multiple comparison. White dot represents a significant difference before FDR correction and black dot represents a significant power difference after FDR correction. 127

Figure 6.5 Non-parametric permutation test ($p<0.05$) between the Baseline and WO for group D, in theta, alpha, lower beta, and higher beta frequency bands FDR correction ($p<0.05$) was applied for multiple comparison. White dot represents a significant difference before FDR correction and black dot represents a significant power difference after FDR correction. 128

Figure 6.6 Non-parametric permutation test ($p<0.05$) between Baseline and BE for group ND, in theta, alpha, lower beta, and higher beta frequency bands. FDR correction ($p<0.05$) was applied for multiple comparison. White dot represents a significant difference before FDR correction and no significant power changes were found after FDR was applied..... .129

Figure 6.7 Non-parametric permutation test ($p<0.05$) between Baseline and WO for group ND, in theta, alpha, lower beta, and higher beta frequency bands. FDR correction ($p<0.05$) was applied for multiple comparison. White dot represents a significant difference before FDR correction and no significant power changes were found after FDR was applied. 130

Figure 6.8 Non-parametric permutation test ($p<0.05$) between BE and WO for group D, in theta, alpha, lower beta, and higher beta frequency bands. FDR correction ($p<0.05$) was applied for multiple comparison. White dot represents a significant difference before FDR correction and no significant power changes were found after FDR was applied. 131

Figure 6.9 Non-parametric permutation test ($p<0.05$) between BE and WO for group ND, in theta, alpha, lower beta, and higher beta frequency bands. FDR correction ($p<0.05$) was applied for multiple comparison. White dot represents a significant difference before FDR correction and no significant power changes were found after FDR was applied. 132

Figure 6.10 Non-parametric permutation test ($p<0.05$) between groups in the Baseline condition, in theta, alpha, lower beta, and higher beta frequency bands. FDR correction ($p<0.05$) was applied

for multiple comparison. White dot represents a significant difference before FDR correction and black dot represents a significant power difference after FDR correction. 133

Figure 6.11 Non-parametric permutation test (p<0.05) between groups in BE condition, in theta, alpha, lower beta, and higher beta frequency bands. FDR correction (p<0.05) was applied for multiple comparison. White dot represents a significant difference before FDR correction and black dot represents a significant power difference after FDR correction. 134

Figure 6.12 Non-parametric permutation test (p<0.05) between groups in the WO condition, in theta, alpha, lower beta, and higher beta frequency bands. FDR correction (p<0.05) was applied for multiple comparison. White dot represents a significant difference before FDR correction and no significant power changes were found after FDR was applied. 135

Figure 6.13 Mean ± std of HFD in all channels during Baseline, BE, and WO condition for (a) group D and (b) group ND. 137

Figure 6.14 Mean ± std of HFD in all channels of both groups during (a) Baseline, (b) BE, and (c) WO..... 138

Figure 6.15 Paired t-statistics (p<0.05) of the source localisation via sLORETA between the average BE and the average Baseline over subjects in group D, in the frequency band of (a) theta, (b) alpha, (c) lower beta, and (d) higher beta. The figures inside the grey box is a 3D representation of the localisation map, and the boxes below it is the 3D slices representing the negative (left side) and the positive (right side) voxel values- blue for negative values and red to yellow for positive values. Voxel's coordinate positioning shown in the 3D slices figures is based on the Montreal Neurological Institute and Hospital (MNI) coordinate system. 141

Figure 6.16 Paired t-statistics (p<0.05) of the source localisation via sLORETA between the average WO and the average Baseline over subjects in group D, in the frequency band of (a) theta, (b) alpha, (c) lower beta, and (d) higher beta. The figures inside the grey box is a 3D representation of the localisation map, and the boxes below it is the 3D slices representing the negative (left side) and the positive (right side) voxel values- blue for negative values and red to yellow for positive values. Voxel's coordinate positioning shown in the 3D slices figures is based on the Montreal Neurological Institute and Hospital (MNI) coordinate system. 142

Figure 6.17 Paired t-statistics (p<0.05) of the source localisation via sLORETA between the average BE and the average WO over subjects in group D, in the frequency band of (a) theta, (b) alpha, (c) lower beta, and (d) higher beta. The figures inside the grey box is a 3D representation of the localisation map, and the boxes below it is the 3D slices representing the negative (left side) and the positive (right side) voxel values- blue for negative values and red to yellow for

positive values. Voxel's coordinate positioning shown in the 3D slices figures is based on the Montreal Neurological Institute and Hospital (MNI) coordinate system..... 143

Figure 6.18 The mean ± std of NASA-TLX scores in each category, such as (a) mental, (b) physical, (c) temporal, (d) performance, (e) effort, and (f) frustration, for both groups of players in three different sessions..... 147

Figure 6.19 The mean ± std of (a-b) NASA-TLX scores in each group, for each category in three sessions, and (c) the overall scores (summed up of the scores in all category) for each group in three sessions..... 147

Figure 7.1 The networks zonation: FF (frontal-frontal), CC (central-central), PoPo (parieto-occipital – parieto-occipital), FC (frontal-central), FPo (frontal-parieto-ocipital), CF (central-frontal), CPo (central-parieto-occipital), PoF (parieto-occipital – frontal), and PoC (parieto-occipital – central). The first letter of the abbreviation indicates the source of the network, and the second letter indicates the sink 159

Figure 7.2 (a-c) The average intra-brain GC matrices of group D for Baseline, BE, and WO. (d-f) The connectivity map for each condition- each map displays the average GC values above the 75th percentile of its corresponding matrix above them. (g-h) The matrices of *p*-values generated from a non-parametric paired permutation ($p<0.01$) of the intra-brain GC values of from all trials between Baseline and each gaming condition, with FDR correction applied. The blue and red squares indicate the significant connections, blue indicates higher average GC value in Baseline and red indicates higher average GC value in gaming..... 161

Figure 7.3 (a-c) The average intra-brain GC matrices of group ND for Baseline, BE, and WO. (d-f) The connectivity map for each condition- each map displays the average GC values above the 75th percentile of its corresponding matrix above them. (g-h) The matrices of *p*-values generated from a non-parametric paired permutation ($p<0.01$) of the intra-brain GC values of from all trials between Baseline and each gaming condition, with FDR correction applied. The blue squares indicate the significantly higher average GC value in Baseline..... 163

Figure 7.4 The bar graphs of the average GC values (mean ± standard error) in each zone for (a) group D, Baseline vs BE, (b) group D, Baseline vs WO, (c) group ND, Baseline vs BE, and (d) group ND, Baseline vs WO. A non-parametric paired permutation ($p<0.01$) was performed to compare the statistic between two conditions, with FDR correction applied. The blue bars indicate the average GC during Baseline and the red bars indicate the average GC during gaming experiment (BE/WO). 164

Figure 7.5 The matrices of *p*-values generated from a non-parametric paired permutation ($p<0.01$) of the intra-brain GC values from all trials between BE and WO for (a) group D and (b) group ND, with FDR correction applied. The blue and red squares indicate the significant connections, blue indicates higher average GC value in BE and red indicates higher average GC value in WO. (c-d) The bar graphs of the average GC values (mean ± standard error) for BE and WO in each zone for (c) group D and (d) group ND. A non-parametric paired permutation ($p<0.01$) was performed to compare the statistic between two conditions, with FDR correction applied. The blue bars indicate the average GC during BE and the red bars indicate the average GC during WO. 166

Figure 7.6 The matrices of *p*-values generated from a non-parametric paired permutation ($p<0.01$) of the intra-brain GC values from all trials between groups (D and ND) in (a) Baseline, (b) BE, and (c) WO, with FDR correction applied. The blue and red squares indicate the significant connections, blue indicates higher average GC value in group D and red indicates higher average GC value in group ND. 167

Figure 7.7 The average DTF matrices for group D for Baseline, BE and WO conditions, in each frequency band. 169

Figure 7.8 The connectivity maps display the average DTF values for group D above the 75^{th} percentile of its corresponding matrix shown in Figure 7.7, for Baseline, BE and WO conditions, in each frequency band. 170

Figure 7.9 The matrices of *p*-values generated from a non-parametric paired permutation ($p<0.01$) of the DTF values from all trials between Baseline and each gaming condition (Baseline vs BE and Baseline vs WO) for group D in each frequency band with FDR correction applied. The blue and red squares indicate the significant connections, blue indicates higher average DTF value in Baseline and red indicates higher average DTF value in gaming. 171

Figure 7.10 The bar graphs of the average DTF values (mean ± standard error) in each zone between Baseline and each gaming condition (Baseline vs BE, and Baseline vs WO) for group D, in each frequency band. A non-parametric paired permutation ($p<0.01$) was performed to compare the statistic between two conditions, with FDR correction applied. The blue bars indicate the average DTF during Baseline and the red bars indicate the average DTF during gaming experiment (BE/WO). 172

Figure 7.11 The average DTF matrices for group ND for Baseline, BE and WO conditions, in each frequency band. 174

Figure 7.12 The connectivity maps display the average DTF values for group ND above the 75th percentile of its corresponding matrix shown in Figure 7.11, for Baseline, BE and WO conditions, in each frequency band. 175

Figure 7.13 The matrices of *p*-values generated from a non-parametric paired permutation ($p<0.01$) of the DTF values from all trials between Baseline and each gaming condition (Baseline vs BE and Baseline vs WO) for group ND in each frequency band with FDR correction applied. The blue and red squares indicate the significant connections, blue indicates higher average DTF value in Baseline and red indicates higher average DTF value in gaming. 176

Figure 7.14 The bar graphs of the average DTF values (mean ± standard error) in each zone between Baseline and each gaming condition (Baseline vs BE, and Baseline vs WO) for group ND, in each frequency band. A non-parametric paired permutation ($p<0.01$) was performed to compare the statistic between two conditions, with FDR correction applied. The blue bars indicate the average DTF during Baseline and the red bars indicate the average DTF during gaming experiment (BE/WO). 177

Figure 7.15 The matrices of *p*-values generated from a non-parametric paired permutation ($p<0.01$) of the DTF values from all trials between BE and WO for each group, in each frequency with FDR correction applied. The blue and red squares indicate the significant connections, blue indicates higher average DTF value in BE and red indicates higher average DTF value in WO. 179

Figure 7.16 The bar graphs of the average DTF values (mean ± standard error) in each zone between BE and WO for both groups, in each frequency band. A non-parametric paired permutation ($p<0.01$) was performed to compare the statistic between two conditions, with FDR correction applied. The blue bars indicate the average DTF during BE and the red bars indicate the average DTF during WO. 180

Figure 7.17 The matrices of *p*-values generated from a non-parametric paired permutation ($p<0.01$) of DTF values from all trials between groups (D and ND) for baseline and each gaming condition (BE and WO), in each frequency with FDR correction applied. The blue and red squares indicate the significant connections, blue indicates higher average DTF value in group D and red indicates higher average DTF value in group ND. 182

Figure 7.18 The matrices of the average inter-brain GC for each condition, i.e. Baseline, BE, and WO for each direction. 183

Figure 7.19 The matrices of *p*-values generated from a non-parametric single-sample permutation ($p<0.001$) with FDR correction applied, of the inter-brain GC from all trials. The white boxes represent the significant connections. 184

Figure 7.20 The significant inter-brain connectivity map based on the significant connections found in Figure 7.19, for both gaming conditions (BE and WO), in both directions..... 184

Figure 8.1 The averaged absolute alpha power at Pz from all players in each group, in each session, for competitive gaming (blue box), and collaborative gaming (orange box) and for their respective baselines..... 193

Figure 8.2 The significant inter-brain connectivity map based on the significant connections generated by a non-parametric single-sample permutation (p < 0,001) with FDR correction applied, for competitive (blue box) and collaborative (orange box) gaming, in both directions (group D to group ND and group ND to group D)..... 196

Publication

(Journal Article)
Vuckovic, Aleksandra, Sara Pangaro, and **Finda Putri**, Unimanual vs Bimanual Motor Imagery Classifiers for Assistive and Rehabilitative Brain Computer Interfaces, IEEE Transactions on Neural Systems and Rehabilitation Engineering, 2018, 26 (12), pp 2407-2415.

(Conferences)
Putri, Finda Dwi, Lulu L. Fitri, Suprijanto and Ulfa O., Evaluation and Analysis of μ Rhythm Desynchronization and Mirror Neuron Activity Related to Motor- related Activity, The 4th International Conference on Mathematics and Natural Sciences, 8-9 November 2012, Bandung Institute of Technology, Bandung, Indonesia. (Poster presentation)

Putri, Finda Dwi, Lulu L. Fitri, and Suprijanto, Analysis of μ Rhythm Desynchronization as a Response to Imagination of Motor-related Activity, International Conference on Women's Health in Science and Engineering, 6-7 December 2012, Bandung Institute of Technology, Bandung, Indonesia. (Oral presentation)

Putri, Finda and Aleksandra Vuckovic, Brain Functional Network During Resting vs Active State: an EEG Study, The BioMedEng18 Conference, Imperial College London, London, 6-7 September 2018. (Poster presentation)

Putri, Finda, Hao Ding, Abdullah Garcia, and Aleksandra Vuckovic, Towards Successful Multi-User Brain-Computer Interface (BCI) Gaming: Analysis of the EEG Signatures and Connectivity, The 3rd International Conference on Computer-Human Interaction Research and Applications (CHIRA) 2019, Vienna, 20-21 September 2019. (Oral presentation – Best Student Paper Award Nomination)

Acknowledgement

I would like to express my gratitude and appreciation to my supervisor Dr Aleksandra Vuckovic for her guidance and support, and for trusting me with this project. Thank you for introducing me with such an interesting topic. I would also like to extend my gratitude to Dr Henrik Gollee for allowing me to take parts in several laboratory organisational events that I really enjoyed doing.

I would like to thank my sponsor, Indonesian Endowment Fund for Education for the financial support during my period of studying.

I would like to thank my parents, Mrs. Augustine Zaini and Mr. Firdaus Ismathuhom, for their endless support, patience, and prayers, I really would not make it without you two. Thank you for believing in me since day 1. You two mean the world to me. My biggest thanks to Mr. James Golding, for all the love and support. Thank you for being there for me and thank you for your patience in good and bad times. I would also like to thank my big brother Renaldi for his guidance all these years and for hosting me at his place every time I am in town, and to my other family member: Sisi Patricia, thank you for teaching me how to read when I was 4 and for always be there ready to pick me up anytime anywhere, and to my sister in law Kak Risza Hijryana, and my baby niece Minerva.

My sincere gratitude to my colleagues who have been very supportive throughout my PhD journey: Alberto Alvarez, thank you for being such a good friend, I owe you a lot man. I wish you nothing but happiness. Ania Sosnowska, thank you for every day that we spent together in and out of the office. Thank you for the beautiful friendship. Margaret Armentano, Ruslinda Binti Ruslee, Manaf Al-taleb, Mohammed Jarjees, Anna Zulauf, Gabriela Cruz, Salim Al-wasity and Sarah Comincioli for welcoming me almost 4.5 years ago in our old laboratory and helping me settling with the PhD life.

I would like to thank my ‘current’ or newer colleagues Ciarán McGeady, Radha Kumari, Jennifer Miller, Nina Petric-Gray, Ina Susnoschi, Lyu Tao, Du Aimin, Keri Anderson, and Thomas Doublein. Thank you for always being there for me, giving me support with experiments and/or personal life. Best of luck with your PhD.

I would also like to express my gratitude to Hao Ding, Abdullah Garcia, and Yannan Yan. Without all of you this project and this thesis would have never come this far.

I would like to thank my community and friends outside the research group: Sheila Scialanga, Silvia Visentin, John Marques, Francesco Gaetano, Silva Doci, Abdu Moh. Ali, Felicity Keefe, Sergio Martin, Luca Rizzo, Moa Safar, Olga Ivanova, Carlos and Kornelija Zamorano, Anneli Pedersen, Lewa Thomas, Melinda Noufal, Zsofia Dobak, Samira Scheenstra, Helen McHugh, Myria Christophini, Sara Vita, Laura GV, Malvina, and many other people from Salsa4Water 2016/2017. Thank you for the dances, the laugh, the tears, the party, and most importantly, thank you for the friendship.

I would also like to express my gratitude to my closest circle in Indonesia: Nungky Patria, Lalita Fitrianti, Arkasha, Abraham and Ardwina Sianipar, Fetriza Rinaldy, Andriani

Oktadianti, Desy Suryani, Roos Haikal, Matiinu, Hanna Panjaitan, Putri Astuti, Astrid Hapsari, Amadea Calista, Waode Nurzara, Amalia Hasnida, Ratna Nindyarani, Dwininta Widyastuti, Ariananda Hariadi, Dila Fauza, Thank you for the endless support this past 13+ years, I will be home soon, and we can finally get together again.

Last but not least I would like to thank Deborah May for the opportunity she has given me to be part of Küche. Topher Love, for both IT support and moral support. Aghnaa Gayatri for being the best kind of friend someone could ask for: I love you so much.

To all other friends, family, colleagues, who have contributed in any form of support during my PhD period: I sincerely thank you and wish good karma will come after you. Since I finished this thesis during the time of COVID-19 pandemic, I would like to thank every healthcare worker out there, whether I know you or not, I sincerely thank you for your service. May God always protect you and us all.

Declaration

I, Finda Dwi Putri, hereby declare that except where explicit reference is made to the contribution of others, this dissertation is the result of the work of the named and has not been submitted for any other degree at the University of Glasgow or any other institution.

Glasgow, September 2020

Abbreviations

ACC	Anterior Cingulate Cortex
ADHD	Attention Deficit Hyperactivity Disorder
ANOVA	Analysis of Variance
BA	Brodmann Area
BCI	Brain-Computer Interface
BNCI	Brain/Neural Computer Interaction
BOLD	Blood-Oxygen Level Dependent
BSD	Biggest Score Difference
CEN	Central Executive Network
CNS	Central Nervous System
DAN	Dorsal Attentional Network
dlPFC	Dorsolateral Prefrontal Cortex
DMN	Default Mode Network
DTF	Directed Transfer Function
ECoG	Electrocorticography
EEG	Electroencephalography
EPSP	Excitatory Post-synaptic Potential
FD	Fractal Dimension
FDR	False-Discovery Rate
fMRI	Functional Magnetic Resonance Imaging
fNIRS	Functional Near Infrared Spectroscopy
GC	Granger Causality
GUI	Graphical User Interface
HFD	Higuchi Fractal Dimension
IA	Individual Alpha
ICA	Independent Component Analysis
IFG	Inferior Frontal Gyrus
IPSP	Inhibitory Post-synaptical Potential
MEG	Magnetoencephalography
MFG	Middle Frontal Gyrus
MI	Motor Imagery
MNI	Montreal Neurological Institute
MTG	Middle Temporal Gyrus
NC	Normalisation Coefficient
PCC	Posterior Cingulate Cortex
PDC	Partial Directed Coherence
PNS	Peripheral Nervous System
RA	Relative Alpha
RSN	Resting State Network
sLORETA	Standardized Low Resolution Electromagnetic Tomography
SMR	Sensory-Motor Rhythm
SN	Salience Network
SPL	Superior Parietal Lobule
SSD	Smallest Score Difference

SSVEP	Steady-state Visually Evoked Potential
std	Standard Deviation
STG	Superior Temporal Gyrus
TPJ	Temporoparietal Junction
vlPFC	Ventrolateral Prefrontal Cortex
vmPFC	Ventromedial Prefrontal Cortex
WSR	Wilcoxon Signed Rank

Chapter I

Introduction

1.1 The Nervous System.

The basic functional unit of the nervous system consists of a functional cellular unit called neuron, a nerve cell that is responsible in transmitting signal within the nervous system. A single neuron consists of a cell body, where the nucleus and cell organelles are located, and extensions of the cell body, which provide pathway for signal transmission, consists of dendrites and axon. Nervous system is divided into two parts, the central nervous system (CNS) which consists of the brain and the spinal cord, and the peripheral nervous system (PNS) which consists of circuits of nerves relaying signals from and to the CNS [1, 2].

1.1.1 The Central Nervous System (CNS) and the Peripheral Nervous System (PNS).

Based on the structural components, the CNS is composed of seven parts, i.e., the spinal cord, the medulla oblongata, the pons, the midbrain, the cerebellum, the diencephalon, and the cerebral hemispheres. The medulla oblongata, pons, and midbrain are forming a

structure called the brainstem. The brainstem major function includes receiving and integrating sensory data to and from other areas of the brain, control of internal body functions like breathing, circulatory system, and digestive system, and coordination of movement and reflexes. The forebrain is formed by the diencephalon and cerebral hemispheres, with the cerebral hemispheres predominantly occupied the forebrain [1-3].

PNS can be classified into two functional systems i.e., the sensory-motor system and the autonomous system. The function of sensory-motor system is mainly to relay signals to and from the skeletal muscles, especially during the presence of external stimuli. The sensory-motor system can be controlled both voluntary and involuntary. The function of autonomous system is to facilitate the functions of the internal body organs by controlling the cardiac muscles and the smooth muscles around the internal organ. The control of the autonomous system is generally involuntary. Based on the ways of the autonomous system function within the body, this system is composed by three divisions i.e., parasympathetic, sympathetic, and enteric divisions. The parasympathetic division is mainly involved in the body regulatory systems that require energy conservation, whereas the sympathetic division works in antagonistic manner to the parasympathetic division, the sympathetic division is involved in energy-consuming systems. The enteric division serves a specific function in controlling the smooth muscles and the glands of the digestive system [1].

1.1.2 Structural and functional organisation of the brain.

The cerebral hemispheres are characterised by the gyri (singular: gyrus), the upper lining of the folded cortical tissues, and the sulci (singular: sulcus), the grooves of the folded cortical tissues, separating one gyrus with another. The topography of cerebral hemispheres is divided into four areas, corresponding the cranial bones that overlie them, i.e., frontal, parietal, temporal, and occipital, with the central sulcus dividing the frontal lobe with the parietal lobe [2].

The cerebral cortex covering the cerebral hemispheres, weighs about 40% of the total weight of the brain and containing more than 100 billion of neurons, forming functional circuitry responsible for variety of physical and cognitive functions. Large portion of cerebral cortex consists of neocortex, which composed of six cellular layers. As the way to identify the organisation of neocortex, Brodmann numbered the neocortex area based on its cytoarchitectural differences (thickness, cell density, and other

histological characteristics of the layers) where the numbers are used to label the area based on its function, known as Brodmann's area (BA) [3, 4].

The cerebral cortex consists of the primary sensory and motor cortex, and the association cortex, where each area responsible to a specific set of functions. The primary sensory cortex consists of cortical areas responsible for sensory processing i.e., somatic sensory processing, visual and auditory processing, and olfactory system. The primary somatic sensory cortex is located in the anterior parietal lobe, just posterior to the central sulcus. The visual cortex is located in the calcarine sulcus on the medial surface of the occipital lobe. The auditory cortex is located in the superior surface of temporal lobe, surrounded by Wernicke's area – the area involved in speech processing, just at the posterior of the temporal lobe. Primary motor cortex is located in the precentral gyrus with the premotor area is located more rostral, adjacent to the primary motor cortex [1, 3]

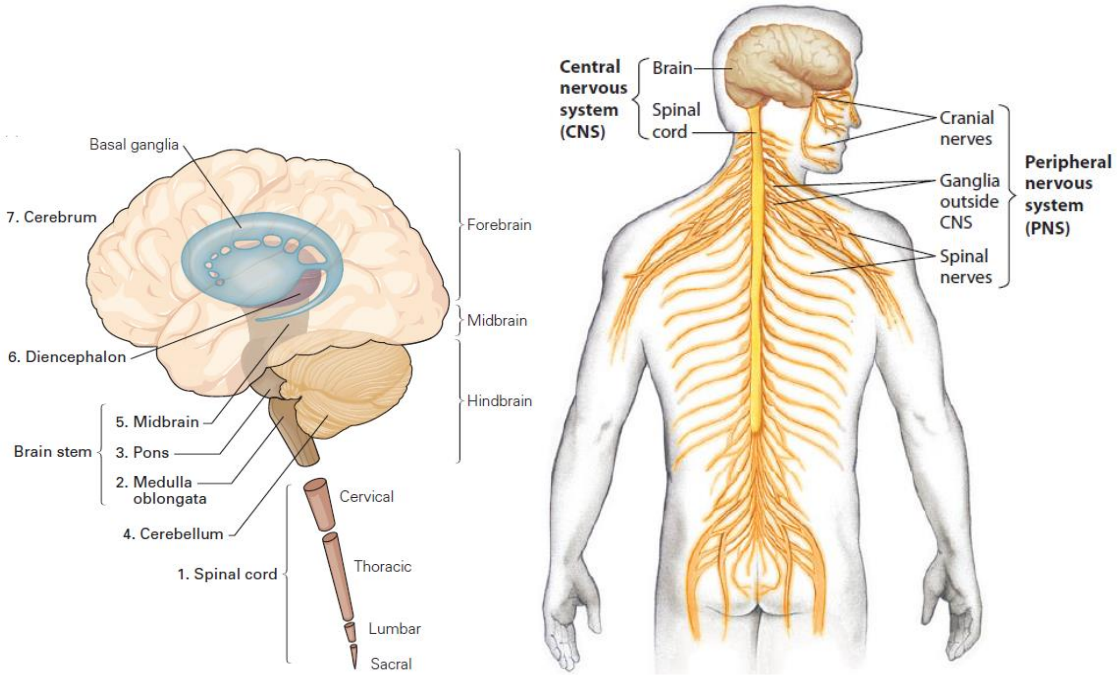

Figure 1.1 Central Nervous System (left) and Peripheral Nervous System (right) [1, 3].

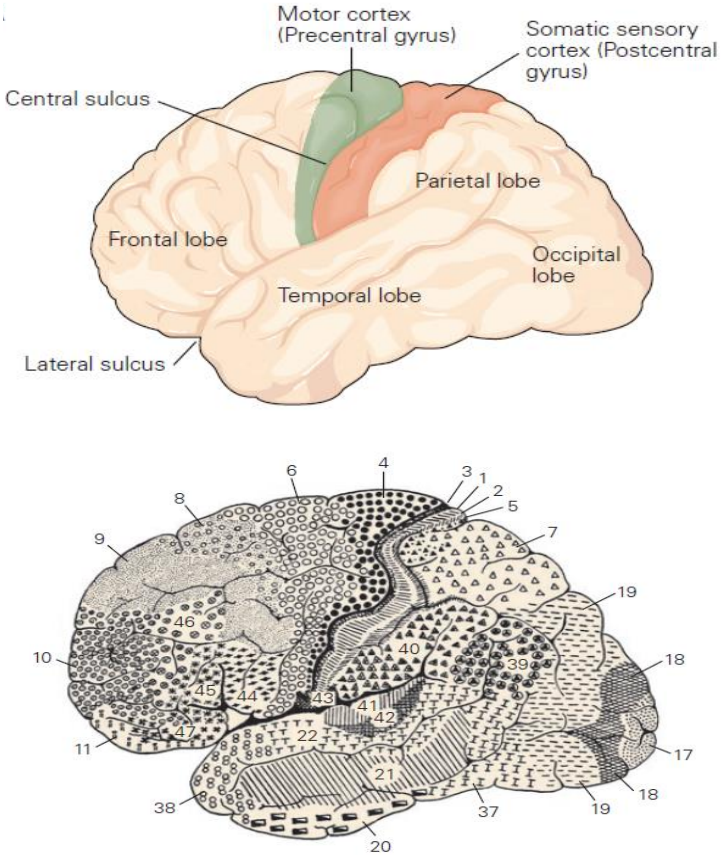

Figure 1.2 The topography of the cerebral hemispheres (top) and the Brodmann's area map [3].

The association cortex, which consist of a large area of cerebral cortex, is involved in mental processing. Each sensory cortex works together with the associate cortex in processing information, allowing the brain to perform higher mental processes like problem solving, decision making, judgement, and planning. The association cortex cooperate with the sub-cortical areas in performing tasks that require memory and emotional processing, involving the limbic system, which includes cortical structures and non-cortical structures [5].

The cerebral cortex composed of different set of intrinsic brain networks that have specific activation patterns that are associated with different mental states. The major brain networks that have been widely studied, including the Resting State Networks (RSNs) – which include the Default Mode Network (DMN), the Dorsal Attention Network (DAN), and the Salience Network (SN) [6-9].

RSNs is an integration of smaller brain networks, that are more active during resting without any task execution present. RSNs activity pattern has been proposed to be used as a biomarker to detect any neurophysiological disturbance that might occur in the brain

[10, 11]. The DMN, a network constituent of RSNs consisting of the ventral medial prefrontal cortex (vmPFC) and the posterior cingulate cortex (PCC) as the core regions [7, 12], has been widely known to have an antagonistic dynamic with DAN [13] and SN [14] during the change of mental states. The DAN is a set of dorsal network that are engaged with attention demanding task and consisting of the dorsolateral prefrontal cortex (dlPFC), frontal eye fields, inferior precentral sulcus, middle temporal motion complex, and superior parietal lobule (SPL) [13]. Whereas the SN is a system that detects stimuli and mediates the network switching between task-free and task-engagement states, consisting of ventrolateral prefrontal cortex (vlPFC), frontoinsular cortex, and anterior cingulate cortex (ACC) [8, 15, 16].

1.2 Electroencephalography (EEG)

Electroencephalography (EEG) is a measurement technique to record and monitor the brain's electrophysiological signals with an electroencephalogram device. EEG setup usually consists of a specially designed cap with electrodes attached on it, and these electrodes can detect the brain's electrical activity from the surface of the scalp. Signal transmissions within the nervous system involve electrical charges. The cumulative electrical charges produced by the neurons in the cerebral cortex, makes it possible for the EEG to record the brain's electrical activity non-invasively [17].

1.2.1 EEG waves generation

The transmembrane neuronal electrical charges occurred due to the potential changes surrounding the neuron's membrane. The electrical charges are facilitated by the protein channels located across the neuronal membrane that work as ion gates to maintain the environment inside and outside the membrane. At the synaptic level, there are two types of post-synaptic potentials i.e., the excitatory post-synaptic potential (EPSP) and the inhibitory post-synaptic potential (IPSP). At EPSP, the transmembrane current brings the positive ions from the extracellular environment into the cell, whereas IPSP works antagonistic to EPSP by bringing the negatively charged ion into the cell and releasing the positively charged ion out of the cell. The transmembrane potential changes leads to the transition of resting potential into an action potential and returning back to resting potential, creating an impulse that propagates along the axons and dendrites allowing the signals to be transmitted among neurons [1, 17, 18]. In the cortex, the summation of this

impulse propagation occurs in layers of abundant pyramidal neurons, allowing the production of the brain's electrophysiological signal to be recorded non-invasively from the skin surface by EEG electrodes [19].

1.2.2 EEG frequency bands

The recorded EEG oscillations can be interpreted based on the different frequency range i.e., delta band (<4 Hz), theta band (4-7 Hz), alpha band (8-13 Hz), beta band (14-30 Hz), and gamma band (> 30 Hz), where each frequency band is associated with different neurophysiological processes occur in the brain [20].

The delta band activity is known to be related to sleeping activity and is not present during wakefulness in adults [20, 21]. The theta band activity is known to be related to the state of drowsiness [18], however the localised high theta power around mid-frontal area has been associated with concentration, especially when higher cognitive loads are involved [22, 23]. The alpha band activity, which has higher distribution in the occipital region of the brain, is known to increase during a relaxed state and also known to be supressed by visual stimulation and cognitive tasks [18, 20]. Alpha oscillation alongside theta, may reflect the cognitive and memory performance [24]. The rolandic mu rhythm is an 8-12 Hz EEG oscillation, which overlaps alpha frequency range. Despite the frequency overlapping, the spatial distribution and the reactivity of mu rhythm is different compared to alpha. Mu rhythm is found to be specifically localised in rolandic area, around the motor cortex, and also found to be reactive to motor-related activity [20, 21, 25]. The beta band lies in the longest frequency band of 14 to 30 Hz. Beta reactivity is often related to higher cognitive functions related to focus, attention, and problem-solving, however the central beta band is also known to be reactive to motor-related processing [18, 20, 21]. The gamma band which lies above 30 Hz, has a rare occurrence and low power, makes it difficult to measure especially the higher frequency range that often overlaps with artefacts. Recorded gamma oscillation have shown to be useful in identifying the laterality of fingers and toes movement as well as tongue movement [18, 20].

1.3 EEG Biofeedback (Neurofeedback)

Biofeedback is a technique of conditioning which is facilitated by any bioindicator that works as a guide to help an individual to self-regulate their biological activation or

behaviour, based on that bioindicator [26]. EEG biofeedback also known as EEG-based neurofeedback, is a form of biofeedback based on the brain's electrophysiological changes, which allows the user to modulate their brain activity based on those changes [27]. The neural indicator in neurofeedback can be presented in various forms of sensory modality (e.g., visual, auditory, and tactile). Neurofeedback has been used to alter the activation of the targeted brain area(s) and in successful training, the alteration will be retained even after the training has finished. Neurofeedback is based on the operant conditioning concept, where it requires the subject to learn to self-regulate their brain activity by using the given feedback within a continuous reinforcement schedule in form of training sessions [28]. Additionally, the efficacy of this feedback-based learning process is dependent to the underlying neurobiological aspects, such as the neural specificity, i.e. the ability to train the neurons on a specific targeted area, and the neural plasticity, i.e. the ability to memorise and to retain the skills to control the targeted area [26, 29]. Frequency/power neurofeedback is one of the most commonly practiced EEG neurofeedback, which allows the user to receive feedback based on their brain's signal power in the assigned frequency band, recorded from one or more surface electrodes [30].

Neurofeedback application has been applied for clinical purposes as a rehabilitative intervention for varieties of neurological and behavioural conditions, for example, in reducing pain in spinal-cord injured patients [31] or in attentional deficit hyperactivity disorder (ADHD) [32, 33]. Neurofeedback can also serve a range of benefits for non-clinical population. The evidences of successful EEG-neurofeedback training in healthy participants have been summed up in an extended review by Gruzelier [34]. The review have listed the different EEG features (i.e. sensory motor rhythm (SMR) ratio, alpha power, beta-gamma, and theta) used in a neurofeedback training protocol, as well as the training outcome that improved of the participant's behaviour, for instance in improving their memory, attention level, and calmness. Moreover, these successful neurofeedback performances were validated as "successful" based on the existence of control group in the study for comparison purpose between the control and the trained group, and the correlation between the performance during learning and post-training assessments to measure the improvement gained from the training [34, 35].

Alkoby et al. [36] in their review addressed the predictors for a successful or non-successful neurofeedback training, by summarising the psychological and

neurophysiological aspects that affecting the neurofeedback performance. The proposed psychological predictors including confidence level of the subjects [37], specific mental strategies [38, 39], and motivation [40]. Whereas the proposed neuropsychological predictors including the signal power spectral density or amplitude recorded during the resting state [41, 42], the initial training session's performance [43, 44], and the inter-individual differences of brain structures revealed through functional imaging [45, 46].

The numerous studies that have been performed to test the neurofeedback efficacy over the past decade have raised more attention towards the methodological and theoretical considerations in designing a neurofeedback training. The considerations that require more attention including the number of sessions, the protocols to measure learning (i.e. across sessions, within session, and successive pre-training baseline), the specified frequency band to train, the individual variability, the trainer-participant interface, the feedback modality and the electrodes placement and montage [29, 30, 35].

1.4 Brain-Computer Interface (BCI)

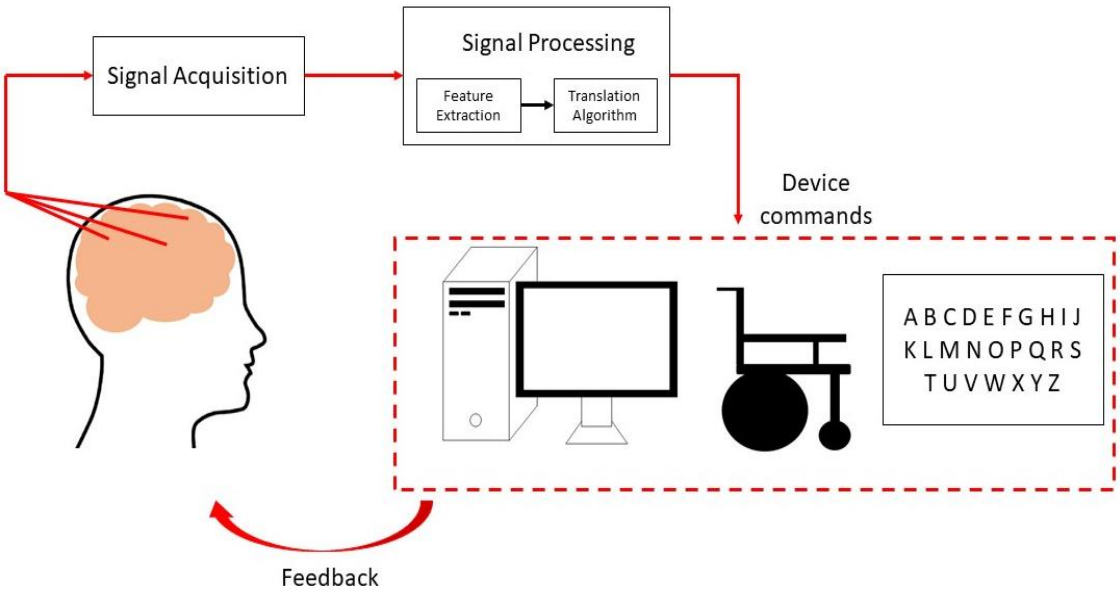

Figure 1.3 The general BCI scheme.

Brain-computer interface (BCI) is a system that can generate commands and control without any muscular involvement [47, 48]. In a BCI system, brain signals are acquired by a signal acquisition unit, and later being processed by the system to produce different variety of output e.g., control over a software or a device, as seen in Fig. 1.3. Based on the type of the input signal, BCIs can be classified as electrophysiological BCIs and

hemodynamic BCIs [49]. Electrophysiological BCIs uses the electrophysiological signal as the input signal, recorded by using electrophysiological signal acquisition unit such as, EEG, magnetoencephalography (MEG), and electrocorticography (ECoG), whereas hemodynamic BCIs uses the BOLD signal, which reflects the brain's metabolic activity as the input signal, recorded by using BOLD signal acquisition unit such as, functional magnetic resonance imaging (fMRI) and functional near infrared spectroscopy (fNIRS). In this thesis, EEG was used as the signal acquisition unit to perform BCI.

On the basis of BCI development for communication and control purposes, Zander et al. [50] categorised BCI based on the directness of the control, such as: directly controlled BCI and indirectly controlled BCI. Direct BCI control is obtained by mapping the assigned mental state performed by the user to produce the output control, for example: mental imagery based BCI. Indirect BCI control obtained from a self-modulated brain activity that elicited in response to a stimulus, for example: P300 – an event-related potential component elicited at 300 milliseconds after stimulus presentation – based BCI [50].

However, the currently existing BCI control paradigms demonstrate how far the technique has grown into a technique that serves broader purposes. Thus, based on the control paradigm used, BCI can be further categorised into active BCI, reactive BCI, and passive BCI. Active BCI, is a BCI system that is controlled by a direct and conscious brain activity of the user that is independent from any external stimulation. Whereas reactive BCI, is a BCI system that is controlled by an elicited brain activity as a reaction to external stimulation. Lastly, passive BCI, is a BCI system that does not require a voluntary control by the user, but instead it monitors the user's brain activity during a certain mental state. When this BCI control paradigms classification is compared to the classification that is based on the directness, active BCI matches the directly controlled BCI and the reactive BCI matches the indirectly controlled BCI, where the passive BCI provides a complementary purpose [50, 51].

From the learnability perspective, the active BCI/directly controlled BCI has been argued to have a limitation, especially for naïve BCI users due to the possible unclear interpretation of the task for each individual user. Bos et al. [52], used the motor imagery task as a case example where naïve users may have the difficulty interpreting what counts as motor imagery (whether it is a visualisation of themselves performing the motor task,

whether or not they feel the actual movement, or whether they should visualise someone else performing the motor task). Therefore, this kind of BCI control may require more training compared to the reactive/indirectly controlled BCI [50, 52].

Due to the growing interest in BCI research, in 2013 the European Commission funded a long-term Brain/Neural Computer Interaction (BNCI) – an extension of BCI that includes other physiological signals such as heart rate and muscle or eye movement – roadmap called Horizon 2020. BNCI Horizon 2020 is aiming to be the guideline for the future direction of BNCI research, including the future applications for clinical population. The roadmap also addressing other key topics such as the ethical guideline, the societal needs and acceptance of BNCI, user-centred approach, evaluation metrics, and the research to market transfer. It is expected that by the development of this program, there will be a coordinated BCI society, that includes the research community and the industrial stakeholders, that will create a more efficient research efforts and collaborations [53].

1.4.1 BCI gaming

By combining both communication and control functions, BCI technology can be used in varieties of applications and serving different purposes. Based on the survey conducted by Ahn et al (2014) to the BCI researchers, developers, and the end users, BCI gaming was perceived to have a significant influence and applicability and was chosen as one of the most promising BCI applications [51]. Gaming is a highly stimulating activity with the ability to induce different kind of cognitive responses of its user. During gaming experience, the users' performance is highly influenced by varieties of factors (e.g., the interface, the tasks' difficulty, the strategies used, etc.) which are engaging them to a complex cognitive and emotional states [54, 55] making BCI gaming technology a very challenging field, yet a very appealing one. The benefits of using games in scientific experiments include: the smaller effort required to recruit participants as it is more approachable to the general public, the familiarity aspects of gaming activity that makes it easier for subjects to engage to the experiment, and the gaming performance of the subjects that are easy to measure based on their daily experience [55].

Nijholt et al. [54], described the stimulated brain activities during BCI gaming, that can be determined by four stages of player experiences. First, the player is experiencing different aspects of the game, such as the task and the interface, and how these aspects

affecting the player's emotion that can be expressed differently (e.g., as engagement, frustration, irritation, boredom, or stress). Second, the player is exposed to variation of external stimuli that would help them in performing the game's tasks and eventually take control of the game. Third, the player is trying to perform the assigned mental tasks as an effort to control the game, producing the brain signals required to control the game. Lastly, the player is trying to control the wider brain activity to control the game, by reacting to the feedback given by the gaming interface.

More advanced BCI-gaming technology has initiated the nascent of multi-user BCI games, that is where the control signal is recorded from more than one brain. The general requirement of a multi-user BCI has been described as the involvement of two or more users with integrated brain activity to a BCI application [56]. Social interaction tasks such as cooperation and competition are ideally implemented in multi-user BCI paradigms, as it has been widely used in the classical video gaming [57].

Multi-user BCI development is a complicated process. Technical challenges including the BCI architecture design, the classification accuracy, and the types of social interaction and its impact on BCI performance, require special attention. Gürkök et al. [58] suggested two descriptors that need to be considered in designing BCI games: the motivations satisfied by the games and the interaction paradigms used by the games. The first descriptor includes the elements that correspond to the fulfilment of psychological needs and the gaming motivation, such as challenge, fantasy, and sociality. Whereas the second predictor addressing the BCI game interaction paradigms, such as mental state regulation, motor imagery, and evoked response generation.

Multi-user BCI gaming experiments have been performed by using both types of brain signals (electrophysiological and hemodynamic signal). BOLD-signal based multi-user BCI has been demonstrated by Goebel et al. [59] by using an fMRI in a Brain Pong game of two users self-regulating their BOLD activity to control a computer ping-pong game by using two separate fMRI machines, and by Duan et al. [60] by using fNIRS in a BOLD-based tug-of-war computer game played by two users. However, until now, EEG is still the most common modality for multi-user BCI gaming, due to the versatility as well as the higher temporal resolution of the EEG features, making it more efficient for multi-user BCI gaming. Several EEG-based multi-user BCI gaming studies have been performed, mainly to test the BCI classification accuracy using different types of control,

e.g. SSVEP [61-63], P300 [64, 65], motor imagery (MI) [66], and the combination of different paradigms such as SSVEP/ P300 with alpha power [67].

1.5 Multi-user BCI gaming and Social Interaction

The brain activity during social interaction has been extensively studied in the field of neuroscience and social psychology. A set of brain structures have been identified to be involved in the "social brain", which are responsible in social cognition. This set of brain structures consists of the amygdala, the temporal poles, the brain's mirror system, the superior temporal sulcus, and the medial prefrontal cortex [68, 69]. These areas were found to be highly relevant to maintain different types of cognitive processes that are the basis of social interaction, for examples, observation, action prediction, mentalising, and imitation [68].

Multi-user BCI gaming is possible due to hyperscanning method. The hyperscanning technology - a method that allows a simultaneous brain activity recording from multiple brain, was introduced to explore the neural mechanisms which occur during a social interaction [70]. The multi-user BCI gaming requires two or more players to interact with each other and to perform the assigned tasks, in order to achieve a personal or a team goal. Different types of social interaction can be applied, such as with collaborative interaction where the players can learn to synchronise their brain activity to achieve their goal with the help of the game's feedback, or with competitive interaction where the players can individually control their brain activity with the help of the game's feedback to achieve their personal goal and outperform the other.

As previously mentioned, most of the available or previously developed multi-user BCI games were focused on the performance aspect (e.g. classification accuracy) and the user preference. To date, the available information related to the underlying neural mechanisms during multi-user BCI gaming interaction is still relatively limited. The literature review surrounding the current state of multi-user BCI topic and the neurological mechanisms obtained from the non-BCI gaming hyperscanning studies, will be explained in Chapter II.

In this thesis, multi-user BCI gaming was performed by applying two different social interactions, such as competitive and collaborative interaction. The general BCI

architecture and the types of the gaming interface that were used in the thesis will be described in Chapter III, along with further technical details.

1.6 Aim and Objectives

The aim of this thesis is to investigate the electrophysiological changes that occur in the brain, due to the multi-user BCI gaming, where the BCI paradigm used is based on the alpha band non-verbalised operant conditioning. Therefore, to achieve this aim, the objectives of the thesis were addressed as the following

- To perform EEG signal analysis techniques, i.e. power spectral analysis, signal complexity analysis, and source localisation analysis to the EEG data of the brain during resting and during multi-user BCI gaming performance.
- To explore the (intra- and inter-) brain connectivity changes by performing Granger Causality and Directed Transfer Function to the EEG data of the brain during resting and during multi-user BCI gaming performance.

With these objectives, the research questions to be answered listed as the followings:

1) What are the strategies applied by the players when they were engaged to the different social interactions applied in the game, judging by the changes of their brainwaves?
2) How relevant is EEG neurofeedback strategy for the multi-user BCI gaming?
3) What are the differences between competing players in competitive gaming?
4) Is there any consistency or differences found in the inter-brain connectivity between competition and collaboration?
5) Is there any resting state prognostic brain marker to characterise the players gaming performance?
6) What are the differences in terms of the brain activities between multi-user interactive BCI gaming and conventional physically controlled video gaming?
7) Is the mental strategy applied during multi-user BCI gaming similar to during single-user neurofeedback BCI gaming?

Two main experiments have been performed to answer these research questions, and the results from each experiment will be described in the upcoming results chapters, organised as the following:

- Chapter IV presents the main finding of the EEG power spectral and source localisation analysis from the multi-user competitive BCI gaming performance.
- Chapter V presents the main finding of the (intra- and inter-) brain connectivity analysis from the multi-user competitive BCI gaming performance.
- Chapter VI presents the main finding of the EEG power spectral and source localisation analysis from the multi-user collaborative BCI gaming performance.
- Chapter VII presents the main finding of the (intra- and inter-) brain connectivity analysis from the multi-user collaborative BCI gaming performance.

Chapter II

Literature Review

2.1 Multi-user BCI gaming applications

One of the earliest implementations of an interactive multi-user human-computer interaction in gaming form was demonstrated in a study for a game called BrainBall [71]. The game consisted of two players competing by controlling the movement of a steel ball on a table by regulating their brain activity through the state of relaxation. The brain's beta/alpha ratio was measured from the frontal EEG electrodes attached to a headband worn by the players. This study focused on controlling stress level through relaxation to control the ball movement, in competitive and cooperative set up. Their results proposed the idea of interactive gaming as a tool for stress-control training.

Similar concept of interaction was later adapted by Bonnet et al. [66], where they introduced BrainArena, a multi-user BCI game, which presented as a simple ball game with two goals on each side of a screen. Unlike in Brainball, in BrainArena the game interface was displayed on a screen complete with instructions directing where the ball should be moved. BrainArena was controlled by imagining hand movement, left hand for directing to the left, and right hand for directing to the right. The game could be provided two options of interaction mode, i.e. competitive mode and collaborative mode. Their study revealed that multi-user operated BCI is possible without compensating the quality

of performance. They also found that, compared to the single player condition, multi-user conditions are preferred by the users and are claimed to be more fun and more motivating.

Gürkök et al. [62] performed a user experience study of collaborative interaction in a multi-user BCI game called Mind The Sheep!. The game's interface consisted of a meadow presented on screen, with a number of sheep that moved freely, fences, and dogs. The aim of the game was for the players to control the movement of the dogs in order to fence and to herd the sheep. In this study, they investigated the different types of game control and their implications on co-experience and social interaction. In this game, two different types of controls were applied, one with BCI control using EEG steady-state visually evoked potential (SSVEP), and the other with a typical mouse pick-and-click control. They found that BCI control reduced co-experience by lowering collaborative interaction. This co-experience reduction was mainly due to the users' concern with losing control if they were paying too much attention on collaboration.

Another SSVEP-based collaborative multi-user BCI gaming was also performed by Cruz et al. [63], with a game called Kessel Run. The game's interface presented a spaceship flying through asteroids in space. The aim of the game was to navigate the spaceship in avoiding the asteroids and to sustain the fuel as long as possible. In this game, they found a relatively low SSVEP performance, however the players reported some co-experience aspects of the game such as inter-dependency and empathy.

Driven by the potential behavioural impact of multi-user BCI gaming for the players, Maby et al. [65] performed a P300-based multi-user BCI gaming experiment by adapting the Connect Four game, a turn-taking computer game where players can block each other when one of them tries to build a line by filling in four blank circles with colours assigned to them (different colour for each player). Apart from high accuracy resulted in their study, they also associated the P300 response to the state of arousal, alertness, and attention by the players, thus promoting the use of multi-user BCI gaming for a wider range of users (i.e. healthy able-bodied and patients) to study social interaction and the level of motivation.

Another study developed quite recently by van Almkerk et al. [72] namely a multi-user BCI game called BrainSnake. The game worked in a cooperative manner that is based on alpha activity. In this study they focused on investigating the role of communication during gaming control by comparing the co-existing condition and

remote condition. They found that the players managed to gain control over the snake character and produced less stress during co-existing condition. The players also preferred to communicate while playing the game.

Multi-user BCI has also been shown to have the potentials for other non-gaming applications. Some of these applications were mostly performed in collaborative fashion rather than in competition. These applications including, collaborative BCI in improving group decision making [73, 74], collaborative BCI for space navigation [75], collaborative control of an SSVEP-based robot arm [76], and collaborative BCI for multi-media science-art installation [77].

Despite the possible variety of applications, the information regarding the underlying neural mechanism as a response to an interactive multi-user BCI gaming is still relatively limited. As previously explained in Chapter I, multi-user BCI gaming elicits different psychological responses, thus such information regarding the cortical activity changes during those responses can be very useful, especially in designing better multi-user BCI games. This information might not yet be provided by any multi-user BCI gaming study, however several non-gaming hyperscanning studies have explored the brain activity changes during social interaction. The following section will further discuss about the non-gaming hyperscanning studies in relation to social behaviours.

2.2 Hyperscannning technology to study social behaviour

The hyperscanning technology allows a simultaneous brain activity recording from multiple brain and it was introduced to explore the neural mechanisms occur during a social interaction [70]. The hyperscanning technology provides a better information regarding the brain response during social interactions, which in the past, such studies were done based on a single brain recording perspective. A number of studies have been performed since the development of the hyperscanning methods.

In social neuroscience studies, experimental games have been widely used, in which the game implement a certain social interaction performed by the players. There are two common approaches in implementing competitive gaming paradigm. The first approach is by providing the opportunity for the participants to choose between competitive or cooperative behaviour, which are often performed in a turn-taking fashion and focusing on the decision-making aspect of the game (decision-induced) [78-80]. The second

approach is a direct competitive gaming, which is performed simultaneously (instead of turn-taking) and the participants were explicitly instructed to compete with each other to achieve a clear goal that can only be rewarded to the winner of the game [81]. This classification has also been explained by Tognoli and Kelso [82] where they introduced the classification of social dynamics i.e. synchronic and diachronic. The synchronic social behaviour occurs when two (or more) individuals participate in simultaneous action and perception activities (e.g. dancing, choir singing, performing surgery), and diachronic social behaviour occurs when one of the two (or more) individuals perform an action at a certain time (e.g. turn-taking interaction, imitation task).

One of the extensively studied turn taking interactions using hyperscanning method is the Prisoner's Dilemma game [80, 83-85], where a pair of players can decide whether to apply cooperation, defect, or tit-for-tat to their gaming partner. Their main findings include the activation of the orbitofrontal cortex and the prefrontal cortex, with a distinctive orbitofrontal activity in defect interaction, particularly in theta band [84]. Moreover, inter-brain connectivity via partial directed coherence (PDC) revealed a smaller number of significant inter-connections formed during defect compared to cooperation with the anterior cingulate cortex (ACC) and the orbitofrontal cortex of the defector were actively sending information to different cortical areas of the other player [84, 85]. They argued that the orbitofrontal cortex activation was likely triggered by the decision-making process made by player in order to decide whether to cooperate or to defect [84].

Another example of diachronic interaction is the Connect Four game, a turn-taking computer game where players can cooperate to build a shape together or to block each other, when one of them tries to build the instructed shape by filling in blank circles with colours assigned to them (different colour for each player) [78, 79]. The studies that applied this game (in both single-brain and hyperscanning experiments) reported that the brain areas such as bilateral superior frontal gyrus, bilateral superior parietal lobe, left inferior parietal cortex, right anterior insula, left medial cerebellum, and right inferior frontal gyrus, are reactive to the cooperative action performed by the gaming partner.

Balconi and Vanutelli [81] along with the studies by Balconi et al. [86, 87] have reported the brain response, particularly around the prefrontal cortex, during a simultaneous-synchronised interaction of a selective attention task between two subjects,

in which they were interacted in collaborative [87, 88] and in competitive [81] manners. They found that prefrontal cortex activity is sensitive to the feedback given to the players to inform them about their performance. They associated this dynamic with the activation of the dorsolateral prefrontal cortex (dlPFC) and ventral medial prefrontal cortex (vmPFC) during adaptation strategy and judgement. Furthermore, they argued that the prefrontal cortex activation is related to the social perception when social hierarchy (based on the player's position, score-wise) is present [81, 87, 88].

Another study of a synchronous interaction, was performed by Toppi et al. [89] in an EEG-hyperscanning study in pairs of pilots during a flight simulation scenario. They reported a significant influence ($p<0.05$) of theta band with the flight phase factor (take-off, cruising, and landing) on connectivity density and efficiency, and the involvement of frontal networks of all the pilots. They also reported a significant increase ($p<0.05$) of theta power in the frontal and parieto-occipital areas of the co-pilots during take-off, and in the frontal area of both pilots during landing. A significant increase of parietal alpha power was also reported in co-pilots during landing (the captain led take-off and the co-pilot led the landing after a deliberate electrical failure applied to the captain's control instrumentation). Higher theta activity around the parieto-occipital area was linked to the visual sensory input during the task, and it was found that with the increase of the task's cognitive demand, the frontal theta activity was also increased.

Hyperscanning methods have also been applied to a re-created situation that is similar to the natural setting of daily social interaction. For example, a series of study exploring the inter-brain neural synchronization during an active conversation found that different level of closeness between the interacting subjects may change the brain activity pattern during a direct conversation. Suda et al. [90] reported an increase of frontal and superior temporal areas activation during a formal and structured conversation between an interviewer and an interviewee. On the other hand, when there is a strong emotional attachment between subjects (e.g. long-term romantic couple), Kinreich et al. [91] reported a stronger inter-brain neural synchrony in the temporal-parietal structures, particularly in gamma rhythms, during a direct and structured communication. Meanwhile in a non-structured direct communication in a group of four individuals revealed an enhanced inter-personal neural synchronization around their frontal area [92]. These studies suggest that, regardless the structure of the interaction, a similar

conversation in a natural setting, can elicit different parts of the brain depends on factors such as emotional attachment or the number of interacting participants.

All of the studies mentioned above have provided the information regarding the underlying neuronal mechanisms that occur during social interactions in different settings. Such information is expected to be the guideline in interpreting the brain activity changes as an impact of a multi-user BCI gaming interaction.

2.3 Summary

This chapter presents the relevant studies surrounding the currently available multi-user BCI gaming studies. Despite its promising potentials, the number of information related to the brain activity changes during multi-user BCI gaming performance are still relatively limited. Such information could be useful, particularly for the future development of the game. To fill in this gap, this chapter reviewed the widely known non-BCI hyperscanning studies, that have been performed to explore the brain activity changes during social interaction. It is expected that this information can be a good guideline in interpreting the brain activity changes in response to an interactive multi-user BCI gaming experiment. Moreover, this thesis is also expected to contribute to the field of multi-user BCI studies by providing the information related to the neurophysiological aspects of multi-user BCI gaming.

Chapter III

Methods

3.1 The BCI paradigm

In this thesis, a general BCI design was implemented for all the experiments. This design is divided into two forms of Graphical User Interface (GUI) and three types of interaction tasks, as presented in Figure 3.1 and 3.2. The BCI GUI was built in Java (version 1.8.0) environment and was previously developed by Pedro [93] and Ling and Vuckovic [94]. All EEG data were acquired through Matlab (Ver. 2015a, The Mathworks, Inc., USA) along with a simulation model operated in Simulink.

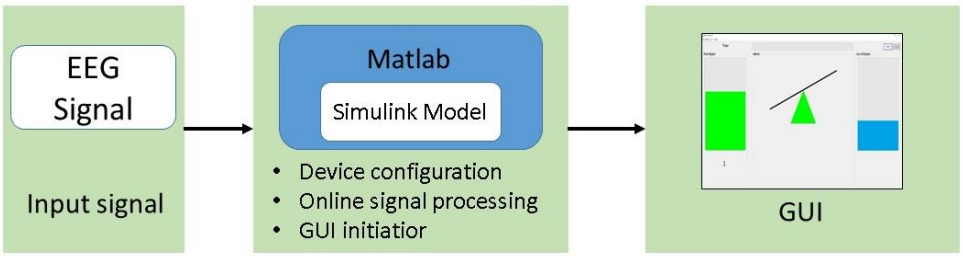

Figure 3.1 The general BCI design.

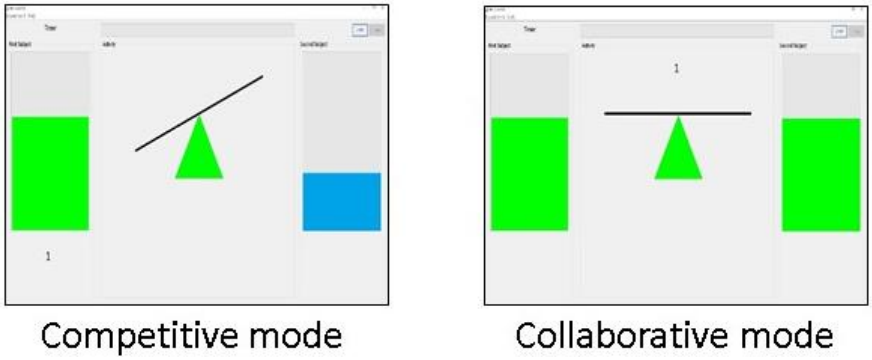

Figure 3.2 The diagram of the BCI GUIs.

The general BCI design implemented in this thesis was controlled by the relative power of EEG signal in specific frequency bands. In a time-series with a finite set of time, power spectrum analysis estimates the power distribution composing the time-series, in the frequency domain [95, 96]. The absolute power, *P(f)*, of a signal can be calculated by dividing the squared amplitude of the signal's Fourier transform output, *X(f)*, by the *N* number of samples, described as the following:

$$P(f) = \frac{1}{N}|X(f)|^2 \tag{3.1}$$

where the power of a specific frequency interval, $P_{band}(f)$, from *i* to *j* Hz can be described as:

$$P_{band}(f) = \sum_{f=i}^{j} P(f) \tag{3.2}$$

in this thesis, the percentage relative alpha power (8-13 Hz) or RA, is calculated by dividing the power of the frequency from 8 to 13 Hz by the power of a wider frequency of 2 to 30 Hz, which is expressed as:

$$RA(f) = \frac{\sum_{f=8}^{13} P(f)}{\sum_{f=2}^{30} P(f)} \quad \text{or} \quad \frac{P_{band\ 8-13}}{P_{band\ 2-30}} \tag{3.3}$$

3.1.1 The gaming interface

The BCI interface was presented as two bars on each side of the screen with a seesaw located in between the bars, as presented in Figure 3.2. The bars were controlled by the fluctuation of the relative alpha power (RA), which was calculated based on the formula in Equation 3.3. The input EEG signal's RA was averaged over 0.5 s of moving average window with the sampling frequency set to 256 and was updated every 8 sample (8/256 s

= 0.03125 s). The game has the option of two different interaction modes, namely competitive and collaborative interaction.

In order to control the interface, the users were asked to control the assigned bar (left bar for player 1 sitting on the left and right bar for player 2 sitting on the right side of the screen), by regulating their RA. The balancing position of the seesaw is affected by the height difference between the two bars, when one side of the bar is higher than the other, the seesaw will be tilted 'heavier' towards the side with the higher bar. This interface incorporated a scoring system which set differently in each gaming interaction. Pre-defined individual threshold was used and calculated based on the users' pre-experimental baseline which was recorded before every session for 2 minutes with eyes open in a relaxed state.

In competitive mode, the players were asked to compete by increasing their RA (which consequently increasing the bar on their side of the screen) to be higher than the other and to eventually gain higher score. When one player increases their bar $\geq$10% higher than the other, the seesaw will be tilted heavier towards the side with higher bar, and if this condition stays for at least 1 s, but less than 2 s, then 1 point will be rewarded to the player with the higher bar. The bar changes colour from blue to green whenever players gain 1 point. The green colour stays as long as the player's power stays 10% above the opponent's and will return to blue when it turns lower or equal. Keeping bar 10% higher than the opponent for 2 s would reward the player with 2 consecutive points. Thereafter, an additional point was awarded for every second RA was maintained. The instruction for competitive gaming required the players to increase their alpha power- which is very similar to the common instruction in frequency-based neurofeedback training. The 10% range was adapted from the threshold used in the single-user frequency-based neurofeedback training by Vuckovic et al.[31] and Hassan et al. [97, 98], however instead of 10% threshold based on the user's own baseline power- like in single-user neurofeedback, in this competitive BCI experiment 10% was set as the threshold of percentage RA difference between players.

In collaborative setup, the players were asked to maintain the seesaw in balanced position, hence the height of the two power bars should be within the range of ± 5% difference between bars of both users. If both players manage to hold this position for at least 0.5 s, but less than 1 s, then 1 point will be rewarded as a joint score. Keeping both

bars within the accepted range for 1 s would reward the player with 2 points. Thereafter, an additional point was awarded for every half a second RA was maintained. Unlike in competitive experiment, the threshold for RA difference was set to 5% due to the training instruction, i.e. to adjust RA based on their partner's level, that is different than in competitive setup as well as in frequency-based neurofeedback training in general. In order to avoid stress due to the difficulty of maintaining the bars at identical level (or zero difference), 5% threshold was chosen.

The daily pre-defined individual baseline RA from each player was used to calculate a normalising coefficient (NC). Due to the individual variability of alpha power [24, 99], one player might have a naturally higher alpha power than the other. It has been reported that inter-individual alpha variability can be caused by number of factors such as age, neurological diseases, memory performance, brain volume, and task demand [24]. Moreover, the existence of the inter-subject variability has also been reported during resting state [100]. As an effort to reduce this alpha imbalance between players in a pair, during gaming, NC was applied to the control signal of the player with a higher individual baseline RA (example is illustrated in Figure 3.3). Consequently, these players would have normalised gaming RA visualised on the interface, instead of the visual feedback based on their original RA. NC was acquired by dividing the daily individual pre-experimental baseline RA of the player with naturally lower RA by the player with higher natural RA, as explained in Equation 3.4. This approach was chosen based on the ratio of RA that the players with higher RA should compensate in order to equalise their RA with their gaming partner at the starting point of the game. This approach is also expected to help the player with lower natural RA to maintain control over their bar even if their opponent has significantly higher baseline RA. Moreover, the level of individual alpha power has been suggested to influence the alpha neurofeedback training outcome in single-user neurofeedback [42], therefore in this study, NC was used to secure the assumption that a higher game performance was caused by the players' mental effort to increase RA in a social interaction setting, rather than by their naturally high RA.

$$NC = RA_{Low} / RA_{High} \tag{3.4}$$

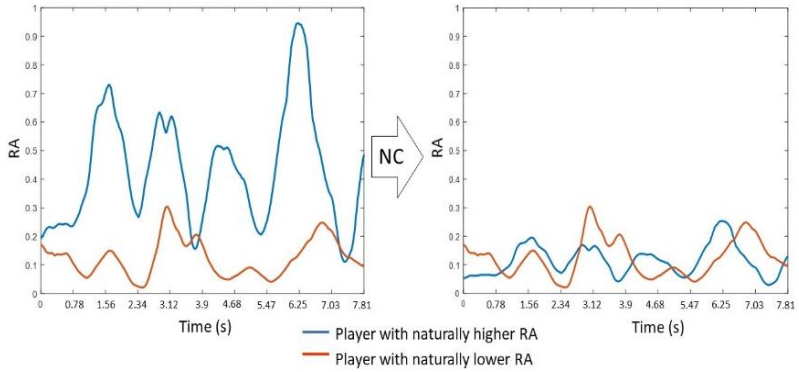

Figure 3.3 The illustration of the before (left) and after (right) effect of NC application on the control signal of a player with naturally higher alpha power, which is expected to balance the average RA of the two players during multi-user gaming experiment.

3.2 EEG recordings

The EEG signal was recorded by a g.USBamp (g.tec Medical Engineering GmbH., Austria) amplifier. The EEG electrodes arrangement was set following the standardised 10-20 EEG electrode placement system [101]. The impedance was kept below 5 kΩ. Linked ear reference was used and FCz was used as the ground. Sampling frequency was set to 256 Hz. Online band-pass filter was set between 0.5 and 60 Hz (and a notch filter at 50 Hz) using 5^{th} order infinite impulse response (IIR) digital Butterworth filter within the g.USBamp [102].

All participants performed three experimental sessions on three separate days, where each session consisted of six sub-sessions (5 minutes each), as explained in Figure 3.4. Two pre-experimental baselines were recorded, one with eyes open (which was used as the main Baseline condition throughout the thesis) and one with eyes closed, along with a post-experimental eyes-open baseline, all in a relaxed state for 2 minutes in every session.

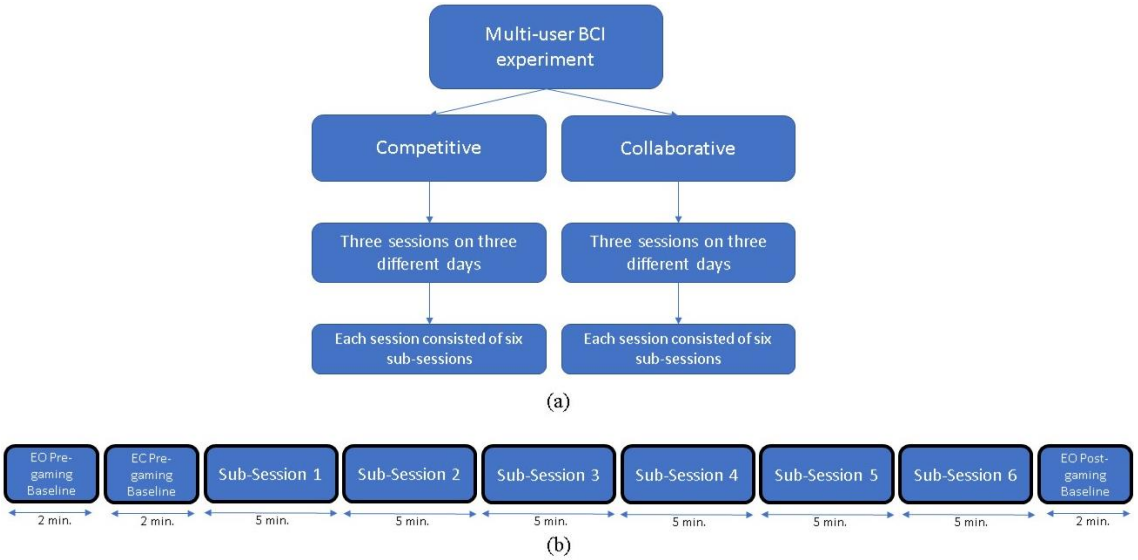

Figure 3.4 The diagram of experimental session: (a) the gaming interaction modes division and (b) the stages of each experimental session.

In all experiments, single-channel EEG (Pz) was used in the first two sessions, and multichannel EEG recording was used for the last session. Due to the limited number of available amplifier units, unequal number of electrodes were used in the last session of the experiment. Multi-channel EEG of 32 and 16 electrodes were used in the last session, where the higher number of electrodes worn by the more dominant group of players (Fig. 3.5). The dominance between players were decided based on the gaming performance in the first two sessions of the experiments.

The experiments were performed by using one computer (Intel® Core™ i7-6700 CPU @ 3.40 GHz) with two screens, where one screen was used for the gaming interface and the other was used by the researcher to monitor the supporting programs. During experiments, a pair of subjects sat still comfortably while looking at a screen, with more or less 50 cm distance between the screen and the user, as seen in Figure 3.6.

After every experimental session, the participants were asked to fill in the NASA-TLX workload index to measure the perceived workload, which will be described further in Section 3.3.

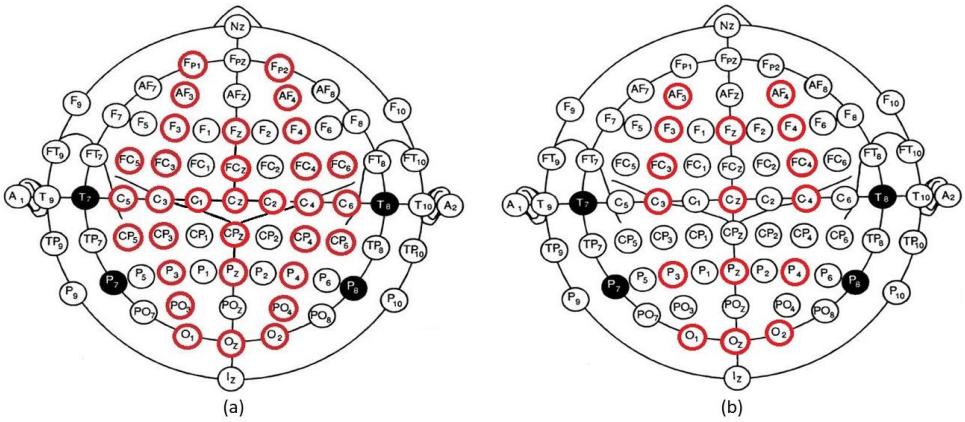

Figure 3.5 EEG electrodes arrangement based on 10-20 system. The used electrodes are marked with red circles, (a) for 32 electrodes set up and (b) for 16 electrodes set up.

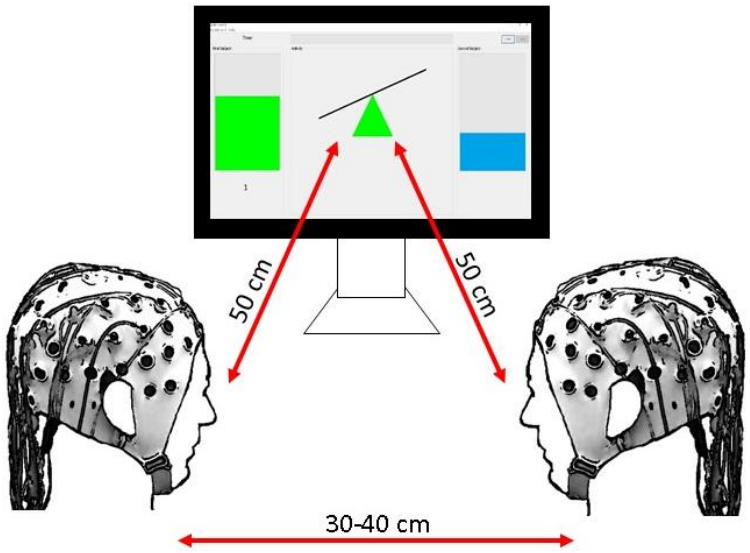

Figure 3.6 The subjects' position relative to the screen in multi-user BCI experiment.

3.3 Data Analysis

Data analysis performed in this thesis consisted of power spectral analysis, signal complexity analysis, source localisation analysis, brain connectivity analysis, and qualitative data analysis through NASA-TLX questionnaires. These analysis techniques were performed separately for baseline and BCI gaming data. The data analysis diagram is illustrated in Figure 3.7. EEG signal analyses (power spectral, signal complexity, and brain connectivity analyses) were performed in a computer with Intel® Core™ i7-6700 CPU @ 3.40 GHz, using Matlab 2018b (The Mathworks, Inc., USA) on Windows 10 operation system.

3.3.1 Data Pre-processing

All raw EEG data were band-pass filtered between the frequency band of 2 and 30 Hz using 5th order infinite impulse response (IIR) digital Butterworth filter. For single-channel data, visual inspection and manual noise (e.g. eye blinking and muscle movement) removal were performed, and as for multi-channel data, independent component decomposition was performed by using the Infomax Independent Component Analysis (ICA) algorithm [103, 104] implemented in EEGLAB (version 14.1.2b) for further noise removal. Noise removal of the multi-channel EEG data was performed to the overall filtered data of 2-30 Hz, from which four different frequency range were later specified, namely theta (4-7 Hz), alpha (8-13 Hz), lower beta (14-20 Hz), and higher beta (21-30 Hz), to be used for power spectral analysis and source localisation analysis.

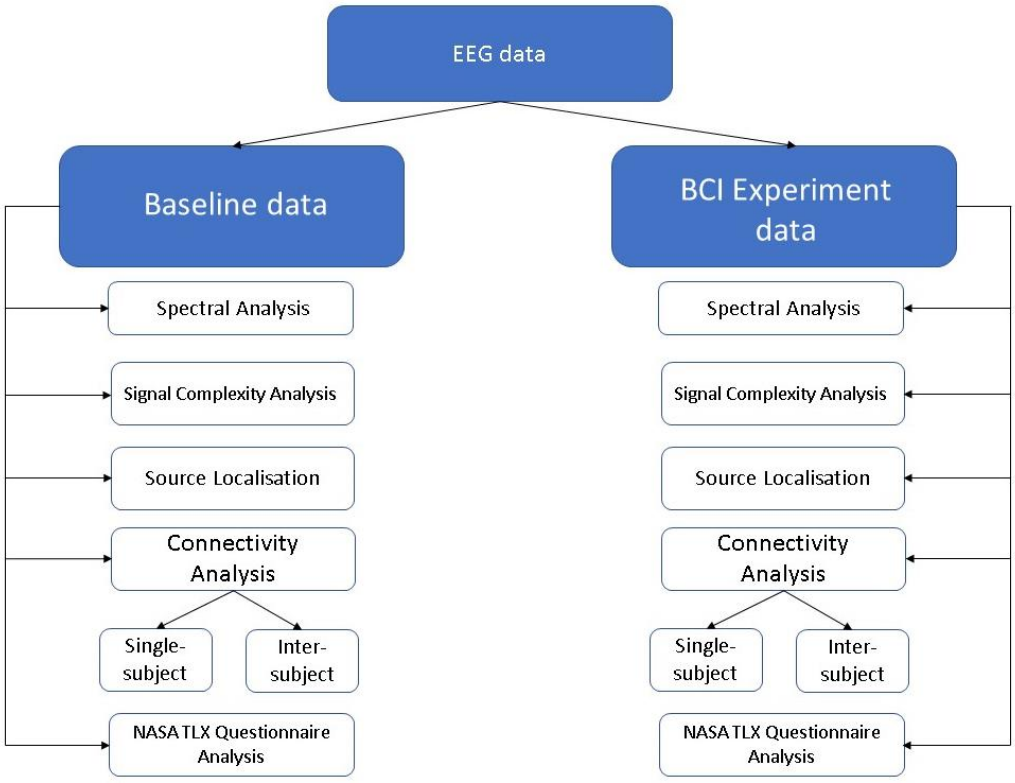

Figure 3.7 Data analysis diagram (there is no specific order for each analysis step).

3.3.2 Power Spectral Analysis

In this thesis, the average power spectrum analysis was calculated by using the Welch's periodogram method, a non-parametrical power spectrum estimator method that is also used as power normalisation method [105]. The equation for Welch's periodogram for a

signal $x_d(n)$ with the intervals of d=1,2,3,…,L and M as the interval length can be described as:

$$\widehat{P_d}(f) = \frac{1}{MU}\left|\sum_{n=0}^{M-1} x_d(n)w(n)\, e^{-j2\pi fn}\right|^2 \tag{3.5}$$

where U works as a normalising factor with the equation of:

$$U = \frac{1}{M}\sum_{n=0}^{M-1}|w(n)|^2 \tag{3.6}$$

with $w(n)$ is the windowed data. The Welch's average power spectrum is the average of the modified periodogram describe in the following equation:

$$\widehat{P_{welch}}(f) = \frac{1}{L}\sum_{n=0}^{L-1}\widehat{P_d}(f) \tag{3.7}$$

3.3.3 Higuchi Fractal Dimension

Fractal dimension (FD) has been used to quantify biological signal dynamic in order to describe the signal's complexity. In this thesis, FD was analysed by applying the Higuchi method as one of the robust methods to measure an object's complexity and self-similarity [106-108]. Higuchi's algorithm is obtained by measuring the mean length of the curve *L(k)*. For each signal in form of a time sequence that is observed as:

X(1), X(2), X(3), …, X(N)

will be constructed into:

$$X_m^k : X(m), X(m+k), X(m+2k), \dots, X\left(m + \left[\frac{N-m}{k}\right]\cdot k\right), m = 1, 2, \dots, k \tag{3.8}$$

where m= 1,2,…,*k* as the initial time and *k*=2,3,…,k_{max} as the time interval. The length, *L(k)*, of the curve X_m^k can be described as:

$$L(k) = \left\{\left(\sum_{i=1}^{\left[\frac{N-m}{k}\right]}|X(m+ik) - X(m+(i-1)\cdot k|\right)\frac{N-1}{\left[\frac{N-m}{k}\right]\cdot k}\right\}/k \tag{3.9}$$

where *N-1/[(N-m)/k]·k* is the normalisation factor for the curve length of the time series. The $\langle L(k)\rangle$ can be defined as the mean of *k* values of *L(k)*, and if the function of $\langle L(k)\rangle$ is proportional to k^{-D}, the curve is said fractal with the dimension of *D* [106, 107].

FD measurement has been applied to EEG signals to further identify the brain's structural and functional organisation during a certain condition or to measure the impact of a neurological impairment. FD has been reported to have a negative correlation with alpha band, the dominant frequency of EEG signal. Accardo et al.[107] reported that FD

is higher during an eyes-open resting state with the level gradient directed from the anterior to the posterior where the highest values were found around the frontal regions, the opposite nature of alpha power that is higher during eyes-closed resting state and predominantly found in the occipital area [107]. Negative correlation was also found between FD and alpha activity during the shift between wakefulness and drowsiness, where they reported an increased in FD along with a reduction of alpha power during drowsy state [109]. With the overlapping frequency band with alpha, mu rhythm desynchronization was found alongside the increase of FD in musicians subjects where they were asked to attend to audio stimulation [110]. Moreover, Accardo et al.[107] also suggested the possibility of lower FD tend to be produced by the presence of a rhythmical and regular wave like the alpha rhythm, as well as by the neural synchronization which corresponds to a higher neural synergism and a lower signal complexity.

Additionally, numbers of studies have been performed in applying FD analysis in brain signals, including the analysis of sleeping and wakefulness stages [109, 111-113], intelligence level [114] and in patient studies for conditions such as: Alzheimer's disease [115], acute stroke [116], schizophrenia [117], epilepsy [118], and depression [119].

Due to the unequal number of EEG channels worn by the players during the last experimental session (the session with multi-channel EEG), only 16 EEG channels were used in HFD analysis, in which the arrangement is identical in both users i.e., AF3, AF4, F3, Fz, F4, FC3, FC4, C3, Cz, C4, P3, Pz, P4, O1, Oz, and O2.

3.3.4 Source Localisation Analysis

The identification of the sources' location where the electrophysiological activation is approximately generated is known as brain source localisation [120-122]. In the effort of identifying the source localisation, there are two types of known problems, namely forward and inverse problem. The forward problem is indicated when the source parameters can be extracted by using a known model, whereas the inverse problem requires an estimation of a model from the available source parameters [122, 123].

The method to solve the forward model in EEG source localisation is more widely available compared to the solution to the inverse problem. The available solution for inverse problem including the two modelling approaches, such as the equivalent current dipole model or the parametric model, based on the assumption of the signal is originated from a small number of active sources, and the distributed source model, based on the

assumption of the signals are generated simultaneously from the distributed location of sources at the cortical level [121-124]. Generally, the accuracy of EEG source localisation depends on several factors, such as the electrodes density and coverage, an accurate head model, and the right inverse model [125].

In this study, the EEG source localisation was estimated by utilising a program called Standardized Low Resolution Electromagnetic Tomography (sLORETA) [126]. Localisation via sLORETA works based on the estimation of the current density which are distributed in the brain [126]. sLORETA can accommodate a total of 6430 voxels at 5mm spatial resolution [122]. sLORETA used a three-shell spherical head model registered to the Talairach human brain atlas [127] based on the digitised Magnetic Resonance Imaging (MRI) from the Brain Imaging Center, Montreal Neurological Institute (MNI) [126]. A three-component vector is estimated at each voxel, where it corresponds to the current density vector with dipole moments along the x, y, and z axes [128]. sLORETA is also equipped with a statistical analysis tool to measure any significant active voxel changes from one condition to another.

sLORETA works under the following mathematical formula:

$$F = \|v - MJ\|^2 + \alpha\|J\| \tag{3.10}$$

where v is the electrical potentials measured from the scalp, M is the lead field matrix, J is the current density, and α is regularisation parameter. The minimum norm $\hat{J}_{mn}$, described as:

$$\hat{J}_{mn} = Tv \text{ where, } T = K^T[KK^T + \alpha C\varepsilon]^{-1} \tag{3.11}$$

the electric potential variance C_x can be calculated by including the source distribution covariance C_j and $C\varepsilon$, described as:

$$C_x = KC_jK^T + C\varepsilon \tag{3.12}$$

and the covariance of the source distribution is calculated as:

$$C_j = T(\alpha)\, C_x\, T(\alpha)^T = K^T[KK^T + \alpha C\varepsilon]^{-1}K \tag{3.13}$$

finally, the sLORETA imaging method for N number of dipoles, can be calculated using the diagonal covariance of the source distribution C_j:

$$\hat{J}_s = [C_j]^{-1/2}\, \hat{J}_{i,} \text{ for } i = 1, \ldots, N \tag{3.14}$$

Due to the unequal number of channels used during the las gaming experimental session for both players (32 channels for one player and 16 channels for the other), only data from the player with 32 channels were subjected to source localisation analysis in

sLORETA. The 32 channels data are expected to provide better source localisation accuracy, as the sensor density is known to directly affect the accuracy as well as in reducing error [125].

3.3.5 Brain Connectivity Analysis

Time-series analysis can be performed in two approaches, i.e., parametric and non-parametric approach. The parametric method requires a model of a data generation, where the method extracts the data property from the assigned model instead of directly from the data, like in non-parametric method [129, 130]. Following the parametric method, one of the most widely used linear model for biological signal is the autoregressive (AR) model [129]. For a sample of data X at a time t : $X(t) = (X_1(t), X_2(t),\ldots.., X_k(t))^T$, AR model can be expressed as:

$$X(t)= \sum_{i=1}^{p} A(i)X(t-i) + E(t) \tag{3.15}$$

where $X(t)$ is a vector of n signals at t, p is the model order, $A(i)$ is a n x n matrix coefficient in the i^{th} order, and $E(t)$ is a matrix with the same size as $X(t)$ containing white noises. In parametric method, the model fitting accuracy depends on the chosen model order. In this thesis, one of the commonly used statistical criteria to estimate AR model order, i.e. the Akaike's information criterion or AIC was used [129, 131], with the maximum order of 30 was chosen, and can be described as:

$$\text{AIC } (p) = \ln[\det(V)] + 2pn^2/N \tag{3.16}$$

where V is the estimated residual variance at the order p, n is number of channels and N is the number of data points.

Brain connectivity can be measured by quantifying the inter-relations between EEG channels, which can be calculated by using more simple methods such as through ordinary coherence in frequency domain or cross correlation function in time domain [35, 37]. However, these two approaches are not depicting the directional and the causal relation between different signal sources. In this thesis, two methods were applied to measure brain connectivity by adapting the AR model, such as Granger Causality (GC) and Directed Transfer Function (DTF). GC was performed to measure both intra-brain connectivity (the measurement among EEG channels within one brain) and inter-brain connectivity (the measurement among EEG channels between two interacting individuals) in time domain, whereas DTF was performed only to estimate the intra-brain connectivity in the frequency domain.

GC is an estimation of a causal influence of two time series *x(t)* and *y(t)*, implying that the past measurement of the second time series *y(t)* will help predicting the future measure of the first time series *x(t)* [38, 39]. Two directional GC from the two time-series can be described as:

$$X'(t) = \sum_{i=1}^{p} A_{11}(i)X(t-i) + \sum_{i=1}^{p} B_{12}(i)Y(t-i) + E_x\,(t)$$

$$Y'(t) = \sum_{i=1}^{p} B_{21}(i)X(t-i) + \sum_{i=1}^{p} A_{22}(i)Y(t-i) + E_y(\mathrm{t}) \qquad (3.17)$$

where time series *x(t-i)* and time series *y(t-i)* are the past values of time series *x(t)* and *y(t)* respectively, with the order of *p*, and the prediction error of *E*.

Bivariate GC was applied to analyse inter-subject connectivity, as there was no physical connectivity between players and multivariate GC was used to analyse intra-subject connectivity. Bivariate GC analysis was performed by using a Matlab toolbox, Brainstorm 3.4 (University of Southern Carolina and McGill University, USA), and multivariate GC analysis was performed by using the MVGC v1.0 Matlab toolbox (the Sackler Centre for Consciousness Science (SCCS), University of Sussex) [132].

DTF was first defined by Kaminski and Blinowska [133] that in the causal influence from *j* to *i*, DTF describes the ratio between the inflow from channel *j* to *i*, relative to all the inflows to *i*, thus focusing on sources of activity that was regarded more relevant due to the nature of the neurofeedback task applied in the experiment (with the Pz as the control channel). In this study DTF was estimated by using asymptotic DTF algorithm in a Matlab package [134]. Four frequency bands were used in DTF analysis: theta (4-7 Hz), alpha (8-13 Hz), lower beta (14-20 Hz), and higher beta (21-30 Hz) bands. DTF from *j* to *i* with the transfer matrix H can be defined as:

$$\gamma^2{}_{j\to i}(f) = \frac{|H_{ij}(f)|^2}{\sum_{m=1}^{k} |H_{im}(f)|^2} \qquad (3.18)$$

Due to a high computational demand of these methods, only ten representative EEG channels were chosen (F3, Fz, F4, C3, Cz, C4, P3, Pz, P4, and Oz) to represent each of the brain area, covering the frontal, central, parietal, and occipital cortex, and distributed in both hemispheres and over the midline areas.

3.3.6 Statistical Analysis

In this thesis, several statistical analysis methods were applied- both parametric and non-parametric analysis- to measure significance in each of EEG analysis component. The parametric statistical analysis includes paired t-test, one-way and two-way analysis of variance (ANOVA), and the non-parametric statistical analysis consisted of Wilcoxon Signed-Rank test, Kruskal-Wallis H test, Friedman test, and permutation test.

Paired t-test analysis was applied to compare means between two groups. In paired t-test, the null hypothesis (H_0) is that the mean difference between two observed groups is zero and paired t-test can be expressed as:

$$t = \frac{\bar{D}}{\left(\frac{SD}{\sqrt{N}}\right)} \tag{3.19}$$

where $\bar{D}$ described the mean of differences between groups for each subject, SD for standard deviation, and N for the number of subjects (N) [135]. The formula for SD can be described as:

$$\text{SD}=\sqrt{\frac{\sum(X-\bar{X})^2}{N-1}} \tag{3.20}$$

One-way ANOVA was applied to compare the means of more than two groups. The H_0 is that the mean of each group is equal, and the alternative hypothesis is the opposite. Based on the source of variance, the way to calculate one-way ANOVA can be divided into one-way ANOVA between groups and one-way ANOVA within groups. The degree of freedom (*df*) used in between groups is the number of groups minus 1, and the *df* used in within groups is the total number of observations minus the number of groups. The total test statistic (*F* statistic) used is the ratio of the variance between groups divided by the variance within groups. However, for one-way ANOVA between groups, F ratio is calculated from the variance between group divided by the variance of error and the same way for one-way ANOVA within groups. All divisions of one-way ANOVA calculation are rooted from the calculation of the sum of squares (SS) and the mean sum of squares (MS)- or variance [136], expressed as followings:

$$\text{SS} = \sum X^2 - \frac{\sum X^2}{N} \tag{3.21}$$

$$\text{MS} = \frac{SS}{df} \tag{3.22}$$

Two-way ANOVA is an extension of the corresponding one-way ANOVA where the same assumptions was adapted. In Two-way ANOVA was performed when there is one measurement variable but with at least two nominal variables/factors. Two-way ANOVA can be used to measure the interaction between-subjects, within-subjects, and in mixed factorial. Thus, the H_0 in two-way ANOVA is that the means for every factorial combination is the same and that there is no interaction between factors. All divisions of two-way ANOVA calculation are rooted from the similar calculation of SS and MS (Eq. 3.21 and 3.22) [137].

Wilcoxon Signed-Rank (WSR) is a non-parametric equivalent of t-test in comparing the means of two groups. The WSR is applicable for comparing the difference of two groups when the sample size of each group is identical and is the equivalent of a paired t-test. The WSR test compares two groups by ranking the differences between observations and then sums up all the ranks for each direction. The WSR test is aiming to determine whether the median difference between pairs of observation is equal to zero. The Z values for WSR can be calculated as the following:

$$\text{Z} = \frac{Tmin - \frac{N(N+1)}{4}}{\sqrt{\frac{N(N+1)(2N+1)}{24} - \sum\frac{t^3-t}{48}}} \tag{3.23}$$

where *Tmin* is the total summation of ranks from negative differences, *N* as the number of observed pairs, and the $\sum \frac{t^3-t}{48}$ extension is applicable when *t* number of ties exist [135, 138].

Kruskal-Wallis H test is a non-parametric statistical test that can be used to compare multiple groups and is a non-parametric equivalent of one-way ANOVA. This test applies ranks to all values from the lowest to the highest, and then sums up all the ranks from each group. The test compares the mean ranks from each group to determine if a group of independent samples are just randomised samples originated from the same population, or from a different population. A test statistic *H* for this test can be computed as:

$$\text{H} = \frac{12}{N(N+1)} \sum \frac{R_k^2}{n_k} - 3(\text{N}+1) \tag{3.25}$$

Where N represents the number of total observed samples, n_k represents the number of samples in each group, and $\sum R_k$ represents the sum of the ranks in each group [136].

Friedman test is the non-parametric statistical test that is equivalent to within-subjects one-way ANOVA. Friedman test can be used to compare scores from two or more conditions, where the one group takes part in all conditions. The test observes each individual subject's scores across all conditions, and later sums up all the ranks from each condition. The test then compares the summed ranks from each condition. Friedman test statistic can be computed as:

$$X_k^2 = \frac{12}{Nk(k+1)} \sum R_k^2 - 3N(k+1) \tag{3.26}$$

Where N represents the size of the group, and $\sum R_k$ represents the sum of the ranks in each group [136].

Permutation or also known as randomisation, is another non-parametric statistical method that can be applied to a sample of data with an unknown normality. In permutation test, when the H_0 says that the correlation between samples in the population is zero, then a test statistic can be carried out under H_0 to see if the outcome from any attempt to randomise the samples. If the H_0 is true, then randomly shuffling the samples has no effect on the outcome, making it possible to generate multiple combination of samples. The decision of rejecting H_0 can be computed from the difference between the shuffled samples and the unshuffled samples [139].

3.3.7 Post-experimental Questionnaire

NASA-TLX questionnaire (Fig. 3.8) was given to all the participants after every experimental session. The questionnaire was chosen as a standardised tool to assess how the players perceive the workload of the BCI gaming experiments. The questionnaire consists of six aspects representing the perceived workload, i.e. mental demand, physical demand, temporal demand, performance, effort, and frustration [140]. The subjects were given 21 gradation of scales rating from high, medium, to low (0= very low, except in performance 0=very low mistakes/perfect; and 21= very high, in performance 21= very high mistakes/failure). This questionnaire is expected to provide an insight whether the behavioural aspects -based on how the players perceive the gaming experiment, affecting the gaming performance.

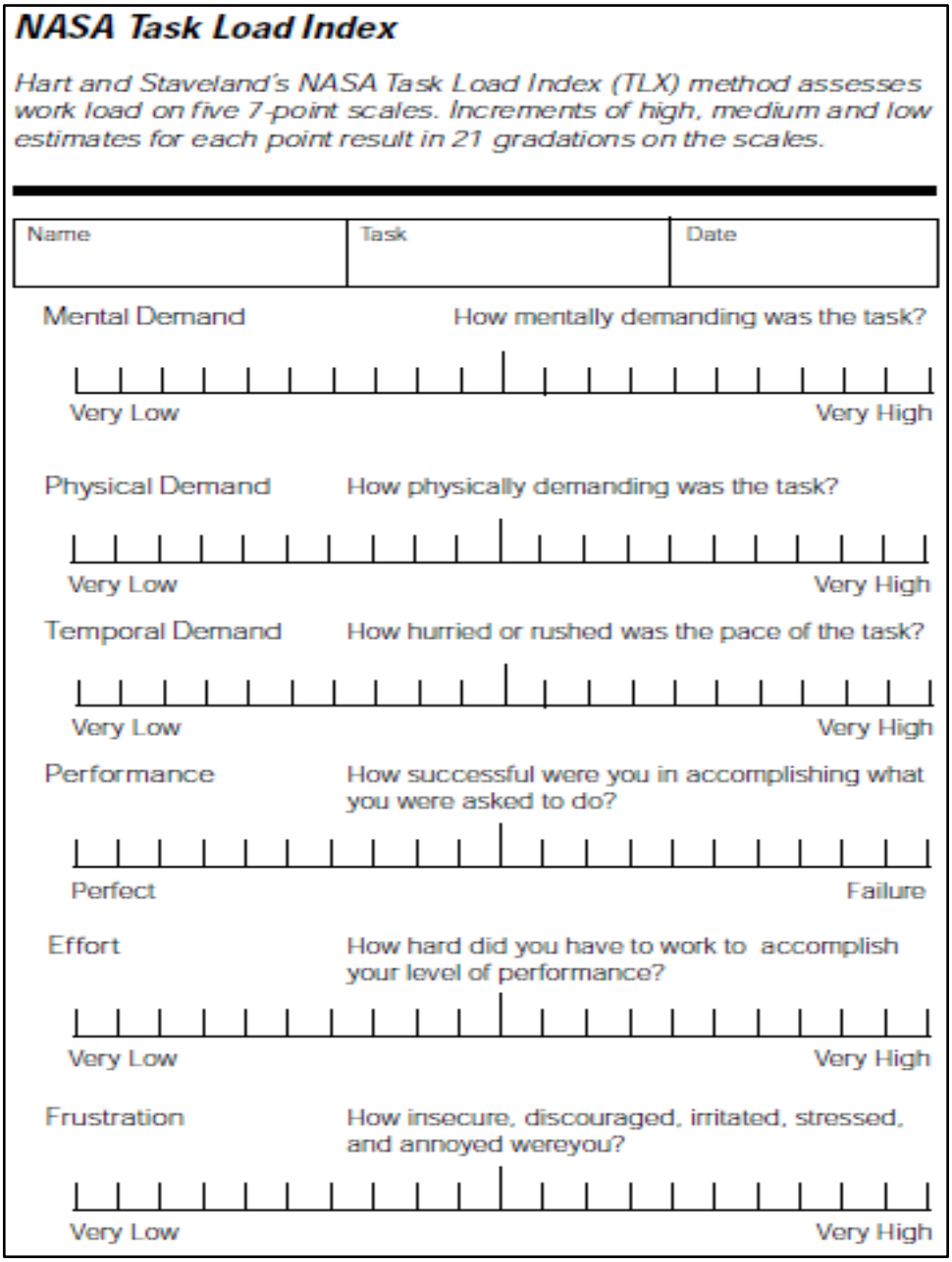

Figure 3.8 NASA-TLX questionnaire.

Chapter IV

Competitive Multi-user BCI:
Part I – Electrophysiological Features

4.1 Introduction

Competitive interaction is an essential mechanism to promote survival in social animals. A single-brain neuroimaging study done by Polosan et al. [141], identified the brain regions that are responsible in a human-to-human competitive interaction, i.e. the superior and inferior frontal gyri, anterior cingulate cortex (ACC), anterior insula, the superior and inferior temporal cortex, hippocampus, fusiform gyrus, cuneus, and precuneus. These findings, however, require further confirmation, especially in a more natural multi-person setting, in which hyperscanning method provides more benefit for this context.

Frontal cortex has been associated to social interaction- including in competition. Astolfi et al. [84], argued that the involvement of the frontal cortex, specifically the orbitofrontal regions during betrayal in Prisoner's Dilemma gaming experiment, reflects the emotional and logical consideration before deciding to betray or to cooperate. The dlPFC has also been linked to social preferences in relation to social norm, where the

decision to violate or to obey the norm is being processed as well as the calculation of reward and punishment [142, 143]. Additionally, competitive interaction that requires error prediction and social loss/gain prediction revealed the involvement of ventromedial prefrontal cortex (vmPFC) and striatum [144-147].

Balconi and Vanutelli [81] also found prefrontal cortex activation during hyperscanning competitive selective attention task and this activation has been linked to the adaptation strategy and judgement. Furthermore, they argued that the prefrontal cortex activation is related to the social perception when social hierarchy is present. Moreover, in a separate study, dlPFC, medial prefrontal cortex, and amygdala have been reported to mediate perception of social hierarchy [148].

Competitive interaction caused one or more of the interacted parties to experience loss. Two brain networks i.e. mentalizing and social pain networks, were reported to play an important role in social interaction, particularly in the one experiencing loss or social exclusion [149, 150]. Mentalizing network consist of dorsal medial prefrontal cortex (dmPFC), vmPFC, precuneus, and TPJ, while social pain network - associated with reaction to social exclusion, consist of ACC and anterior insula [149].

In this study, a competitive multi-user BCI gaming that is based on the alpha band, non-verbalised operant conditioning, were performed. The recorded EEG signatures were measured and analysed during both resting and gaming states, in order to explore the cortical dynamics that occur during a simultaneous competitive task. Moreover, the alpha band activity, particularly during resting has been proposed as a predictor of a successful cognitive performance [42, 151]. In this study, EEG resting state of two competing players will be recorded and compared, to see whether there is any resting state EEG characteristic that can predict competitive BCI performance.

4.2 Methods

4.2.1 EEG experiments

Twenty healthy able-bodied adults (age 26.9 ± 4.7 years old, eight females and twelve males) participated in EEG experiments where they were grouped into ten pairs based on the order of their appearance. Eight out of ten pairs of participants have known each other before the experiment. They signed the written consent form prior to the experiments. Ethical permission was granted by the University's College Ethical Committee.

The groups of players were divided into group D (dominant players) and group ND (non-dominant players), determined based on the highest average scoring performance (out of six sub-sessions in each session) in the first two gaming sessions (the single-channel experiments). If during the first two sessions the pair is tied in scores, then highest average gaming RA between players during the first two sessions was used to determine the dominance between players. The gaming conditions for each pair were classified into 'successful' and 'non-successful' sub-sessions based on their gaming performance in the third session. These conditions were decided by calculating the score difference between players which was obtained by subtracting the fixed scores gained by the players, in each sub-session. These conditions include: the gaming sub-session with the biggest score difference between players (BSD) and the gaming sub-session with the smallest score difference between players (SSD). Further technical details regarding the game interface, the scoring rules, the EEG experiment setup and sessions have been covered in the Method chapter (Chapter III).

4.2.2 Data analysis

Power Spectral Analysis

Prior the analysis, each continuous time-series was segmented into 4 s epoch with a 50% overlap. Statistical analysis for individual RA at Pz and individual alpha (IA) peak frequency at Pz from all sessions were performed in SPSS 25.0 (IBM corp., USA). Prior the statistical analysis, Shaphiro-Wilk normality test was performed to confirm the normal distribution of the data. Non-parametric statistical analyses were performed for RA and scores data, by using Kruskal-Wallis H test and Wilcoxon signed rank (WSR) test. Kruskal-Wallis H test was used to compare more than two groups and the WSR was used to compare two groups, i.e. the group of players, D and ND. Parametric statistical analyses were performed for IA peak frequency data, by using. two-way ANOVA to compare different variables (Session and Group) in one measurement.

All multi-channel EEG data were uploaded to a STUDY structure in EEGLAB for power spectral group analysis. The uploaded data were divided into groups (i.e. group D and ND) and into different conditions (i.e. Baseline, BSD, and SSD). In a STUDY structure, spatial distribution of power for all conditions was calculated in the four pre-defined frequency bands (theta, alpha, lower beta, and higher beta). A non-parametric unpaired permutation analysis for 800 repetition ($p<0.05$) [139] was applied to test the statistical significance of the absolute power difference between groups or conditions in

each frequency band, and False Discovery Rate (FDR) statistical correction method [152] was applied for multiple comparisons.

Fractal Dimension

The k*max* value of 8, as the most commonly used k*max* values in EEG signal analysis [109, 153, 154] and a 5 s epoch length were chosen for HFD analysis. Prior the HFD analysis, data were down-sampled to 128 Hz sampling frequency [155]. Non-parametric statistical analysis such as Kruskal-Wallis H test and WSR test were performed to the mean HFD data. Kruskal-Wallis H test was used to compare the three conditions (i.e. Baseline, BSD, and SSD) and WSR test was used to compare the two groups (i.e. group D and ND). Both tests used confidence level of 95%. Holm-Bonferroni statistical correction method was applied for multiple comparisons [156].

Source Localisation

Prior exporting data to sLORETA, 2 minutes of data length from each participant from each condition (i.e. Baseline, BSD, and SSD) were divided into 4 s epoch with no overlap. The 2 minutes length was chosen based on the duration of the shortest time-series (baseline), due to the data length uniformity required for paired statistic in sLORETA. The extracted 2 minutes data were taken from the two minutes where the average RA of both players have the biggest difference (for BSD) and the smallest difference (for SSD). Four pre-defined frequency bands (theta, alpha, lower beta, and higher beta) were selected. Paired t-test statistic was performed using statistical analysis package implemented in sLORETA, to compare each of the gaming condition with the baseline in each frequency band. The paired t-statistic was calculated on log-transformed data with 5000 non-parametric randomizations ($p < 0.05$).

Post-experimental Workload Analysis

The post-experimental NASA-TLX scales obtained from all participants were compared to find the statistically significant difference between sessions and between groups, for each category (i.e. mental, physical, temporal, performance, effort, and frustration). Non-parametric statistical tests were performed in SPSS, namely Friedmann's test, WSR test, and Kruskal-Wallis H test ($p < 0.05$). Friedmann's test was used to determine any statistical difference between measurements across multiple variables, namely Sessions and Groups (i.e. group D and ND). WSR test was used to compare the scores between

groups in each session for each category. Lastly, Kruskal-Wallis H test was performed to measure the statistical difference in the overall NASA-TLX scores over sessions.

4.3 Results

4.3.1 RA, scoring performance, and individual alpha peak frequency

In this study, RA was used as a control parameter in gaming, where the scoring results were used to measure the users' gaming performance, as previously mentioned in the method section. Figure 4.1 shows the absolute power at alpha band from Pz during Baseline and during the highest-scoring sub-session, averaged from all players in each group, for each session. This figure indicates that, on average, both groups managed to increase their alpha power during gaming and during baseline, however the increase is less clear in ND. Moreover, in the last session, group ND showed higher average alpha power during Baseline, indicating the possibility of training effect on the last day of experiment.

Table 4.1 and Table 4.2 show the daily sessions' average (mean and standard deviation) and median (median and interquartile range), respectively of the % gaming RA recorded from channel Pz along with the gaming scores from all participants across sub-sessions. Due to the large values of standard deviations of % RA, the results of median and interquartile range were also provided.

Table 4.3 shows Kruskal-Wallis H test ($p < 0.05$) found a significant difference over sessions in gaming scores, only in group D. No significant difference was found in RA of both groups and in scoring over sessions of group ND. Table 4.4 shows that Wilcoxon signed-rank test ($p < 0.05$) found a significant difference in RA and gaming scores in both groups, for RA between Session I and Session III for group D and between Session I and Session II for group ND, and for scores, between Session I and Session II in both groups, and between Session I and Session III in group D.

Figure 4.2 shows the % RA during pre-gaming Baseline in each player in three experimental sessions. The results showed that the players with higher pre-gaming Baseline RA can be different in each session, for example, group ND in pair 4, 6, and 7 in Session III had higher Baseline RA, compared to the previous two sessions.

Results in Figure 4.3 shows the mean ±standard deviation (std) of each single player's gaming RA (Fig. 4.3(a-c)) and gaming scores (Fig. 4.3 (d-f)), averaged over 6

gaming sub-sessions in each daily session. Mean ±std were used in this figure to show the impact of NC on the individual RA, which is more evident if the graphs are presented based on mean. The bars with an asterisk represent the mean gaming RA from players with higher Baseline RA in each pair. The players marked with asterisks received feedback of their normalised RA (NC was applied to their RA during gaming) instead of their real RA. In some pairs, the players who had larger/smaller Baseline RA can be different on different days, they can be from either group D or ND (i.e. pair 4, 6, and 7 on session III). This was likely caused by the individual variability of natural alpha power that not only differs from one person to another, but also from one day to another [157]. This also suggests how important it is to adjust the individual alpha threshold daily, before each gaming session.

Our results also suggest that lower Baseline RA due to normalisation does not guarantee a balanced performance between players, e.g. in pair 1 in all sessions, pair 9 in Session I and Session III, and in pair 10 Session I., where the players who received normalised RA won the game in all three sessions. In order to score, one player should maintain their RA 10% above the other for at least 1 s, thus, timing is essential to achieve better performance. In these pairs, one player did not manage to sustain their RA higher for longer time, which led them to a lower score despite having a higher average RA. The mean ± std of the individual RA before normalisation are displayed on Figure 4.4, to provide a comparison between before and after NC application to the player with higher Baseline RA. In some pairs, the player with higher Baseline RA did not always have a larger average RA during gaming even before the normalisation was applied (e.g. pair 8 Session I and pair 2 Session II), confirming that the better gaming performance relied on the skill to sustain higher RA within the appointed duration, rather than based on the natural Baseline RA.

Furthermore, the individual alpha (IA) peak at Pz in all participants from each session was measured from the power spectrum within the wide band of 6-16 Hz [158], from eyes-closed baseline and eyes-open baseline. The frequency of the beginning of ‘ascent’ and the end of ‘descent’ from the dominant power spectrum within the selected frequency width were visually inspected and the decrease of spectral power by more than 20% from the eyes-closed condition to the eyes-open condition was defined as IA frequency with the maximum decrease as the maximum peak [158]. Table 4.5 shows the

different IA peak frequency in each player from one session to another, along with the mean ± std of IA peak frequency for each group, in every session. Shapiro-Wilk normality test was performed prior the parametric statistical analysis to confirm the normal distribution of the IA peak frequency data. Table 4.6 shows that two-way ANOVA analysis ($p < 0.05$) found no significant difference in IA peak frequency across sessions and between groups in each session.

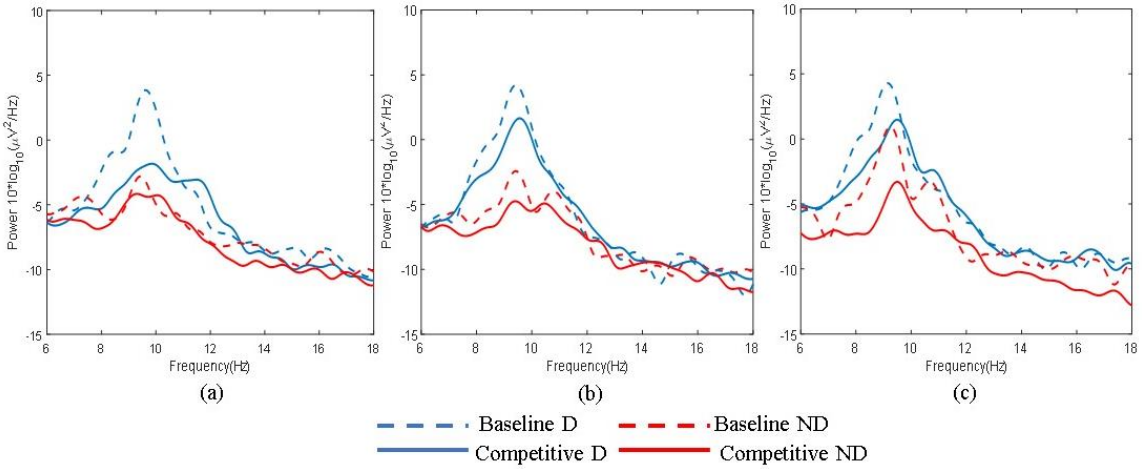

Figure 4.1 The absolute alpha power spectral density at Pz, averaged from all baselines and all the highest-scoring sub-sessions, in (a) Session I, (b) Session II, and (c) Session III, for each group of players.

Table 4.1 The mean ± std of gaming RA from channel Pz and gaming scores from all participants averaged over all sub-sessions on each experimental day.

RA		
Session	*Group D*	*Group ND*
I	33.1 ± 14.3	21.8 ± 10.4
II	36.9 ± 17.8	23.4 ± 11.9
III	35.2 ± 10.0	23.7 ± 14.4
Scores		
Session	*Group D*	*Group ND*
I	23.5 ± 15.1	19.7 ± 14.7
II	38.5 ± 27.9	16.3 ± 13.4
III	34.4 ± 24.6	18.1 ± 12.4

Table 4.2 The median and interquartile range of gaming RA from channel Pz, and gaming scores from all participants averaged over all sub-sessions on each experimental day.

RA		
Session	*Group D*	*Group ND*
I	33.7 (20.2-40.4)	18 (14.1-28.3)
II	30.4(21.5-50.9)	21 (15.3-26.9)
III	33.6 (20.5-44.8)	19 (17.1-22.3)
Scores		
Session	*Group D*	*Group ND*
I	25.5 (11-32.75)	16.5 (8-26.75)
II	35.5 (14-57)	11(7-24)
III	28.5 (15-45.75)	16.5(7.25-24.75)

Table 4.3 Table of *p*-values and H scores obtained from Kruskal-Wallis H test ($p<0.05$) of gaming RA (of each group) and gaming scores, across all sessions.

RA		
Group	*p*-values	H-statistic
D	0.578	1.096
ND	0.737	0.610
Scores		
Group	*p*-values	H-statistic
***D**	0.011	9.111
ND	0.282	2.535

Table 4.4 Table of *p*-values and *Z* scores obtained from Wilcoxon signed rank test ($p<0.05$) of gaming RA (of each group) and gaming scores between sessions.

RA			
Group	**Comparison**	***p*-values**	***Z*-score**
D	Session I - Session II	0.058	-1.899
	*Session I - Session III	0.049	-1.966
	Session II- Session III	0.095	-1.610
ND	*Session I - Session II	0.033	-2.135
	Session I - Session III	0.143	-1.465
	Session II- Session III	0.924	-0.096
Scores			
	Comparison	***p*-values**	***Z*-score**
D	*Session I - Session II	0.51×10^{-4}	-4.050
	*Session I - Session III	0.23×10^{-3}	-3.677
	Session II- Session III	0.216	-1.238
ND	*Session I - Session II	0.049	-1.967
	Session I - Session III	0.396	-0.849
	Session II- Session III	0.244	-1.166

*) Comparison with significant *p*-value.

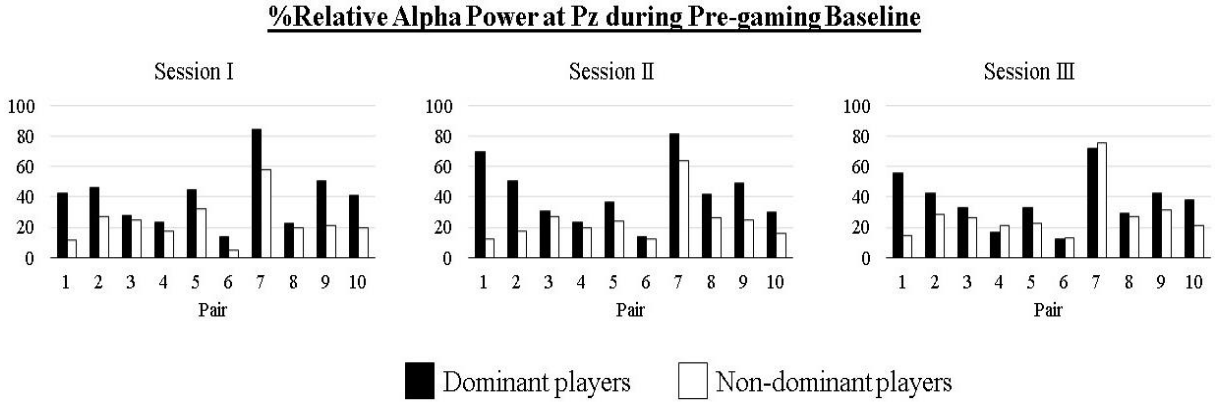

Figure 4.2. The individual pre-gaming RA (%) at Pz for all players in all three experimental sessions.

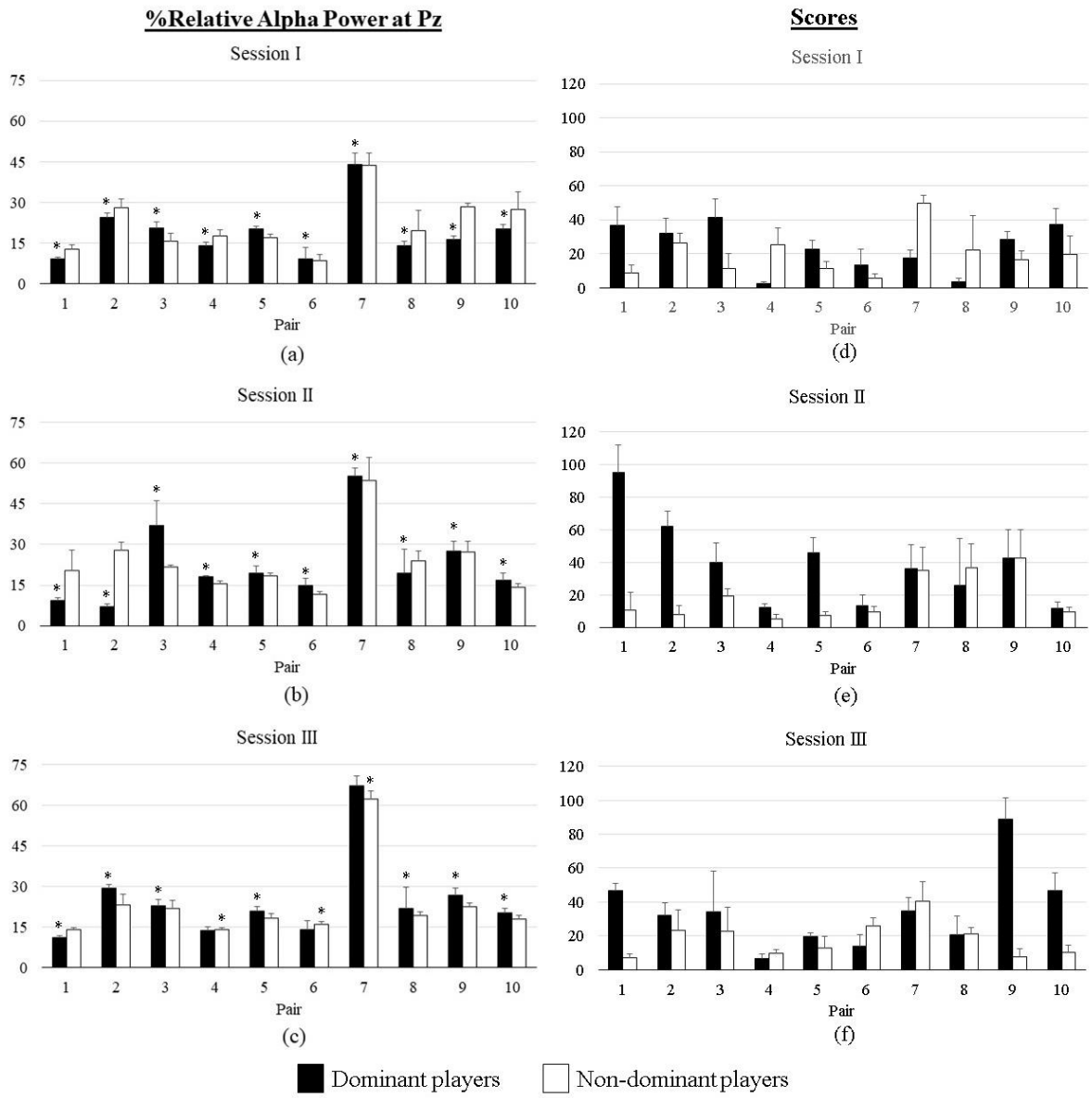

Figure 4.3 (a-c) Mean ± std of individual gaming RA (%) at Pz and (d-f) gaming scores from all sub-sessions in each session -the bars with asterisks (a-c) indicate normalisation of RA during gaming.

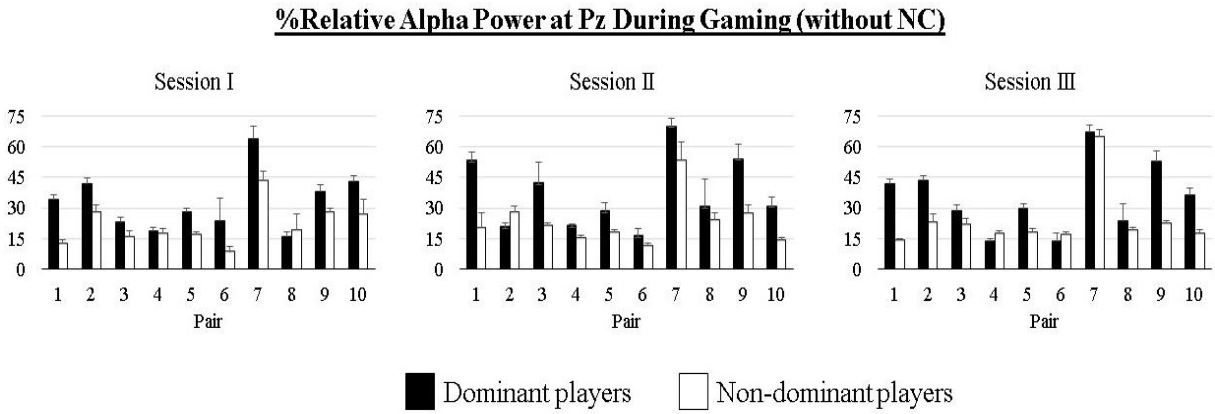

Figure 4.4 Mean ± std of the real individual gaming RA (%) at Pz from all sub-sessions in all three experimental sessions, without any normalisation applied during gaming.

Table 4.5 The mean ± std of IA peak (Hz) from each participant in each session.

Pair	Session I		Session II		Session III	
	D	ND	D	ND	D	ND
1	10.5	11.3	10.3	11.2	9.7	11.1
2	9.5	9.7	10.1	9.9	11.3	10.7
3	10.6	11.3	9.8	11.6	11.1	10.4
4	10.1	9.9	10.0	9.8	9.9	10.1
5	11.3	11.3	10.8	12.0	9.9	11.7
6	11.0	10.9	10.8	10.5	11.1	10.4
7	9.1	10.1	9.7	10.0	9.3	9.9
8	10.8	10.0	10.4	9.8	10.4	9.3
9	9.3	8.4	9.5	8.8	9.5	8.5
10	10.6	10.0	10.5	10.7	10.3	9.5
Mean	**10.3**	**10.3**	**10.2**	**10.4**	**10.2**	**10.2**
Std	0.7	0.9	0.4	1.0	0.7	0.9

Table 4.6 Table of F and *p*-values obtained from two-way ANOVA analysis ($p<0.05$) of IA peak frequency.

Comparison	F	*p*-value
Group	0.002	0.969
Session	0.130	0.878
Group*Session	0.304	0.739

4.3.2 Spatial power spectral density

The spatial power spectral density obtained from the multichannel EEG data between tasks (i.e. between baseline and BSD, between baseline and SSD, and between BSD and SSD) in each group (i.e. group D and ND) and between groups in each condition were compared by performing a non-parametric unpaired permutation test ($p<0.05$) in a STUDY structure provided in EEGLAB.

The comparison of the power spatial distribution between Baseline and BSD in group D (Fig. 4.5) shows an uncorrected significant power changes occur around the bilateral frontal channels in alpha band. While theta and both beta bands show fewer changes occur on the isolated frontal electrodes., such as at FC6 for theta band and at F3 for both beta bands. No significant changes were found after FDR correction was applied in any channels in any frequency band. No significant changes were found at control channel Pz in any frequency band, indicating that the winning strategy was to maintain the alpha power rather than to increase it. No significant changes were found in any channels in any frequency band for SSD condition compared to Baseline. Despite the lack of significant changes, the results during BSD suggesting the tendency to maintain alpha power at Pz during successful gaming to be closer to Baseline, followed by a frontal decrease of alpha power.

The comparison of spatial power distribution between Baseline and BSD in group ND (Fig 4.6) shows a significant decrease of alpha and lower beta bands. In alpha band, a significant power decrease was found in all channels, while in lower beta band, was found around the bilateral frontal channels (i.e. AF3, AF4, F3, Fz, F4, FC3, FC4, C3, Cz, and C4). No significant changes were found in the theta and higher beta bands. The comparison between baseline and SSD (Fig. 4.7) shows power changes were found in alpha band at Fz, F4, FC6, C3, C4, P3, and Pz, and no significant changes were found after FDR was applied. In contrast to BSD, Pz was found unchanged after FDR correction, indicating the slight effort to gain better performance by maintaining power at Pz (and globally). The global decrease or maintenance of alpha power that occur in BSD suggesting that group ND did not apply any task-specific strategy during their successful gaming.

The comparison of spatial power distribution between BSD and SSD in group D (Fig. 4.8) shows a significant power difference in lower beta band in channel C1, with

SSD shows higher power than BSD. No significant difference was found after FDR correction in any frequency band, however uncorrected power differences were found in theta band around the central-parietal-occipital area and in higher beta band in the left frontal area. The comparison between BSD and SSD in group ND (Fig. 4.9) show no significant difference was found in any channel in both groups, in any frequency band, after FDR correction. However, uncorrected power changes were found around the left frontal area in theta and alpha bands.

The comparison of spatial power distribution between groups in different condition, i.e. Baseline (Fig. 4.10), BSD (Fig. 4.11), and SSD (Fig. 4.12), were presented with 16 out of 32 channels of group D that are the same location to the channels of group ND, due to the unequal number of channels used by the two groups during the experiment. Significantly lower occipital alpha power was found in group ND compared to group D, during Baseline. No statistically significant difference was found in BSD and SSD, after FDR correction. However, uncorrected power differences were found in the bilateral central area and the posterior midline area in alpha band (and around the occipital channels only in SSD). Generally lower posterior alpha power exhibited by group D during Baseline might support the idea that resting alpha can be used to predict learning ability in alpha neurofeedback training [42], which is consistent with our results, where most players in group D outperformed group ND in all gaming sessions.

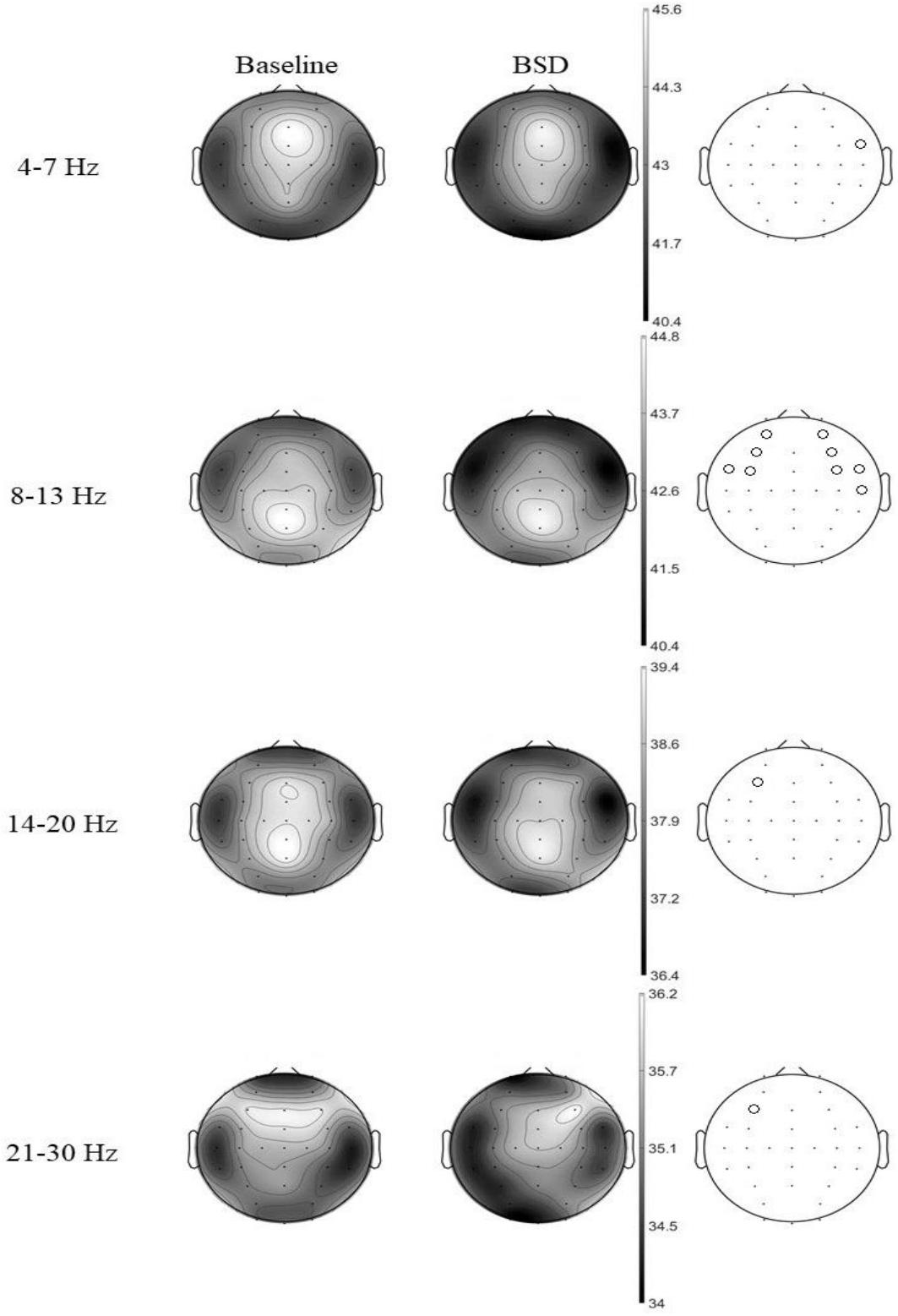

Figure 4.5 Non-parametric permutation test ($p<0.05$) between the BSD condition and Baseline for group D, in theta, alpha, lower beta, and higher beta frequency bands. FDR correction was applied for multiple comparison (FDR was not performed if the significant activation after permutation only occur in one channel). White dot represents a significant difference before FDR correction ($p<0.05$) and no significant power changes were found after FDR was applied.

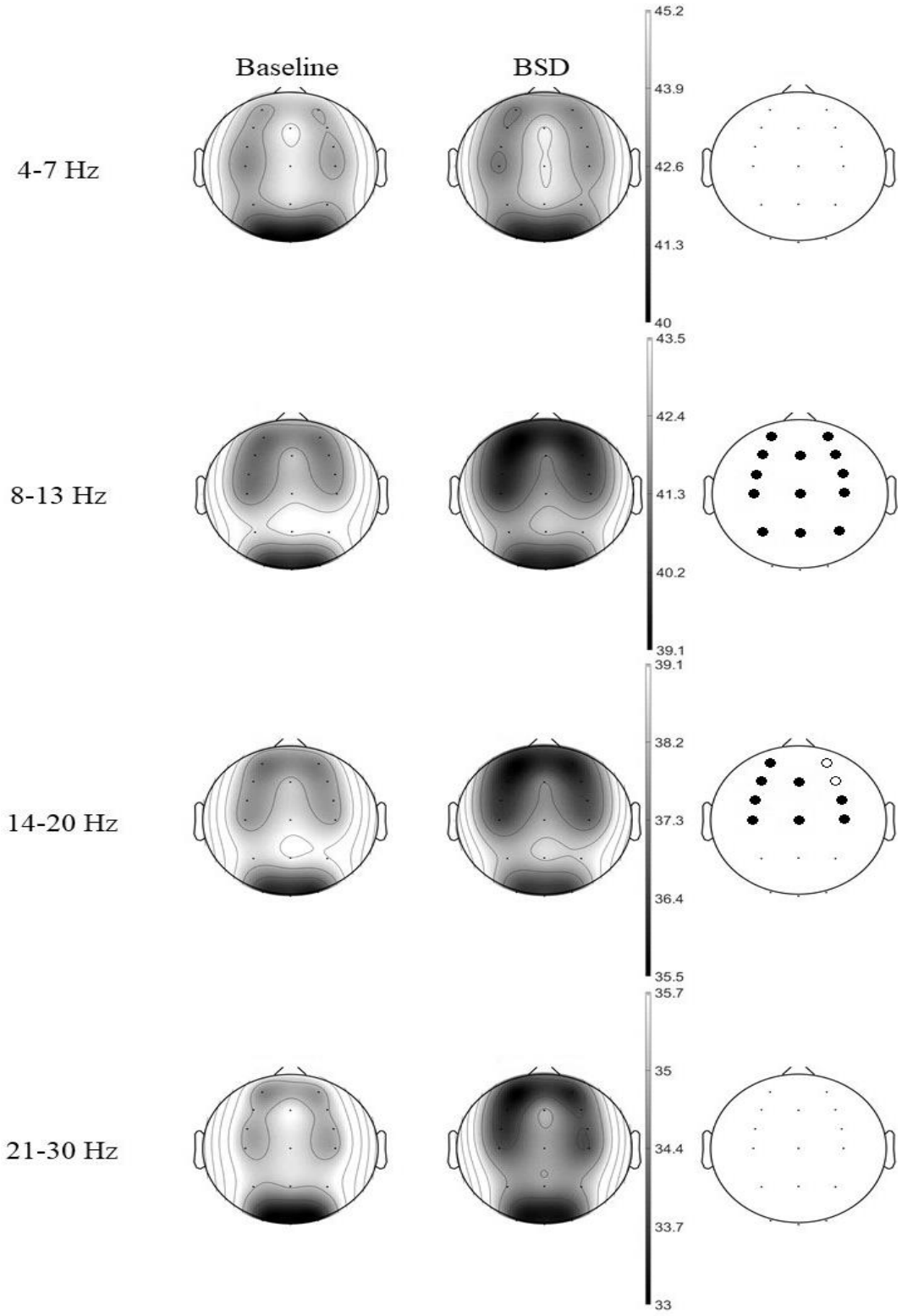

Figure 4.6 Non-parametric permutation test (p<0.05) between the BSD condition and Baseline for group ND, in theta, alpha, lower beta, and higher beta frequency bands. FDR correction was applied for multiple comparison (FDR was not performed if the significant activation after permutation only occur in one channel). White dot represents a significant difference before FDR correction (p<0.05), and black dot represents a significant difference after FDR correction.

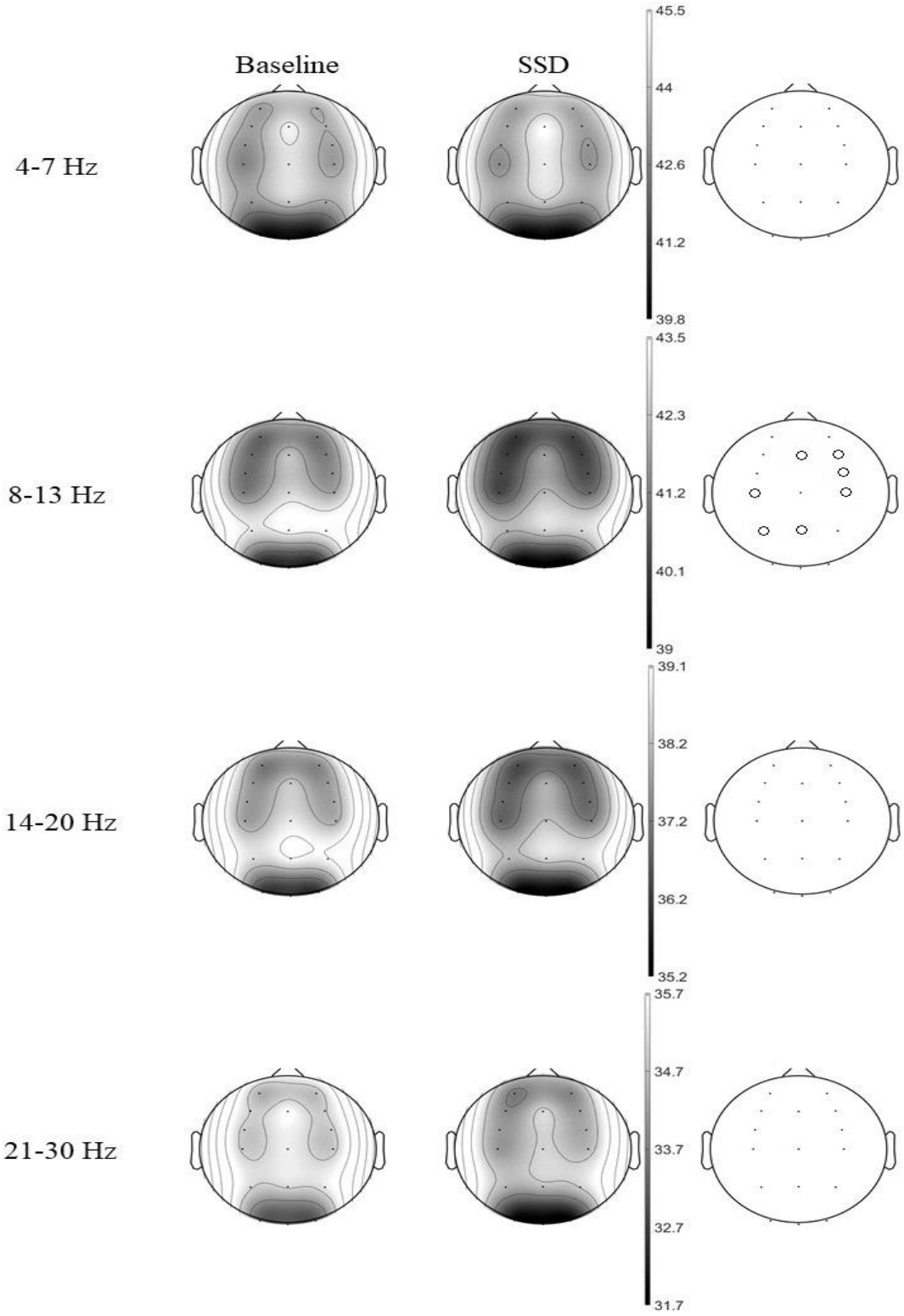

Figure 4.7 Non-parametric permutation test (p<0.05) between the SSD condition and Baseline for group ND, in theta, alpha, lower beta, and higher beta frequency bands. FDR correction was applied for multiple comparison (FDR was not performed if the significant activation after permutation only occur in one channel). White dot represents a significant difference before FDR correction (p<0.05) and no significant power changes were found after FDR was applied.

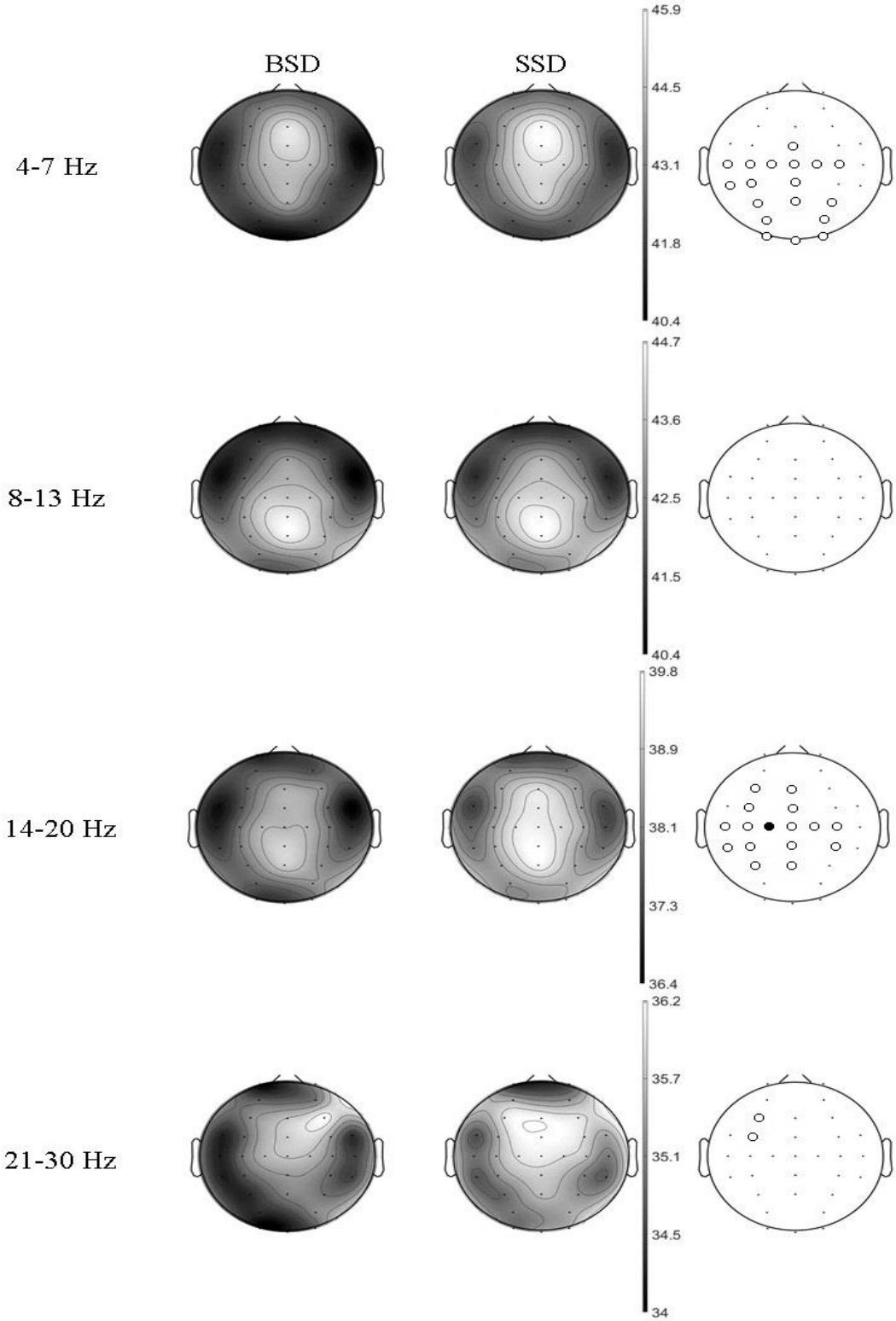

Figure 4.8 Non-parametric permutation test ($p<0.05$) between BSD and SSD for group D, in theta, alpha, lower beta, and higher beta frequency bands. FDR correction ($p<0.05$) was applied for multiple comparison. White dot represents a significant difference before FDR correction and black dot represents a significant difference after FDR correction.

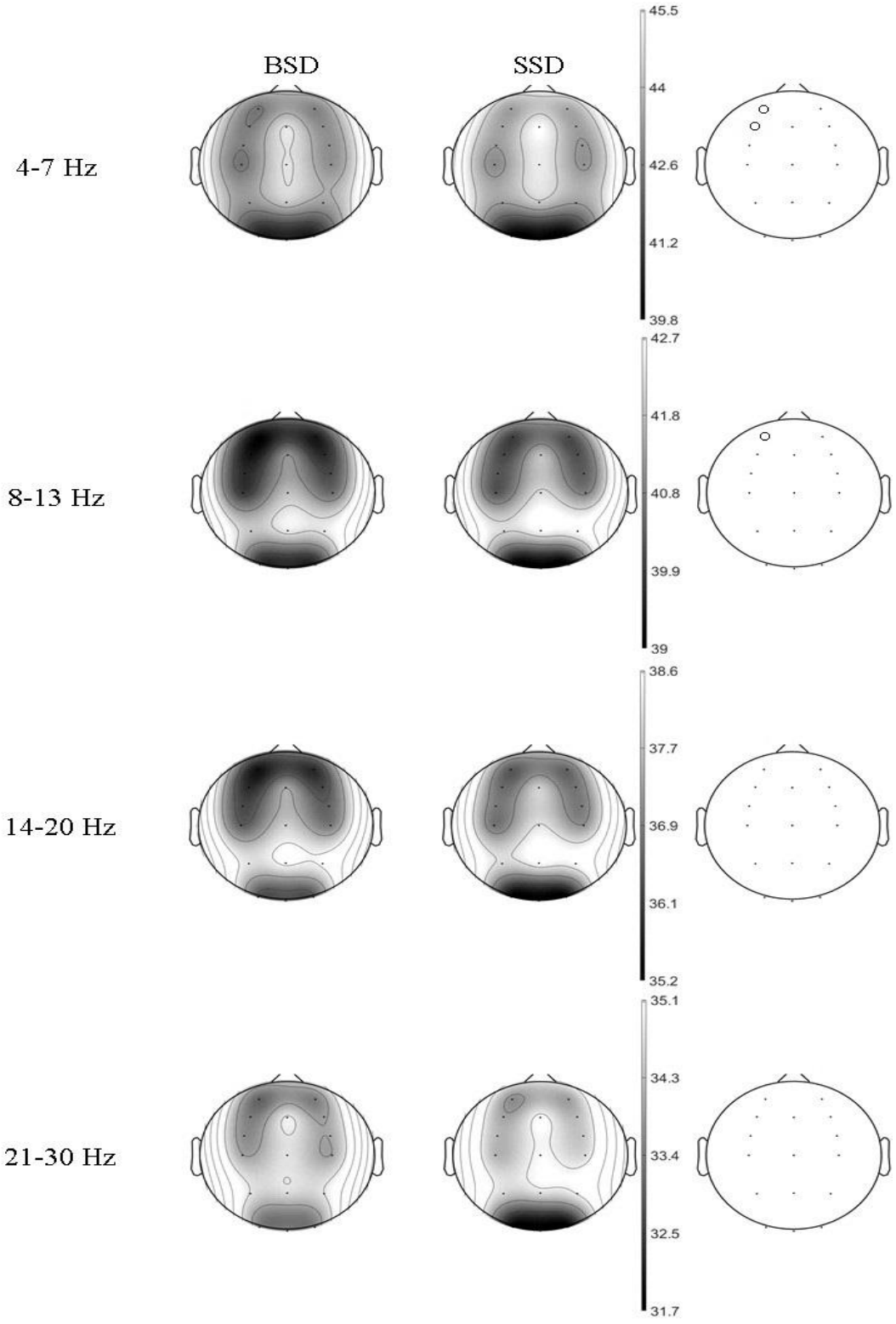

Figure 4.9 Non-parametric permutation test (p<0.05) between BSD and SSD for group ND, in theta, alpha, lower beta, and higher beta frequency bands. FDR correction (p<0.05) was applied for multiple comparison. White dot represents a significant difference before FDR correction and no significant power changes were found after FDR was applied.

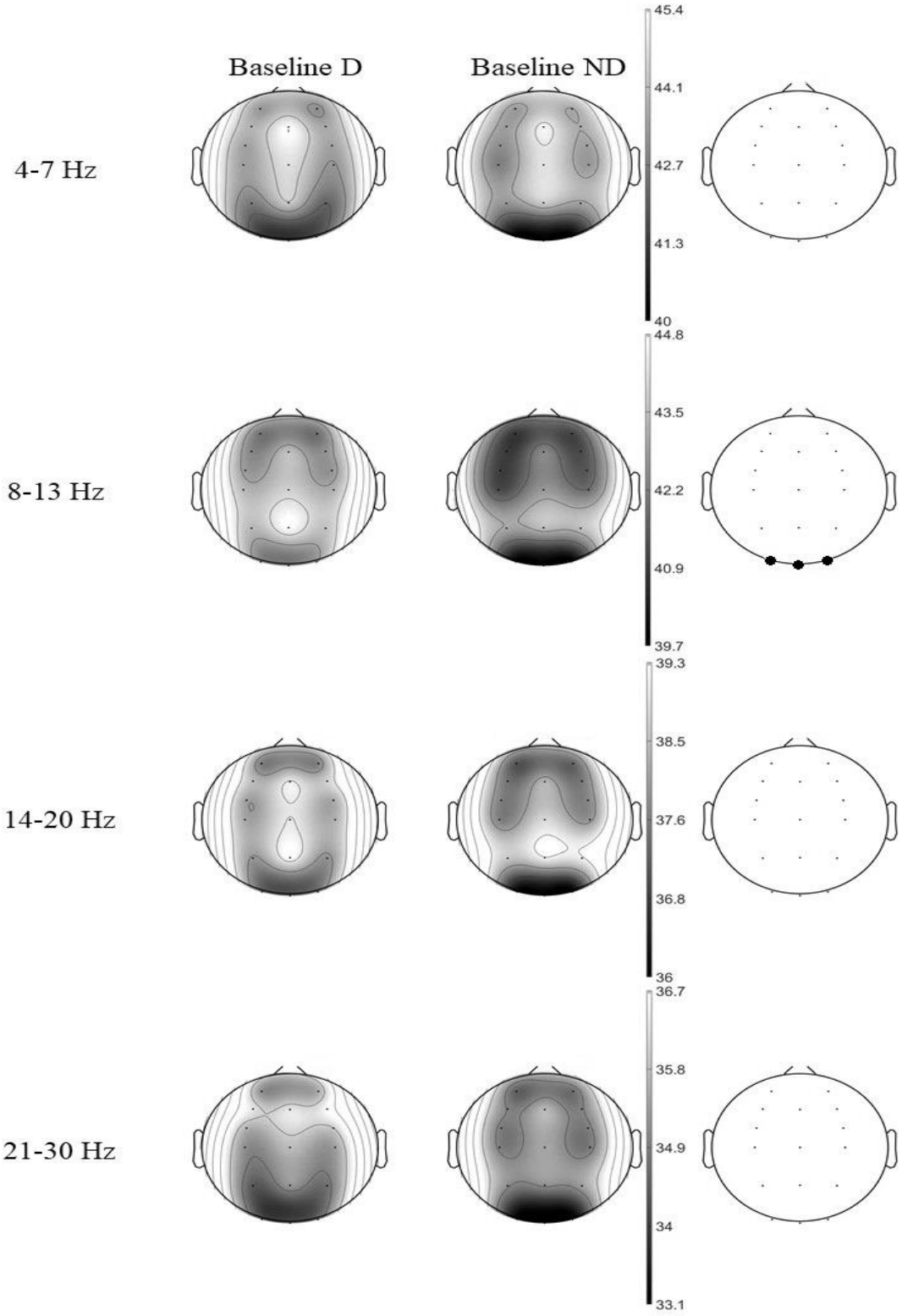

Figure 4.10 Non-parametric permutation test (p<0.05) between groups in the Baseline condition, in theta, alpha, lower beta, and higher beta frequency bands. FDR correction was applied for multiple comparison (FDR was not performed if the significant activation after permutation only occur in one channel). Black dot represents a significant power difference after FDR correction (p<0.05).

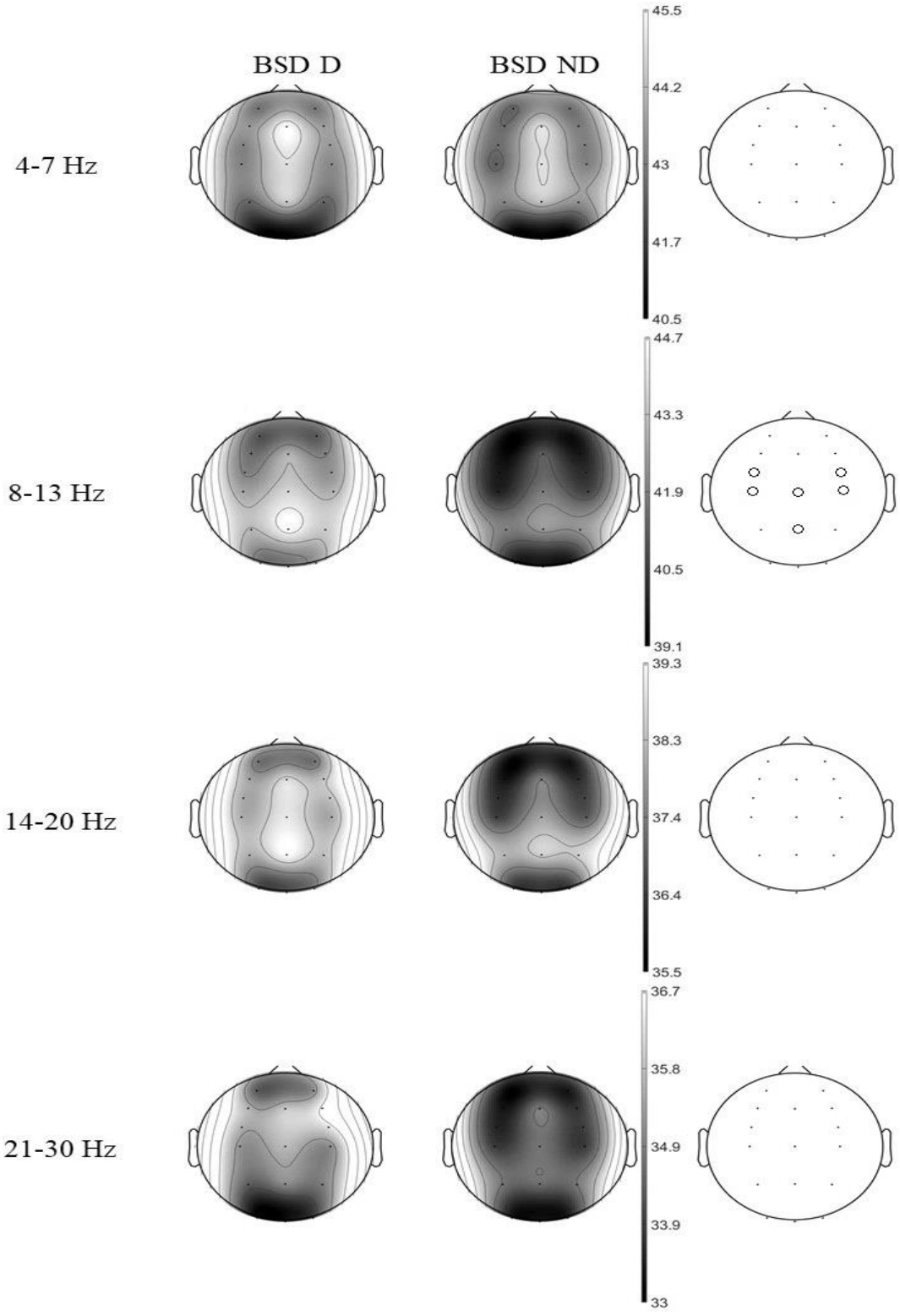

Figure 4.11 Non-parametric permutation test (p<0.05) between groups in the BSD condition, in theta, alpha, lower beta, and higher beta frequency bands. FDR correction was applied for multiple comparison (FDR was not performed if the significant activation after permutation only occur in one channel). White dot represents a significant difference before FDR correction (p<0.05) and no significant power changes were found after FDR was applied.

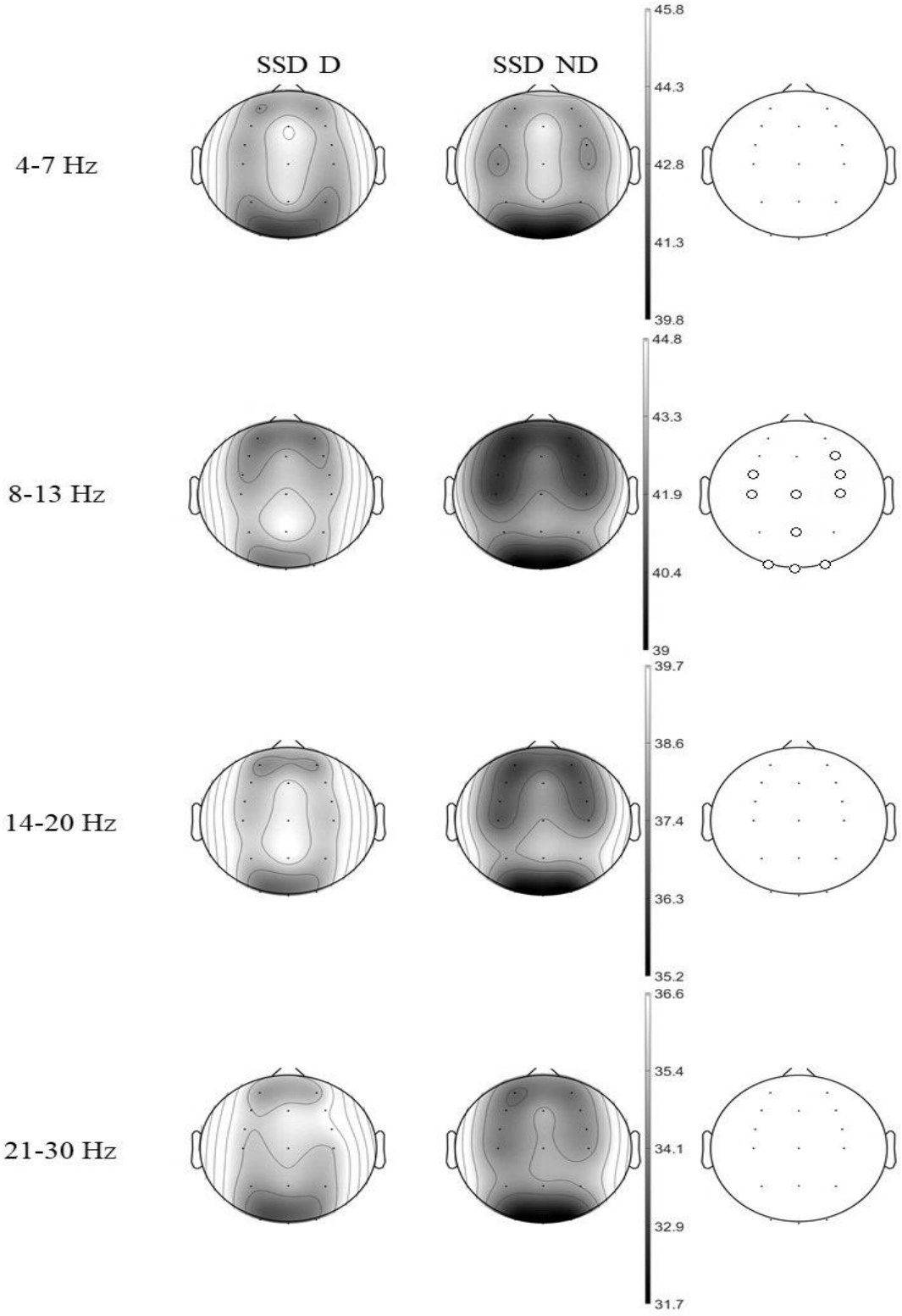

Figure 4.12 Non-parametric permutation test (p<0.05) between groups in the SSD condition, in theta, alpha, lower beta, and higher beta frequency bands. FDR correction was applied for multiple comparison (FDR was not performed if the significant activation after permutation only occur in one channel White dot represents a significant difference before FDR correction (p<0.05) and no significant power changes were found after FDR was applied.

4.3.3 Higuchi Fractal Dimension

To measure the signal complexity during different conditions in all channels, Higuchi's Fractal Dimension (HFD) analysis was performed in both groups. Non-parametric statistical test such as Wilcoxon signed rank test and Kruskal-Wallis H test (both with $p<0.05$) were performed to see if there are any significant changes in EEG signal complexity between conditions at any of the channels.

Figure 4.13 shows the mean ± std of HFD for different conditions (i.e. Baseline, BSD, and SSD) in each group. Group D shows a relatively unchanged trend of average HFD values during the three different conditions, however, the average HFD at F4 is seen higher during BSD compared to the other conditions, and AF4 and FC4 show slightly higher average HFD during gaming compared to Baseline. Meanwhile, the trend of average HFD in group ND shows that HFD during gaming were generally lower compared to Baseline, particularly in the frontal and central areas. However, HFD trend during SSD were lower than Baseline in all channels.

Kruskal-Wallis H test ($p<0.05$) of HFD values found no significant difference of HFD values from Baseline, BSD, and SSD, in each group (Appendix 1.1). Wilcoxon signed rank test found significant HFD decrease from Baseline to SSD in group ND at channel F3, FC3, and C3 (Appendix 1.3), however there were no significant changes found in any channels after Holm-Bonferroni correction ($p<0.05$) was applied. No significant changes were found between Baseline and BSD in both groups at any channels, and between Baseline and SSD at any channels in group D (Appendix 1.2 and 1.3).

Figure 4.14 shows the mean ± std of HFD for both groups in each different condition (i.e. Baseline, BSD, and SSD). The trend of average HFD values during Baseline indicate a very similar trend between the groups, with group D shows slightly higher HFD around the fronto-central channels. In BSD, group D was shown to have higher HFD around the frontal and fronto-central areas, while group ND shows higher HFD around the parieto-occipital area. In SSD, group D shows higher HFD around the frontal and central channels, as well as the occipital channels, and the trend between the two groups were very similar at parietal channels. However, Wilcoxon signed rank test comparing the two groups found no significant differences in HFD at any channel, for the three conditions (Appendix 1.4).

Signal complexity has been linked to alpha/mu activity [107, 110]. Our results in group D- where there was no statistically significant alpha activity found after correction in any channel during gaming compared to Baseline, show that signal complexity also relatively unchanged in both BSD and SSD when compared to Baseline. Group ND showed a significant decrease of alpha power over all cortical areas during BSD compared to Baseline, however there was no significant changes in signal complexity found during the same condition. This result indicates that alpha power decrease in group ND during BSD was not accompanied by any changes in signal complexity, confirming the non-task-specific nature of the decrease. Moreover, we found a very similar level of signal complexity around the parietal areas during Baseline and SSD between the two groups, indicating the effort of group ND to regulate their parietal activity by maintaining their brain activity closer to Baseline state in order to perform better, which is consistent to the unchanged alpha power by group ND during SSD when compared to Baseline.

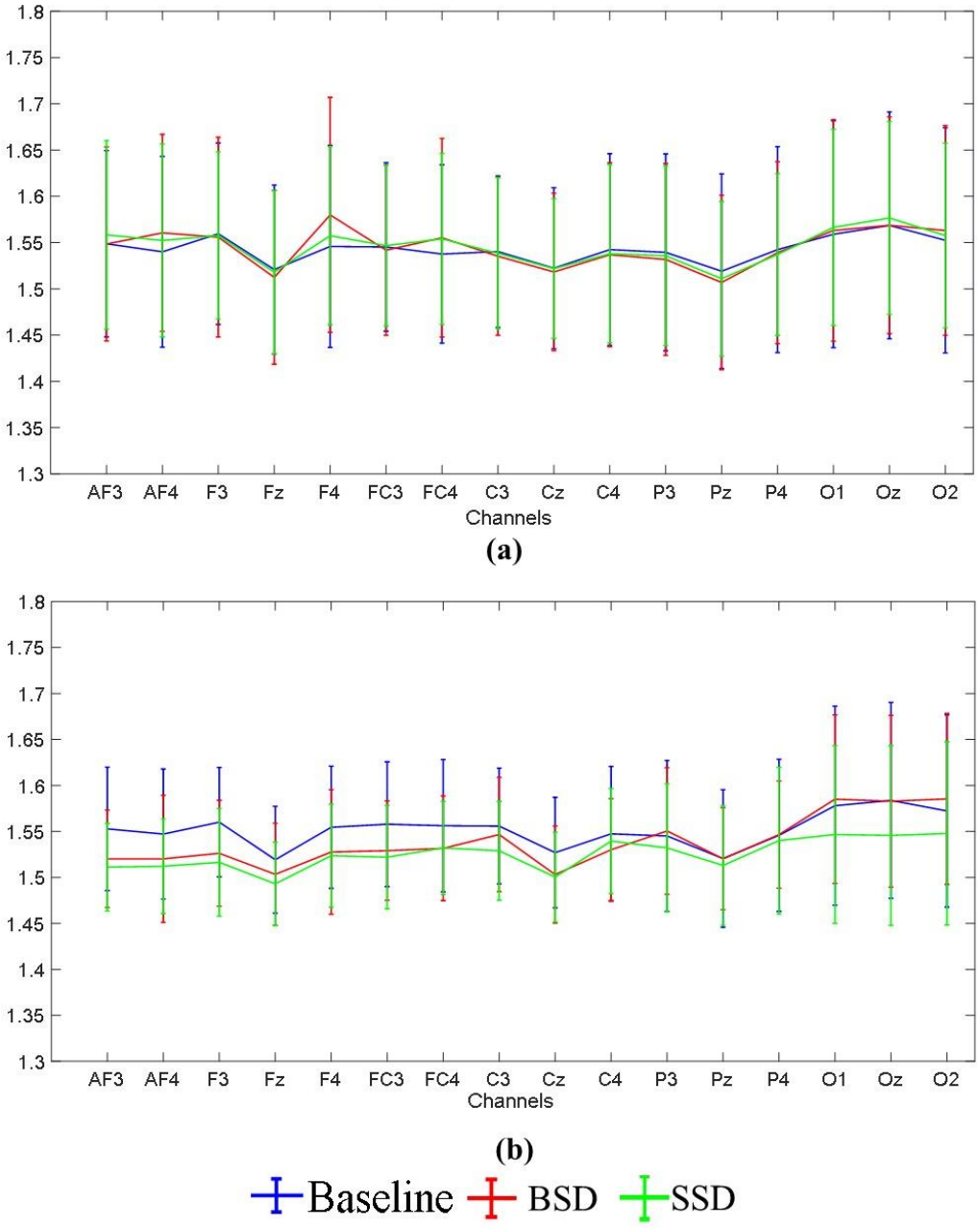

Figure 4.13 Mean ± std of HFD in all channels during Baseline, BSD, and SSD condition for (a) group D (a) and (b) group ND.

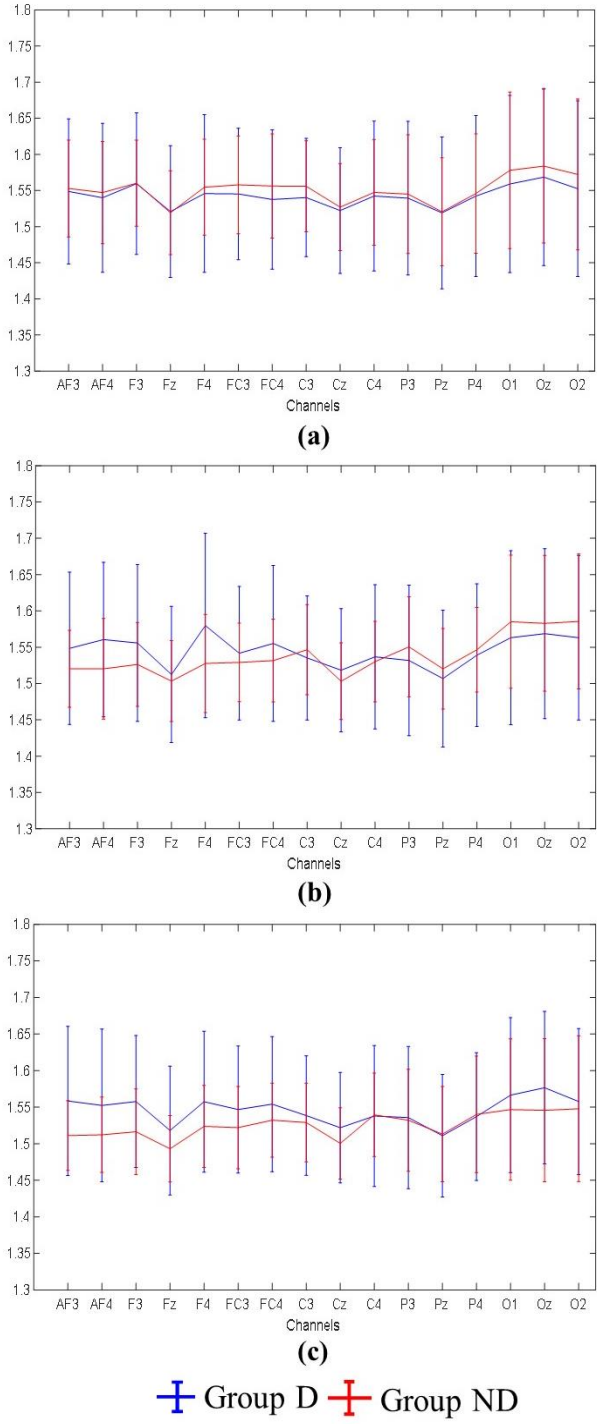

Figure. 4.14 Mean ± std of HFD in all channels of both groups during (a) Baseline, (b) BSD, and (c) SSD.

4.3.4 sLORETA source localisation analysis

Source localisation activity was performed only to group D during the third experimental day. Non-parametric paired t-statistics ($p < 0.05$) which is implemented in the sLORETA software was applied to the source localisation data for each gaming condition against Baseline (BSD against Baseline, and SSD against Baseline), and for BSD against SSD, for each frequency band. There was no statistically significant source activity found in BSD and SSD against Baseline and between BSD and SSD, in any frequency band. The maximum and minimum source activity from each condition and each frequency band was reported in Table 4.7 and 4.8, and in Figure 4.15, 4.16, and 4.17. The areas with the highest count of positive and negative source activity were presented in Table 4.9 and 4.10.

For BSD against Baseline (Fig. 4.15), an increase of source activity was found in the bilateral frontocentral and bilateral parietal areas for theta band, in the right frontal and bilateral parietal areas for alpha band, in the right frontal and right parietal for lower beta band, and in the right frontal area for higher beta band. A decrease of source activity was found around bilateral limbic area for theta band, around the left frontocentral and left temporal areas for alpha band, and around the left frontal-central-parietal areas for both beta bands. The highest source activity was found in the parietal area for theta, alpha, and lower beta bands, and in the frontal area for higher beta band, all in the right hemisphere. While the lowest source activity was found in the limbic lobe for theta and higher beta bands, in the temporal area for alpha band, and in the parietal area for lower beta band, mostly in the left hemisphere (midline area for higher beta band).

For SSD against Baseline (Fig. 4.16), an increase of source activity was found mainly around the right parietal and temporal areas for all frequency bands. While a decrease of source activity was mainly around the left frontal areas as well as the anterior portion of the left temporal area, for all frequency bands. The highest source activity was found in the temporal area for theta and higher beta bands, in the parietal area for alpha band, and in the limbic area for lower beta band, all in the right hemisphere. While the lowest source activity was found in the frontal area for theta, and both beta bands, and in the temporal area for alpha band, all in the left hemisphere.

In both gaming conditions (BSD and SSD), the largest increase of source activity in alpha band, despite not significant, occurred in the parietal cortex, indicating the effort

to modulate alpha from Pz by the players. Both gaming conditions also show a highly lateralised source activation and deactivation. In BSD against Baseline, the brain structures with the highest count of increased source activity was found in the middle frontal gyrus (MFG) for theta and both beta bands, and in the precuneus for alpha band, and the highest count of decreased source activity was found in the superior temporal gyrus (STG) for theta and lower beta bands, in MFG for alpha band, and in precuneus in higher beta band. Meanwhile, in SSD against Baseline, precuneus constantly shows highest count of increased source activity in all frequency bands with the frontal area, i.e. inferior frontal gyrus (IFG) and MFG, show the highest count of decreased source activity. These results revealed the source activation dynamic between precuneus, MFG and STG during successful gaming, as well as the specificity of precuneus activation that only occurred in BSD.

For BSD against SSD (Fig. 4.17), higher source activity was found in the bilateral frontal area in all frequency bands and lower source activity was found in the bilateral temporal area in all frequency bands, suggesting that the different gaming performance might occurred due to the activity of other brain areas, rather than a failing attempt on regulating the parietal activity. The highest count of increased source activity was found in MFG in all frequency bands and the highest count of decreased source activity was found in precuneus for theta and both beta bands, and in the middle temporal gyrus (MTG) in alpha band.

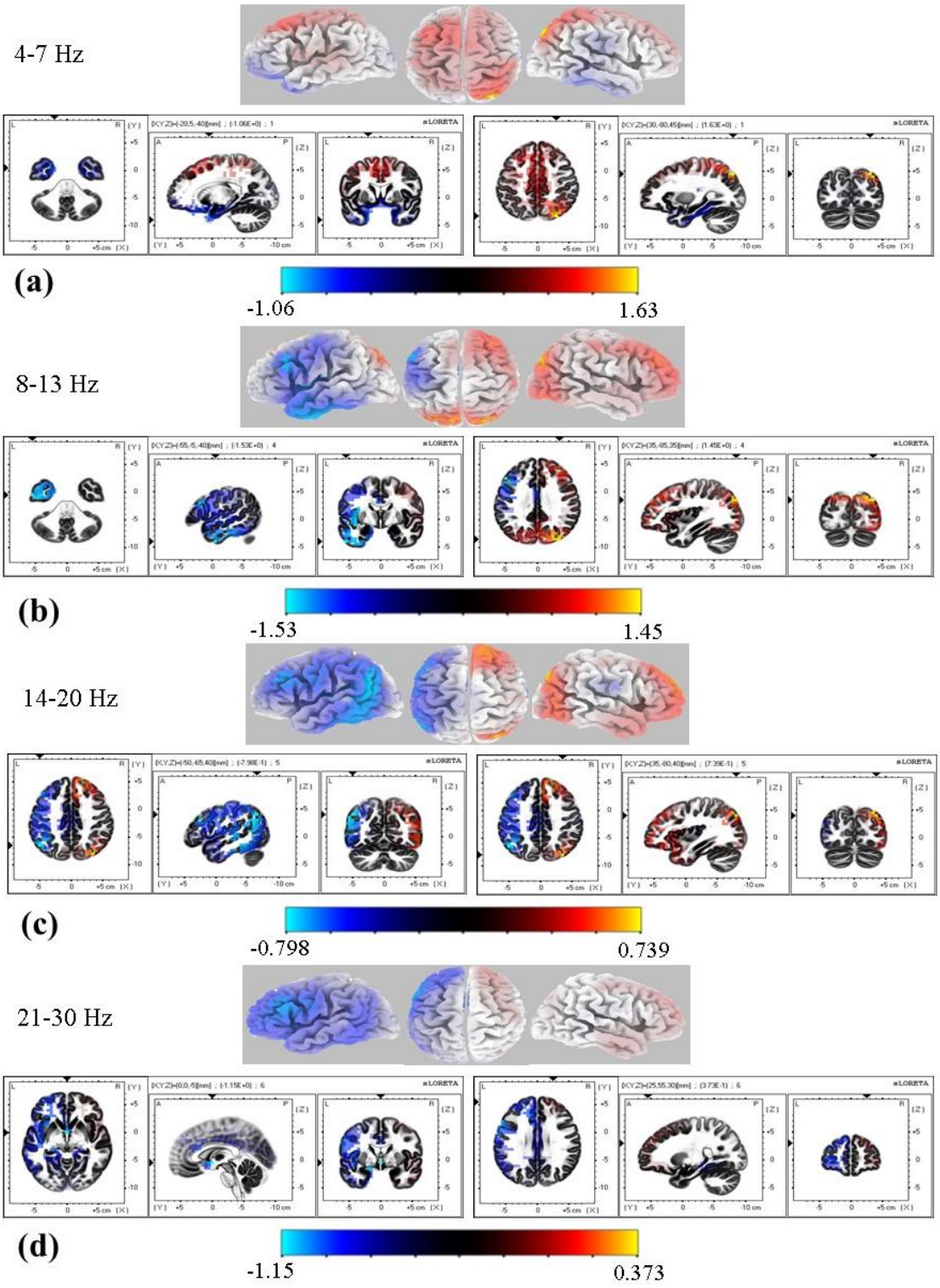

Figure 4.15 Paired t-statistics (p<0.05) of the source localisation via sLORETA between the average BSD and the average Baseline over subjects in group D, in the frequency band of (a) theta, (b) alpha, (c) lower beta, and (d) higher beta. The figures inside the grey box is a 3D representation of the localisation map, and the boxes below it is the 3D slices representing the negative (left side) and the positive (right side) voxel values- blue for negative values and red to yellow for positive values. Voxel's coordinate positioning shown in the 3D slices figures is based on the Montreal Neurological Institute (MNI) coordinate system.

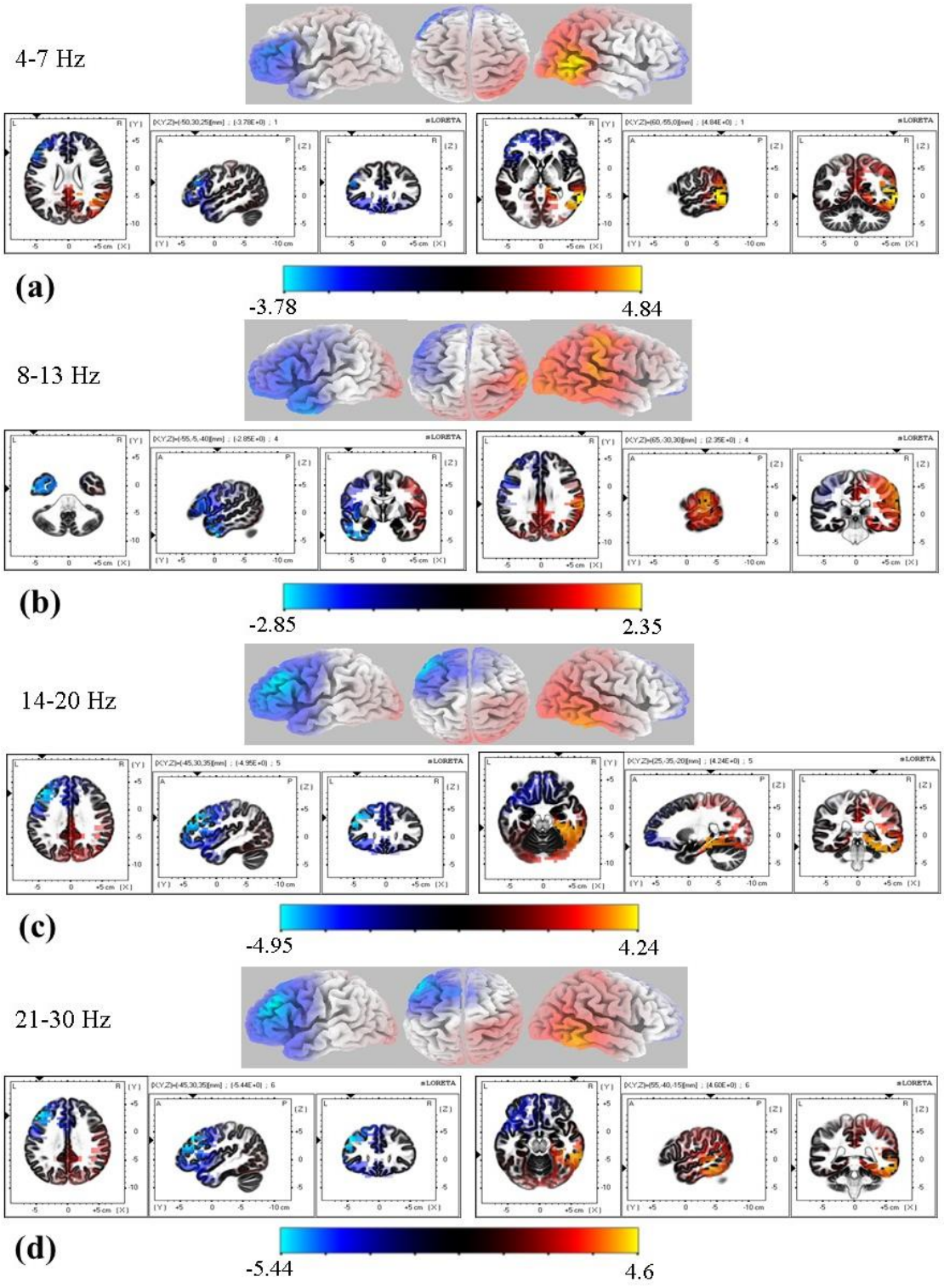

Figure 4.16 Paired t-statistics (p<0.05) of the source localisation via sLORETA between the average SSD and the average Baseline over subjects in group D, in the frequency band of (a) theta, (b) alpha, (c) lower beta, and (d) higher beta. The figures inside the grey box is a 3D representation of the localisation map, and the boxes below it is the 3D slices representing the negative (left side) and the positive (right side) voxel values- blue for negative values and red to yellow for positive values. Voxel's coordinate positioning shown in the 3D slices figures is based on the Montreal Neurological Institute (MNI) coordinate system.

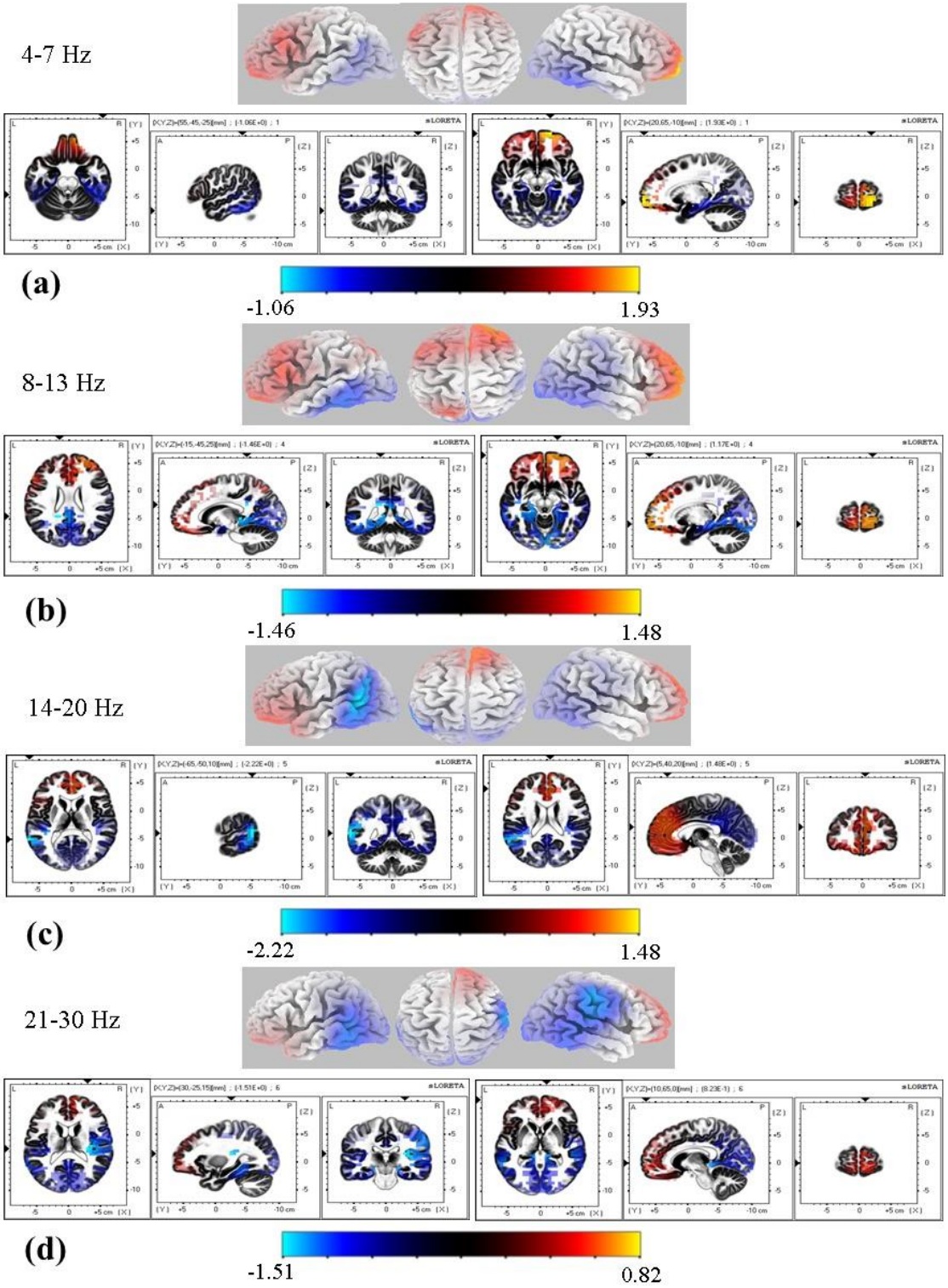

Figure 4.17 Paired t-statistics (p<0.05) of the source localisation via sLORETA between the averaged BSD and the average SSD over subjects in group D, in the frequency band of (a) theta, (b) alpha, (c) lower beta, and (d) higher beta. The figures inside the grey box is a 3D representation of the localisation map, and the boxes below it is the 3D slices representing the negative (left side) and the positive (right side) voxel values- blue for negative values and red to yellow for positive values. Voxel's coordinate positioning shown in the 3D slices figures is based on the Montreal Neurological Institute (MNI) coordinate system.

Table 4.7 The location of the maximum and minimum source activity obtained from paired t-test analysis in sLORETA between gaming condition (BSD/SSD) and Baseline.

Frequency and dynamic			Brain lobe	Hem.	BA	Structure	Max/MinValue	MNI coordinate (x,y,z)
BSD	Theta	Increase	Parietal	R	7	Superior Parietal Lobule	1.63	30,-80,45
		Decrease	Limbic	L	38	Uncus	-1.06	-20,5,-40
	Alpha	Increase	Parietal	R	19	Precuneus	1.45	35,-85,35
		Decrease	Temporal	L	20	Inferior Temporal Gyrus	-1.53	-55,-5,-4
	Lower Beta	Increase	Parietal	R	19	Precuneus	0.739	35,-80,40
		Decrease	Parietal	L	39	Inferior Parietal Lobule	-0.798	-50,-65,40
	Higher Beta	Increase	Frontal	R	10	Superior Frontal Gyrus	0.373	25,55,30
		Decrease	Limbic	Midline	25	Anterior Cingulate	-1.15	0,0,-5
SSD	Theta	Increase	Temporal	R	21	Middle Temporal Gyrus	4.84	60,-55,0
		Decrease	Frontal	L	46	Middle Frontal Gyrus	-3.78	-50,30,25
	Alpha	Increase	Parietal	R	40	Inferior Parietal Lobule	2.35	65,-30,30
		Decrease	Temporal	L	20	Inferior Temporal Gyrus	-2.85	-55,-5,-40
	Lower Beta	Increase	Limbic	R	36	Parahippocampal Gyrus	4.24	25,-35,-20
		Decrease	Frontal	L	9	Middle Frontal Gyrus	-4.95	-45,30,35
	Higher Beta	Increase	Temporal	R	20	Middle Temporal Gyrus	4.6	55,-40,-15
		Decrease	Frontal	L	9	Middle Frontal Gyrus	-5.44	-45,30,35

*Hem. = Hemisphere

Table 4.8 The location of the maximum and minimum source activity obtained from paired t-test analysis in sLORETA between BSD and SSD.

Frequency and dynamic		Brain Lobe	Hem.	BA	Structure	Max/Min value	MNI coordinate (x,y,z)
Theta	Increase	Frontal	R	11	Superior Frontal Gyrus	1.93	29,65,-10
	Decrease	Temporal	R	37	Inferior Temporal Gyrus	-1.06	55,-45,-25
Alpha	Increase	Frontal	R	11	Superior Frontal Gyrus	1.17	20,65,-10
	Decrease	Limbic	L	31	Cingulate Gyrus	-1.46	-15,-45,25
Lower Beta	Increase	Limbic	R	32	Anterior Cingulate	1.48	5,40,20
	Decrease	Temporal	L	22	Superior Temporal Gyrus	-2.22	-65,-50,10
Higher Beta	Increase	Frontal	R	10	Medial Frontal Gyrus	0.82	10,65,0
	Decrease	Sub-lobar	R	13	Insula	-1.51	30,-25,15

*Hem. = Hemisphere

Table 4.9 The brain structures with the highest counts of source activity, found after paired t-test analysis in sLORETA between gaming condition (BSD/SSD) and Baseline.

Task	Frequency	Activity	Brain Structure	No. of voxels
BSD	Theta	Increase	Middle Frontal Gyrus	375
		Decrease	Superior Temporal Gyrus	274
	Alpha	Increase	Precuneus	359
		Decrease	Middle Frontal Gyrus	235
	Lower beta	Increase	Middle Frontal Gyrus	241
		Decrease	Superior Temporal Gyrus	253
	Higher beta	Increase	Middle Frontal Gyrus	240
		Decrease	Precuneus	329
SSD	Theta	Increase	Precuneus	364
		Decrease	Inferior Frontal Gyrus	360
	Alpha	Increase	Precuneus	364
		Decrease	Middle Frontal Gyrus	293
	Lower beta	Increase	Precuneus	364
		Decrease	Middle Frontal Gyrus	399
	Higher beta	Increase	Precuneus	364
		Decrease	Middle Frontal Gyrus	373

Table 4.10 The brain structures with the highest counts of source activity, found after paired t-test analysis in sLORETA between BSD and SSD.

Task	Frequency	Activity	Brain Structure	No. of voxels
BSD vs SSD	Theta	Increase	Middle Frontal Gyrus	481
		Decrease	Precuneus	353
	Alpha	Increase	Middle Frontal Gyrus	472
		Decrease	Middle Temporal Gyrus	310
	Lower beta	Increase	Middle Frontal Gyrus	393
		Decrease	Precuneus	364
	Higher beta	Increase	Middle Frontal Gyrus	358
		Decrease	Precuneus	364

4.3.5 NASA-TLX questionnaire

The perceived experimental workload was measured by performing non-parametric statistical analysis to the post-experiment NASA-TLX questionnaire scores, shown in Figure 4.18 and 4.19, and Table 4.11. No significant difference was found from Friedman's test ($p<0.05$) across the three sessions in each category for each group. No significant difference was found from Wilcoxon signed rank test ($p<0.05$) to compare the scores between groups in each category. Lastly, no significant difference was found from Kruskal-Wallis H test ($p<0.05$) of the overall scores across the three sessions for each group.

The lack of significant difference in our data may suggest that both groups perceived the workload of the experiment in a relatively similar way from time to time regardless their gaming outcome. However, three categories (i.e., mental, effort, and performance) are shown to have generally higher scores compare to the rest categories, with the higher scores achieved in 'effort' , followed by 'mental' and 'performance' in group D, whereas in group ND higher scores were achieved in 'effort', followed by relatively similar scores of 'mental' and 'performance' categories. These results, despite being not statistically significant, might reflect that both groups perceived a higher effort during gaming. Moreover, the highest scores in 'effort' of both groups were achieved in the first session, suggesting that both players were still not familiar with the gaming task.

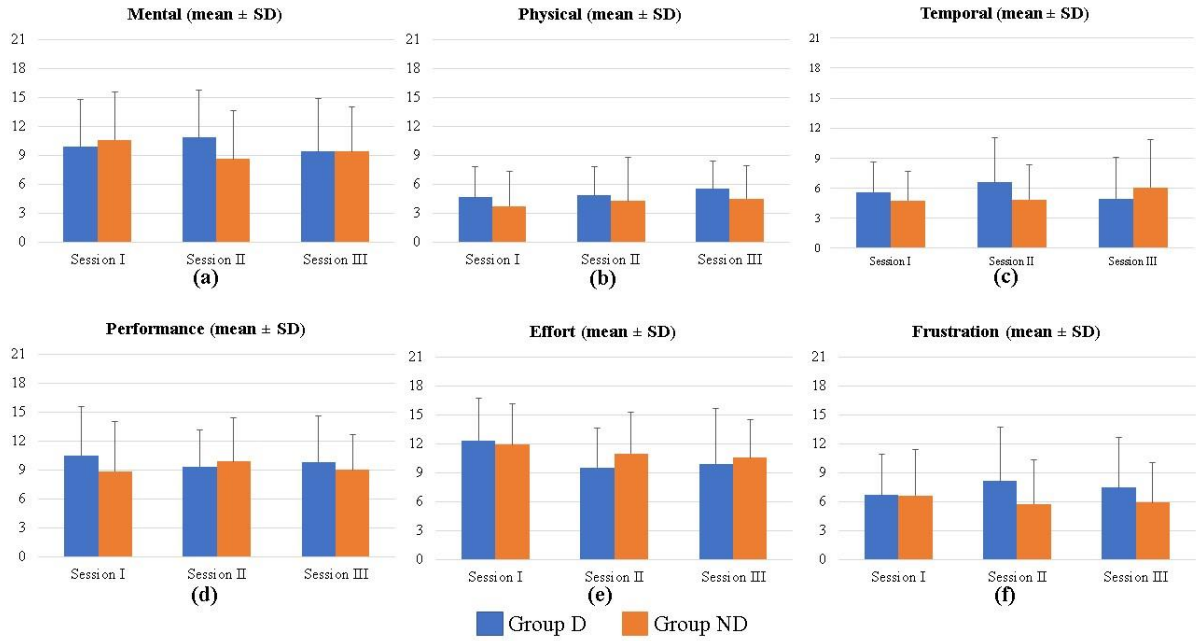

Figure 4.18 The mean ± std of NASA-TLX scores in each category, such as (a) mental, (b) physical, (c) temporal, (d) performance, (e) effort, and (f) frustration, for both groups of players in three different sessions.

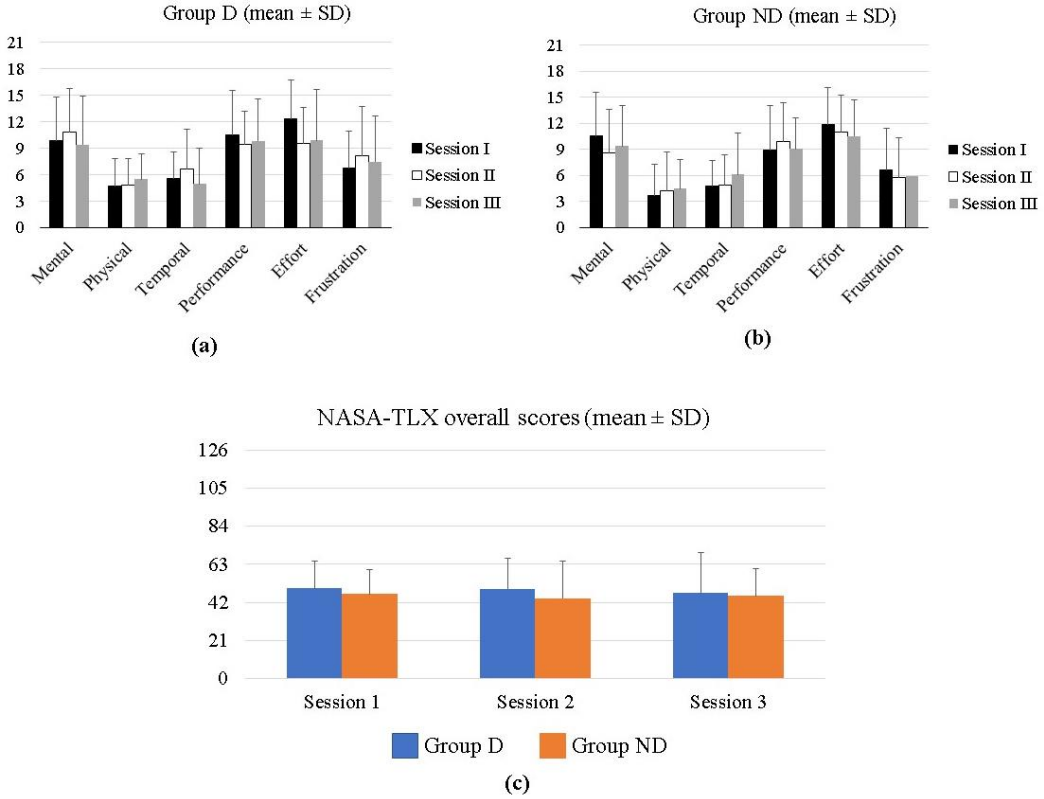

Figure 4.19 The mean ± std of (a-b) NASA-TLX scores in each group, for each category in three sessions, and (c) the overall scores (summed up of the scores in all category) for each group in three sessions.

Table 4.11 Table of statistical results of NASA-TLX scores for each category and for the overall score.

Statistical test	Category	Group	*p*-values	Chi-square
Friedman Test	Mental	D	0.509	1.351
		ND	0.201	3.211
	Physical	D	0.499	1.389
		ND	0.317	2.296
	Temporal	D	0.439	1.647
		ND	0.315	2.313
	Performance	D	0.332	2.205
		ND	0.479	1.474
	Effort	D	0.275	2.579
		ND	0.423	1.722
	Frustration	D	0.717	0.667
		ND	0.697	0.722
	Category	**Session**	***p*-values**	**Z-scores**
Wilcoxon signed rank test	Mental	I	0.813	-0.237
		II	0.262	-1.122
		III	0.959	-0.051
	Physical	I	0.313	-1.009
		II	0.261	-1.123
		III	0.357	-0.921
	Temporal	I	0.514	-0.653
		II	0.262	-1.122
		III	0.683	-0.408
	Performance	I	0.506	-0.665
		II	0.726	-0.350
		III	0.610	-0.510
	Effort	I	0.759	-0.306
		II	0.261	-1.124
		III	0.953	-0.059
	Frustration	I	0.919	-0.102
		II	0.176	-1.355
		III	0.415	-0.816
	Category	**Group**	***p*-values**	**H-statistic**
Kruskal-Wallis H test	Overall score across sessions	D	0.774	0.512
		ND	0.934	0.137

4.4 Discussion

Multi-user BCI competitive gaming has been previously studied [66, 159], however, the information regarding the EEG signatures changes within the interacting brain are still relatively limited. In this study, we analysed the EEG signatures in order to explore the impact of competitive multi-user BCI gaming on brain cortical activity. Three different conditions were measured such as pre-gaming Baseline, BSD and SSD, with the players divided into group D and group ND. The results from each offline analysis (i.e. power spectral analysis, signal complexity analysis, and source localisation analysis) were compared based on the types of task (i.e. Baseline-BSD ,Baseline-SSD, and BSD-SSD) and based on the groups (i.e. between group D and group ND). Power spectral density analysis found that alpha activity at Pz behaved differently in group D and group ND. The consequence of a successful game control was characterised by the similar level of Pz alpha activity to the level during Baseline. Source localisation analysis found the highest source activity as well as the highest number of increased source activations in alpha band at the precuneus, which is located close to channel Pz. Resting EEG comparison between group revealed a different posterior alpha activity between the group, suggesting the use of resting alpha activity as a predictor for the game performance.

RA, scoring performance, and individual alpha peak frequency

Statistically significant increases of RA at Pz and the game scores were found in both groups, and to some extent, these results might reflect the effort to learn by both groups to upregulate their RA to control the game. The averaged game scores, however, shows an increasing trend for group D and a decreasing trend for group ND, though there were no statistical significance found across sessions and between groups. The increasing scores over sessions might indicate a successful learning process done by the players in group D. We did not perform any measurement to assess the post-training outcome to validate whether the players manage to retain the learned skills, as proposed by Gruzelier [34] as one of the methods to validate a successful neurofeedback training. However, the training paradigm used in this study did not apply a typical single-user neurofeedback paradigm, where the user was asked to maintain their brain activity based on their own feedback. In this study, the users were asked to maintain their RA level at Pz while

engaging in a competitive interaction- and for them to train not only based on their own performance, but also in relative their opponent's performance/feedback which is changing over time. Therefore, there are more factors to be considered in learning measurement and training design (e.g. member of the pair, level of Baseline RA of the players in a pair, level of motivation, etc.).

Despite of not having a consistent increase over sessions, RA level of group D in the later sessions was better than the first one, while in group ND the increase of RA stopped after the second session. Psychological factors that can be associated with these conditions namely the lack of motivation and reduced confidence level, as most of the group ND players experienced losing more often than winning. Motivation and confidence level have been suggested in promoting the success of neurofeedback training [37, 40]. Additionally, physical factors e.g. the multi-channel EEG used in the third experiment, might also influence the overall performance of both groups, i.e. there is no significant increase of RA was found in group D from Session II to Session III. Higher number of channels requires longer pre-experimental preparation time as well as physically heavier for the players' head as they were used to the single-channel setup in the previous sessions, thus may increase the chance of fatigue or distraction.

Our results also revealed that the players who received NC in a pair, i.e. the individual with higher Baseline RA, is not always the same person in every session. This is caused by the variability of natural alpha power that differs from one person to another, even can varied in one person from time to time, suggesting that it is important to perform a daily adjustment of individual RA threshold. Our individual alpha peak frequency analysis further confirmed the inter-individual alpha power as well as the intra-individual alpha power showing that alpha peak can be varied for one person in different days [157, 158, 160, 161].

Scoring performance also shows that despite receiving normalisation due to higher Baseline RA, which was consequently lowering their gaming RA, the majority of players with higher Baseline RA still managed to outperform their opponents. Players with lower average gaming RA after normalisation, might still produce higher average score. This condition might be related to the timing aspect of the game. Timing is an essential factor in scoring, as one can only score if they managed to increase their bar at least 10% higher than their opponent's for at least 1 s. Thus, in our case, the losing players simply did not

manage to sustain higher relative alpha power long enough to score more often, though on average their RA during gaming might be higher. In addition, our scoring results show that not all players with higher Baseline RA (the one receiving NC) always end up as the winner of the game or guaranteed to have higher gaming RA. In some cases, one player can be a winner in one session and be a loser in the next one, regardless which player receiving NC. These conditions suggest that our approach of normalising feedback for players with high Baseline RA does not guarantee a balanced level of competitive performance in every pair of participants, however it surely reduces the chance of bias in scoring, indicating that the scoring performance was obtained due to the mental effort of the players rather than based on their natural alpha power.

Spatial distribution of power spectral density

Our results revealed that there were no significant alpha power changes found at channel Pz or nearby channel in group D during both BSD and SSD, when compared to Baseline. This indicates that the group dominated the game by upregulating their alpha at Pz to the similar level to Baseline. Alpha activity has been known to be higher during resting state (Baseline), especially during eyes-closed, and supressed by eyes-opening as well as by higher cognitive processing [160]. Group D, managed to increase their alpha power at Pz during gaming as instructed, however the increase did not exceed the level of alpha power during Baseline, as commonly expected in a traditional alpha operant conditioning training/neurofeedback. This condition might be due to the fact that the alpha neurofeedback approach used in the experiment required the players to control their RA based on their own and their opponent's performance, rather than just based on their own performance like in the traditional alpha neurofeedback.

In group ND, alpha power was significantly decreased in all channels during BSD, which indicate a non-task-specific power decrease, which potentially caused their poor gaming performance. Significant decrease of lower beta power was also found over the left and midline frontal area and bilateral frontocentral area, during BSD. Decreasing beta power in the left inferior prefrontal cortex has been related to memory encoding process [162]. During the SSD condition, there were no significant power changes found in all channels compared to Baseline, indicating their effort to apply the same strategy applied by the dominant players: maintaining alpha power at Pz to the similar level during

Baseline. However, this improved performance during SSD was not strong enough to outperform group D.

The spatial power distribution comparison between groups show that significant statistical difference occurs in the occipital alpha band during Baseline, with higher alpha power in group D than in group ND. This result supports the idea of using resting alpha power level as a training predictor for alpha neurofeedback proposed by Wan et al. [42].

Signal complexity analysis via Higuchi Fractal Dimension

The signal complexity analysis did not find any statistically significant differences in different conditions and between groups after Holm-Bonferroni correction. However, prior to correction, significant decreases of HFD from Baseline to SSD were found at channel F3, FC3 and C3 (left frontal-central area). The average HFD at parietal channels of the two groups show almost identical values only during SSD, despite there is no statistical significance found for group comparison of HFD at Pz in any condition. This close similarity around the parietal area may reflect the closer parietal brain activation of the two groups, causing the smallest scoring difference between players. Moreover, the uncorrected statistically significant changes in group ND during SSD reflect that the maintenance of power similar to Baseline during SSD promoting changes in signal complexity. This idea suggests that the 'similar to Baseline' response was actually a more task-specific response, especially compared to the global decrease of alpha power occurred during BSD in group ND. Previous studies have proven the inverse relationship between alpha/mu activity signal complexity [107, 109, 110]. The antagonistic interaction of signal complexity with the brain resting network have also been proposed, since lower signal complexity has been reported during resting condition and higher during mentally demanding tasks [163, 164]. However, statistical significance is required to further validate the relationship between alpha activity and signal complexity level.

sLORETA source localisation analysis

Source localisation analysis did not find any statistical significance between gaming and Baseline, in any frequency bands, which is consistent to the spatial power distribution results. Despite being not statistically significant, our sLORETA results displayed the lateralization tendency in source activation and deactivation patterns. Our results show

that the increasing activity mostly occurred in throughout the right hemisphere and the decreasing activity mostly occurred in the right hemisphere. The increasing activity found in the right frontal area might be related to the reactivity of the right frontal cortex (e.g. rSFG and rIFG) in response to the competitive interaction, as suggested in the literature [78, 79]. The rIFG activity has also been linked to response inhibition as well as to attention-demanding tasks [165-167]. The increasing activity found in the right hemisphere around the temporal and parietal areas might indicate the activation of the right temporo-parietal junction, an area that has been linked to attention, specifically when social interaction is present [168]. Meanwhile, the activation of left frontal cortex has been linked to self-relevance process [169]. Therefore, the decreasing source activity in the left hemisphere might indicate the lack of internal-processing tasks (non-self-referential taught).

Our results also found the highest count of increased source activity in the precuneus (parietal lobe) in alpha band, particularly during BSD (while SSD showed non-frequency-specific precuneus activity), followed the high count of increased source activity in MFG for other frequency bands. Precuneus activity has been linked to visuo-spatial imagery, episodic memory retrieval, and self-referential processing [170]. Additionally, Utevsky et al. [171] reported when the connectivity between precuneus and the frontoparietal control network was found increasing during a task performance, where the connectivity between precuneus and the DMN was found increasing during rest, suggesting the role of precuneus in control-resting network switching.

NASA-TLX questionnaire

The NASA-TLX workload questionnaire revealed that there is no significant difference of the perceived workload between the groups of players and across experimental sessions in any categories. Our results suggest that the level of dominance between players in the game does not necessarily change the way the players perceive the task load given to them during the experiment. Despite being non statistically significant, the highest scores were achieved in ‘effort’ category during the initial session and decreasing over time for both groups, implying that during the initial session, both groups perceived the game’s difficulty higher due to the lack of familiarity. Moreover, the results show that effort, mental, and performance are the categories with higher scores in both groups, indicating that, the players mainly are more concern to the factors that they can internally control,

i.e. how demanding the task is, how they perceive the task mentally, and how they predict their performance, rather than to the situational and physical categories such as temporal and physical. Frustration category however, remained low, despite being able to be controlled internally by the players.

Notable findings

Our study has incorporated a competitive interaction in an alpha operant-conditioning training paradigm. The efficacy of this paradigm for individual control of alpha power, similar to the classical alpha neurofeedback [172], still requires further validation. Nonetheless, this study has revealed the electrophysiological signatures during a competitive interaction between two groups, while they were regulating parietal alpha activity at the same time. This study focused on the electrophysiological response of a single-brain during a two-person interaction. In order to investigate how these activated brain areas influencing one another and how different brain areas in different individuals interacting with each other during competition, we performed intra-brain and inter-brain connectivity analysis to the data obtained by the experiment of this study, which will be presented and discussed further in the upcoming chapter.

Limitations

The limitations of this study including the different number of channels used by the two groups during the third experimental day. A larger and balance number of channels (for both players) will provide the opportunity to gain better results, especially in spatial power spectral and source localisation analyses. More training sessions are needed in the future to produce more information related to the learning process when competitive interaction is present. Larger number of participants are also required to produce better statistical analysis, therefore better and more precise validation over the statistically significant results can be made. In order to further study the efficacy of the competitive BCI training, control group, post-training baseline analysis and post-training assessment should be performed in the future.

4.5 Conclusion

This study introduced a multi-user competitive BCI game that is based on alpha band operant conditioning. Our results show that group D consistently outperformed group ND in all experimental sessions, even when they received normalisation which consequently decreasing their average gaming RA. Spatial spectral distribution analysis revealed that the strategy applied by both groups in order to perform better, involving the maintenance of brain activity closer to the baseline state. This study also found that the level of alpha power during Baseline was higher in group D than in group ND, supporting the idea to use baseline alpha power as a predictor of gaming performance. Signal complexity analysis did not show any statistically significant changes, however the highly similar level of signal complexity around the parietal area was found in both groups during SSD, which is consistent to gaming condition- the condition with the smallest scores difference. Source localisation analysis in group D found that, despite being statistically not significant, the highest increase of source activity and the highest count of increased source activity in alpha band were found in the precuneus in both gaming conditions, indicating the upregulation of alpha power by the target channel (Pz). Lastly, NASA-TLX workload post-experimental questionnaire revealed that all players perceived the gaming task in a similar way for each category across sessions, despite having a very different gaming outcome.

Chapter V

Competitive Multi-user BCI:
Part II- Connectivity

5.1 Introduction

The extensive information regarding the cortical dynamics that occur during a specific cognitive task can be achieved by estimating the brain's network connectivity. Connectivity analysis quantifies the inter-relations between EEG channels that are located within the same brain/single person (intra-brain) and that are located in different brains/multi personal (inter-brain). In this chapter, the results of the connectivity analysis of the EEG data that were obtained from the multi-user BCI competitive experiment performed in Chapter IV are presented.

Competition consequently elicit the different social perception responses in the brain of the winning and losing participant. The responses related to reward, motivation, arousal, attention, and dominance [173, 174] might be experienced by the winner, whereas the response related to lower social rank, social exclusion, and error awareness [81, 149, 175] might be experienced by the loser.

Functional connectivity studies in social reciprocity revealed that, the connectivity between the right central executive network (CEN) and the salience network (SN) during resting state may predict social performance [176]. CEN is a brain network that is engaged during cognitive tasks, which comprises of the dorsolateral prefrontal cortex (dlPFC) and the posterior parietal cortex [9, 16], whereas SN is a brain network that responses to salient events and comprises of the ventrolateral prefrontal cortex (vlPFC), anterior insula, and anterior cingulate cortex (ACC) [8]. Rewards processing has also been reported as an important part of competitive dynamic [144-146]. Past studies have shown the functional connectivity between the striatal network consisted of the orbitofrontal cortex, insula, amygdala, and hippocampus, during reward processing [177, 178], and the dorsal striatum has also been shown active in regulating motivation [178]. Moreover, competition has also been associated with the activation of the mentalizing network, consisted of the medial prefrontal cortex (mPFC), precuneus, and temporoparietal junction (TPJ) [149, 150]. It was revealed that social exclusion increases the functional connectivity of the mentalizing network, compared to social inclusion [149].

Additionally, Astolfi et al. [84] during their hyperscanning study in Prisoner's Dilemma game revealed lower count of significant inter-brain connections when the players were performing defective (competitive) interaction, compared to cooperative interaction. The lower inter-connectivity found during defective behaviour might indicate a selfish behaviour by the betrayers [84, 85]. Apart from the reduction of connection density/count, reduction of inter-brain connectivity strength was also reported during multi-player competitive selective attention task [86].

In this chapter, connectivity analysis was performed to the data obtained from the competitive multi-user BCI gaming that is based on the alpha band, non-verbalised operant conditioning in Chapter IV. Connectivity analysis will be divided into two approaches, such as the intra-brain connectivity, performed by multivariate GC and DTF and the inter-brain connectivity, performed by bivariate GC.

5.2 Methods

5.2.1 Connectivity Analysis

GC and DTF were used for connectivity estimation, where GC provides multivariate connectivity analysis in time domain and DTF multivariate connectivity analysis in frequency domain. Due to the limited computational speed, 2 minutes out of each 5

minutes time-series data (BSD and SSD data from the third experimental session) were extracted for further connectivity analyses. In each pair, these 2 minutes data were extracted within the identical time points for both players, based on the 2 minutes where the RA values of both players have the biggest difference in both gaming conditions. The 2 minutes were segmented into 6 s epoch with 50% overlap. Independent Component Analysis (ICA) algorithm [103, 104] implemented in EEGLAB (version 14.1.2b) was performed for further noise removal (e.g. eye blinking, muscle movement, or other biological signal). The pre-processed 2 minutes data were later analysed by using GC and DTF connectivity analyses, which have been described in Chapter III.

5.2.2 Statistical Analysis

A non-parametric paired permutation statistical test ($p<0.01$) was performed in MATLAB with 10000 repetition of all the estimated connectivity data. The method was used for the analyses of GC and DTF in order to compare the brain connectivity between the gaming conditions (Baseline and BSD; Baseline and SSD; BSD and SSD) and between groups (D and ND) for the three conditions (Baseline, BSD, and SSD). Statistically significant connections ($p<0.01$) found in each comparison were later projected into a connectivity matrix. False Discovery Rate correction method [152] was applied for multiple comparisons.

A non-parametric single-sample permutation statistical test ($p<0.001$) was performed in MATLAB with 10000 repetition, with FDR correction applied, to all the estimated inter-brain connectivity data. The method was used to find the significant connections found in inter-brain GC during BSD and SSD, in different directions between players.

5.3 Results

5.3.1 Intra-brain Granger Causality

Intra-brain GC results are presented in three ways: as matrices presenting the grand average of GC values of all epochs from all players in each group (Fig. 5.2 and 5.3 (a-c)), as connectivity maps displaying only the average values above the 75^{th} percentile of its corresponding matrix for an easy visual representation of spatial connectivity localisation (Fig. 5.2 and 5.3 (d-f)), as a set of *p*-value matrices (Fig. 5.2, 5.3 (g-h), 5.5 (a-b), and 5.6),

and as bar graphs displaying the average GC values in each zone- following the zonation in Figure 5.1 (Fig. 5.4 and 5.5 (c-d)).

The statistical comparisons from the GC data were performed as the following: between Baseline and BSD/SSD, between BSD and SSD, and between groups. Based on these presentations, the results will be explained in the following structure:

(i) the significant connection changes found in the connections involving Pz.

(ii) the pattern shaped by the most prominent connections shown by the connectivity maps (does not apply in the comparisons between BSD and SSD, and between groups).

(iii) the network with a high count of significantly increase/decrease connections in found in the *p*-values matrices. The networks in the *p*-values matrices will be described based on the zonation shown in Figure 5.1.

(iv) the significant average GC changes in each zone (does not apply in the comparison between group D and group ND) as the results of a non-parametric paired permutation.

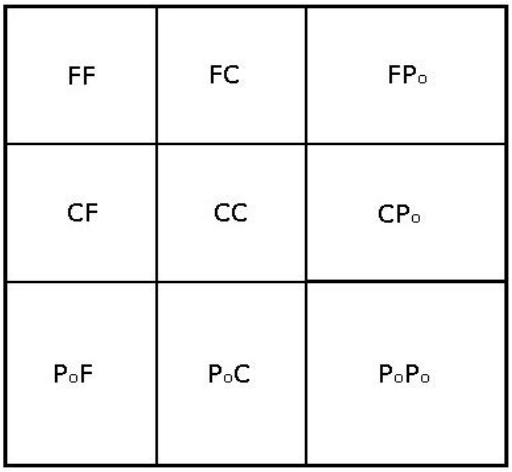

Figure 5.1 The networks zonation: FF (frontal-frontal), CC (central-central), PoPo (parieto-occipital – parieto-occipital), FC (frontal-central), FPo (frontal-parieto-ocipital), CF (central-frontal), CPo (central-parieto-occipital), PoF (parieto-occipital – frontal), and PoC (parieto-occipital – central). The first letter of the abbreviation indicates the source of the network, and the second letter indicates the sink.

Intra-brain GC of group D

(i) *Baseline vs BSD*: in BSD, for Pz as a source, increased connections were flowing to all frontal, central, and parietal channels. For Pz as a sink, increased connections were coming from F4 and P3, and the decreased connections from C3 and Cz.

Baseline vs SSD: in SSD, for Pz as a source, increased connections were flowing to almost all frontal, central, and parietal channels, except Cz. For Pz as a sink, increased connections were coming from P3 and Oz, and the decreased connections from C3 and Cz.

(ii) The most prominent connections during baseline are distributed around all areas with Cz sending information to all region. In BSD, the prominent connections are formed by a higher count of bidirectional GC mainly clustered around the right hemisphere of fronto-central and centro-parietal areas, as well as around bilateral occipital area. In SSD, the prominent connections were also found clustered around the right hemisphere, particularly around the right fronto-central area compared to Baseline and BSD. The causality around the left fronto-central area during SSD was found below the 75^{th} percentile, thus displaying a lack of connections cluster.

(iii) *Baseline vs BSD*: PoPo was found as the network with the highest count of significantly active connections in BSD, while CPo shows higher count of significantly active connections in Baseline.

Baseline vs SSD: PoPo was found as the network with the highest count of significantly active connections in SSD, followed by PoF, while CPo shows higher count of significantly active connections in Baseline.

(iv) *Baseline vs BSD*: significant decreases of average GC during BSD were found in CC and CPo, and significant increases during BSD were found in all zones coming from Po.

Baseline vs SSD: A significant decrease of average GC during SSD was found in CPo and significant increases during SSD were found in FF, FC, and in all zones coming from Po.

Intra-brain GC of group ND

(i) *Baseline vs BSD*: in BSD, for Pz as a source, decreased connections were flowing to F4, Cz, C4, and P4. For Pz as a sink, an increased connection was coming from F4, and decreased connections were coming from F3, Fz, Cz, P3, P4, and Oz.

Baseline vs SSD: in SSD, for Pz as a source, an increased connection was coming to Oz and a decreased connection was coming to P4. For Pz as a sink, an increased

connection was coming from C4, and the decreased connections from F3, Fz, C3, P3, P4, and Oz.

(ii) The most prominent connections in Baseline clustered over the midline area, the occipital area, and the left fronto-central area, with a lack of connections between the bilateral central area and the bilateral parietal area. In BSD, the prominent connections are clustered around the localised frontal and occipital areas, and the connection between Pz and Cz became one directional. In SSD, the connectivity pattern is relatively similar to baseline with the connections from P3 to C3 and from Oz to F4 remain, similar to BSD.

(iii) *Baseline vs BSD*: FPo was found as the network with the highest count of significantly active connections in BSD, while PoPo shows higher count of significantly active connections in Baseline.

Baseline vs SSD: CPo was found as the network with the highest count of significantly active connections in SSD, while FPo and PoPo show higher count of significantly active connections in Baseline.

(iv) *Baseline vs BSD and Baseline vs SSD*: significant decreases of average GC during BSD were found in FC, FPo, CF, CC, and in all zones coming from Po.

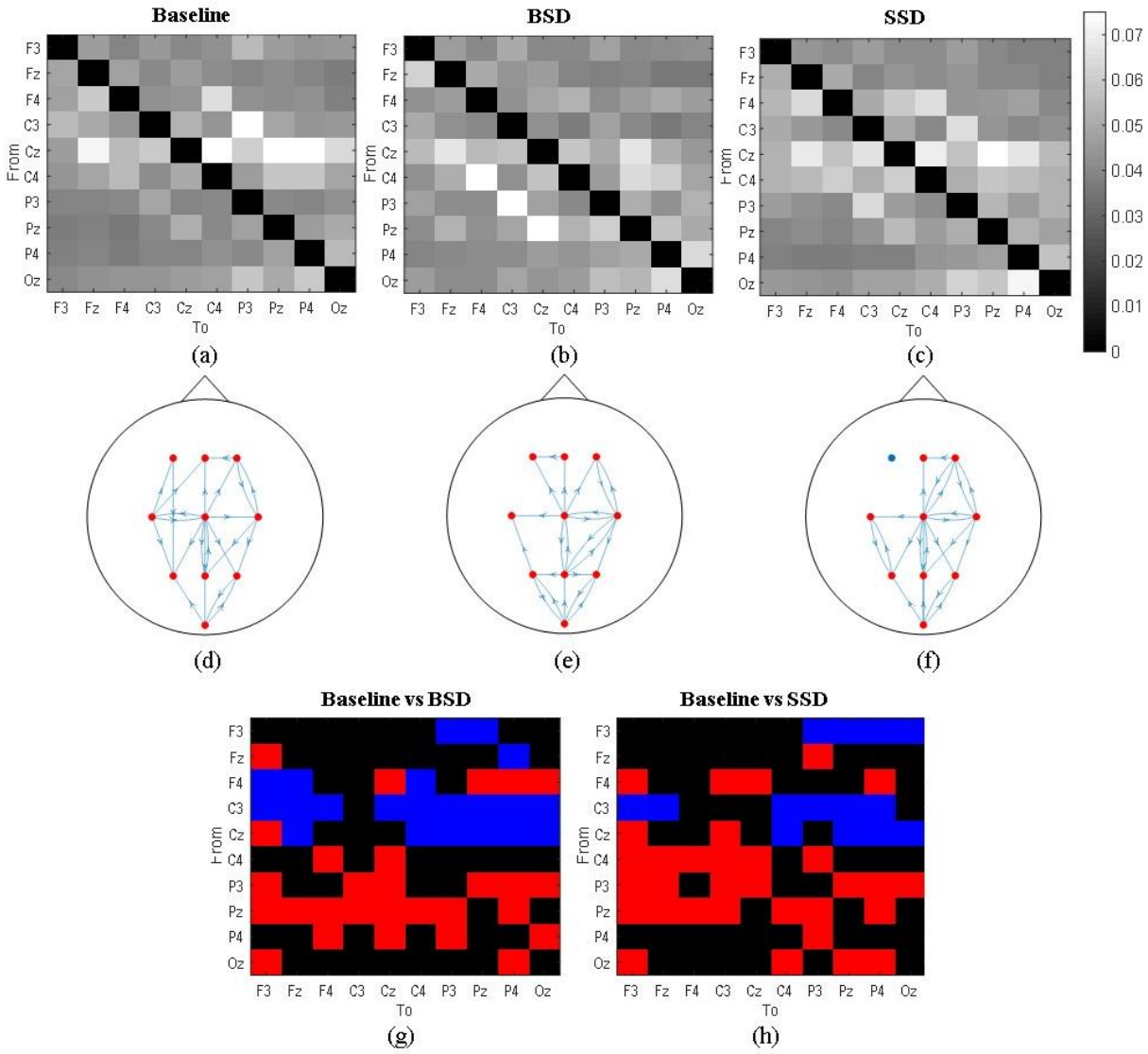

Figure 5.2 (a-c) The average **intra-brain GC** matrices of **group D** for Baseline, BSD, and SSD. (d-f) The connectivity map for each condition- each map displays the average GC values above the 75th percentile of its corresponding matrix above them. (g-h) The matrices of *p*-values generated from a non-parametric paired permutation ($p<0.01$) of the intra-brain GC values from all trials between Baseline and each gaming condition, with FDR correction applied. The blue and red squares indicate the significant connections, blue indicates higher average GC value in Baseline and red indicates higher average GC value in gaming.

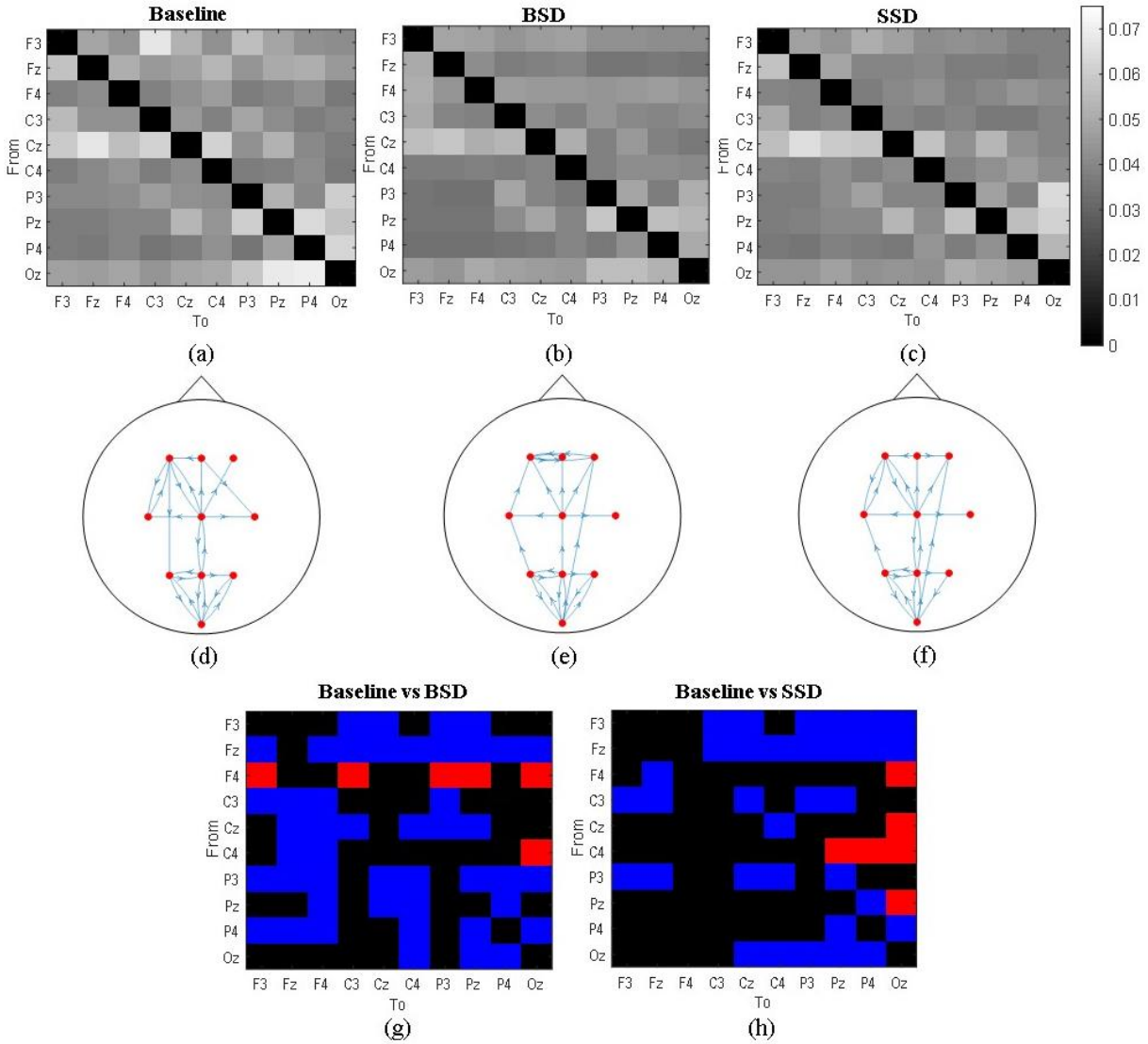

Figure 5.3 (a-c) The average **intra-brain GC** matrices of **group ND** for Baseline, BSD, and SSD. (d-f) The connectivity map for each condition- each map displays the average GC values above the 75th percentile of its corresponding matrix above them. (g-h) The matrices of *p*-values generated from a non-parametric paired permutation ($p<0.01$) of the intra-brain GC values from all trials between Baseline and each gaming condition, with FDR correction applied. The blue and red squares indicate the significant connections, blue indicates higher average GC value in Baseline and red indicates higher average GC value in gaming.

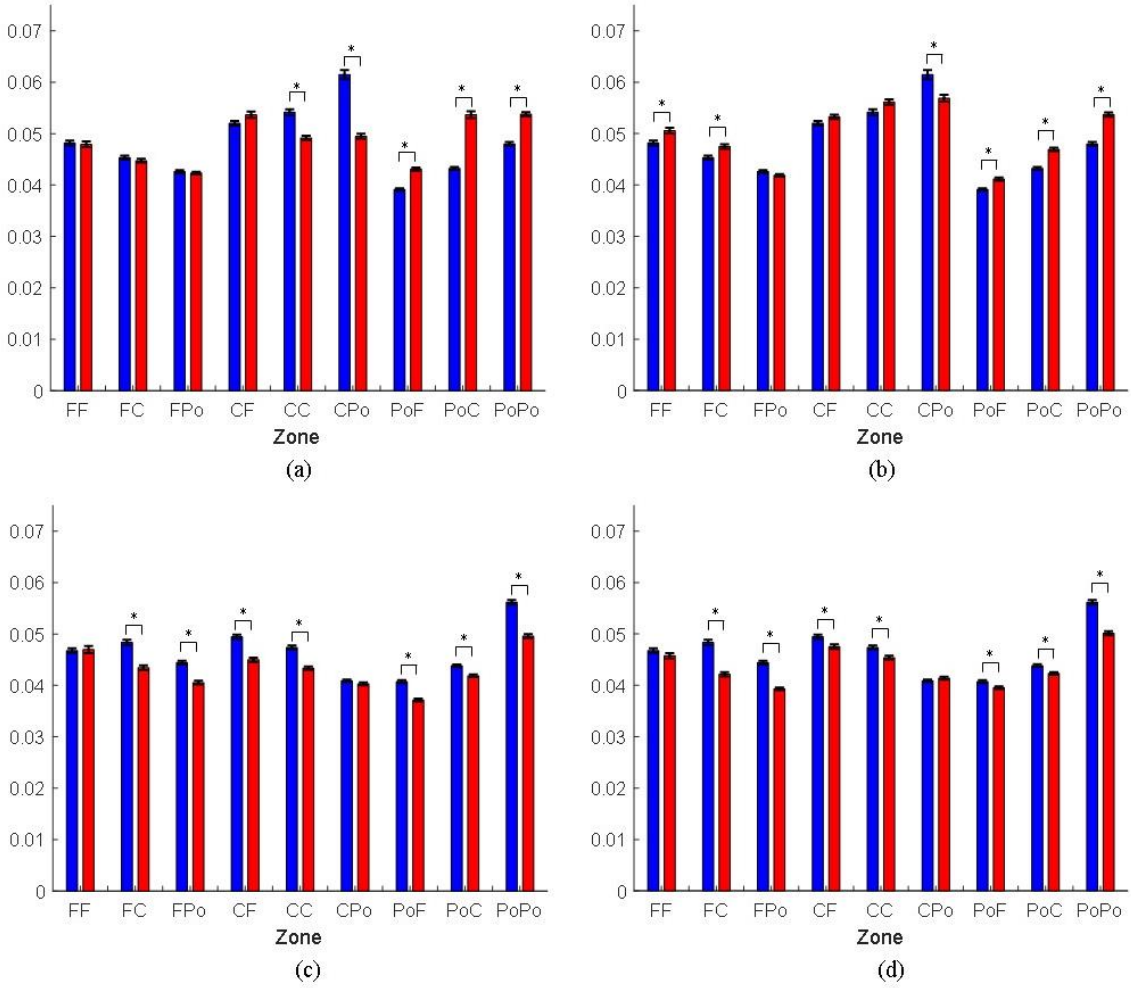

Figure 5.4 The bar graphs of the average GC values (mean ± standard error) in each zone for (a) group D, Baseline vs BSD, (b) group D, Baseline vs SSD, (c) group ND, Baseline vs BSD, and (d) group ND, Baseline vs SSD. A non-parametric paired permutation (p<0.01) was performed to compare the statistic between two conditions, with FDR correction applied. The blue bars indicate the average GC during Baseline and the red bars indicate the average GC during gaming experiment (BSD/SSD).

Comparisons between BSD vs SSD

(i) *Group D*: in BSD, for Pz as a source, stronger connections were flowing to most channels in the cortical areas (frontal, central, parietal, and occipital areas). For Pz as a sink, weaker connections were coming from C3, Cz, and Oz, and a stronger connection was coming from C4.

Group ND: in BSD, for Pz as a source, weaker connections were flowing to Fz, F4, Cz, and Oz. For Pz as a sink, a weaker connection was coming from Cz, and stronger connections were coming from F4, C3, and Oz.

(ii) *Group D*: in BSD, group D shows higher count of significant connections in PoPo, while in SSD, higher count of significant connections was found in CPo.

Group ND: in BSD, group ND shows higher count of significant connections in CPo (left), while in SSD, higher count of significant connections was found in PoF and CPo (from midline/Cz).

(iii) *Group D*: significantly higher average GC during BSD compared to SSD were found in PoF and PoC, and significantly lower average GC during BSD compared to SSD were found in FF, FC, CC, and CPo.

Group ND: A significantly higher average GC during BSD compared to SSD was found in FPo, and significantly lower average GC during BSD compared to SSD were found in CF, CC, CPo, and PoF.

Comparisons between group D and group ND

(i) *Baseline*: for Pz as a source, group D shows weaker connections to F4, C4, P3, P4, and, and Oz. For Pz as a sink, group D shows stronger connections from all central channels, and weaker connections from Fz, P3, and Oz.

BSD: for Pz as a source, group D shows stronger connections to all fronto-central channels. For Pz as a sink, group D shows stronger connections from Fz, Cz, C4, and P4.

SSD: for Pz as a source, group D shows stronger connections to P3 and Oz, and weaker connections to Fz, C3, and C4. For Pz as a sink, group D shows stronger connections from Fz, F4, C3, Cz, C4, P3, and Oz.

(ii) *Baseline*: group D shows higher count of significant connections in CPo, while group ND shows higher count of significant connections in PoPo.

BSD: group D shows higher count of significant connections in PoF and PoC, while group ND shows higher count of significant connections in FF and FC.

SSD: group D shows higher count of significant connections in CPo, while group ND shows higher count of significant connections in PoPo.

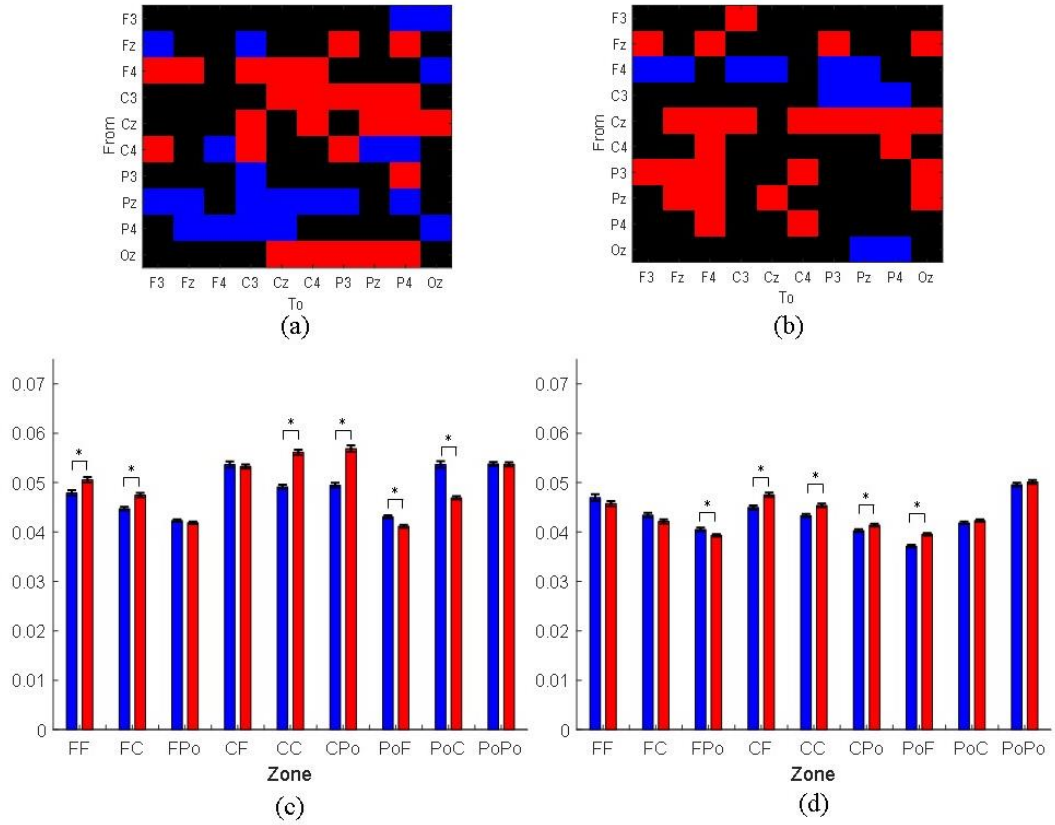

Figure 5.5 (a-b) The matrices of *p*-values generated from a non-parametric paired permutation ($p<0.01$) of the **intra-brain GC values from all trials between BSD and SSD** for (a) group D and (b) group ND, with FDR correction applied. The blue and red squares indicate the significant connections, blue indicates higher average GC value in BSD and red indicates higher average GC value in SSD. (c-d) The bar graphs of the average GC values (mean ± standard error) for BSD and SSD in each zone for (c) group D and (d) group ND. A non-parametric paired permutation ($p<0.01$) was performed to compare the statistic between two conditions, with FDR correction applied. The blue bars indicate the average GC during BSD and the red bars indicate the average GC during SSD.

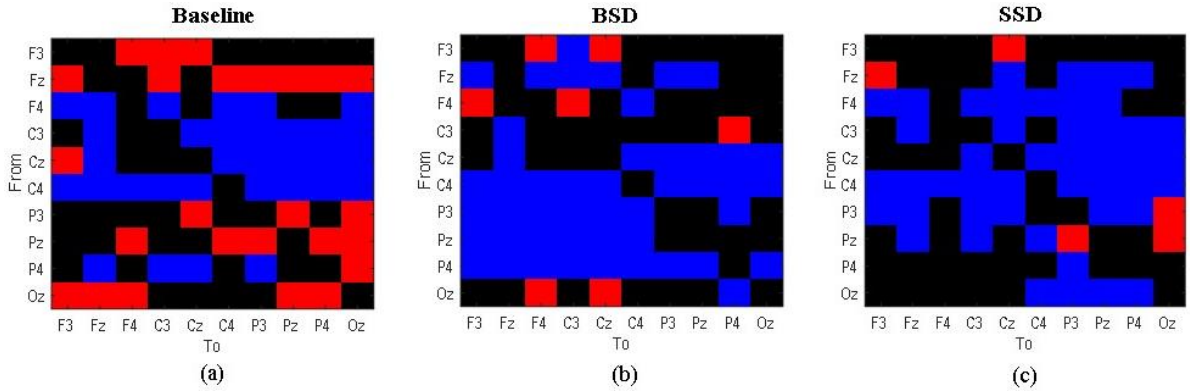

Figure 5.6 The matrices of *p*-values generated from a non-parametric paired permutation ($p<0.01$) of the **intra-brain GC values from all trials between groups** (D and ND) in (a) Baseline, (b) BSD, and (c) SSD, with FDR correction applied. The blue and red squares indicate the significant connections, blue indicates higher average GC value in group D and red indicates higher average GC value in group ND.

5.3.2 Directed Transfer Function

DTF results are presented in three ways: as matrices presenting the grand average of DTF values of all epochs from all players in each group (Fig. 5.7 and 5.11), as connectivity maps displaying only the average values above the 75th percentile of its corresponding matrix for an easy visual representation of spatial connectivity localisation (Fig. 5.8 and 5.12), as a set of *p*-value matrices (Fig. 5.9, 5.13, 5.15, and 5.17) and as bar graphs displaying the average GC values in each zone (Fig. 5.10, 5.14, and 5.16).

The statistical comparisons from the DTF data were performed as the following: between Baseline and BSD/SSD, between BSD and SSD, and between groups. Based on these presentations, the results will be explained following the same structure as in intra-brain GC results presentation.

DTF of group D

(i) *Baseline vs BSD*: in BSD, for Pz as a source, increased connections were flowing to Fz and F4 (in lower beta band), to C3 (in theta band), and to Cz (in theta, alpha, and lower beta bands), and decreased connections to P4 (in alpha band) and Oz (in all frequency bands). For Pz as a sink, increased connections were flowing from F3, Fz, and C3 (in all frequency bands), and decreased connections from Cz and C4 (in all frequency bands), and from Oz (in theta and both beta bands).

Baseline vs SSD: in SSD, for Pz as a source, decreased connections were flowing to P4 (in lower beta band) and Oz (in alpha and both beta bands). For Pz as a sink,

increased connections were flowing from F3 and C3 (in all frequency bands), and decreased connections from C4 (in theta, alpha, and higher beta bands).

(ii) In all frequency bands and all conditions, the prominent connections were evenly distributed throughout all channels and densely clustered over the midline channels.

(iii) *Baseline vs BSD*: FPo was found to have higher significant connection count in BSD in all frequency bands, followed by FC in theta and alpha bands, while CPo was found to have higher significant connection count in Baseline in all frequency bands, followed by PoF in theta and alpha bands.

Baseline vs SSD: FPo and CPo (from the left hemisphere) were found to have higher significant connection count in SSD in all frequency bands. In Baseline, higher significant connection count was found in CF in all frequency bands and in CPo in theta, alpha, and lower beta bands, all from the right hemisphere.

(iv) *Baseline vs BSD*: significant decreases of average DTF during BSD were found in FC (theta, alpha, and lower beta), FPo (theta, alpha, and higher beta), CC and PoPo (all frequency bands), and significant increases of average DTF during BSD were found in FF, CF, and PoF (all frequency bands) and in CPo (lower beta).

Baseline vs SSD: significant decreases of average DTF during SSD were found in FC (alpha), FPo (all frequency bands), and PoPo (theta and both beta bands), and significant increases of average DTF during SSD were found in FF (all frequency bands), CF and PoF (theta, alpha, and higher beta), and PoC (both beta bands).

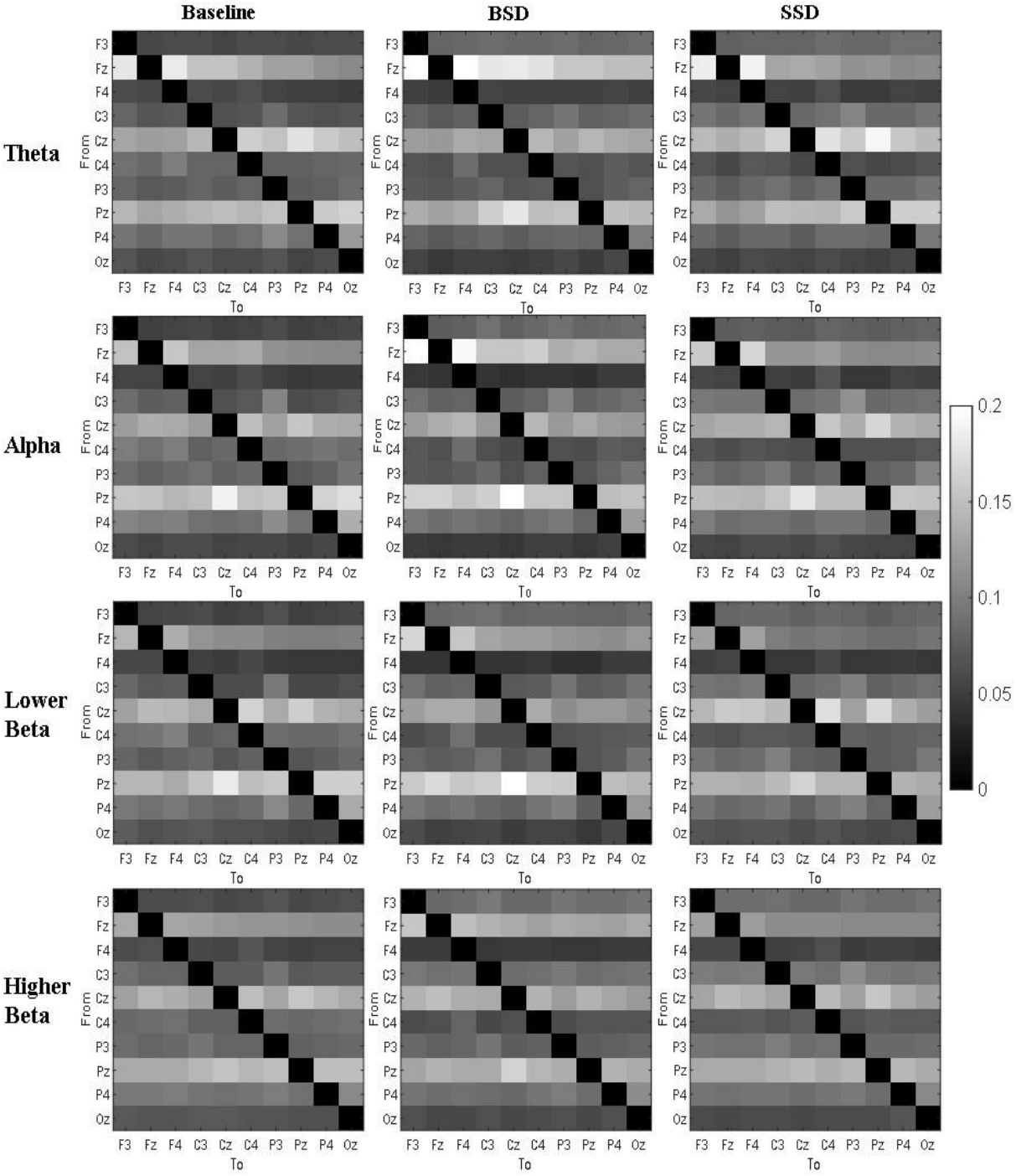

Figure 5.7 The average DTF matrices **for group D** for Baseline, BSD and SSD conditions, in each frequency band.

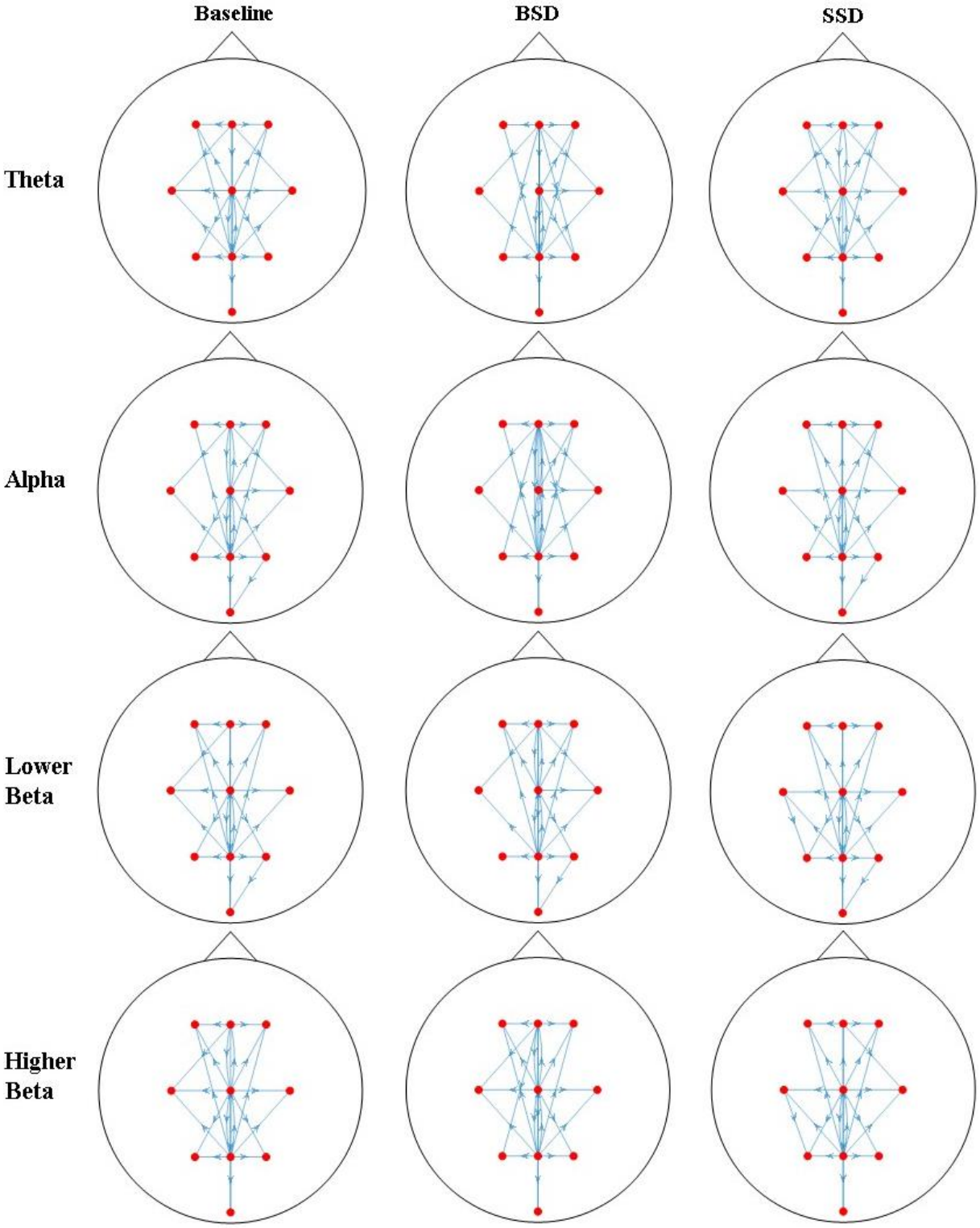

Figure 5.8 The connectivity maps display the average DTF values for group D above the 75th percentile of its corresponding matrix shown in Figure 5.7, for Baseline, BSD and SSD conditions, in each frequency band.

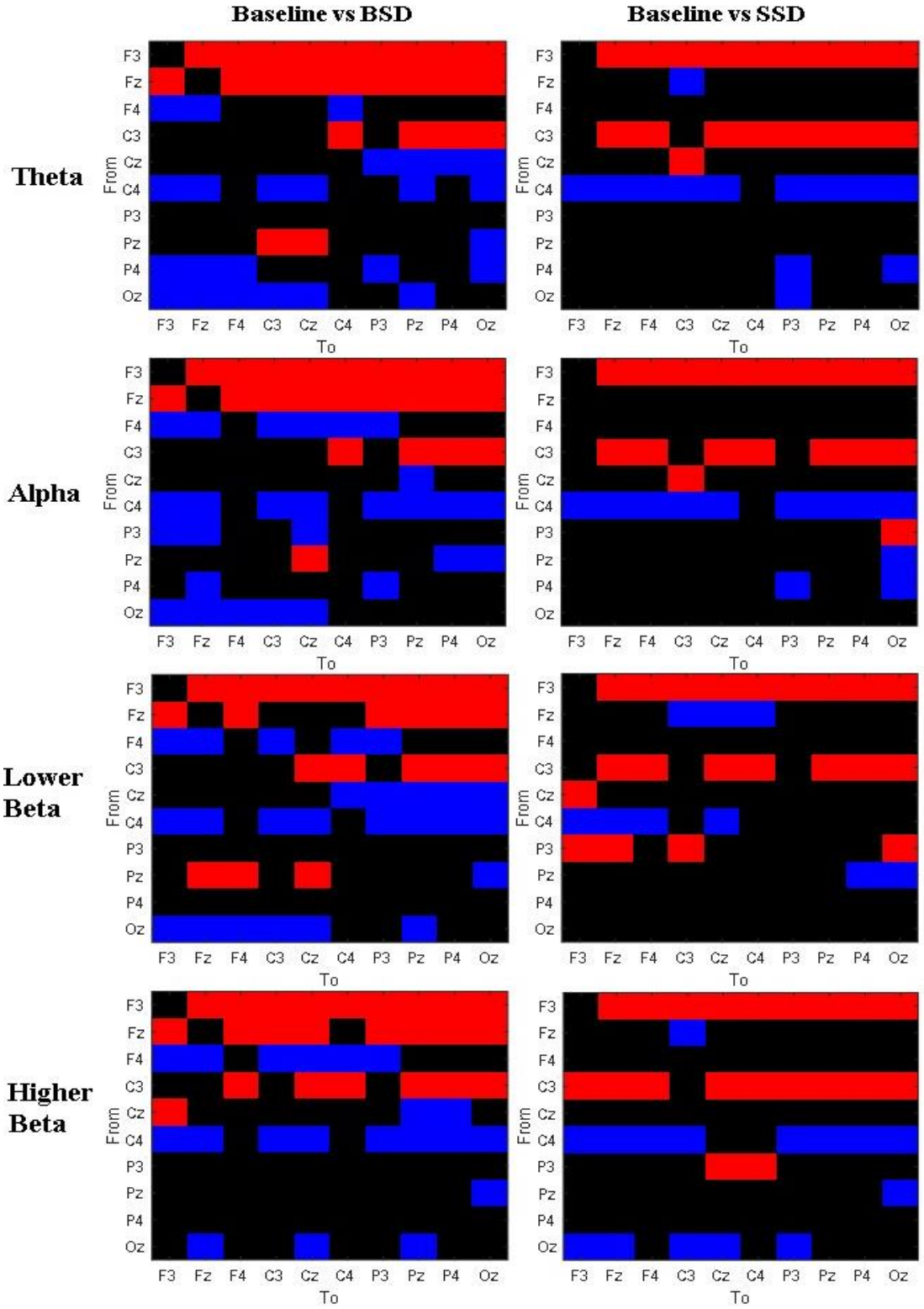

Figure 5.9 The matrices of *p*-values generated from a non-parametric paired permutation ($p<0.01$) of the DTF values from all trials **between Baseline and each gaming condition** (Baseline vs BSD and Baseline vs SSD) for **group D** in each frequency band with FDR correction applied. The blue and red squares indicate the significant connections, blue indicates higher average DTF value in Baseline (lower in gaming) and red indicates lower average DTF value in Baseline (higher in gaming).

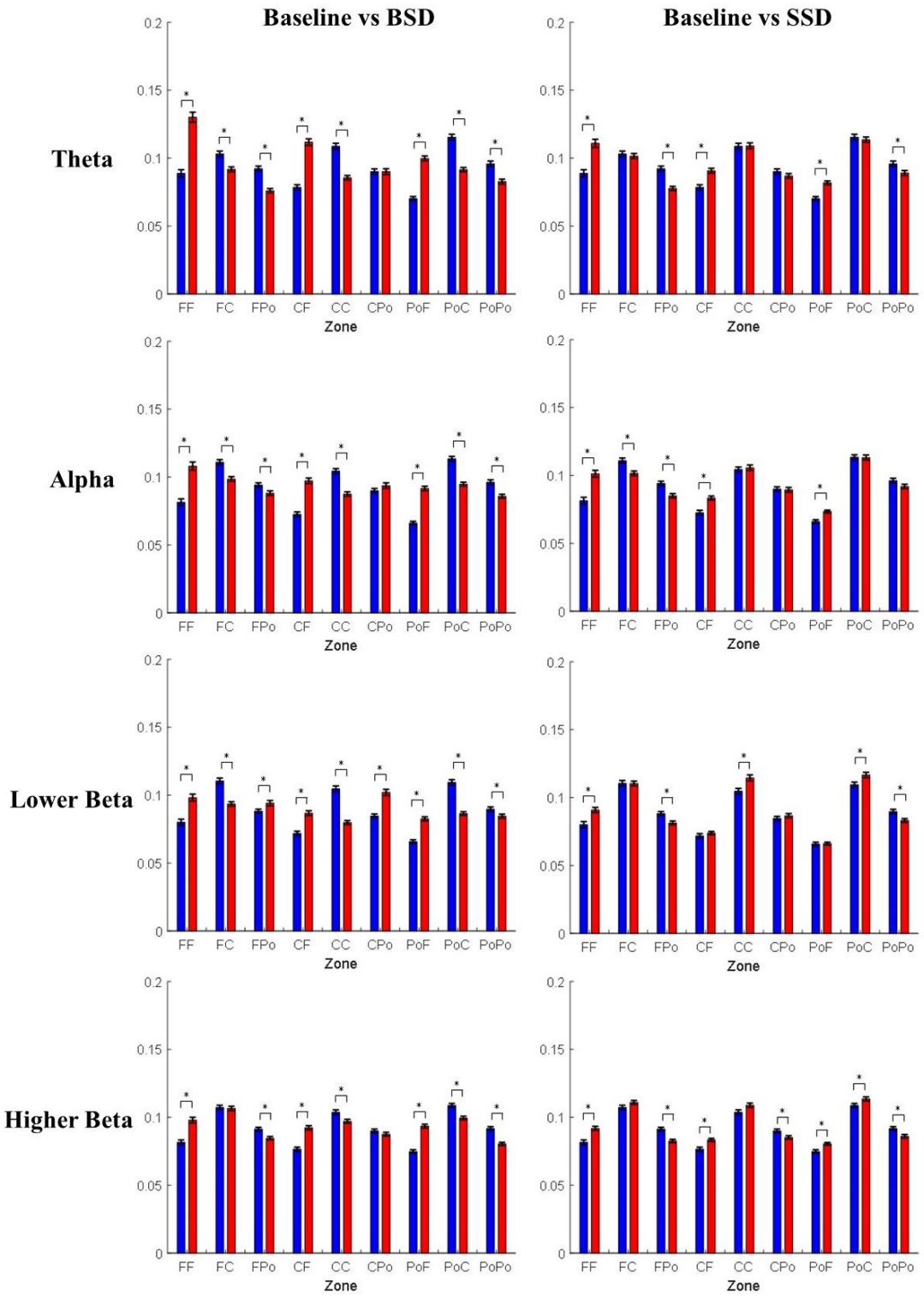

Figure 5.10 The bar graphs of the average DTF values (mean ± standard error) in each zone between Baseline and each gaming condition (Baseline vs BSD, and Baseline vs SSD) for group D, in each frequency band. A non-parametric paired permutation (p<0.01) was performed to compare the statistic between two conditions, with FDR correction applied. The blue bars indicate the average DTF during Baseline and the red bars indicate the average DTF during gaming experiment (BSD/SSD).

DTF of group ND

(i) *Baseline vs BSD*: in BSD, for Pz as a source, decreased connections were flowing to all channels in all frequency bands. For Pz as a sink, increased connections were coming from F3 and C4 (in all frequency bands), Fz (in both beta bands), and C3 (in theta and both beta bands), and decreased connections were coming from P3 (in both beta bands), P4 (in theta and both beta bands), and Oz (in higher beta band).

Baseline vs SSD: in SSD, for Pz as a source, decreased connections were flowing to all channels in all frequency bands. For Pz as a sink, increased connections were coming from F3, F4, and C3 (in all frequency bands), and decreased connections were coming from Cz and P4 (in all frequency bands), P3 and Oz (in higher beta band).

(ii) The most prominent connections in Baseline were evenly distributed around all areas in all frequency bands, with a dense cluster formed over the midline channels. During both gaming conditions, the most prominent connections are clustered around the left fronto-central channels with larger area of the left-hemisphere become more involved in SSD compared to BSD.

(iii) *Baseline vs BSD*: in BSD, higher significant connection count was found in FPo and CPo in all frequency bands, while in Baseline, higher significant connection count was found PoF and PoC in all frequency bands.

Baseline vs SSD: in SSD, higher significant connection count was found in FC, FPo, and left hemispheric CF, CC, and CPo, in all frequency band, while in Baseline, higher significant connection count was found in PoF, PoC, and PoPo in all frequency bands.

(v) *Baseline vs BSD*: significant decreases of average DTF during BSD were found in FC and CC (theta and both beta bands), FPo, CPo, PoC, and PoPo (all frequency bands), and significant increases of average DTF during BSD were found in FF, CF, PoF in all frequency bands.

Baseline vs SSD: significant decreases of average DTF during SSD were found in FC, FPo, CPo, and PoPo (all frequency bands) and PoC (theta) and significant increases of average DTF during SSD were found in FF, CF, PoF in all frequency bands.

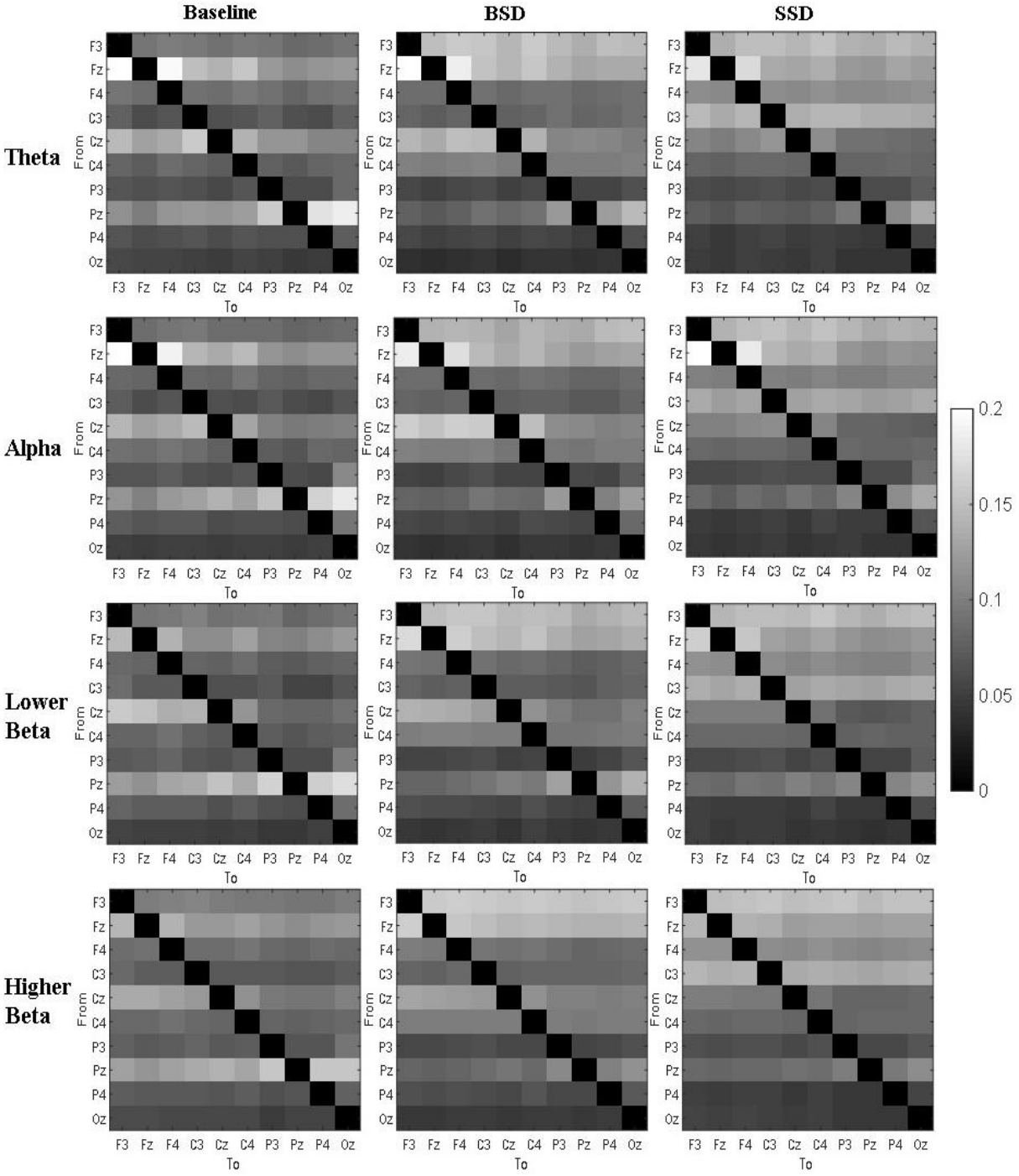

Figure 5.11 The average DTF matrices **for group ND** for Baseline, BSD and SSD conditions, in each frequency band.

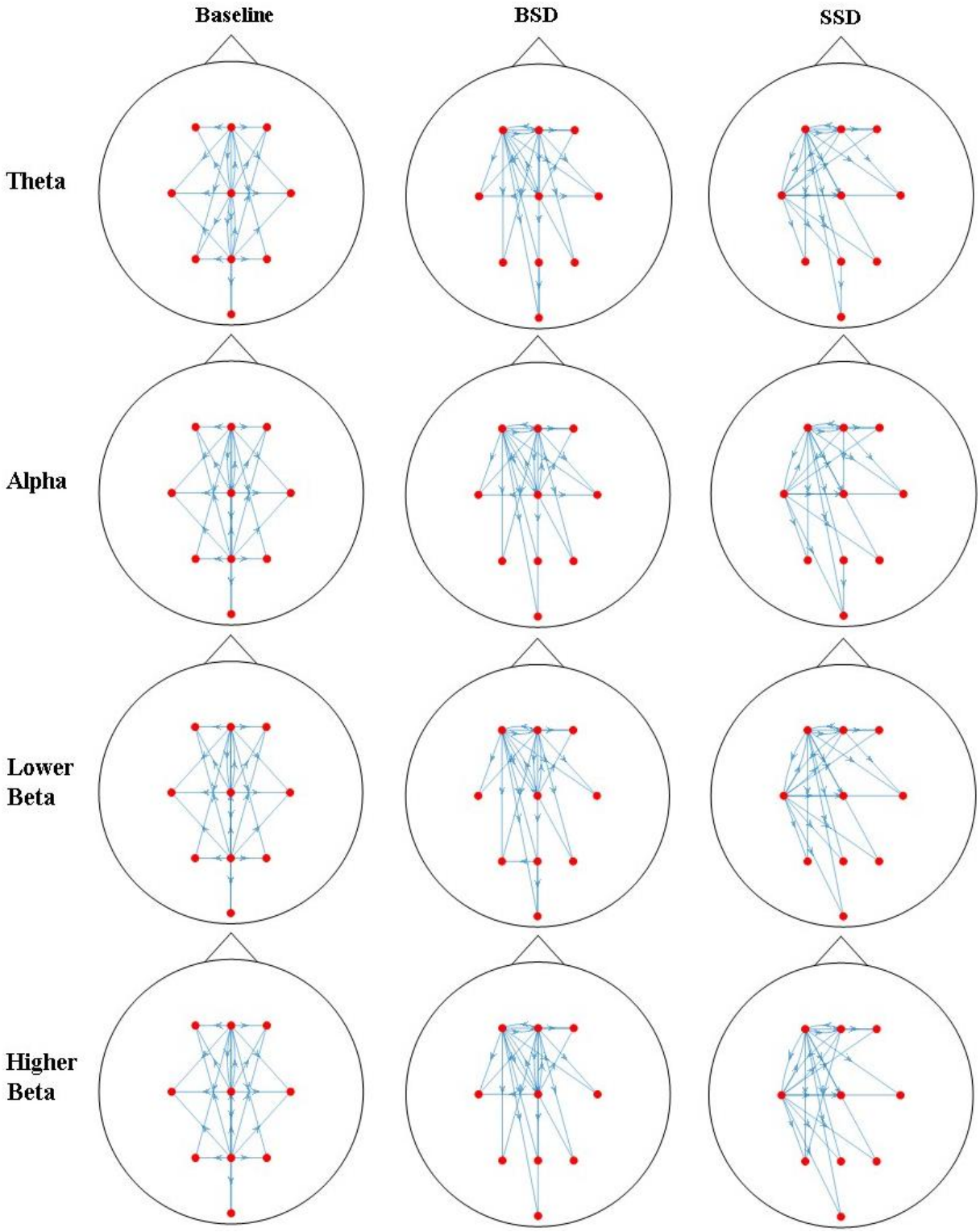

Figure 5.12 The connectivity maps display the average DTF values for group D above the 75th percentile of its corresponding matrix shown in Figure 5.11, for Baseline, BSD and SSD conditions, in each frequency band.

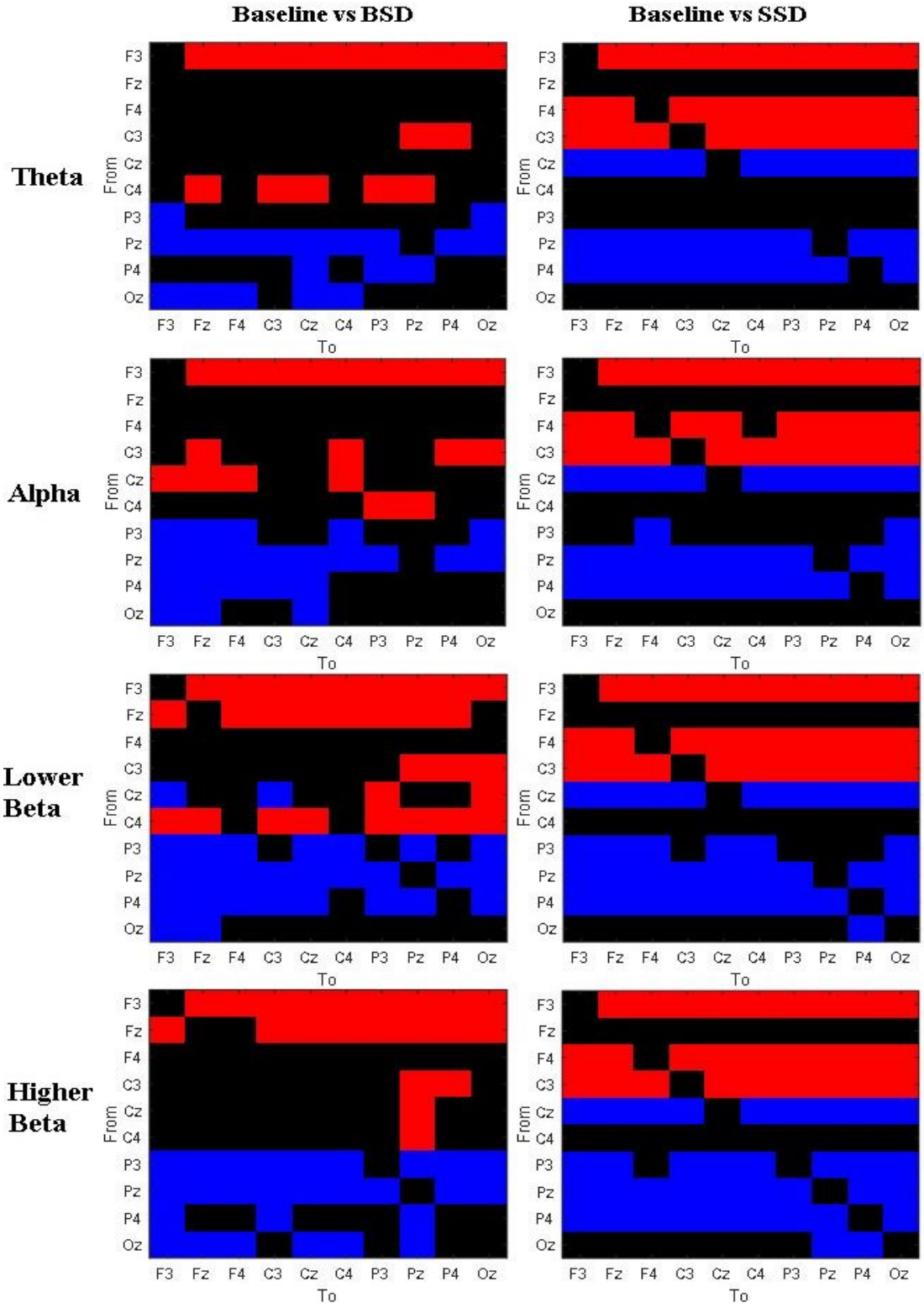

Figure 5.13 The matrices of *p*-values generated from a non-parametric paired permutation ($p<0.01$) of the DTF values from all trials **between Baseline and each gaming condition** (Baseline vs BSD and Baseline vs SSD) for **group ND** in each frequency band with FDR correction applied. The blue and red squares indicate the significant connections, blue indicates higher average DTF value in Baseline (lower in gaming) and red indicates lower average DTF value in Baseline (higher in gaming).

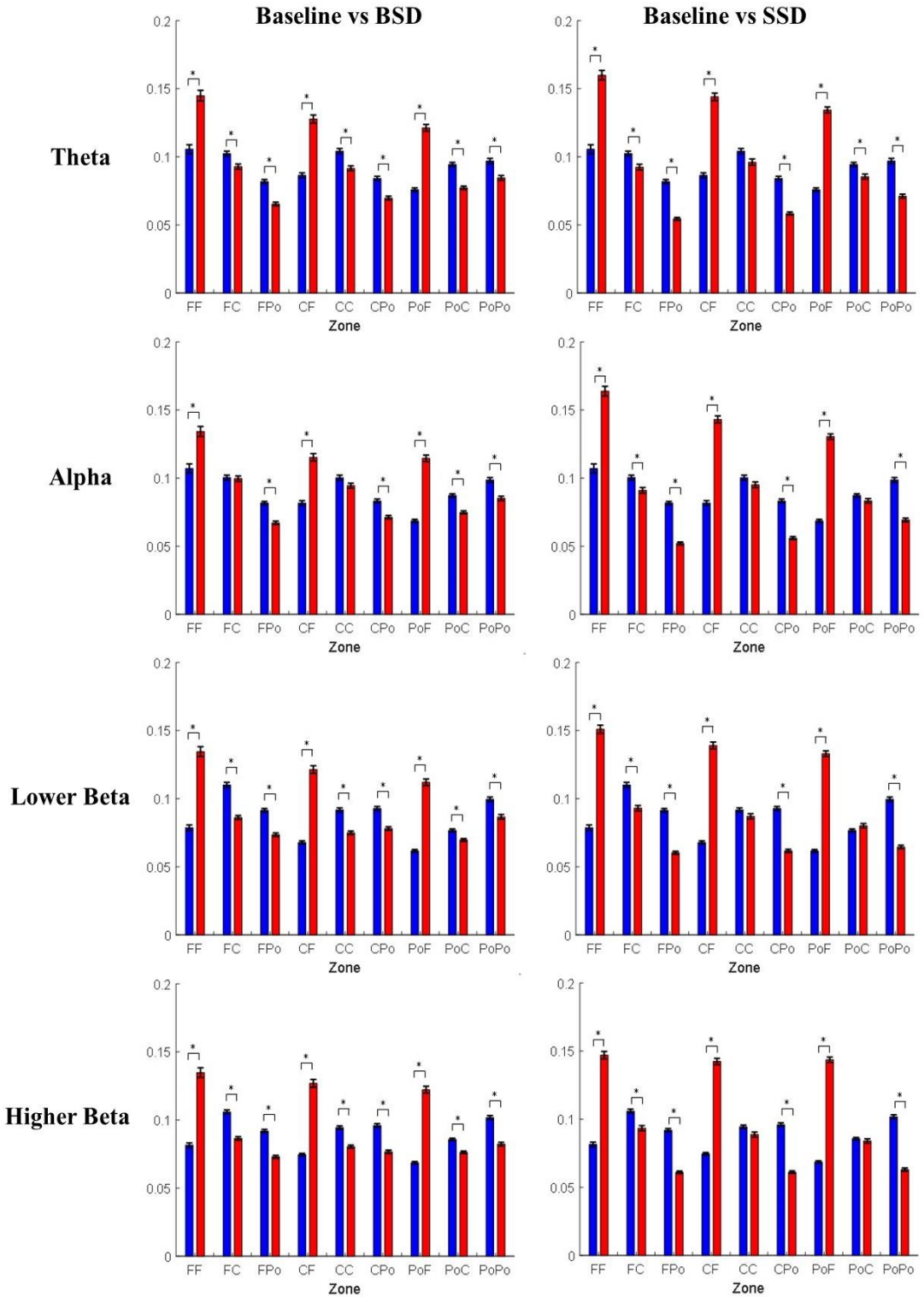

Figure 5.14 The bar graphs of the average DTF values (mean ± standard error) in each zone between Baseline and each gaming condition (Baseline vs BSD, and Baseline vs SSD) for group ND, in each frequency band. A non-parametric paired permutation (p<0.01) was performed to compare the statistic between two conditions, with FDR correction applied. The blue bars indicate the average DTF during Baseline and the red bars indicate the average DTF during gaming experiment (BSD/SSD).

Comparisons between BSD vs SSD

(i) *Group D*: in BSD, for Pz as a source, stronger connections were flowing to Fz and Cz (in all frequency bands), and to P3 (in alpha band) and Oz (in alpha and lower beta bands), and a weaker connection was flowing to P3 (in theta and higher beta bands). For Pz as a sink, stronger connections were coming from F3 (in lower beta band) and Fz (in alpha and lower beta bands), and weaker connections were coming from F4 and C4 (in lower beta band), and from Cz (in all frequency bands).

Group ND: in BSD, for Pz as a source, stronger connections were flowing to C3 (in all frequency bands), to Cz (in theta and higher beta bands), and to C4 (in theta band), and weaker connections were flowing to Fz (in higher beta band), to F4 and C4 (in all frequency bands), and to Cz (in alpha and lower beta bands). For Pz as a sink, stronger connections were coming from Cz (in theta band) and from P4 and Oz (in lower beta band), and weaker connections were coming from C3 (in theta band) and from P3 (in theta and lower beta bands).

(ii) *Group D:* in BSD, higher significant connection count was found in FPo in alpha and both beta bands, while in SSD, higher significant connection count was found in CC and CPo in alpha and lower beta bands.

Group ND: in BSD, higher significant connection count was found in FC in theta and both beta bands and in CC and PoC (higher from midline and the right hemisphere in theta, and both beta bands). In SSD higher significant connection count was found in PoC (higher from the occipital midline and the left hemisphere in theta and both beta bands), while in alpha band PoC activity was higher in SSD, particularly coming from the parietal midline and left hemisphere (Pz and P3).

(iii) *Group D*: significantly higher average DTF during BSD compared to SSD were found in FF (alpha), CF and PoF (all frequency bands) , and CPo (lower beta), and significantly lower average DTF during BSD compared to SSD were found in FC (theta and lower beta), CC, PoC, and PoPo (all frequency bands).

Group ND: significantly higher average DTF during BSD compared to SSD were found in FC (alpha), FPo, CPo, and PoPo (all frequency bands), and significantly lower average DTF during BSD compared to SSD were found in FF, CF, PoF, and PoC (all frequency bands), and FC and CC (both beta bands).

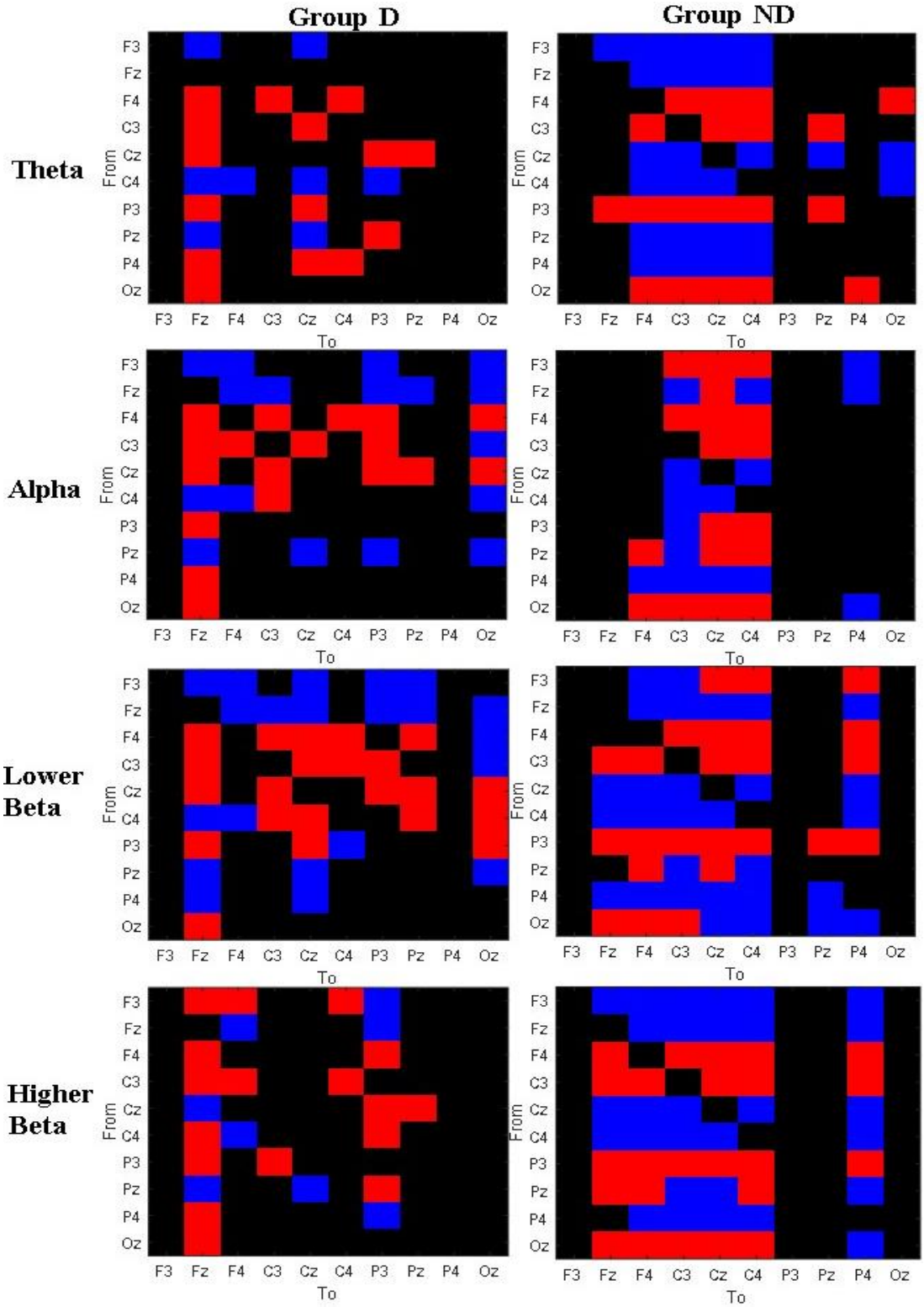

Figure 5.15 The matrices of *p*-values generated from a non-parametric paired permutation ($p<0.01$) of the DTF values from all trials **between BSD and SSD for each group,** in each frequency band with FDR correction applied. The blue and red squares indicate the significant connections, blue indicates higher average DTF value in BSD (lower in SSD) and red indicates lower average DTF value in BSD (higher in SSD).

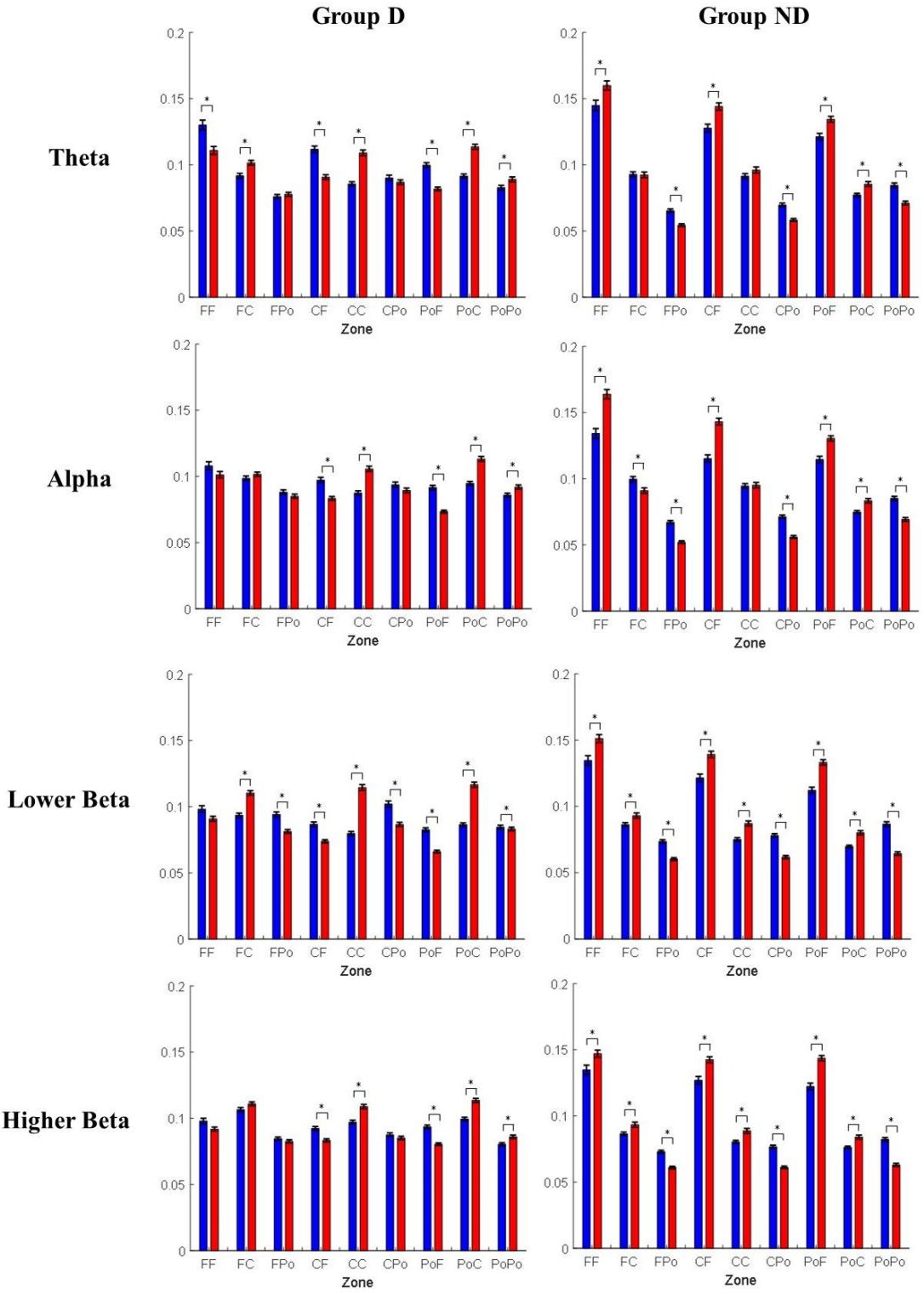

Figure 5.16 The bar graphs of the average DTF values (mean ± standard error) in each zone between BSD and SSD for both groups, in each frequency band. A non-parametric paired permutation (p<0.01) was performed to compare the statistic between two conditions, with FDR correction applied. The blue bars indicate the average DTF during BSD and the red bars indicate the average DTF during SSD.

Comparisons between group D and group ND

(i) *Baseline*: for Pz as a source, group D shows stronger connections to most fronto-central channels (in theta, alpha, and lower beta bands), to Fz and C4 (in higher beta band). For Pz as a sink, group D shows stronger connections from Cz and P4 (in all frequency bands), from C4 (in lower beta band), from P3 (in theta and higher beta bands), and from Oz (in theta and both beta bands), and weaker connections from F3 and F4 (in all frequency bands).

BSD: for Pz as a source, group D shows stronger connections to all channels (in all frequency bands, except to Oz in theta and lower beta bands). For Pz as a sink, group D shows stronger connections from Fz (in theta and alpha bands), from Cz, P3, and P4 (in all frequency bands), and from Oz (in higher beta band), and weaker connections from F3, F4 and C4 (in all frequency bands).

SSD: for Pz as a source, group D shows stronger connections to all channels (in all frequency bands, except to Oz in alpha and lower beta bands). For Pz as a sink, group D shows stronger connections from Cz, P3, P4, and Oz (in all frequency bands), and weaker connections from F3, F4, and C3 (in all frequency bands), from Fz (in higher beta band), and from C4 (in theta band).

(ii) *Baseline, BSD, and SSD*: group D shows higher significant connection count in PoF and PoC in all frequency bands, while group ND shows higher significant connection count in FC and FPo in all frequency bands, with Baseline shows more scarce significant connections compared to gaming.

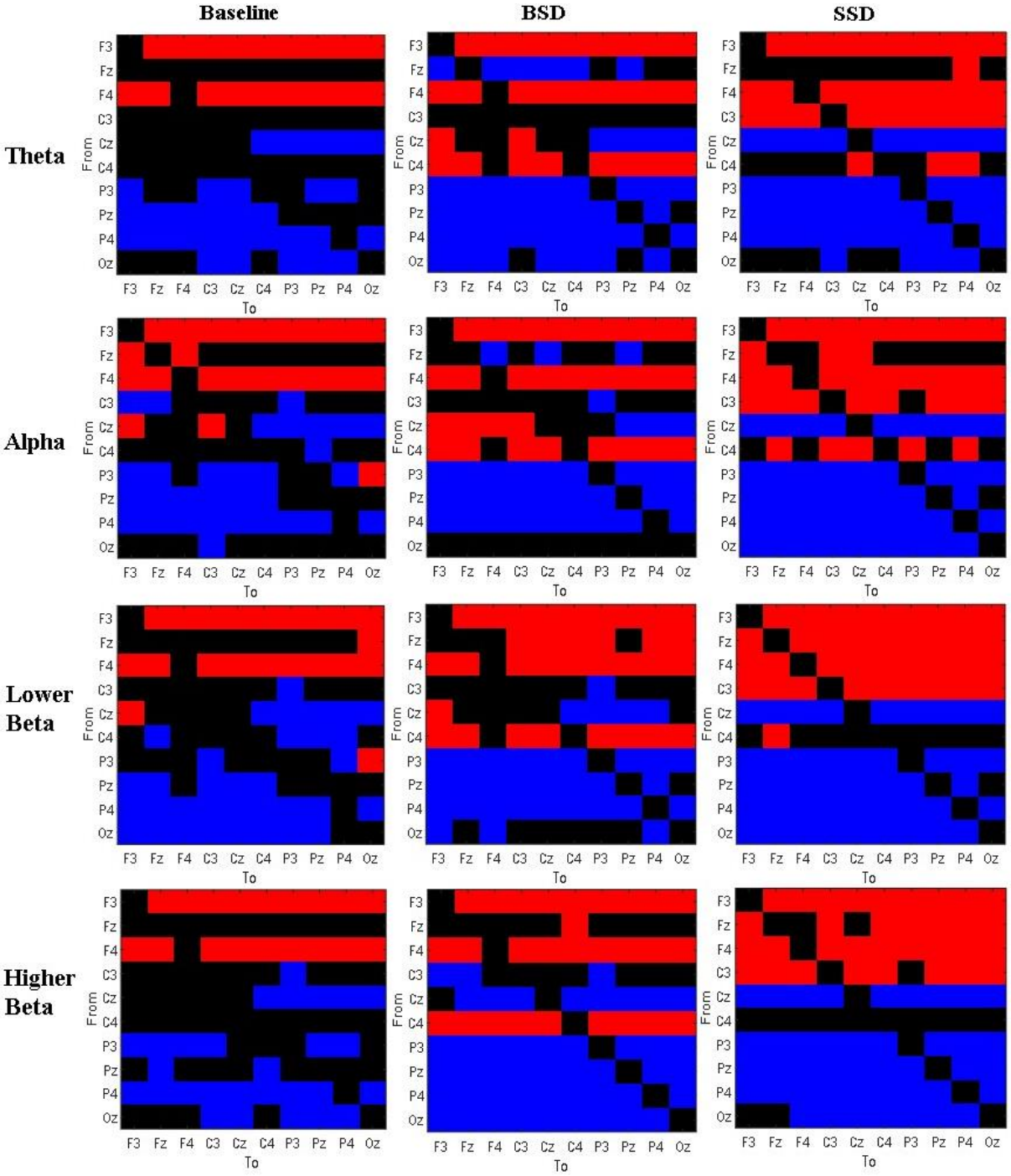

Figure 5.17 The matrices of *p*-values generated from a non-parametric paired permutation ($p<0.01$) of DTF values from all trials **between groups** (D and ND) for Baseline and each gaming condition (BSD and SSD), in each frequency band with FDR correction applied. The blue and red squares indicate the significant connections, blue indicates higher average DTF value in group D (lower in group ND) and red indicates lower average DTF value in group D (higher in group ND).

5.3.3. Inter-brain Granger Causality

Inter-brain GC results are presented in two ways: as matrices presenting the grand average of GC values of all epochs from all pairs in each direction (i.e. from group D to group ND will be called 'direction I' and from group ND to group D will be called 'direction II') (Fig. 5.18), as a set of *p-values* matrices displaying the significant connections, as a result of a non-parametric single-sample permutation test (Fig. 5.19), and as inter-brain connectivity maps displaying the significant connections obtained from the *p-values* matrices (Fig. 5.20).

The significant connections found in the inter-brain GC showed that more connections were found in direction I during BSD, while there was no significant connection found during SSD. This condition indicates that group D achieved their best gaming performance (BSD), not only by modulating their intra-brain activity, but also by engaging in the social aspect of the game (i.e. competing with their opponent). Meanwhile, group D reached their worst gaming performance (SSD) by isolating themselves. On the other hand, direction II showed the same amount of significant connections during both gaming conditions. During group ND's best gaming performance (SSD), all channels were found active in sending significant connections to group D, compared to during BSD. This condition indicates that SSD was achieved due the larger brain activation area combined with the lack of social engagement by group D.

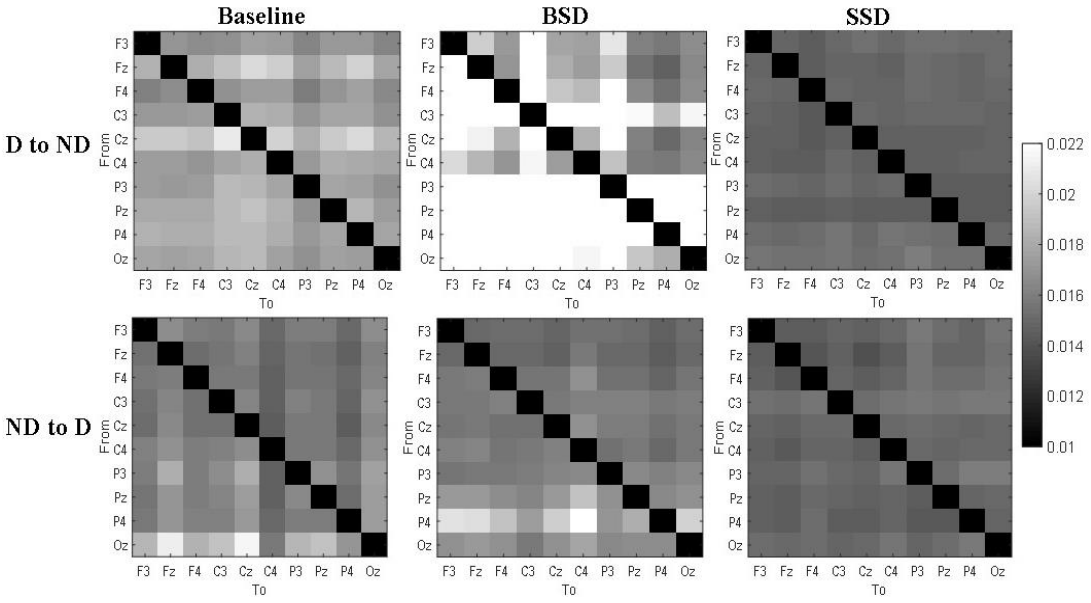

Figure 5.18 The matrices of the average inter-brain GC for each condition, i.e. Baseline, BSD, and SSD for each direction.

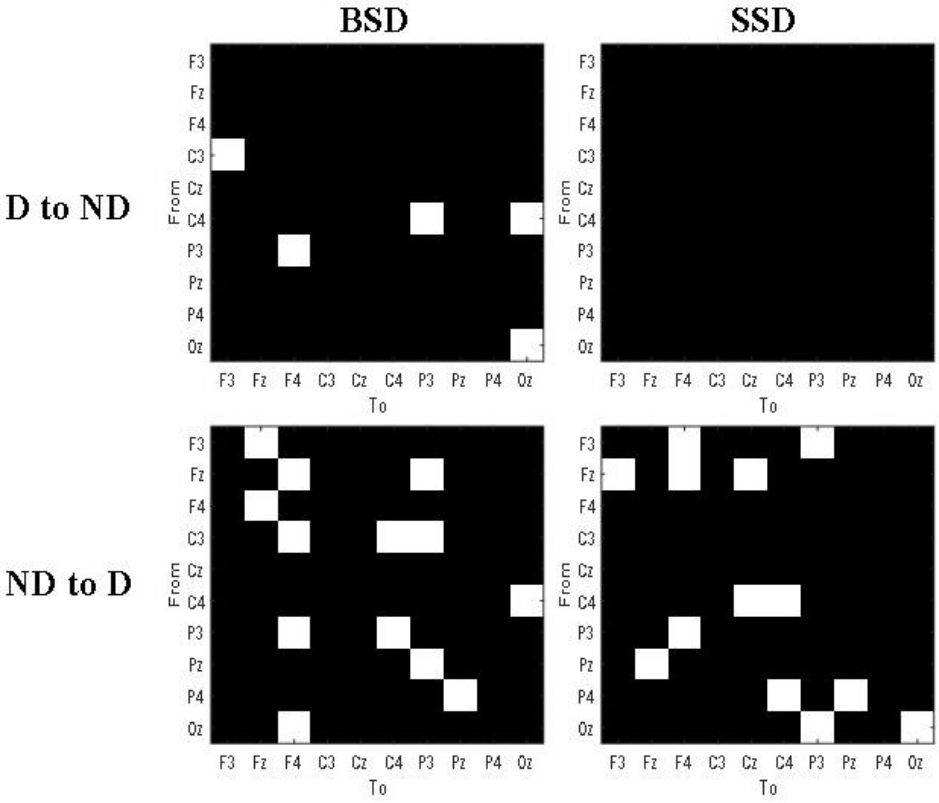

Figure 5.19 The matrices of *p*-values generated from a non-parametric single-sample permutation ($p<0.001$) with FDR correction applied, of the inter-brain GC of all pairs for both gaming conditions. The white boxes represent the significant connections.

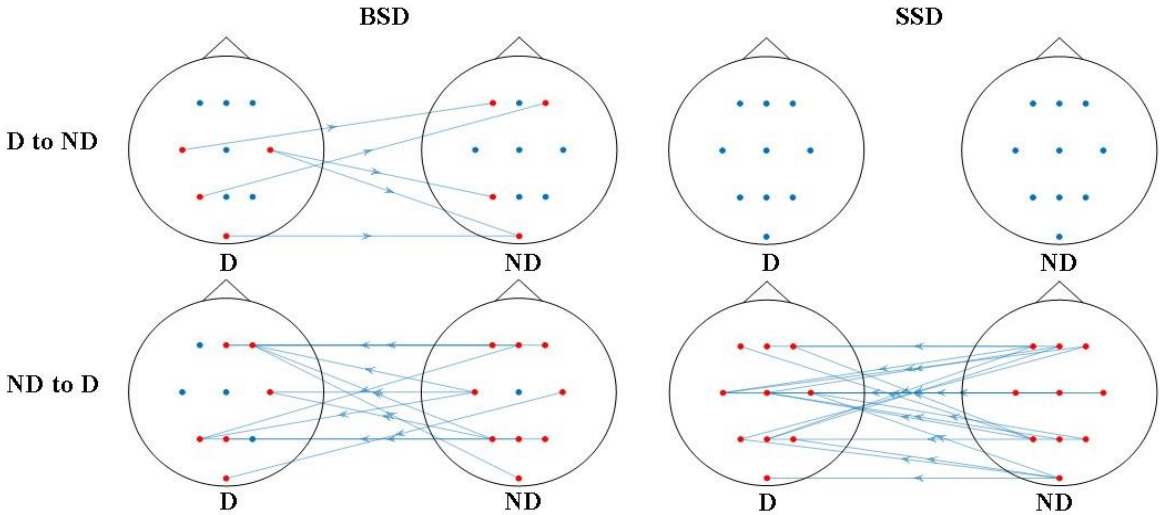

Figure 5.20 The significant inter-brain connectivity map based on the significant connections found in Figure 5.19, for both gaming conditions (BSD and SSD), in both directions.

5.4 Discussions

Multi-user BCI competitive gaming has been previously studied [66, 159], however, the information regarding the cortical activation within and between the interacting brain are still relatively limited. In this study, we performed intra-brain and inter-brain connectivity analysis in order to explore the impact of competitive BCI gaming that is based on alpha band operant conditioning, to the brain cortical activity. Three different conditions were measured such as pre-gaming Baseline, BSD, and SSD, with the group of players divided based on their resting state alpha power, into group D and group ND. Connectivity analysis were divided into intra-brain GC, DTF, and inter-brain GC, with a non-parametric statistical analysis to compare the results based on the types of condition (i.e. Baseline-BSD and Baseline-SSD) in order to find out the difference between Baseline and each gaming condition, and based on the groups (i.e. between group D and group ND) in order to compare the different network activation between players during Baseline and both gaming conditions. Intra-brain connectivity detected the dominance of group D during gaming, characterised by the stronger connections coming from the parietal area (in GC) and by a frequency specific Pz activity as a source channel (in DTF). Inter-brain connectivity also found best gaming performance of group D was achieved due to their ability to modulate their intra-brain activity as well as by engaging to the social aspect of the game, while group ND only engaged in the social interaction with weaker ability to modulate their intra-brain activity.

Intra-brain GC

Intra-brain GC analysis for group D in both gaming conditions detected an increased connectivity around the localised parietal network as well as the bilateral fronto-parietal network, and the most successful gaming was characterised by the increased of connectivity from Pz to Cz. These results might suggest that they managed to upregulate the activity around the Pz channel by increasing its activity as a source, sending information to other channels compared to its activity as a sink in receiving information from other channel, despite there was no significant alpha power changes occurred at Pz (Chapter IV). The activation of fronto-parietal network might reflect the level of task-engagement performed by the group during gaming. Fronto-parietal network is known to be activated during cognitive control, it has been proposed that its role is to regulate the

activities of antagonistic networks of default mode network (DMN) and the dorsal attention network (DAN) [179, 180]. Intra-brain GC also detected a decreased of network connections that are originated from the left central channel in both gaming conditions in group D, indicating that the left central area of the brain is more active during Baseline. Left-lateralised brain activity during resting state has been reported along with its relation to the DMN [181, 182]. The decreasing activity around this part during gaming might indicate the deactivation of DMN. In contrast to group D, group ND did not show much of a significant increase of connectivity during gaming, instead, they tend to deactivate most of the brain networks during gaming.

Intra-brain GC comparison between BSD and SSD revealed that during their most successful gaming (BSD), group D significantly increased their fronto-parietal network, with higher connections coming from Pz towards the fronto-central area, confirming the control of channel Pz, while maintaining a higher level of task-engagement. Similar analysis in group ND showed that during their most successful gaming (SSD), the fronto-parietal connectivity and the activity of Pz as a source channel are significantly higher compared to during BSD, indicating the effort for a better performance, thus reducing the score difference between the groups. However, their effort was not enough to outperform their opponent.

Intra-brain GC comparison between groups show that, even during Baseline, the two groups displayed statistically significant differences in their connectivity, with stronger connectivity found in group D around the fronto-parietal and the localised parieto-occipital networks. Based on this result, the connectivity difference during resting period between the groups may allow the prediction of a gaming/training outcome, as previously studied with the functional resting connectivity and its ability to predict task performance [45, 183]. This result also supports our findings in Chapter IV, which revealed a statistically significant difference of occipital alpha power between groups during Baseline. During gaming, generally higher connectivity was found in all of the brain networks in group D regardless the gaming outcome, while group ND showed a very few significant connections. This result reflects that group ND has no substantial role in achieving SSD condition- as their successful performance, and it is more likely that SSD was achieved due to a weaker performance by group D.

Directed Transfer Function

DTF results in group D showed that there was a significant frequency specific increase of connectivity from Pz to Cz in the alpha band (as well as in the frequency band that might overlap with alpha band, i.e. theta and lower beta band) during BSD. However, similar increase did not occur during SSD, which might reflect the effort of the group to regulate the parietal activity within a specific frequency range. DTF also detected higher posterior midline connectivity (between Pz and Oz) during Baseline when compared to both gaming conditions that was not frequency specific. This higher Baseline connectivity might be associated to the posterior cingulate cortex (PCC) activity, a brain structure that is a part of DMN [184], which is deactivated during gaming performance. Additionally, DMN (consisted of mPFC, PCC and TPJ), has been linked to the brain's social function and an abnormal PCC activity has been associated with an impaired social function in autistic individuals [185-189], which is relevant to the social interaction aspect of the experiment.

The DTF results during gaming in group D may suggest the mental strategy that potentially caused group D to perform poorly during SSD. In BSD, group D in all frequency bands, tend to increase the connectivity around the left frontocentral and left frontoparietal areas and to decrease the posterior midline area. While in SSD, group D showed a lack of activation around midline area, leaving a separated, lateralised connectivity (increasing in the left-frontal and decreasing in the right-central compared to Baseline). This result suggests the importance of maintaining the brain activity around the midline area as a successful gaming strategy. Moreover, midline area has been reported as the system responsible to a self-referential thought and self-evaluation [190, 191]. Midline areas also included in the brain's major networks, e.g. DMN and SN [184, 192].

On the other hand, the DTF results in group ND show that, despite having the similar connectivity pattern coming from the frontal area like in group D, the group showed a significant decrease of connectivity in the fronto-parietal network that is coming from the parietal channels, as well as in the localised parietal area, in all frequency bands. This indicates that the group not only failed to regulate a frequency specific parietal activity during gaming, but also, they show less active fronto-parietal network, suggesting a lower level of task engagement performed during gaming.

DTF results from group D and from group ND during SSD consistently showing a decrease of connections that are coming from the left fronto-central area. This activity can be associated with the activation of the left dlPFC, a structure that has been linked to planning and perceptual decision making [193, 194] and has been reported to be active in multiple competitive experiments [81, 84]. However, the lateralization of brain connectivity detected by DTF is very different to the lateralization pattern found in GC. This difference will be discussed later in the chapter.

Furthermore, the frequency specific increase of connection in group D from Pz and Cz, suggest that only the targeted area (Pz) can modify their connectivity within a specific frequency band. In addition, taken from the sLORETA results in alpha band presented in Chapter IV, the highest increase of source activation and the highest count of increased source activation during BSD, all were found in precuneus, a portion of parietal cortex that is located closer to the midline area [170], while precuneus activity in SSD was not frequency-specific. This result can be associated with our DTF results in alpha band, where the increase of connectivity from Pz to Cz was found in alpha band (as well as in the frequency which might overlap with alpha, i.e. theta and lower beta band), only during BSD.

Similarly with intra-brain GC, DTF comparison between groups show that, even during resting, the two groups displayed statistically different Baseline connectivity in all frequency bands, with higher connectivity around the centro-parietal area was found in group D, while group ND exhibited higher frontal connectivity. **These connectivity differences during resting might be useful to predict a successful/non-successful gaming interaction [45, 183]**, in line with the results found in intra-brain GC as well in spatial alpha power distribution in Chapter IV.

Inter-brain GC

Inter-brain GC analysis revealed the influence of the engagement level of the players to the social aspect of the game, with the gaming performance. Best gaming performance in both groups was achieved when there are more significant inter-connections found (e.g. from group D to group ND in BSD) and when there are more channels actively sending the significant inter-connections (from group ND to group D in SSD). Moreover, the lack of significant connections from group D to group ND in both conditions, may reflect the tendency of isolation by the players when they tried to perform better, as presented by

Fallani et al. [85] that the weaker significant connections during defective gaming interaction compared to collaboration may reflect selfish behaviour. Additionally, the inter-connectivity in our results may not necessarily depicting that signal is physically transmitted between brains during interaction. However, our results managed to show that the gaming paradigm is not only depending on the player's individual performance (based on their own brain activity), but also depending on the level of engagement to their opponent's performance.

Notable findings

Our study analysed the brain intra- and inter- connectivity as a response to competitive interaction in an alpha operant-conditioning training paradigm. We found that different method of multivariate connectivity analyses, i.e. GC and DTF, might show different results, particularly evident after the statistical analysis comparing gaming condition with Baseline. The differences between these two methods have been discussed before by Eichler [195], stating that despite the close relation in concept between the two methods in estimating directed connectivity, DTF estimates the total information affecting one time series on another, while GC mainly estimates the direct effect that one series can give to another. Moreover, GC can have the tendency to promote type I spurious causality, which likely to cause a false detection of a direct effect between two time series [195], while DTF detects not only a direct effect but also a cascade effect [196]. Different connectivity detection during Baseline and gaming by these two methods, consequently, resulted different trend of brain activation pattern after statistical analysis. However, both approaches are equally needed in our study to provide connectivity information in both time and frequency domain.

Moreover, we found that intra-brain connectivity results in this study to some extent, complement the single-brain analysis electrophysiological signatures, performed in the previous chapter (Chapter IV). Our results revealed that significant connectivity changes in a specific frequency band might appear, despite the power spectral density results did not find any significant activation in the localised area. These significant connections displayed the brain activity as multiple separate networks and depicted their influences on each other during resting and active states. In addition, we found that individual intra-brain connectivity during resting is potentially useful in predicting gaming performance. Lastly, we also revealed the inter-brain connections between

players, suggesting that the level of engagement to the social aspect of the game is related to the gaming performance.

Limitations

The limitations of this study including small number of channels as well as the shorter time-series length that were used in connectivity analysis. A larger number of channels that evenly distributed throughout the brain areas will provide a better connectivity resolution. Faster computational facility was also required in order to perform connectivity analysis efficiently. Inter-brain synchrony analysis could be added for future direction to provide the information of inter-brain synchronization activity when competitive interaction is present [197, 198]. Moreover, there is always a room to increase the number of players in order to get better and more precise group statistical results.

5.5 Conclusion

The study performed intra- and inter- brain connectivity analysis of the data obtained by multi-user competitive BCI game that is based on alpha band operant conditioning. Our results suggest that group D outperformed group ND regardless the gaming outcome. Intra-brain connectivity results showed the effort of group D to upregulate their parietal activity within the alpha frequency band while keeping their engagement level to the task, which is characterised by the activation of fronto-parietal control network. Results in group D also proposed the role of midline activity for a successful gaming strategy. In contrast, group ND did not show any indication of successful parietal alpha regulation nor a higher level of task engagement. Our results also found that Baseline connectivity might be useful in predicting the gaming performance, as the groups showed a different resting connectivity pattern. Finally, our inter-brain connectivity results suggest that successful gaming condition was achieved when the players are not only modulating their intra-brain activity, but also while being engaged to the social aspect of the game.

Chapter VI

Collaborative Multi-user BCI:
Part I – Electrophysiological Features

6.1 Introduction

Collaborative behaviour holds a crucial role in human survival- along with competitive behaviour. If competitive behaviour is beneficial to win a limited resource, collaborative behaviour is beneficial in gaining a communal benefit [199]. Due to the frequency of collaborative interaction in everyday scenarios and its importance in maintaining human survival as a community, it is important to explore and to understand the underlying principles of collaborative interaction.

Li and Nam [76] defined the collaborative Brain-Computer Interface (BCI) as a non-invasive BCI system that maintains collaborative interaction by working in a group of users, where the users can help each other to perform their joint task. In BCI application, collaborative interaction has been used in several BCI paradigm, for example: in collaborative BCI speller [200], collaborative BCI for robot arm control [76], collaborative BCI involving joint decision making [73], and in collaborative BCI gaming [62, 63]. These studies have proven the possibilities of employing social interaction in a BCI system, as well as the possibilities to combine brain signatures from multiple

individuals as the input of the system and potentially bring benefits to the outcome of the system.

The brain areas such as bilateral superior frontal gyrus, parietal cortex, right inferior frontal gyrus, and anterior insula, were reported to be activated by cooperative behaviour [78, 79, 89]. The superior frontal gyrus activity is related to a higher memory processing [201, 202] as well as serving a broader functions, from cognitive to motor functions [203], and the right inferior frontal gyrus has been linked to response inhibition and to attention during a target detection task [165-167]. The superior parietal cortex activity is related to cognitive functions, such as in spatial shifting during goal-directed attention state [204-206], and in working memory [207], and the inferior parietal cortex was reported to be involved in the mental construction of an object shape [208] - which is relevant to the experimental task in Connect Four [78]. Lastly, the anterior insula has been linked to emotional awareness and conscious perception [175, 209-212].

In this study we performed a synchronic [82] collaborative multi-user BCI gaming that is based on the alpha band, non-verbalised operant conditioning. The recorded EEG signatures from the gaming experiment were measured and analysed during both resting and gaming states, in order to explore the cortical dynamics that occur during an active synchronic collaborative task. Moreover, the alpha EEG activity, particularly during resting has been proposed as a predictor of a successful cognitive performance [42, 151]. In this study, EEG activity resting state of two collaborating players will be recorded and compared, to see whether there is any resting state EEG characteristic that can predict collaborative BCI performance.

6.2 Methods

6.2.1 EEG experiments

Twenty healthy able-bodied adults (age 26.9 ± 3.7 years old, eight females and twelve males) participated in EEG experiments where they were grouped into ten pairs based on the order of their appearance. Eight out of ten pairs of participants have known each other before the experiment. They signed the written consent form prior to the experiments. Ethical permission was granted by the University's College Ethical Committee.

The groups of players were divided as group D (dominant players) and group ND (non-dominant players). The dominance level between players was determined based on

the highest average gaming RA (out of six sub-sessions in each session) in the first two gaming sessions. If during the first two sessions the pair is tied in achieving the higher average gaming RA, then the highest average gaming RA between players for the first two sessions was used to determine the dominance between players. The gaming conditions were classified into 'successful' sub-session and 'non-successful' sub-sessions based on their gaming performance in the third session. These conditions were decided based on the gaming sub-session where both players gained the highest\lowest mutual score. These conditions include: the gaming sub-session with the highest score (Best/BE) and the gaming sub-session with the lowest score (Worst/WO). Further technical details regarding the game interface, the scoring rules, the EEG experiment setup and sessions have been covered in the Method chapter (Chapter III).

6.2.2 Data analysis

Power Spectral Analysis

Prior the analysis, each continuous time-series was segmented into 4 s epoch with a 50% overlap. Statistical analysis for individual RA at Pz and individual alpha (IA) peak frequency at Pz from all sessions were performed in SPSS 25.0 (IBM corp., USA). Prior the statistical analysis, Shaphiro-Wilk normality test was performed to confirm the normal distribution of the data. Non-parametric statistical analyses were performed for RA and scores data, by using Kruskal-Wallis H test and Wilcoxon signed rank (WSR) test. Kruskal-Wallis H test was used to compare more than two groups and the WSR was used to compare two groups, i.e. the group of players, D and ND. Parametric statistical analyses were performed for IA peak frequency data, by using. two-way ANOVA to compare different variables (Session and Group) in one measurement.

All multi-channel EEG data were uploaded to a STUDY structure in EEGLAB for power spectral group analysis. The uploaded data were divided into groups (i.e. group D and ND) and into different conditions (i.e. Baseline, BE, and WO). In a STUDY structure, spatial distribution of power for all conditions was calculated in the four pre-defined frequency bands (theta, alpha, lower beta, and higher beta). A non-parametric unpaired permutation analysis for 800 repetition ($p<0.05$) [139] was applied to test the statistical significance of the absolute power difference between groups or conditions in each frequency band, and False Discovery Rate (FDR) statistical correction method [152] was applied for multiple comparisons.

Fractal Dimension

The k*max* value of 8, as the most commonly used k*max* values in EEG signal analysis [109, 153, 154] and a 5 s epoch length were chosen for HFD analysis. Prior the HFD analysis, data were down-sampled to 128 Hz sampling frequency [155]. Non-parametric statistical analysis such as Kruskal-Wallis H test and WSR test were performed to the mean HFD data. Kruskal-Wallis H test was used to compare the three conditions (i.e. Baseline, BE, and WO) and WSR test was used to compare the two groups (i.e. group D and ND). Both tests used confidence level of 95%. Holm-Bonferroni statistical correction method was applied for multiple comparisons [156].

Source Localisation

Prior exporting data to sLORETA, 2 minutes of data length from each participant from each condition (i.e. Baseline, BE, and WO) were divided into 4 s epoch with no overlap. The 2 minutes length was chosen based on the duration of the shortest time-series (baseline), due to the data length uniformity required for paired statistic in sLORETA. The extracted 2 minutes data were taken from the two minutes where the average RA of both players have the smallest difference (for BE) and the biggest difference (for WO). Four pre-defined frequency bands (theta, alpha, lower beta, and higher beta) were selected. Paired t-test statistic was performed using statistical analysis package implemented in sLORETA, to compare each of the gaming condition with the baseline in each frequency band. The paired t-statistic was calculated on log-transformed data with 5000 non-parametric randomizations ($p < 0.05$).

Post-experimental Workload Analysis

The post-experimental NASA-TLX scales obtained from all participants were compared to find the statistically significant difference between sessions and between groups, for each category (i.e. mental, physical, temporal, performance, effort, and frustration). Non-parametric statistical tests were performed in SPSS, namely Friedmann's test, WSR test, and Kruskal-Wallis H test ($p < 0.05$). Friedmann's test was used to determine any statistical difference between measurements across multiple variables, namely Sessions and Groups (i.e. group D and ND). WSR test was used to compare the scores between groups in each session for each category. Lastly, Kruskal-Wallis H test was performed to measure the statistical difference in the overall NASA-TLX scores over sessions.

6.3 Results

6.3.1 RA, scoring performance, and individual alpha peak frequency

In this study, RA was used as a control parameter in gaming, where the scoring results were used to measure the user's gaming performance, as previously mentioned in the method section. Figure 6.1 shows the absolute power at alpha band from Pz during Baseline and during the highest-scoring sub-session, averaged from all players in each group, for each session. This figure indicates that, on average, both groups managed to adjust their alpha power during gaming to a similar level over time.

Table 6.1 and Table 6.2 show the daily sessions' average (mean ±std) and median (median and interquartile range), respectively of the % gaming RA recorded from channel Pz along with the gaming scores from all participants across sub-sessions. Due to the large values of standard deviations of % RA, the results of median and interquartile range were also provided.

Table 6.3 shows Kruskal-Wallis H test ($p < 0.05$) found no significant difference over sessions in both RA and gaming scores in both groups. Table 6.4 shows that a Wilcoxon signed-rank test ($p < 0.05$) found a significant difference in RA and in gaming scores, in both groups between Session I and II, and between Session I and III. Our results indicate an increased trend for RA over sessions and a decreased trend for scores.

Figure 6.2 shows the individual pre-gaming Baseline RA for both groups over the three sessions (Fig. 6.2 a-c), mean ±std in each daily session of each single player's gaming RA (Fig. 6.2d-f) averaged over 10 players in each group, and the average gaming scores (Fig. 6.2g) in each pair. Mean ±std were used in this figure to show the impact of NC on the individual RA, which is more evident if the graphs are presented based on mean. The bars with an asterisk represent the mean gaming RA from players with higher Baseline RA in each pair (as displayed in Fig. 6.2a-c). The players marked with asterisks received feedback of their normalised RA (NC was applied to their RA during gaming) instead of their real RA. In some pairs, the players who had larger/smaller Baseline RA can be different on different days, they can be from either group D or ND (i.e. pair 3, Session II and III, pair 8 and 9 on Session III). This was likely caused by the individual variability of natural alpha power that not only differs from one person to another, but also from one day to another [157]. However, in a special case like in pair 3, since the dominance between players was decided prior the experiment on Session III, the player

with the highest Baseline RA in the past two experiments was chosen as the dominant player-thus that player received NC, even though that player ended up having lower Baseline RA on Session III. In this case, it is suggested that the length of EEG preparation time during the last session, where multiple channels were used, might affect the Baseline RA level of the player. Generally, the different daily individual Baseline RA suggests how important it is to adjust the individual alpha threshold daily before each gaming session. To show the difference of average RA values before and after NC was applied, the mean ± std of the players' individual RA in each daily session without NC application were presented in Figure 6.3

Furthermore, the individual alpha (IA) peak at Pz in all participants from each session was measured from the power spectrum within the wide band of 6-16 Hz [158], from eyes-closed baseline and eyes-open baseline. The frequency of the beginning of 'ascent' and the end of 'descent' from the dominant power spectrum within the selected frequency width were visually inspected and the decrease of spectral power by more than 20% from the eyes-closed condition to the eyes-open condition was defined as IA frequency with the maximum decrease as the maximum peak [158]. Table 6.5 shows the different IA peak frequency in each player from one session to another, along with the mean ± std of IA peak frequency for each group, in every session. Shapiro-Wilk normality test was performed prior the parametric statistical analysis to confirm the normal distribution of the IA peak frequency data. Table 6.6 shows that two-way ANOVA analysis ($p < 0.05$) found no significant difference in IA peak frequency across sessions and between groups in each session.

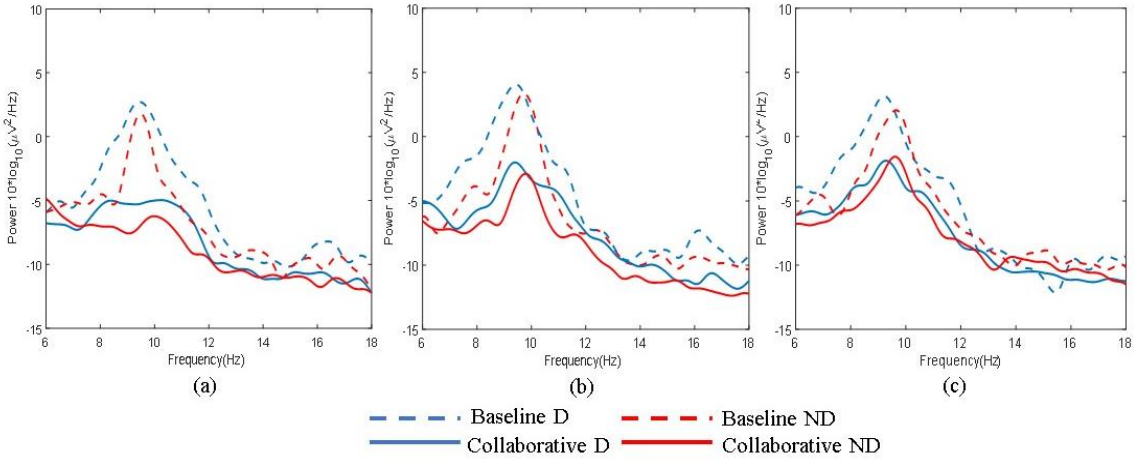

Figure 6.1 The absolute alpha power spectral density at Pz, averaged from all baselines and all the highest-scoring sub-sessions, in (a) Session I, (b) Session II, and (c) Session III, for each group of players.

Table 6.1 The mean ± std of RA from channel Pz and gaming scores from all pairs averaged over all sub-sessions on each experimental day.

RA		
Session	***Group D***	***Group ND***
I	29.0 ± 13.4	20.5 ± 13.6
II	33.4 ± 15.3	24.5 ± 12.7
III	31.9 ± 16.2	24.1 ± 12.5
Scores		
Session		
I	95.4± 76.2	
II	62.5± 40.7	
III	68.7±31.1	

Table 6.2 The median and interquartile range of RA from channel Pz, and gaming scores from all pairs averaged over all sub-sessions on each experimental day.

RA		
Session	***Group D***	***Group ND***
I	28.6(18.7-37.5)	16.4(11.9-28.8)
II	28.8(20.7-41.3)	20.8(15.5-29.0)
III	29.5(17.7-38.5)	20.9(17.1-24.9)
Scores		
Session		
I	89.5(32.25-113.5)	
II	65(23-95.25)	
III	74(45.5-91.75)	

Table 6.3 Table of *p*-values and H scores obtained from Kruskal-Wallis H test ($p<0.05$) of RA (of each group) and gaming scores, across all sessions.

RA		
Group	*p*-values	H-statistic
D	0.392	1.875
ND	0.054	5.838
Scores		
	p-values	H-statistic
	0.060	5.624

Table 6.4 Table of *p*-values and *Z* scores obtained from Wilcoxon signed rank test ($p<0.05$) of RA (of each group) and gaming scores between sessions.

RA			
Group	**Comparison**	***p*-values**	***Z*-score**
D	*Session I - Session II	0.000	-4.226
	*Session I - Session III	0.017	-2.385
	Session II- Session III	0.074	-1.789
ND	*Session I - Session II	0.000	-4.829
	*Session I - Session III	0.003	-2.967
	Session II- Session III	0.208	-1.259
Scores			
	Comparison	***p*-values**	***Z*-score**
	*Session I - Session II	1.6×10^{-7}	-5.300
	*Session I - Session III	0.004	-2.853
	Session II- Session III	0.325	-0.983

*) Comparison with significant *p*-value.

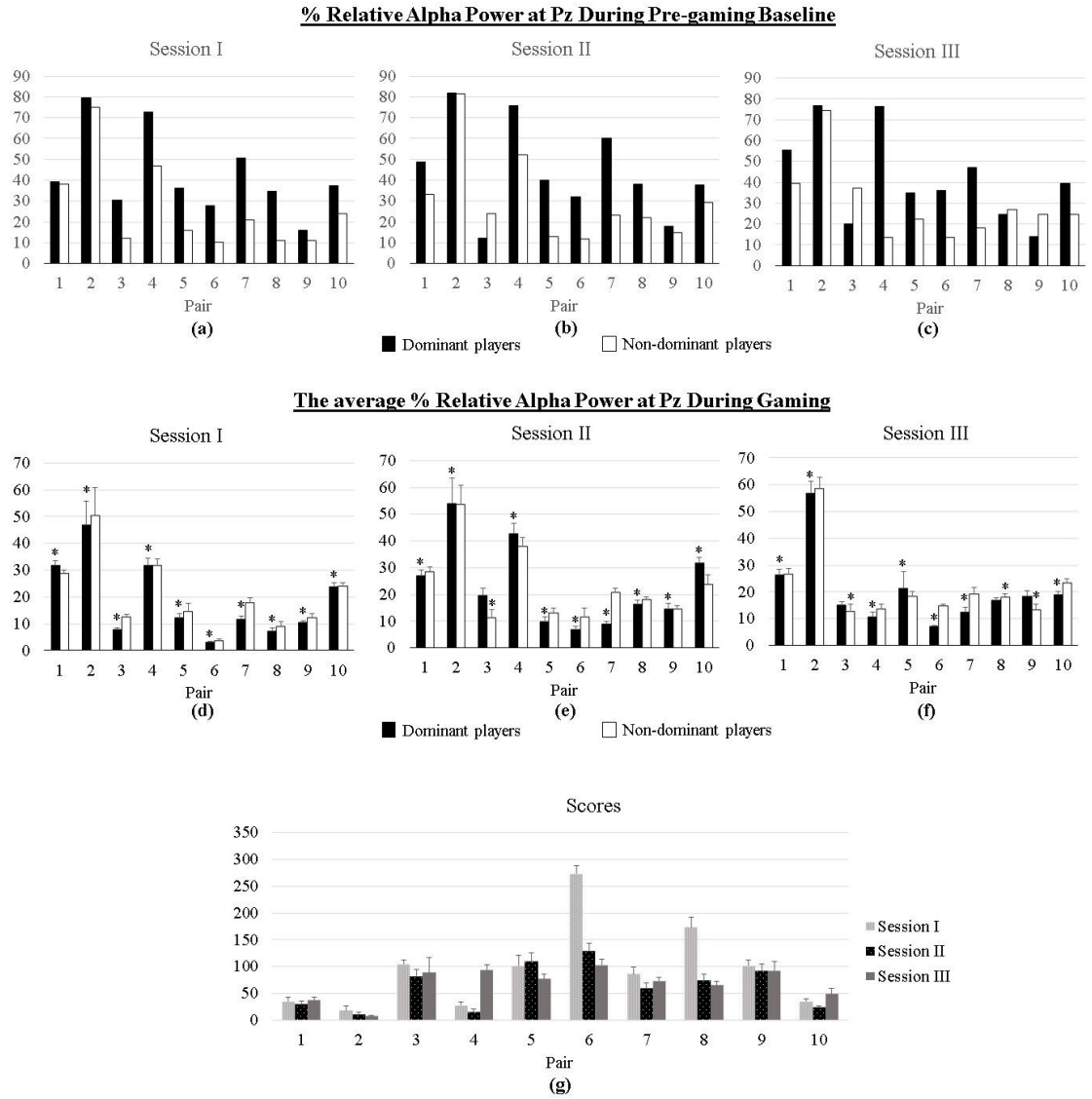

Figure 6.2 (a-c) The individual pre-gaming RA (%) at Pz for all players in all three experimental sessions. (d-f) Mean ± std of individual gaming RA (%) at Pz during gaming and (g) the gaming scores, all taken from all sub-sessions in each session -the bars with asterisks (d-f) indicate normalisation of RA during gaming.

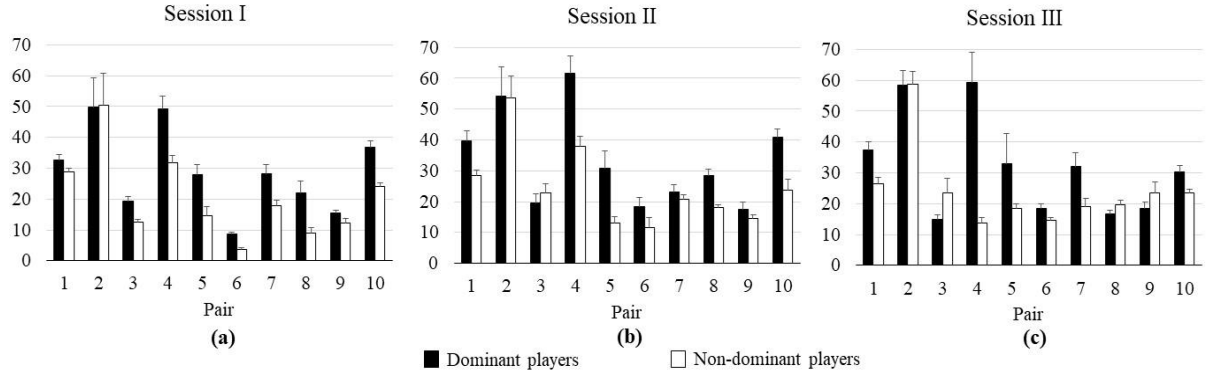

Figure 6.3 (a-c) Mean ± std of the real individual gaming RA (%) at Pz from all sub-sessions, without any normalisation applied during gaming.

Table 6.5 The mean ± std of IA peak frequency (Hz) from each participant in each session.

Pair	Session I		Session II		Session III	
	D	**ND**	**D**	**ND**	**D**	**ND**
1	9.7	10.3	11.8	10.8	10.1	10.8
2	10	9.6	10.1	9.5	10.9	10.6
3	10.6	9.1	10.8	9.0	10.4	10.7
4	9.5	10.2	9.7	9.8	9.9	10.1
5	9.8	10.1	9.8	10.6	9.9	10.7
6	11.3	10.6	11.2	10.3	11.7	10.3
7	9.2	10.4	7.8	11.2	8.7	10.8
8	7.6	10.2	7.7	10.3	7.7	10.2
9	9.7	9.8	9.8	9.5	9.5	9.6
10	9.5	8.7	9.5	8.6	9.5	8.8
mean	**9.7**	**9.9**	**9.8**	**9.9**	**9.8**	**10.3**
std	0.9	0.6	1.3	0.8	1.1	0.6

Table 6.6 Table of F and *p*-values obtained from two-way ANOVA analysis ($p<0.05$) of IA peak frequency.

Comparison	**F**	***p*-value**
Group	0.676	0.415
Session	0.131	0.877
Group*Session	0.014	0.986

6.3.2 Spatial power spectral density

The spatial power spectral density obtained from the multichannel EEG data between tasks (i.e. between Baseline and BE, between Baseline and WO, and between BE and WO) in each group (i.e. group D and ND) and between groups in each condition were compared by performing a non-parametric unpaired permutation test ($p<0.05$) in a STUDY structure provided in EEGLAB.

The comparison of the power spatial distribution between Baseline and BE in group D (Fig. 6.4) shows a significant decrease of alpha around the central and parietal channels, such as at C1, C3, C5, Cz, CP3, CPz, CP6, Pz, and P4. There were no significant changes in other frequency bands. While between Baseline and WO in group D (Fig. 6.5), significant decrease of power was only found in lower beta at FC6. No significant changes were found at control channel Pz in any frequency band during WO, indicating that the winning strategy for group D was to significantly decrease their parietal alpha power

(which was also extended to the central area), presumably to maintain their alpha level as close as possible to their partner's alpha level.

No significant changes were found in any channel in group ND in neither of gaming conditions as compared to Baseline, in any frequency bands (Fig. 6.6 and 6.7) after FDR correction, indicating the group's inability to modulate alpha power regardless the gaming condition. Although uncorrected power changes were found around the left hemisphere in beta band for both BE and WO conditions.

The comparison of spatial power distribution between BE and WO in group D (Fig. 6.8) and group ND (Fig. 6.9) show no significant difference was found in any channel in both groups, in any frequency band, after FDR correction. However, uncorrected power differences were found around the central channels in alpha band for group D, and in some frontal and parietal channels in beta band for group ND.

The comparison of spatial power distribution between groups in different condition, i.e. Baseline (Fig. 6.10), BE (Fig. 6.11), and WO (Fig. 6.12), were presented with 16 out of 32 channels of group D that are the same location to the channels of group ND, due to the unequal number of channels used by the two groups during the experiment. Significantly lower occipital alpha power was found in group ND compared to group D, during Baseline and BE. No significant difference of alpha power was found at Pz for all three conditions. Significantly lower theta power was found in bilateral occipital channels in group ND compared to group D, during BE. There was no significant difference found beta bands for Baseline and BE, and there was no significant difference found in any frequency band for WO.

Generally lower posterior alpha power shown by group ND consequently forced group D to maintain their alpha power closer to their partner's level, thus explaining the significant decrease of alpha occurred during BE (Fig. 6.4). Moreover, the significantly higher natural occipital alpha, found in group D during Baseline (Fig. 6.10) might support the idea that resting alpha can be used to predict learning ability in alpha neurofeedback training [42], as based on our results, group D shows the ability to adjust their alpha activity easier than group ND.

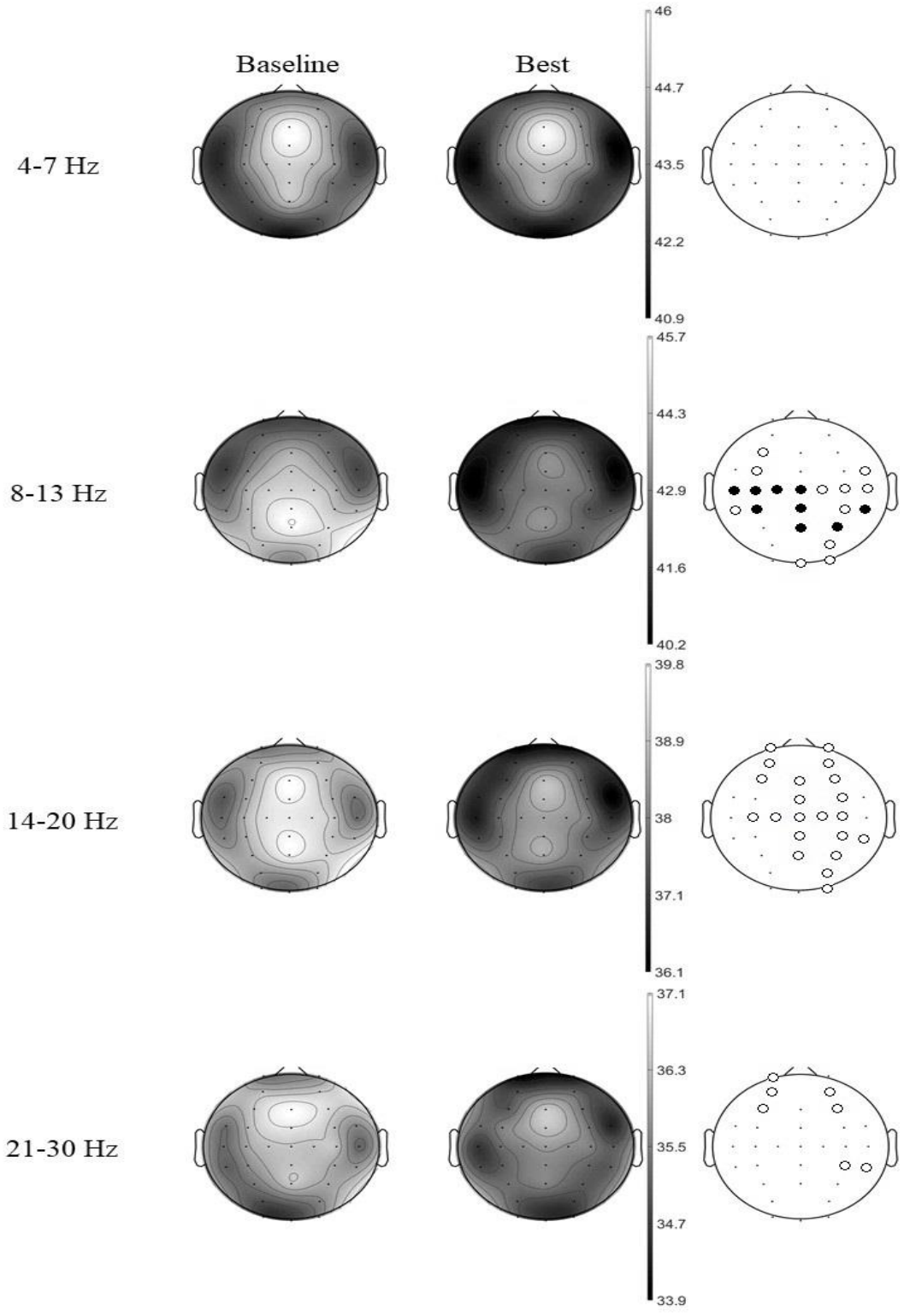

Figure 6.4 Non-parametric permutation test (p<0.05) between Baseline and BE for group D, in theta, alpha, lower beta, and higher beta frequency bands. FDR correction (p<0.05) was applied for multiple comparison. White dot represents a significant difference before FDR correction and black dot represents a significant power difference after FDR correction.

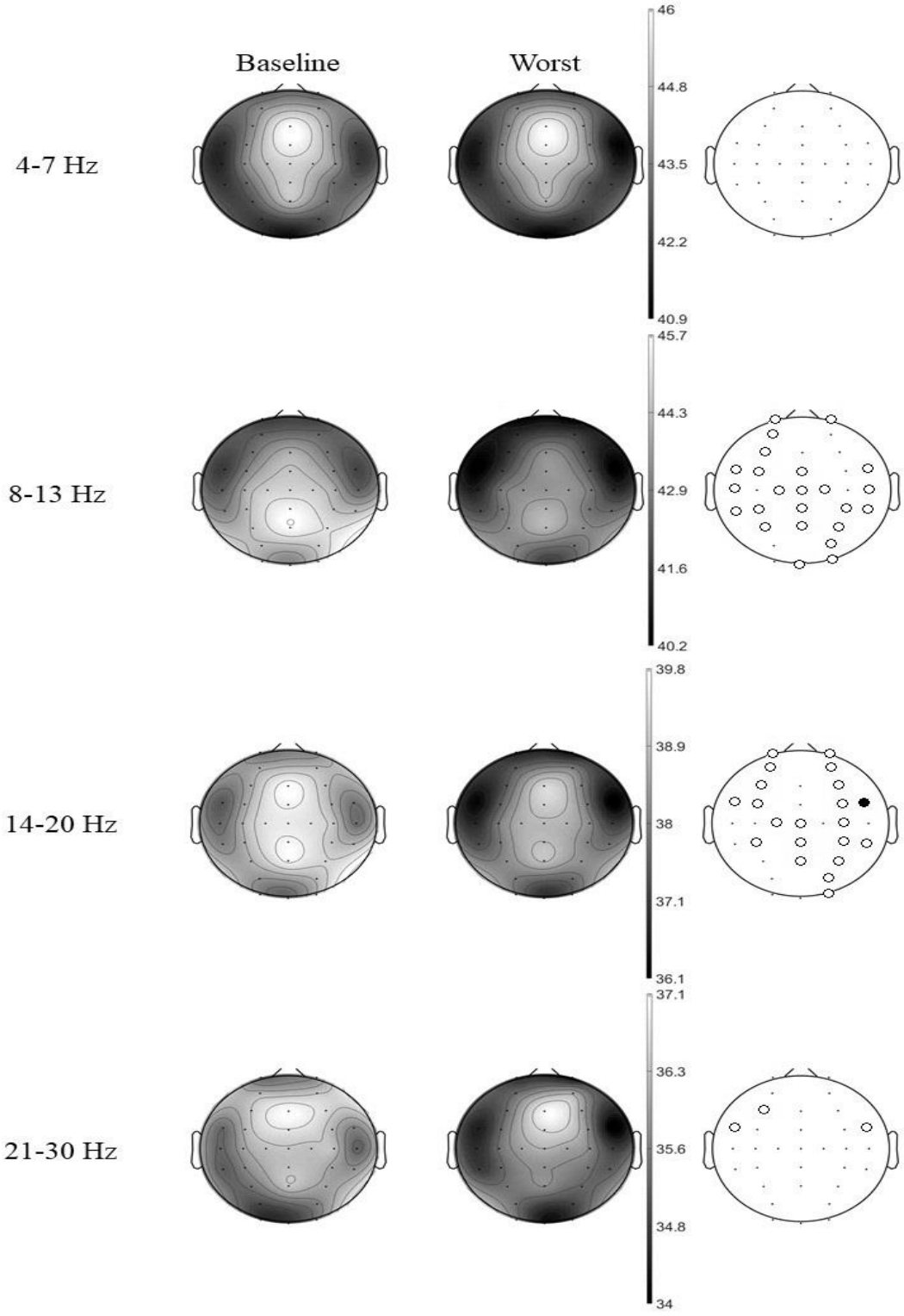

Figure 6.5 Non-parametric permutation test (p<0.05) between the Baseline and WO for group D, in theta, alpha, lower beta, and higher beta frequency bands FDR correction (p<0.05) was applied for multiple comparison. White dot represents a significant difference before FDR correction and black dot represents a significant power difference after FDR correction.

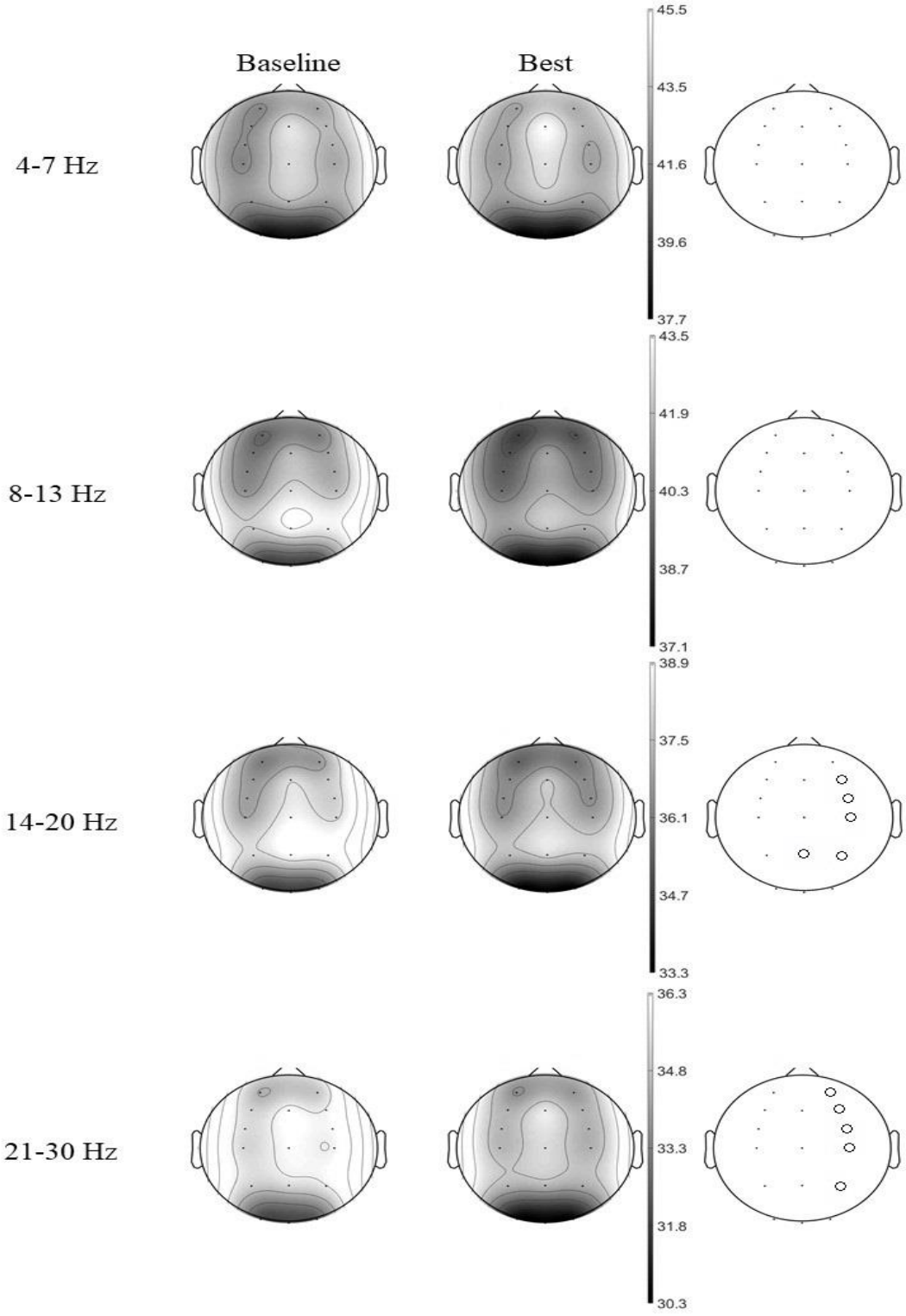

Figure 6.6 Non-parametric permutation test (p<0.05) between Baseline and BE for group ND, in theta, alpha, lower beta, and higher beta frequency bands. FDR correction (p<0.05) was applied for multiple comparison. White dot represents a significant difference before FDR correction and no significant power changes were found after FDR was applied.

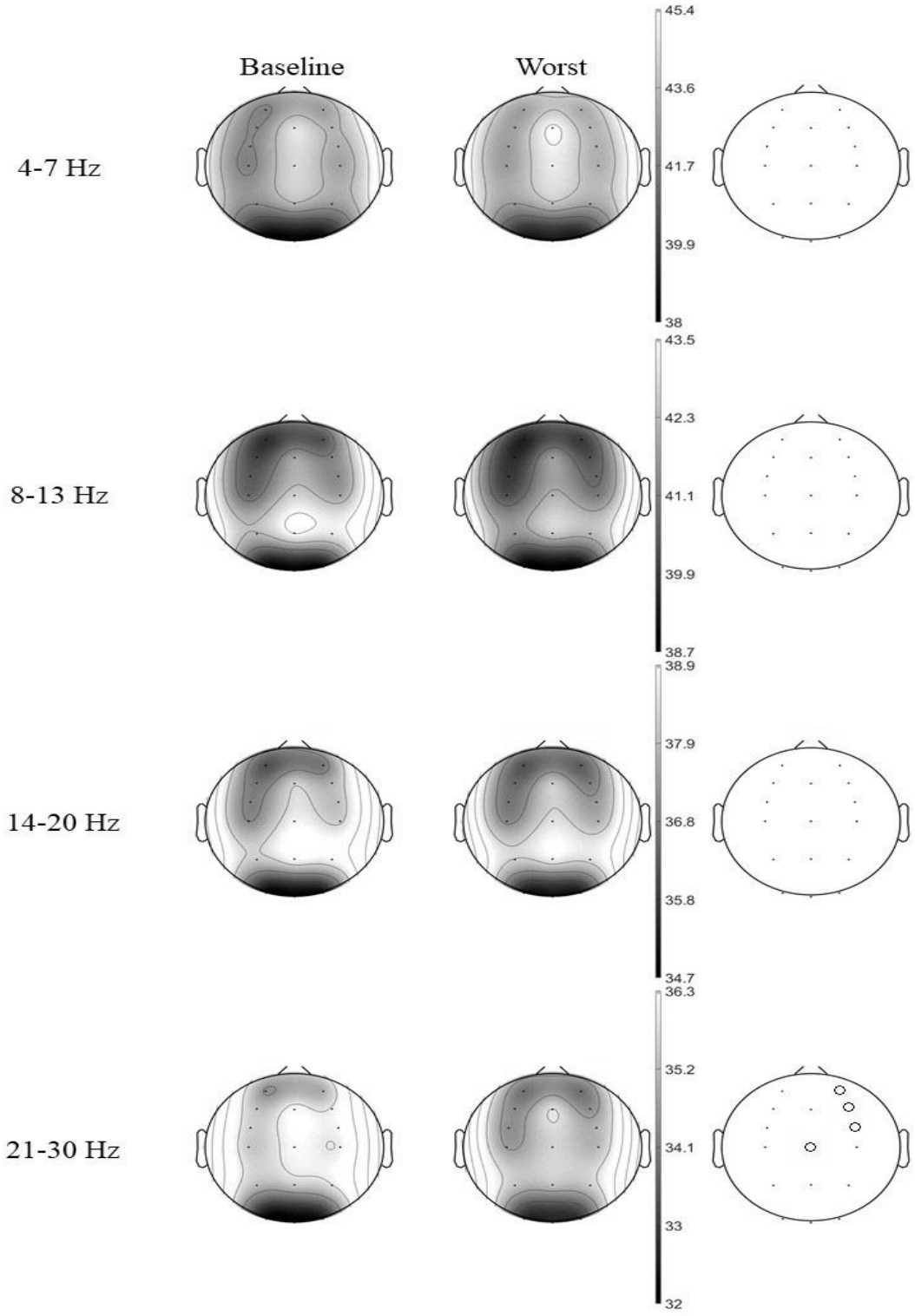

Figure 6.7 Non-parametric permutation test ($p<0.05$) between Baseline and WO for group ND, in theta, alpha, lower beta, and higher beta frequency bands. FDR correction ($p<0.05$) was applied for multiple comparison. White dot represents a significant difference before FDR correction and no significant power changes were found after FDR was applied.

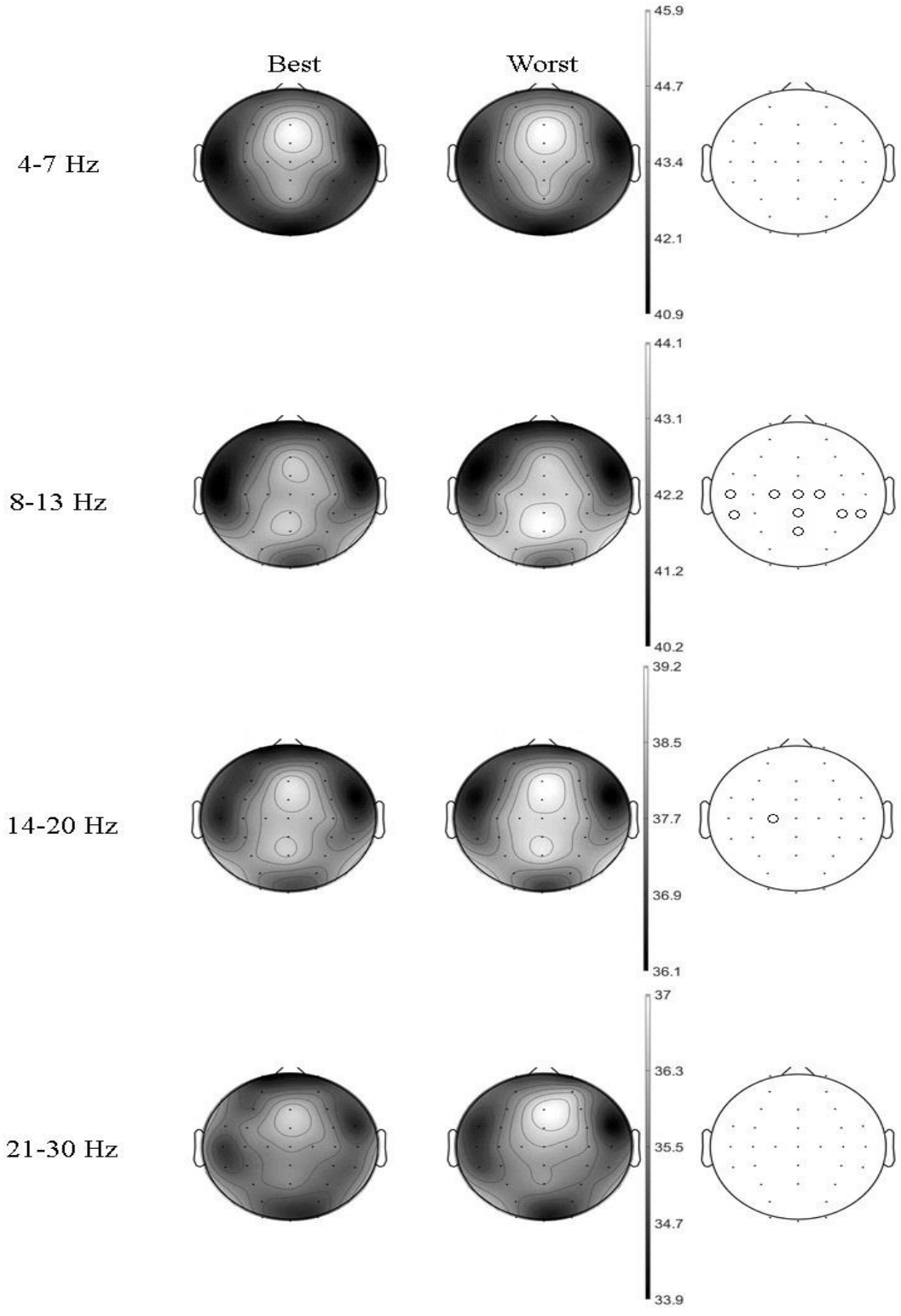

Figure 6.8 Non-parametric permutation test (p<0.05) between BE and WO for group D, in theta, alpha, lower beta, and higher beta frequency bands. FDR correction (p<0.05) was applied for multiple comparison. White dot represents a significant difference before FDR correction and no significant power changes were found after FDR was applied.

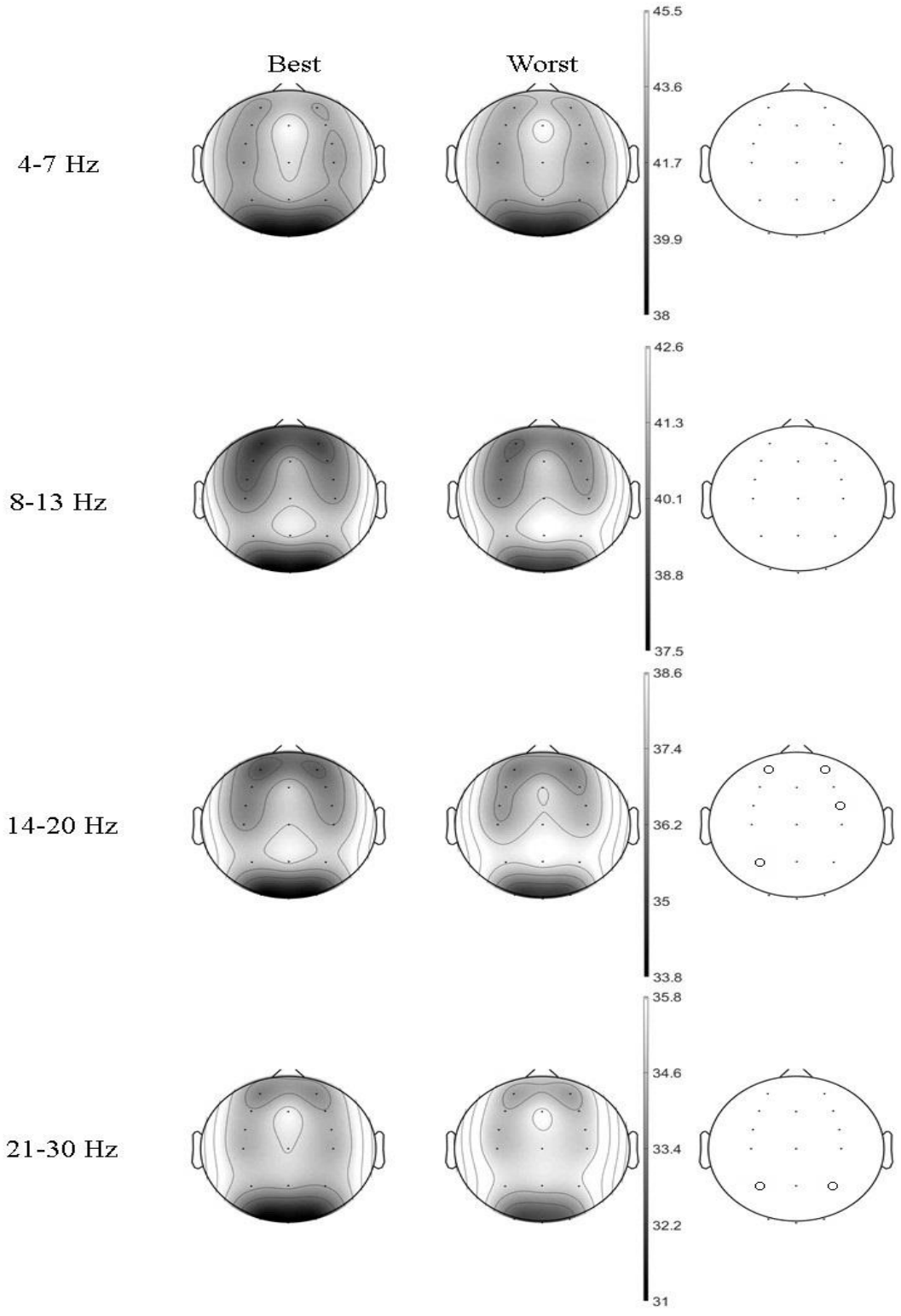

Figure 6.9 Non-parametric permutation test ($p<0.05$) between BE and WO for group ND, in theta, alpha, lower beta, and higher beta frequency bands. FDR correction ($p<0.05$) was applied for multiple comparison. White dot represents a significant difference before FDR correction and no significant power changes were found after FDR was applied.

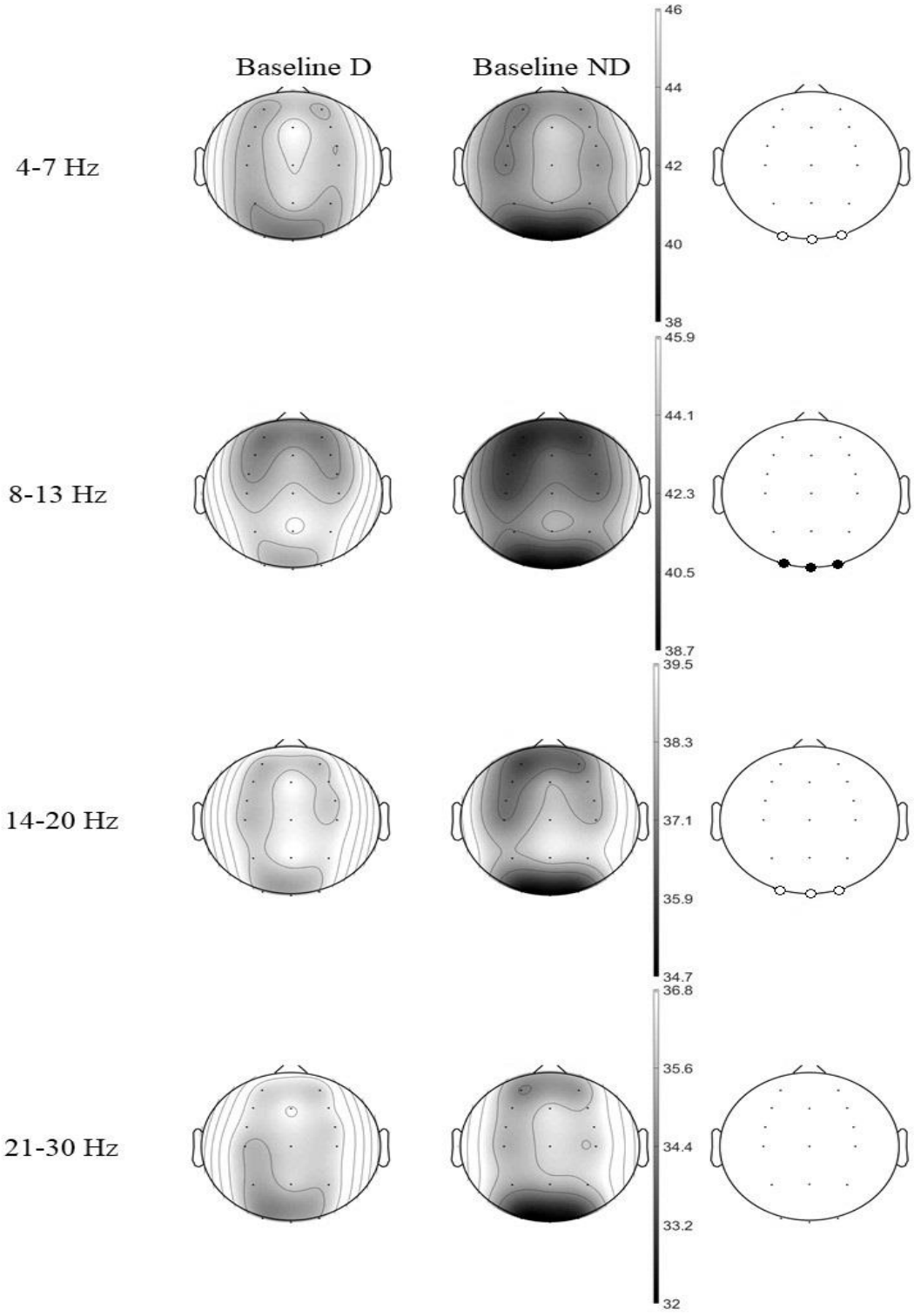

Figure 6.10 Non-parametric permutation test (p<0.05) between groups in the Baseline condition, in theta, alpha, lower beta, and higher beta frequency bands. FDR correction (p<0.05) was applied for multiple comparison. White dot represents a significant difference before FDR correction and black dot represents a significant power difference after FDR correction.

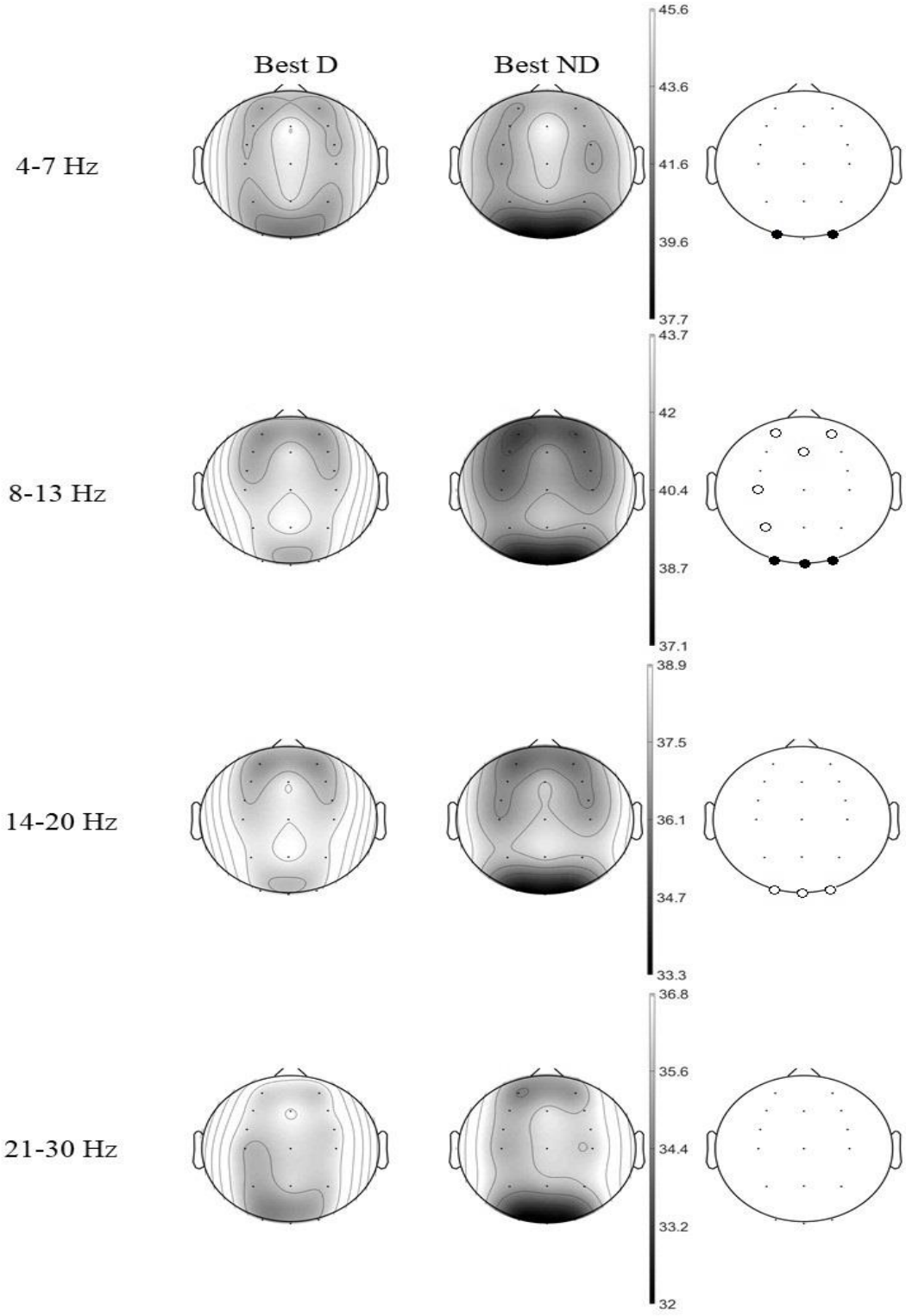

Figure 6.11 Non-parametric permutation test (p<0.05) between groups in BE condition, in theta, alpha, lower beta, and higher beta frequency bands. FDR correction (p<0.05) was applied for multiple comparison. White dot represents a significant difference before FDR correction and black dot represents a significant power difference after FDR correction.

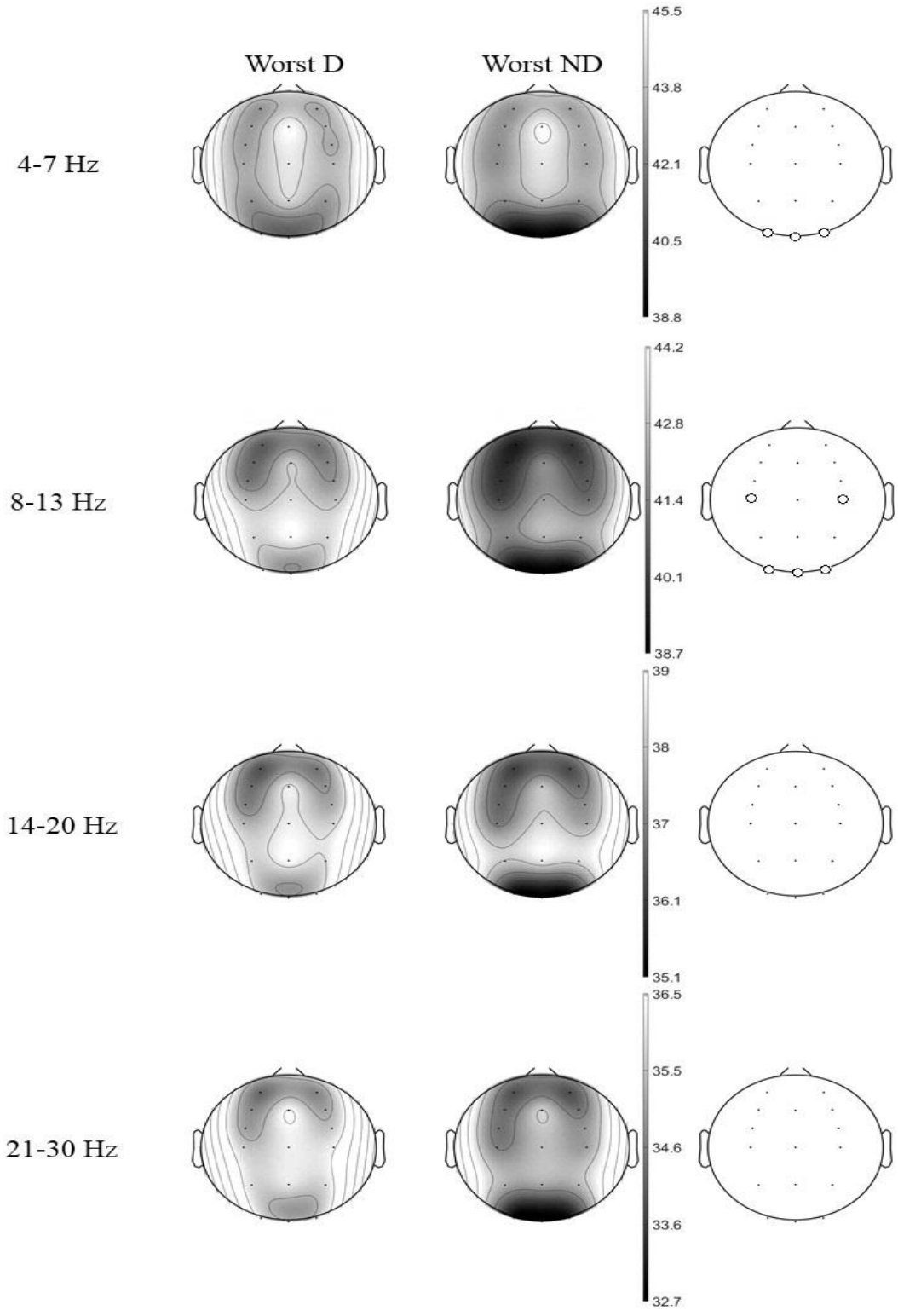

Figure 6.12 Non-parametric permutation test ($p<0.05$) between groups in the WO condition, in theta, alpha, lower beta, and higher beta frequency bands. FDR correction ($p<0.05$) was applied for multiple comparison. White dot represents a significant difference before FDR correction and no significant power changes were found after FDR was applied.

6.3.3 Higuchi Fractal Dimension

To measure the signal complexity during different conditions in all channels, Higuchi's Fractal Dimension (HFD) analysis was performed in both groups. Non-parametric statistical test such as Wilcoxon signed rank test and Kruskal-Wallis H test (both with $p<0.05$) were performed to see if there are any significant changes in EEG signal complexity between conditions at any of the channels.

Figure 6.13 shows the mean ± std of HFD for different conditions (i.e. Baseline, BE, and WO) in each group. The trend of average HFD values shows an increasing trend of HFD values in group D during gaming at the posterior channels compared to Baseline. While results in group ND indicate an increasing trend of HFD values at the posterior channels only occurs during WO, compared to Baseline and BE. This increasing trend might reflect the tendency of both players to decrease their EEG power in the posterior area during gaming, which only reported to be significant in the alpha band of group D during BE. However, Kruskal-Wallis H test ($p<0.05$) of HFD values found no significant difference of HFD values from Baseline, BE, and WO, in each group (Appendix 2.1). Wilcoxon signed rank test found significant HFD increase from Baseline to BE in group D at channel P3 and O1 (Appendix 2.2), however there were no significant changes found in any channel, after Holm-Bonferroni correction ($p<0.05$) was applied. No significant changes were found between Baseline and BE in group ND at any channels, and between Baseline and WO at any channels in both groups (Appendix 2.2 and 2.3).

Figure 6.14 shows the mean ± std of HFD for both groups in each different condition (i.e. Baseline, BE, and WO). The trend of average HFD values during Baseline and WO show lower HFD in group D over the central, parietal, and occipital area, compared to group ND. While BE shows a very similar trend for both groups However, Wilcoxon signed rank test comparing the two groups found no significant differences in HFD at any channel, for the three conditions (Appendix 2.4).

Antagonistic relationship between HFD values and alpha activity has been previously reported [107, 110]. However, no significant HFD differences were found between Baseline and BE at central and parietal channels and between groups in Baseline and BE at occipital channels, where significantly different alpha power were found, thus our results failed to verify the antagonistic relationship between HFD and alpha activity. However, despite the lack of statistical significance, Figure 6.13 shows the HFD trend at

channel Pz between the two groups during Baseline and during gaming, where HFD at Pz in group D was lower compared to group ND in Baseline and WO, and became very similar in BE. This trend might indicate the groups' effort to mutually maintain their EEG activity at Pz at the same level.

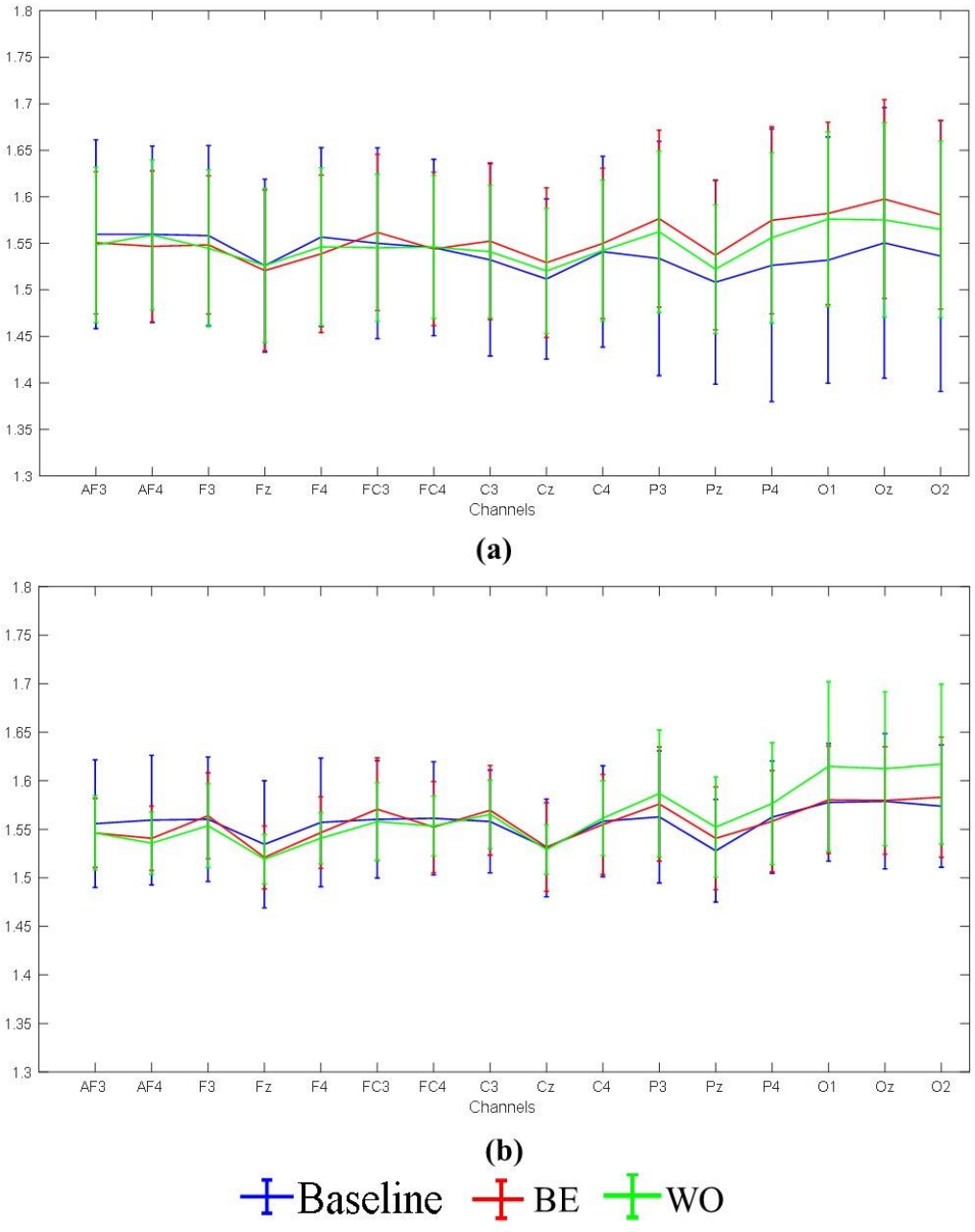

Figure 6.13 Mean ± std of HFD in all channels during Baseline, BE, and WO condition for (a) group D and (b) group ND.

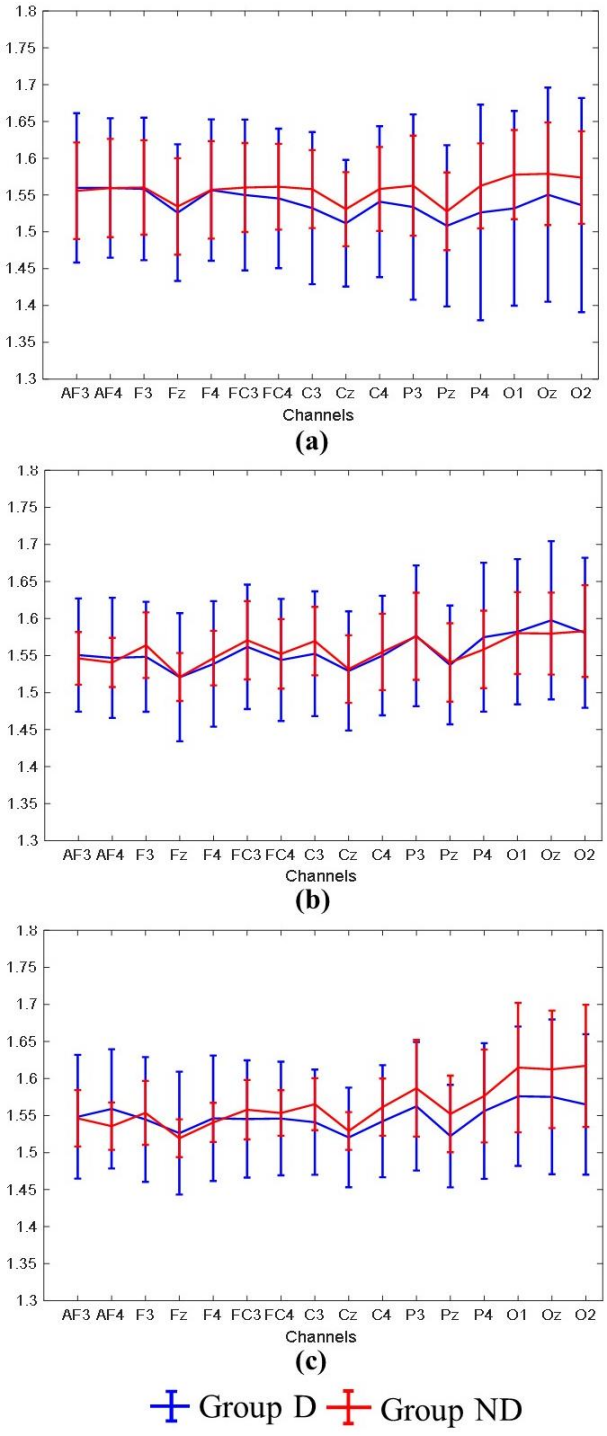

Figure 6.14 Mean ± std of HFD in all channels of both groups during (a) Baseline, (b) BE, and (c) WO.

6.3.4 sLORETA source localisation analysis

Source localisation activity was performed only for group D during the third experimental day. Non-parametric paired t-statistics ($p < 0.05$) which is implemented in the sLORETA software was applied to the source localisation data for each gaming condition against Baseline (BE against Baseline, and WO against Baseline), and for BE against WO, for each frequency band. Statistically significant voxel activation was found between BE and Baseline conditions in higher beta band and between WO and Baseline conditions in lower beta band (Appendix 2.5 and 2.6). No statistical significance was found in the other frequency bands in any of the gaming conditions. No statistical significance was found in any frequency between BE and WO. The maximum and minimum strength of the voxel values from each comparison for each frequency band, was reported in Table 6.7 and 6.8, Figure 6.15, 6.16, and 6.17. The areas with the highest count of positive and negative source activity were presented in Table 6.9 and 6.10.

For BE against Baseline (Fig. 6.15), increase of source activity were found around the bilateral frontocentral, left temporo-parietal area in theta band, around the left temporal and left parietal areas in alpha band, and around the left parietal and left occipital areas in both beta bands. Decreasing source activity were found around the right parietal and occipital areas in theta band, around the right parietal-occipital-temporal area in alpha band, and around the bilateral frontal area in both beta bands. The largest increase of source activity were found around the cingulate cortex and the frontocentral area in theta band, around the parietal cortex in alpha band, and around the occipital cortex in both beta bands- including the significant increase found in higher beta band (Appendix 2.5), with the majority of increasing activity occurred in the left hemisphere. Whereas the largest decrease of source activity were found around the parietal cortex in theta band, around the parahippocampal gyrus (limbic lobe) in alpha and lower beta bands, and around the frontal cortex in higher beta band, with the majority of decreasing activity occurred in the right hemisphere.

For WO against Baseline (Fig. 6.16), increase of source activity were found mainly around bilateral central and the left parietal areas in theta band, and around the left parietal and left occipital areas in alpha and both beta bands. Decreasing source activity were found around the right frontal-temporal-parietal areas in theta and alpha bands, and around the right frontal and right temporal areas in both beta bands. The largest increase

of source activity were found around the right frontal cortex in theta band, around the left parietal cortex in alpha and lower beta bands- including the significant increase found for lower beta band (Appendix 2.6), and around the left occipital cortex in higher beta band. Whereas the largest decreasing source activity were found around the right temporal cortex in theta band, around the right uncus (limbic lobe) in alpha band, and around the right frontal cortex for both beta bands, with the majority of decreasing activity occurred in the right hemisphere.

In both gaming conditions (BE and WO), the largest increase of source activity in alpha band, despite not significant, occurred in the parietal cortex and it is more alpha frequency-specific in BE, indicating the effort to modulate alpha from Pz by the players, which is in line with our spatial power distribution results. The significant increase of source activity in beta bands around the posterior area (parietal and occipital) might be related to visual attention task, as it was previously reported that occipital beta activity facilitates visual attention task [213, 214] . In both gaming conditions, the brain structures with the highest count of increased source activity was found in MFG for theta and alpha bands, and in precuneus for both beta bands, while the highest count of decreased source activity was found in precuneus for theta and alpha bands, and in MFG for both beta bands. This shows a clear activation pattern between MFG and precuneus that is specific to the lower and higher frequency bands.

For BE against WO (Fig. 6.17), higher source activity were found around the bilateral temporal area and bilateral frontal-temporal area in theta band, around the right temporal and right frontal areas in alpha band, and around the right temporo-parietal cortex in both beta bands. Whereas the lower source activity was found around the bilateral parietal cortex (postcentral gyrus) in theta and alpha bands and extended to the frontal area for both beta bands. The highest count of increased source activity was found in the superior temporal gyrus (STG) in all frequency bands and the highest count of decreased source activity was found in precuneus for theta, alpha, and lower beta bands, and in the medial frontal gyrus (medFG) for higher beta band.

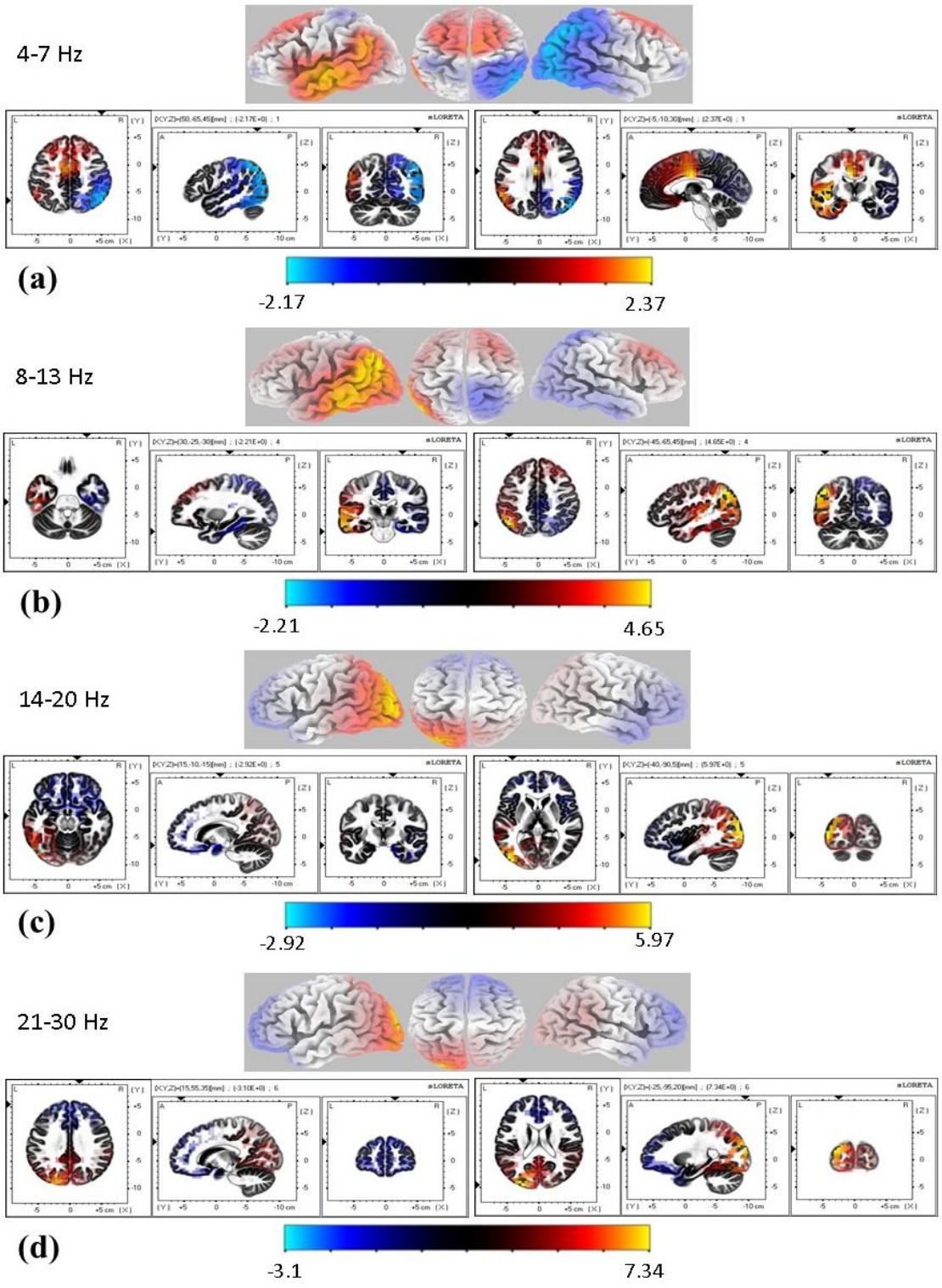

Figure 6.15 Paired t-statistics (p<0.05) of the source localisation via sLORETA between the average BE and the average Baseline condition of group D, in the frequency band of (a) theta, (b) alpha, (c) lower beta, and (d) higher beta. The figures inside the grey box is a 3D representation of the localisation map, and the boxes below it is the 3D slices representing the negative (left side) and the positive (right side) voxel values- blue for negative values and red to yellow for positive values. Voxel's coordinate positioning shown in the 3D slices figures is based on the Montreal Neurological Institute (MNI) coordinate system.

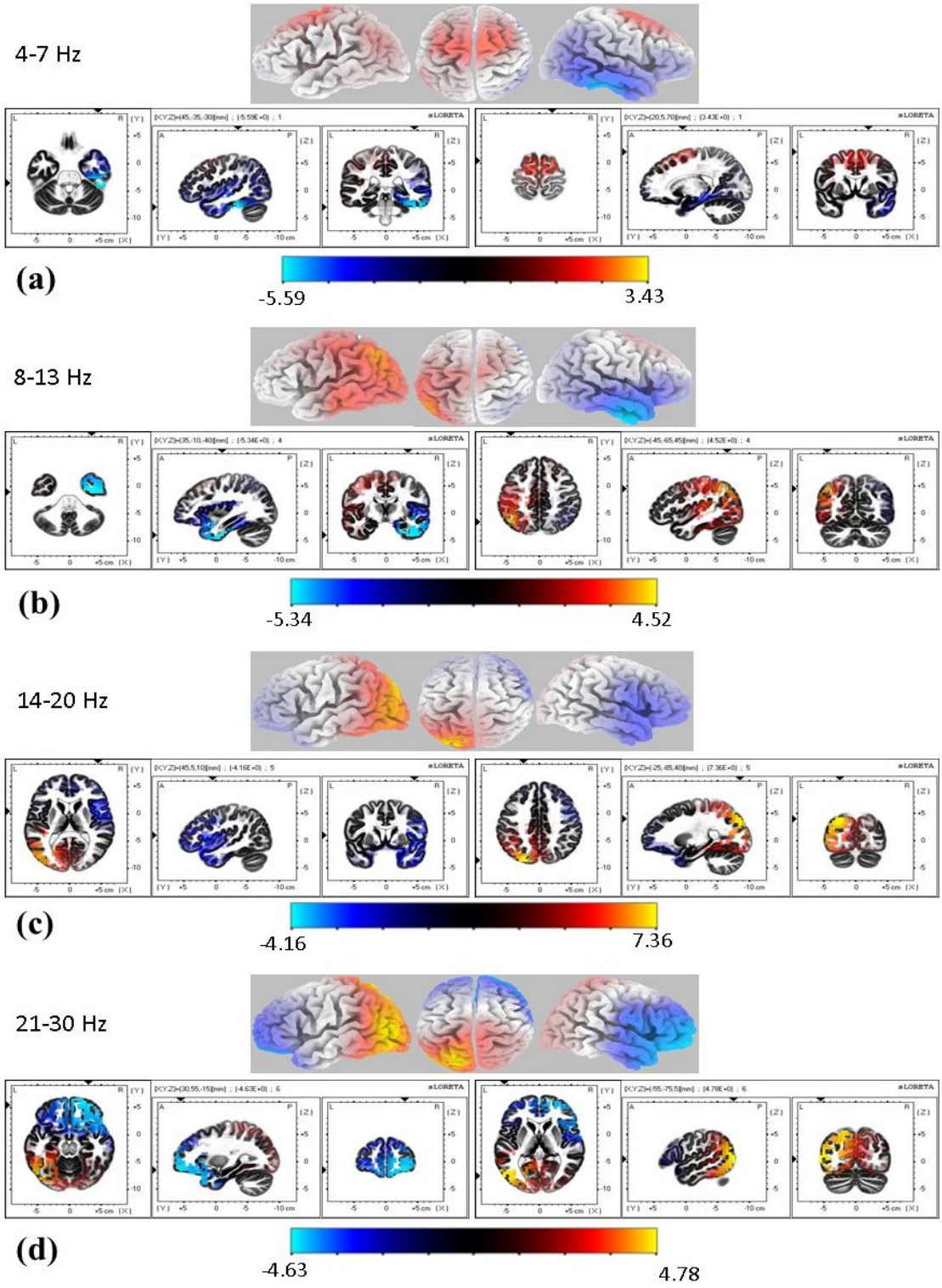

Figure 6.16 Paired t-statistics (p<0.05) of the source localisation via sLORETA between the average WO and the average Baseline condition of group D, in the frequency band of (a) theta, (b) alpha, (c) lower beta, and (d) higher beta. The figures inside the grey box is a 3D representation of the localisation map, and the boxes below it is the 3D slices representing the negative (left side) and the positive (right side) voxel values- blue for negative values and red to yellow for positive values. Voxel's coordinate positioning shown in the 3D slices figures is based on the Montreal Neurological Institute (MNI) coordinate system.

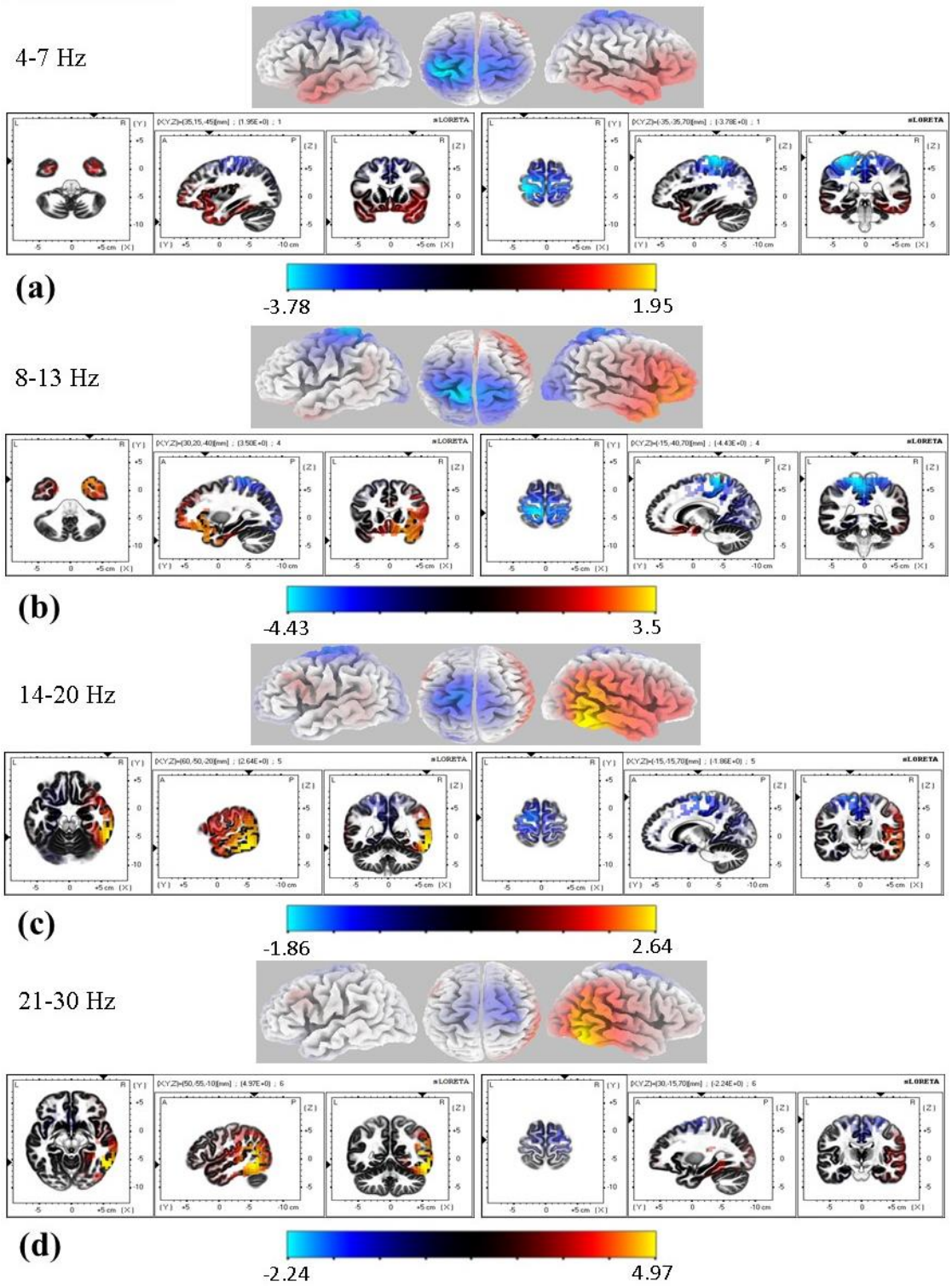

Figure 6.17 Paired t-statistics (p<0.05) of the source localisation via sLORETA between the average BE and the average WO conditions of group D, in the frequency band of (a) theta, (b) alpha, (c) lower beta, and (d) higher beta. The figures inside the grey box is a 3D representation of the localisation map, and the boxes below it is the 3D slices representing the negative (left side) and the positive (right side) voxel values- blue for negative values and red to yellow for positive values. Voxel's coordinate positioning shown in the 3D slices figures is based on the Montreal Neurological Institute (MNI) coordinate system.

Table 6.7 The location of the maximum and minimum voxel values obtained from paired t-test analysis in sLORETA between gaming condition (BE/WO) and Baseline.

	Frequency and dynamic		Brain lobe	Hem.	BA	Structure	Max/ Min value	MNI coordinate (x,y,z)
BE	Theta	Increase	Limbic	L	24	Cingulate Gyrus	2.37	-5,-10,30
		Decrease	Parietal	R	39	Inferior Parietal Lobule	-2.17	50,-65,45
	Alpha	Increase	Parietal	L	40	Inferior Parietal Lobule	4.65	-45,-65,45
		Decrease	Limbic	R	36	Parahippocampal Gyrus	-2.21	30,-25,-30
	Lower Beta	Increase	Occipital	L	19	Middle Occipital Gyrus	5.97	-40,-90,5
		Decrease	Limbic	R	28	Parahippocampal Gyrus	-2.92	15,-10,-15
	Higher Beta	Increase	Occipital	L	19	Cuneus	7.34	-25,-95,20
		Decrease	Frontal	R	9	Superior Frontal Gyrus	-3.1	15,55,35
WO	Theta	Increase	Frontal	R	6	Superior Frontal Gyrus	3.43	20,5,70
		Decrease	Temporal	R	20	Fusiform Gyrus	-5.59	45,-35,-30
	Alpha	Increase	Parietal	L	40	Inferior Parietal Lobule	4.52	-45,-65,45
		Decrease	Limbic	R	20	Uncus	-5.34	35,-10,-40
	Lower Beta	Increase	Parietal	L	19	Precuneus	7.36	-25,-85,40
		Decrease	Frontal	R	44	Precentral Gyrus	-4.16	45,5,10
	Higher Beta	Increase	Occipital	L	19	Middle Occipital Gyrus	4.78	-55,-75,5
		Decrease	Frontal	R	11	Superior Frontal Gyrus	-4.63	30,55,-15

*Hem. = Hemisphere

Table 6.8 The location of the maximum and minimum voxel values obtained from paired t-test analysis in sLORETA between BE and WO gaming conditions.

Frequency and dynamic		Brain Lobe	Hem.	BA	Structure	Max/Min value	MNI coordinate (x,y,z)
Theta	Increase	Temporal	R	38	Superior Temporal Gyrus	1.95	35,15,-45
	Decrease	Parietal	L	1	Postcentral Gyrus	-3.78	-35,-35,70
Alpha	Increase	Temporal	R	38	Superior Temporal Gyrus	3.5	30,20,-40
	Decrease	Parietal	L	3	Postcentral Gyrus	-4.43	-15,-40,70
Lower Beta	Increase	Temporal	R	20	Inferior Temporal Gyrus	2.64	60,-50,-20
	Decrease	Frontal	L	6	Superior Frontal Gyrus	-1.86	-15,-15,70
Higher Beta	Increase	Temporal	R	37	Inferior Temporal Gyrus	4.97	50,-55,-10
	Decrease	Frontal	R	6	Precentral Gyrus	-2.24	30,-15,70

*Hem. = Hemisphere

Table 6.9 The brain structures with the highest counts of source activity, found after paired t-test analysis in sLORETA between gaming condition (BE/WO) and Baseline.

Task	Frequency	Activity	Brain Structure	No. of voxels
BE	Theta	Increase	Middle Frontal Gyrus	341
		Decrease	Precuneus	337
	Alpha	Increase	Middle Frontal Gyrus	462
		Decrease	Precuneus	296
	Lower beta	Increase	Precuneus	364
		Decrease	Middle Frontal Gyrus	482
	Higher beta	Increase	Precuneus	364
		Decrease	Middle Frontal Gyrus	480
WO	Theta	Increase	Middle Frontal Gyrus	316
		Decrease	Superior Temporal Gyrus	254
	Alpha	Increase	Middle Frontal Gyrus	318
		Decrease	Inferior Frontal Gyrus	255
	Lower beta	Increase	Precuneus	364
		Decrease	Middle Frontal Gyrus	445
	Higher beta	Increase	Precuneus	364
		Decrease	Middle Frontal Gyrus	434

Table 6.10 The brain structures with the highest counts of source activity, found after paired t-test analysis in sLORETA between BE and WO.

Task	Frequency	Activity	Brain Structure	No. of voxels
BE vs WO	Theta	Increase	Superior Temporal Gyrus	383
		Decrease	Precuneus	364
	Alpha	Increase	Superior Temporal Gyrus	333
		Decrease	Precuneus	364
	Lower beta	Increase	Superior Temporal Gyrus	308
		Decrease	Precuneus	338
	Higher beta	Increase	Superior Temporal Gyrus	277
		Decrease	Medial Frontal Gyrus	352

6.3.5 Nasa TLX questionnaire

The perceived experimental workload was measured by performing non-parametric statistical analysis to the post-experiment NASA-TLX questionnaire scores, shown in Figure 6.18 and 6.19. Table 6.11 shows that no significant difference was found from Friedman's test (p<0.05) across the three sessions in any category for neither of the groups, and Wilcoxon signed rank test (p<0.05) comparing the scores between groups in each category found a statistically significant difference in performance category in Session II. Lastly, no significant difference was found from Kruskal-Wallis H test (p<0.05) when comparing the overall scores across the three sessions for each group.

Three categories (i.e., mental, effort, and performance) are shown to have generally higher scores compare to the rest categories, with the higher scores achieved in 'performance' , followed by 'effort' and 'mental' in group D, whereas in group ND the generally higher scores were achieved in 'mental', followed by 'effort' and 'performance' categories. The trend of higher scores in 'performance' by group D reflects that the group felt that they performed poorly, particularly in Session II, despite the average gaming scores from that Session Is not the lowest. Moreover, despite being non-statistically significant, the scores trend for 'effort' shows that both players felt that they put similar level of effort to the game, which is important in our collaborative gaming setup. Meanwhile, the scores trend for group ND indicate that they felt higher mental load as well as physical load during the last experimental session. The results of the mean overall data (Fig. 6.19c) may suggest that both groups perceived the workload of the experiment in a relatively similar way from time to time regardless their gaming outcome (the average gaming scores is the highest during Session I and the lowest during Session III).

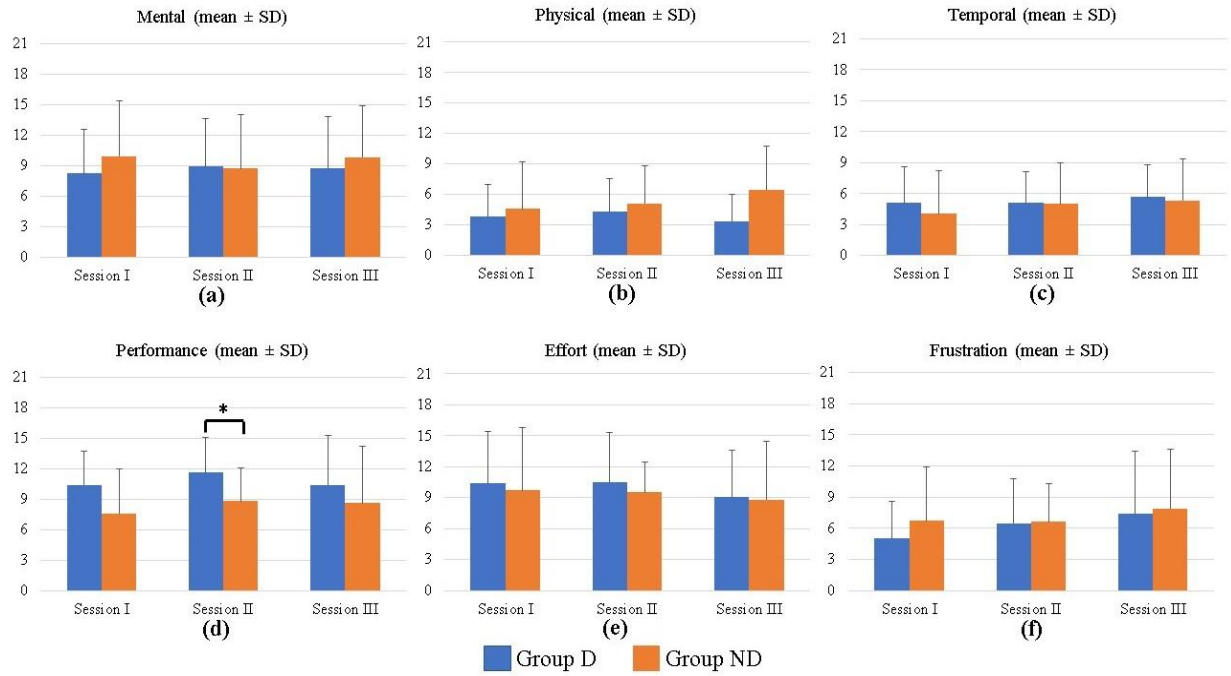

Figure 6.18 The mean ± std of NASA-TLX scores in each category, such as (a) mental, (b) physical, (c) temporal, (d) performance, (e) effort, and (f) frustration, for both groups of players in three different sessions.

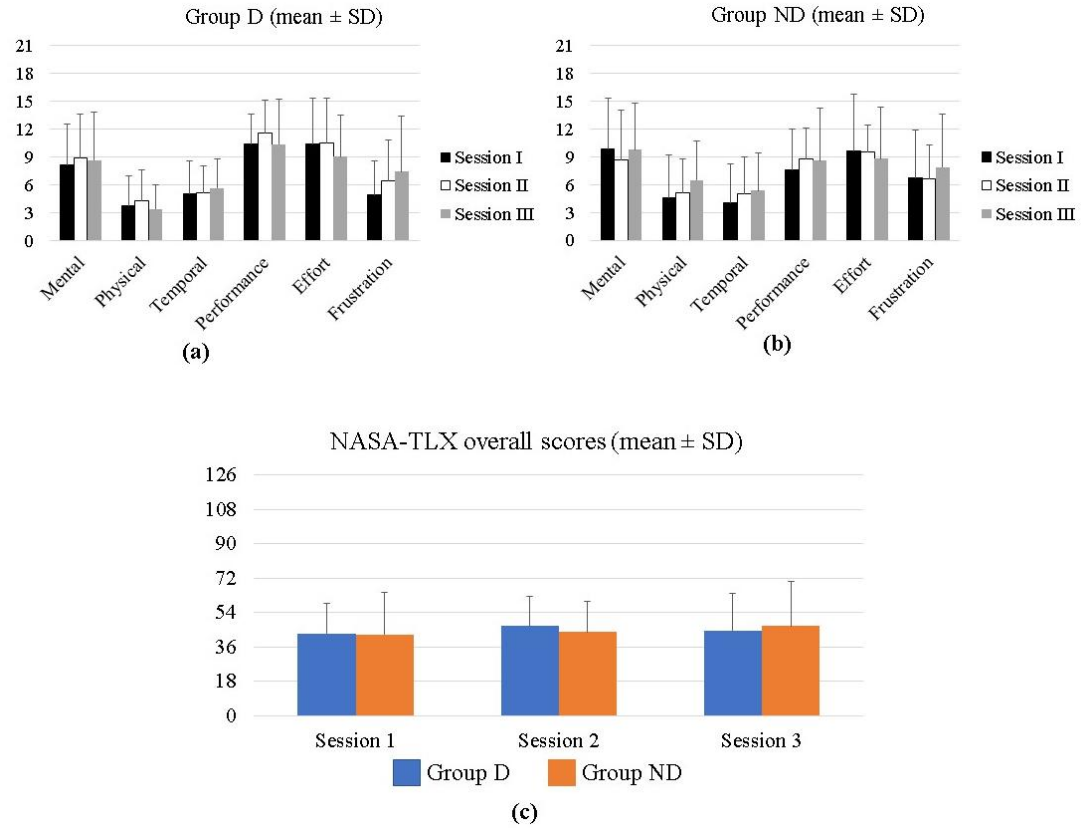

Figure 6.19 The mean ± std of (a-b) NASA-TLX scores in each group, for each category in three sessions, and (c) the overall scores (summed up of the scores in all category) for each group in three sessions.

Table 6.11 Table of statistical results of NASA-TLX scores for each category and for the overall score.

Statistical test	Category	Group	*p*-values	Chi-square
Friedman Test	Mental	D	0.972	0.057
		ND	0.886	0.242
	Physical	D	0.066	5.429
		ND	0.078	5.091
	Temporal	D	0.508	1.355
		ND	0.135	4.000
	Performance	D	0.966	0.069
		ND	0.452	1.588
	Effort	D	0.607	1.000
		ND	0.558	1.167
	Frustration	D	0.128	4.108
		ND	0.779	0.500
	Category	**Session**	***p*-values**	**Z-scores**
Wilcoxon signed rank test	Mental	I	0.283	-1.074
		II	0.553	-0.593
		III	0.528	-0.632
	Physical	I	0.483	-0.701
		II	0.506	-0.665
		III	0.066	-1.836
	Temporal	I	0.248	-1.156
		II	0.959	-0.051
		III	1.000	.000
	*Performance	I	0.122	-1.548
		*II	0.038	-2.075
		III	0.283	-1.074
	Effort	I	0.553	-0.594
		II	0.575	-0.561
		III	0.760	-0.306
	Frustration	I	0.441	-0.771
		II	0.767	-0.297
		III	0.833	-0.210
	Category	**Group**	***p*-values**	**H-statistic**
Kruskal-Wallis H test	Overall score across sessions	D	0.750	0.576
		ND	0.651	0.859

*) Category with significant *p*-value.

6.4 Discussion

Multi-user BCI collaborative gaming has been previously studied [62, 63], however, the information regarding the EEG signatures changes within the interacting brain are still relatively limited. In this study, we analysed the EEG signatures in order to explore the impact of collaborative multi-user BCI gaming on brain cortical activity. Three different conditions were measured such as pre-gaming Baseline, BE, and WO, with the players divided into group D and group ND. The results from each offline analysis (i.e. power spectral analysis, signal complexity analysis, and source localisation analysis) were compared based on the types of task (i.e. Baseline-BE ,Baseline-WO, and BE-WO) and based on the groups (i.e. between group D and group ND). Power spectral density analysis found that alpha activity at Pz behaved differently in group D and group ND. The consequence of a successful game control was characterised by downregulation of alpha power at Pz by group D, and by the similar level of Pz alpha activity to the level during Baseline by group ND. Source localisation analysis found a significant increase of source activity in beta band around the parieto-occipital cortex of group D in both gaming conditions. Resting EEG comparison between group revealed a different posterior alpha activity between the group, suggesting the use of resting alpha activity as a predictor for the game performance.

RA, scoring performance, and individual alpha peak frequency

Statistically significant increases of RA at Pz was found between Session I and II, and Session I and III in both groups, and statistically significant decrease of scores was found also from Session I and II, and Session I and III. The trend for averaged RA in both groups increases from Session I to II and slightly decreases from Session II and III, whereas the trend for the average score is consistently decreasing from Session I to Session III.

Both players significantly increased their RA level at the same period (from Session I to Session II and from Session I to Session III), suggesting that multi-user BCI collaborative training is beneficial for communal learning. In order to explore about the community learning, more training sessions as well as a post-experimental assessment were required in the experimental design [34, 35]. Furthermore, collaborative BCI training has been proposed for other community benefits, e.g. in improving communal decision making [73, 74, 215]. Both groups show that their RA level was better during the later training sessions, compared to the first one. However, there is no significant

increase of RA was found from Session II to Session III, indicating a plateau during the later sessions, which is likely caused by the physical factors e.g. heavier EEG setup from the multi-channel EEG used in the third experiment. Higher number of channels requires longer pre-experimental preparation time and it is physically heavy for the players' head as they were used to the single-channel setup in the previous sessions, the longer preparation time and the higher physical effort may increase the chance of fatigue or distraction. The decreasing scores over sessions might reflect the complexity of the task, which not only required the players to adjust alpha power to the same level with each other but also to retain the condition in a certain duration in order to score.

Similar to the competitive experiment in Chapter IV, the neurofeedback training paradigm used in this study did not apply a typical single-user neurofeedback paradigm, where the user was asked to maintain their brain activity based on their own feedback. In this study, the users were asked to maintain their RA level at Pz while engaging in a collaborative interaction- and for them to train not only based on their own performance, but also in relative to their opponent's performance/feedback which is changing over time. It is therefore important to take other factors into account (e.g. the collaborating member of the pair and their natural Baseline RA level) in measuring the efficacy of this training paradigm.

The comparison of average RA before and after NC application revealed that the players who were labelled as 'NC' (players who received NC), managed to equalise their RA to the same level as their partner. In this case, normalisation of RA might play a role in helping the players to navigate the collaborative game. This indicates that unlike in competitive gaming where NC was used to avoid bias, in collaborative gaming there is a chance for NC to create bias, suggesting that the scores were not only achieved due to the players gaming strategy, but also due to the normalisation. It was also revealed that the player who were labelled 'NC' in a pair was not always the same person in every session. This is caused by the variability of natural alpha power that can vary from one person to another due to multiple reasons, such as the time of the day, caffeine consumption, and fatigue [216-219], suggesting that it is important to perform a daily adjustment of individual RA threshold. Our individual alpha peak frequency analysis further confirmed this variability, showing that alpha peak can be varied for one person over different days [158, 161].

Spatial distribution of power spectral density

The spatial power distribution results revealed a significant decrease of alpha power around the left-central and centroparietal areas, including channel Pz, during BE compared to Baseline in group D. Whereas during the same condition, group ND did not show any statistically significant changes in any channel/frequency band. This indicates that group D was the one that actively (and efficiently) adapting their power level to the same level as group ND, hence the significant alpha decrease at Pz, while group ND maintained their alpha power level similar to Baseline. Generally, alpha activity has been known to be higher during resting state, especially during eyes-closed, and supressed by eyes-opening as well as by higher cognitive processing [160]. The decrease of alpha power shown by group D in the results of this study may also indicate the level of task engagement. The participants were asked to control alpha, however since the majority of group ND have lower alpha, group D had to level down their alpha power in order to gain better join-performance. Additionally, group comparisons revealed that during resting, group D showed a significantly higher natural alpha around the occipital area compared to group ND. This suggests that individuals with higher natural alpha power during resting can adjust their alpha level easier when they are required to, compared to the ones with lower natural alpha power, supporting the idea proposed by Wan et al. [42], in which they reported that the alpha amplitude during eyes-open or eyes-closed condition could predict the outcome of an alpha neurofeedback training.

Signal complexity analysis via Higuchi Fractal Dimension

The signal complexity analysis did not find any statistically significant differences in different conditions and between groups after Holm-Bonferroni correction. However, prior to correction, significant increases of HFD from Baseline to BE were found at channel P3 and O1 (left parieto-occipital area). The average HFD at Pz of the two groups show almost identical values only during BE, despite there is no statistical significance found for group comparison of HFD at Pz in any condition. This close similarity of signal complexity at Pz during BE may reflect the condition in which both players not only managed to adjust their RA to the same level, but also their signal complexity level. Alpha (and mu) activity has been reported to have a negative relationship with HFD values [107, 109, 110], however due to the lack of statistical significance in our HFD results, we failed to validate this relationship between alpha and HFD based on our results.

Additionally, the trend of average HFD values in group D tend to increase during gaming compared to Baseline, particularly around the posterior channels. Similar tendency also occurs in group ND only during WO compared to Baseline. Previous studies have reported lower complexity of EEG signal are associated to resting condition or other internally engaged task (e.g. in meditation) [163] and higher EEG signal complexity are associated to problem solving [164], self-focused emotion regulation [220], and divergent thinking- particularly higher in the occipital area [221]. The increasing tendency of HFD values in the posterior channels during gaming might be related to the thinking process to achieve higher gaming scores, which is consistent in group D regardless the gaming conditions, while in group ND only occurs during WO.

sLORETA source localisation analysis

The results from sLORETA source localisation show that increasing source activity was found in the parietal area for both gaming conditions. This result, despite not statistically significant, might indicate the effort of parietal alpha modulation, as instructed by the gaming task. Significant increase of source activity was found in beta bands around the left parietooccipital areas for both gaming conditions when compared to Baseline. The lateralisation of beta activation around the brain posterior areas (i.e. parietal and occipital) might be associated to visual attention control [213, 214].

Source localisation analysis also detected the dynamic around the limbic lobe during BE condition, showing an increase of theta activity around the anterior cingulate cortex (ACC) and decreasing of alpha and lower beta activity around the parahippocampal gyrus. Cingulate cortex is engaged in processing information about an outcome of an action, including rewards and punishment processing [222], while theta activity around the ACC has been linked to a task's rule prediction as well as in task's error adjustment [223]. Moreover, ACC has also been reported as the structure involved in social synchrony [224]. The increasing activity around this area might indicate the increasing of engagement level of the players to the social interaction task. Parahippocampal gyrus has been reported to connect the default-mode network (DMN) with the memory processing area around the temporal lobe during resting state [225], the decreasing activity of this structure might indicate the weaker activation of DMN as a consequence of task engagement. Increasing theta activity was also found around the frontal area during WO condition. Frontal theta activity has been reported to be negatively

correlated with the DMN and also known as the indicator of cognitive control [226, 227]. Additionally, the highest number increased/decreased source activity in both gaming conditions revealed the activation pattern between MFG and precuneus that is frequency specific. MFG was more active in lower frequency band (theta and alpha) and precuneus was more active in higher frequency band (both beta bands). The MFG activity has been associated to attention and lingual and numerical processing [103, 204, 228] and generally prefrontal cortex has been associated with emotional processing and the regulation of motivation or withdrawal [229]. Precuneus activity has been linked to visuo-spatial imagery, episodic memory retrieval, and self-referential processing [170].

Comparison between BE and WO revealed that higher source activity was found around the right temporo-frontal (in theta and alpha bands) and temporo-parietal (in lower and higher beta bands) areas in BE, and higher source activity was found around the bilateral parietal area (extended to the frontal area) in all frequency bands in WO. These results suggest the tendency to support the previous reports of temporal cortex as a part of the 'social brain', particularly as a mentalizing system [149, 230, 231]. To be more specific, the right temporoparietal junction has been linked to social interaction and attention orientation [168, 232, 233].

The results of spectral power distribution, signal complexity, and source localisation analyses show the tendency of lateralised brain activity in group D in the left hemisphere, during BE compared to Baseline. The number of channels that show significant alpha power changes are higher in the midline and left hemisphere compared to the right hemisphere. Despite the lack of statistically significant difference after correction, higher HFD values were found at the left parieto-occipital channels. Lastly, most of the increasing dynamics of source activity mainly take place in the left parieto-occipital areas. It has been reported that, the left inferior parietal lobe is active during the detection of perspective differences [234], which in our collaborative gaming condition might imply to the effort of the players in trying to interpret their partner's perspective of the game, in order to achieve the joint goal. Moreover, the activity of the left posterior parietal cortex has been linked to the ability of attending and selecting salient stimuli in the environment [235].

NASA-TLX questionnaire

Our results show that mental, effort, and performance are the categories that generally obtained higher scores in both groups, indicating that throughout the gaming experiments, the players mainly are more concern to the factors that they can internally control, such as how they perceive the mental load of the task, the effort they put on the task, and the ability to predict their own performance, rather than to the other situational categories such as temporal and physical. Whereas the frustration category, despite being able to be internally controlled by the players, the scores are lower compared to mental, effort, and performance. The scores trend indicates less confidence in group D in judging their own performance, meaning that they felt that they performed poorly compared to group ND, particularly in Session II, despite the fact that their EEG analysis results show the opposite.

Notable findings

Our study has demonstrated the application of collaborative interaction in an alpha operant-conditioning training paradigm. Further testing and exploration are still needed to measure the efficacy of this paradigm for individual control of alpha power. This study has revealed the characteristics of electrophysiological signatures in response to collaborative interaction of both groups, while they were regulating parietal alpha activity at the same time. This study focused on the electrophysiological response of a single-brain during a two-person interaction. In order to investigate how these activated brain areas influencing one another and how different brain areas in different individuals interacting with each other during collaboration, we performed intra-brain and inter-brain connectivity analysis to the data obtained by the experiment of this study, which will be presented and discussed further in the upcoming chapter.

Limitations

The limitations of this study including the different number of channels used by the two groups during the third experimental day. A larger and balance number of channels (for both players) will provide the opportunity to gain better results, especially in spatial power spectral and source localisation analyses. More training sessions are needed in the future to produce more information related to the learning process when collaborative interaction is present. Larger number of participants are also required to produce better

statistical analysis, therefore better and more precise validation over the statistically significant results can be made. In order to further study the efficacy of the collaborative BCI training, control group, post-training baseline analysis and post-training assessment should be performed in the future.

6.5 Conclusion

The study introduced a multi-user collaborative BCI game that is based on alpha band operant conditioning. Our results suggest that group D have the better ability to adjust their alpha power at Pz to be closer to their partner, and this ability can be predicted based on their resting alpha power. This study also found that the level of alpha power during Baseline was higher in group D than in group ND, supporting the idea to use Baseline alpha power as a predictor of gaming performance. Signal complexity analysis confirmed that both players managed to adjust their signal complexity level at channel Pz during BE. Spatial power distribution, signal complexity analysis, and source localisation analysis revealed that during BE, group D activated their left-parietal area which might reflect the perspective adjustment (to their partner's). Source localisation analysis in group D found a significant increase of source activation in beta band during both gaming conditions (i.e. higher beta in BE and lower beta in WO). Source localisation analysis also revealed that during BE, a higher number of increased source activity was found in the MFG in lower frequency bands (theta and alpha bands) and was found higher in the precuneus in beta band, suggesting the role of the two brain structures in regulating a frequency-specific brain response to a successful collaborative gaming. Finally, post-experimental questionnaire revealed that the players perceived the gaming task in a relatively similar way in most of the categories across sessions, apart from the performance category, where group D felt like they performed poorly, particularly in Session II.

Chapter VII

Collaborative Multi-user BCI:
Part II- Connectivity

7.1 Introduction

In this chapter, the results of the connectivity analysis of the EEG data that were obtained from the multi-user BCI collaborative experiment described in Chapter VI are presented. In this chapter, robust connectivity measurements such as Granger Causality (GC) and Directed Transfer Function (DTF) will be estimated.

Hyperscanning studies to explore the brain connectivity during collaborative interaction have been performed by applying the different types of collaborative tasks [84, 87-89, 236]. Stronger activity of the frontal area has been reported in both types of collaborative tasks (i.e., synchronic and diachronic) [79, 237]. During a synchronic collaborative selective attention task, Balconi et al. [87], found that intra-brain connectivity was generally higher around dorsolateral prefrontal cortex (dlPFC). Sänger et al. [236] also reported an enhanced intra-brain connectivity around the frontal and central areas during a musical coordination task

Furthermore, several studies have explored the brain-to-brain coupling during collaborative interaction, which represents the mutual effort performed by the participants in order to achieve the common goal. Synchronic collaborative experiments have shown an evidence of brain-to-brain signal coupling between the participants during an explicit communication, such as verbal communication and/or face-to-face condition. These experiments reported the neural synchrony during a face-to-face structured communication between strangers [90] and in romantic couples [91], as well as the non-structured one [92]. These studies suggest that, regardless the structure of the interaction in collaborative task and the strength of inter-personal emotional attachment, collaborative interaction has been found to elicit different parts of the brain (i.e. frontal cortex, superior temporal lobe, and temporo-parietal junction). Additionally, social synchronisation between mothers and their infants was revealed, involving a specific set of brain structures, such as the anterior cingulate cortex (ACC), inferior parietal lobule, fusiform, cuneus, and supplementary motor area [224], which may indicate the roots of collaborative interaction brain activation, particularly the areas that are involved in emotional processing and empathy.

In this chapter, connectivity analysis was performed on EEG data collected during the collaborative multi-user BCI gaming that is based on the alpha band, non-verbalised operant conditioning, as described in Chapter VI. Connectivity analysis will be divided into two approaches, namely the intra-brain connectivity, performed by multivariate GC and DTF and the inter-brain connectivity, performed by bivariate GC.

7.2 Methods

7.2.1 Connectivity Analysis

GC and DTF were used for connectivity estimation, where GC provides multivariate connectivity analysis in time domain and DTF multivariate connectivity analysis in frequency domain. Due to the limited computational speed, 2 minutes out of each 5 minutes time-series data (BE and WO data from the third experimental session) were extracted for further connectivity analyses. In each pair, these 2 minutes data were extracted within the identical time points for both players, based on the 2 minutes where the RA values of both players have the smallest difference in both gaming conditions. The 2 minutes were segmented into 6 s epoch with 50% overlap. Independent Component

Analysis (ICA) algorithm [103, 104] implemented in EEGLAB (version 14.1.2b) was performed for further noise removal (e.g. eye blinking, muscle movement, or other biological signal). The pre-processed 2 minutes data were later analysed by using GC and DTF connectivity analyses, which have been described in Chapter III.

7.2.2 Statistical Analysis

A non-parametric paired permutation statistical test ($p<0.01$) was performed in MATLAB with 10000 repetition of all the estimated connectivity data. The method was used for the analyses of GC and DTF in order to compare the brain connectivity between the gaming conditions (Baseline and BSD; Baseline and SSD; BSD and SSD) and between groups (D and ND) for the three conditions (Baseline, BSD, and SSD). Statistically significant connections ($p<0.01$) found in each comparison were later projected into a connectivity matrix. False Discovery Rate correction method [152] was applied for multiple comparisons.

A non-parametric single-sample permutation statistical test ($p<0.001$) was performed in MATLAB with 10000 repetition, with FDR correction applied, to all the estimated inter-brain connectivity data. The method was used to find the significant connections found in inter-brain GC during BSD and SSD, in different directions between players.

7.3 Results

7.3.1 Intra-brain Granger Causality

Intra-brain GC results are presented in three ways: as matrices presenting the grand average of GC values of all epochs from all players in each group (Fig. 7.2 and 7.3 (a-c)), as connectivity maps displaying only the average values above the 75^{th} percentile of its corresponding matrix for an easy visual representation of spatial connectivity localisation (Fig. 7.2 and 7.3 (d-f)), as a set of *p*-value matrices (Fig. 7.2, 7.3 (g-h), 7.5 (a-b), and 7.6), and as bar graphs displaying the average GC values in each zone- following the zonation in Figure 7.1 (Fig. 7.4 and 7.5 (c-d)).

The statistical comparisons from the GC data were performed as the following: between Baseline and BE/WO, between BE and WO, and between groups. Based on these presentations, the results will be explained in the following structure:

(v) the significant connection changes found in the connections involving Pz,

(vi) the pattern shaped by the most prominent connections shown by the connectivity maps (does not apply in the comparisons between BE and WO, and between groups)

(vii) the network with a high count of significantly increase/decrease connections in found in the *p*-values matrices. The networks in the *p*-values matrices will be described based on the zonation shown in Figure 7.1.

(viii) the significant average GC changes in each zone (does not apply in the comparison between group D and group ND) as well as the results of a non-parametric paired permutation.

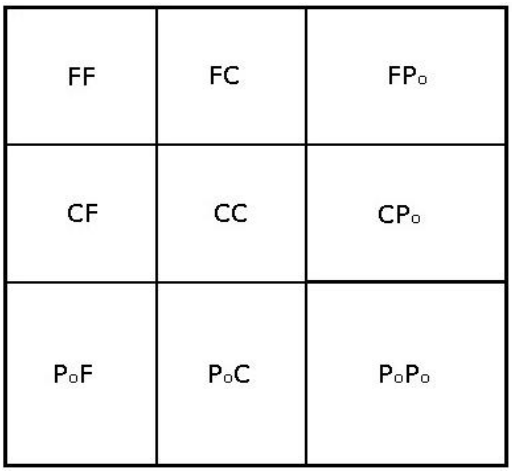

Figure 7.1 The networks zonation: FF (frontal-frontal), CC (central-central), PoPo (parieto-occipital – parieto-occipital), FC (frontal-central), FPo (frontal-parieto-ocipital), CF (central-frontal), CPo (central-parieto-occipital), PoF (parieto-occipital – frontal), and PoC (parieto-occipital – central). The first letter of the abbreviation indicates the source of the network, and the second letter indicates the sink.

Intra-brain GC of group D

(i) *Baseline vs BE*: in BE, for Pz as a source, increased connections were flowing to F3 and the decreased connections to Cz, C4, and P4. For Pz as a sink, increased connections were coming from P3 and P4, and the decreased connections from F3, Fz, Cz, and C4.

Baseline vs WO: in WO, for Pz as a source, increased connections were flowing to F3 and F4, and the decreased connections to Cz, P3, P4, and Oz. For Pz as a sink, increased connections were coming from C3 and Oz, and the decreased connections from Fz, Cz, C4, and P4.

(ii) The prominent connections in Baseline and BE are relatively similar, showing clustered bidirectional connections over the midline and the right fronto-central areas. In WO, bidirectional connections were found clustered around the frontal area and in some midline channels, and weaker connections towards Oz and around the localised parieto-occipital area.

(iii) *Baseline vs BE*: Compared to Baseline, most of the networks were deactivated during BE. PoPo was found as the network with the highest count of significantly active connections in BE, followed by PoF.

Baseline vs WO: Compared to Baseline, most of the networks were deactivated during WO. FC, CP, CC, and PoF show an equal number of significant connections found in WO.

(iv) *Baseline vs BE*: significant decreases of average GC during BE were found in FC, FPo, all zones coming from C, and PoC, and a significant increase was found in PoF.

Baseline vs WO: significant decreases of average GC during WO were found in FPo, CC, CPo, and in all zones coming from Po, and a significant increase was found in FF.

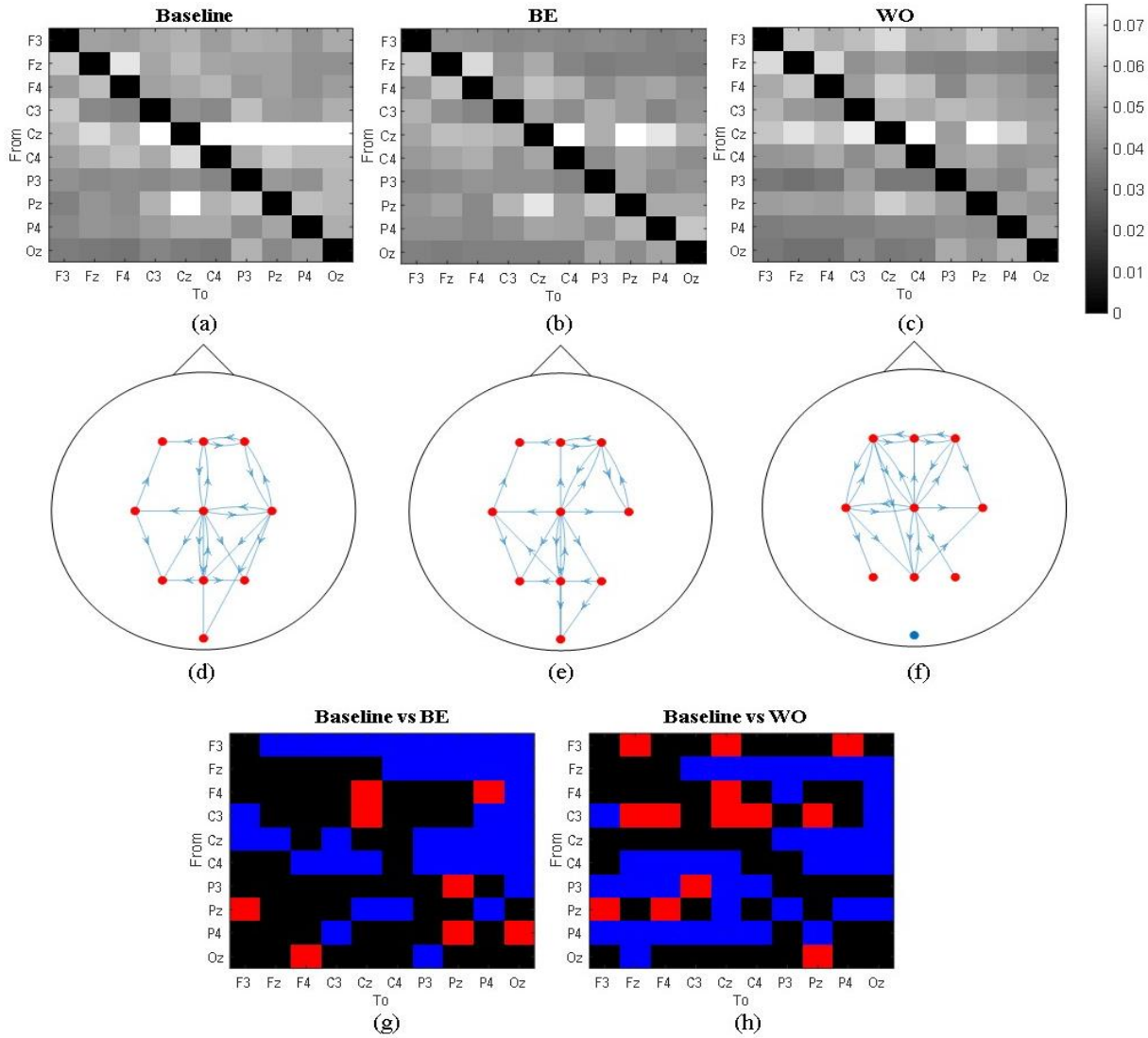

Figure 7.2 (a-c) The average **intra-brain GC** matrices of **group D** for Baseline, BE, and WO. (d-f) The connectivity map for each condition- each map displays the average GC values above the 75th percentile of its corresponding matrix above them. (g-h) The matrices of *p*-values generated from a non-parametric paired permutation ($p<0.01$) of the intra-brain GC values of from all trials between Baseline and each gaming condition, with FDR correction applied. The blue and red squares indicate the significant connections, blue indicates higher average GC value in Baseline and red indicates higher average GC value in gaming.

Intra-brain GC of group ND

(i) *Baseline vs BE*: in BE, for Pz as a source, decreased connections were flowing to all frontal channels and C4. For Pz as a sink, decreased connections were coming from F3, Cz, P3, P4, and Oz.

Baseline vs WO: the significant changes involving Pz were only found as a sink, with decreased connections coming from F4, Cz, P3, P4, and Oz.

(ii) In Baseline, the prominent connections were clustered around the left fronto-central area and the localised parieto-occipital area, with a lack of connections between the two localised areas. In BE, the prominent connections were e evenly distributed across all areas, while in WO, the prominent connections were clustered around the left hemisphere of all cortical areas (frontal, central, parietal, and occipital).

(iii) *Baseline vs BE* and *Baseline vs WO*: all the significant changes found in this group are characterised by the deactivation of the most networks during gaming when compared to Baseline, particularly the deactivation of CF, PoF, PoC, and PoPo.

(iv) *Baseline vs BE* and *Baseline vs WO*: significant decreases of average GC during BE and WO compared to Baseline were found in all zones.

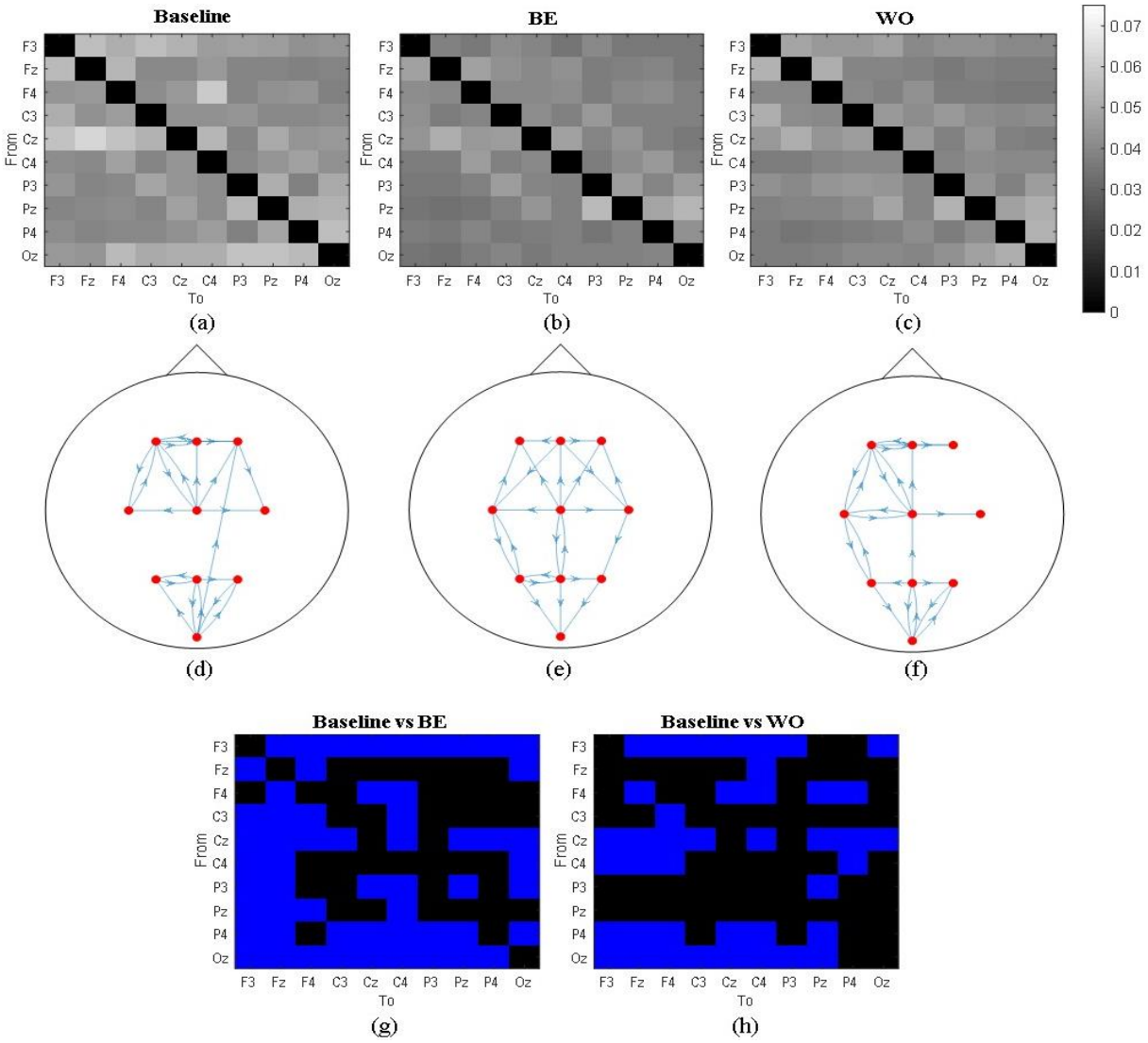

Figure 7.3 (a-c) The average **intra-brain GC** matrices of **group ND** for Baseline, BE, and WO. (d-f) The connectivity map for each condition- each map displays the average GC values above the 75th percentile of its corresponding matrix above them. (g-h) The matrices of *p*-values generated from a non-parametric paired permutation ($p<0.01$) of the intra-brain GC values of from all trials between Baseline and each gaming condition, with FDR correction applied. The blue squares indicate the significantly higher average GC value in Baseline.

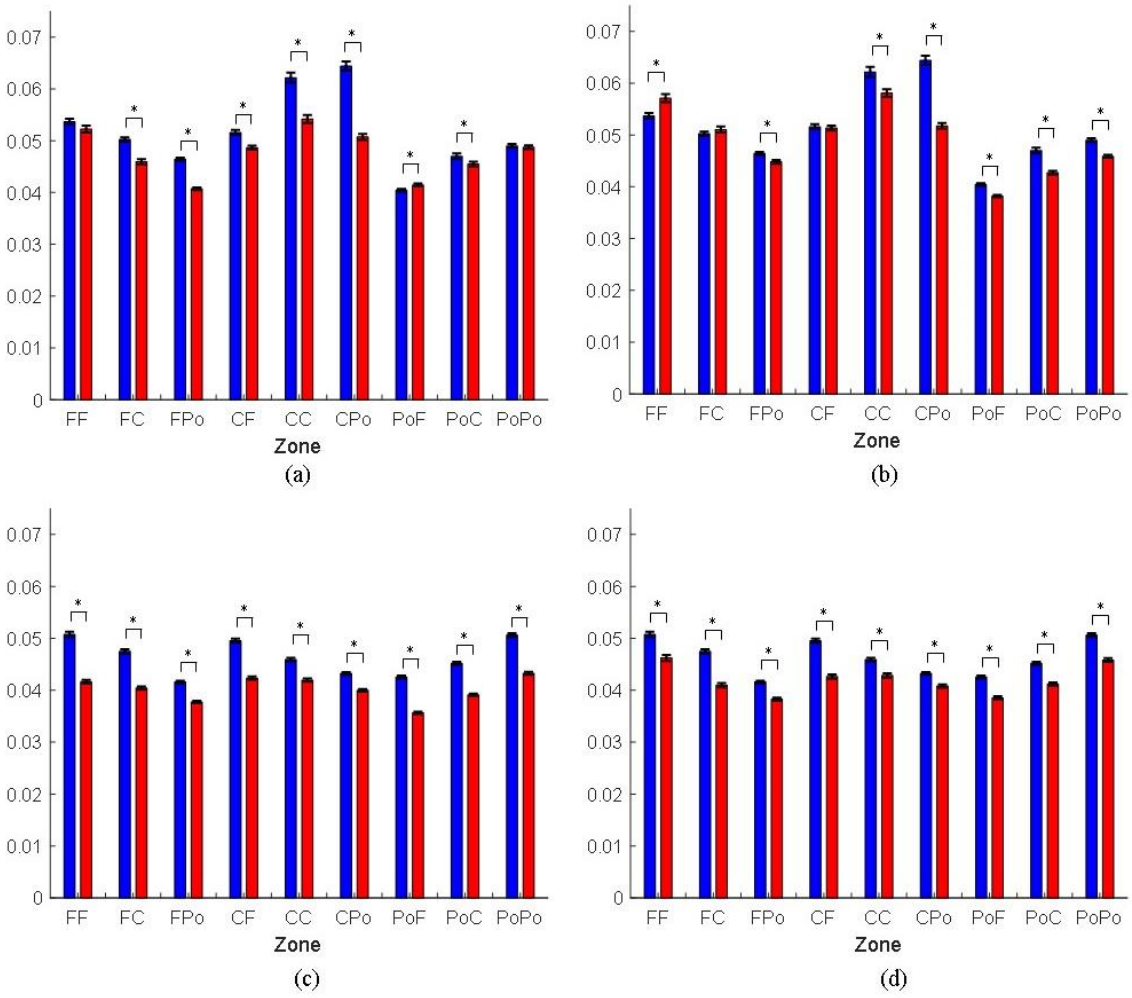

Figure 7.4 The bar graphs of the average GC values (mean ± standard error) in each zone for (a) group D, Baseline vs BE, (b) group D, Baseline vs WO, (c) group ND, Baseline vs BE, and (d) group ND, Baseline vs WO. A non-parametric paired permutation (p<0.01) was performed to compare the statistic between two conditions, with FDR correction applied. The blue bars indicate the average GC during Baseline and the red bars indicate the average GC during gaming experiment (BE/WO).

Comparisons between BE vs WO

(i) *Group D*: in BE, for Pz as a source, weaker connections were flowing to F4 and C4, and stronger connections to P3 and Oz. For Pz as a sink, weaker connections were coming from F3, Fz, and C3, and stronger connections were coming from P3 and P4.

Group ND: in BE, for Pz as a source, weaker connections were flowing to all frontal channels and to Cz. For Pz as a sink, weaker connections were coming from F3, P4, and Oz.

(ii) *Group D*: in BE, group D shows higher count of significant connections in PoF, PoC, and PoPo. While in WO, higher count of significant connections was found in FPo.

Group ND: most areas remained the similar in both BE and WO. There is one significant connection in FC, FPo, CF,CPo, and PoF, showing higher activity in BE. While in WO, higher count of significant connections was found in PoF and PoPo.

(iii) *Group D*: significantly higher average GC during BE compared to WO were found in all zones coming from Po, and significantly lower average GC during BE compared to WO were found in all zones coming from F, CF, and CC.

Group ND: significantly lower average GC during BE compared to WO were found in FF and all zones coming from Po.

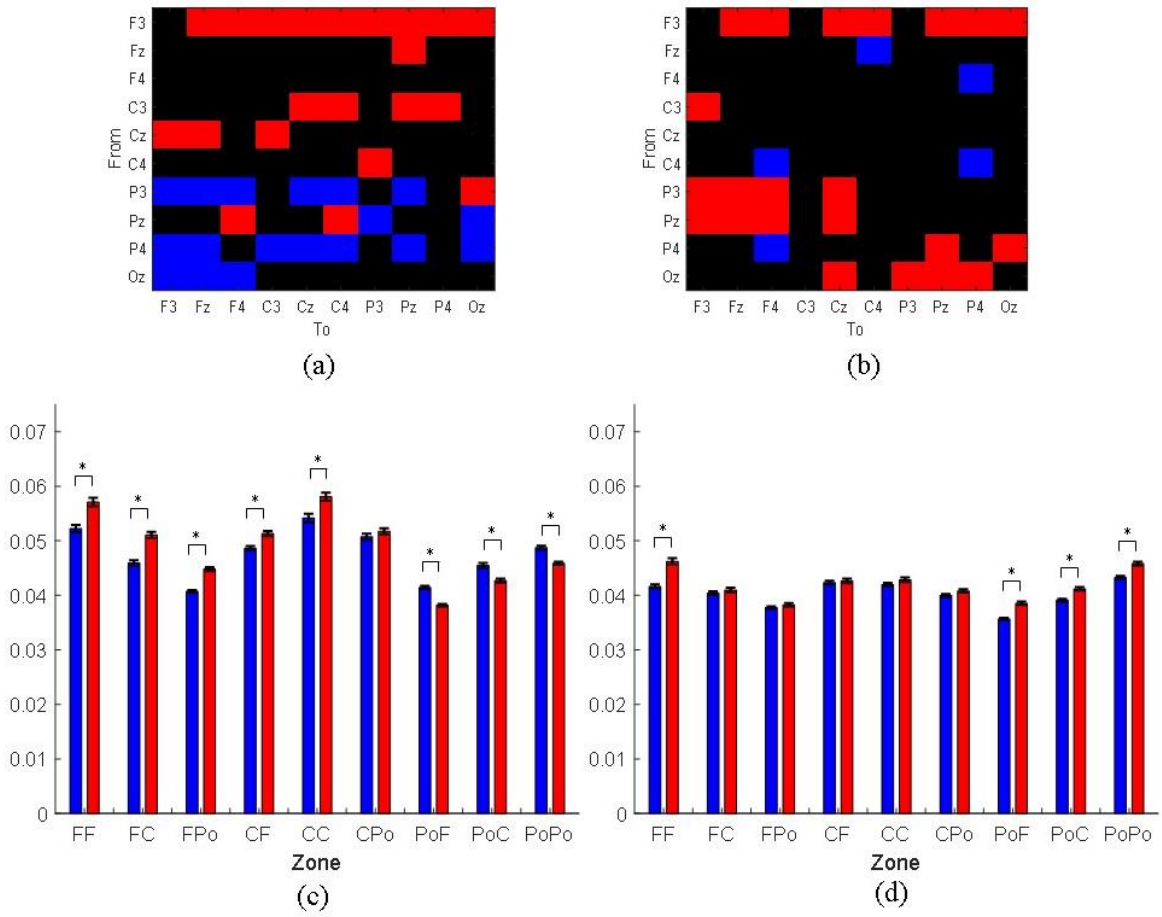

Figure 7.5 (a-b) The matrices of *p*-values generated from a non-parametric paired permutation ($p<0.01$) of the **intra-brain GC values from all trials between BE and WO** for (a) group D and (b) group ND, with FDR correction applied. The blue and red squares indicate the significant connections, blue indicates higher average GC value in BE and red indicates higher average GC value in WO. (c-d) The bar graphs of the average GC values (mean ± standard error) for BE and WO in each zone for (c) group D and (d) group ND. A non-parametric paired permutation ($p<0.01$) was performed to compare the statistic between two conditions, with FDR correction applied. The blue bars indicate the average GC during BE and the red bars indicate the average GC during WO.

Comparisons between group D and group ND

(i) *Baseline*: for Pz as a source, group D shows stronger connections to Fz, C3, Cz, and C4. For Pz as a sink, group D shows stronger connections from Fz, F4, C3, Cz, and C4, and weaker connections from P3 and Oz.

BE: for Pz as a source, group D shows stronger connections to all fronto-central channels. For Pz as a sink, group D shows stronger connections from F3, F4, C3, Cz, C4, P4, and Oz.

WO: for Pz as a source, group D shows stronger connections to all fronto-central channels. For Pz as a sink, group D shows stronger connections from F3, F4, C3, Cz, and C4, and weaker connections from P4 and Oz.

(ii) *Baseline*: group D shows higher count of significant connections in CPo and FPo, while group ND generally shows lower significant connection count. For group ND, the highest number of significant connections was found in PoC and PoPo.

BE: All the significant connections found indicated that group D has higher connectivity compared to group ND during BE. The highest significant connection count was found in PoF and CPo.

WO: Most of the significant connections found indicated that group D has higher connectivity compared to group ND during WO. The highest significant count was found in CPo and FPo for group D and in PoF for group ND.

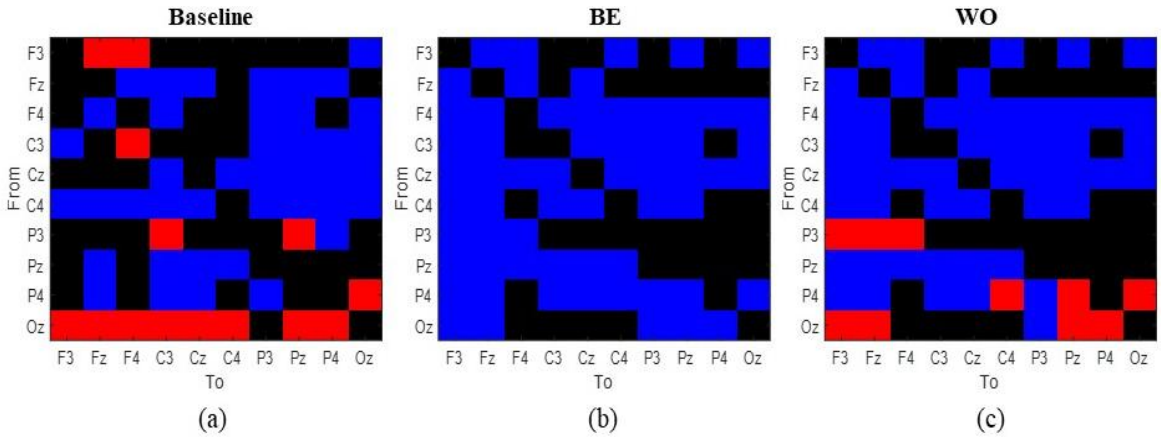

Figure 7.6 The matrices of *p*-values generated from a non-parametric paired permutation ($p<0.01$) of the **intra-brain GC values from all trials between groups** (D and ND) in (a) Baseline, (b) BE, and (c) WO, with FDR correction applied. The blue and red squares indicate the significant connections, blue indicates higher average GC value in group D and red indicates higher average GC value in group ND.

7.3.2 Directed Transfer Function

DTF results are presented in three ways: as matrices presenting the grand average of DTF values of all epochs from all players in each group (Fig. 7.7 and 7.11), as connectivity maps displaying only the average values above the 75th percentile of its corresponding matrix for an easy visual representation of spatial connectivity localisation (Fig. 7.8 and 7.12), as a set of *p*-value matrices (Fig. 7.9, 7.13, 7.15, and 7.17) and as bar graphs displaying the average GC values in each zone (Fig. 7.10, 7.14, and 7.16).

The statistical comparisons from the DTF data were performed as the following: between Baseline and BE/WO, between BE and WO, and between groups. Based on these presentations, the results will be explained following the same structure as in intra-brain GC results presentation.

DTF of group D

(i) *Baseline vs BE*: in BE, for Pz as a source, increased connections were flowing to P3 (in theta, alpha, and lower beta bands) and P4 (in theta band). For Pz as a sink, increased connection was flowing from Fz (in alpha and both beta bands), F4 (in all frequency bands), and C4 (in alpha and both beta bands), and decreased connections were coming from C3 (in both beta bands), Cz (in theta, alpha, and lower beta bands), P3 (in both beta bands), P4 (in all frequency bands), and Oz (in theta and higher beta bands).

Baseline vs WO: in WO, for Pz as a source, decreased connections were flowing to Fz (in higher beta band), Cz (in alpha band), P3 (in alpha and lower beta bands), P4 (in alpha band), and Oz (in alpha band).

(ii) In all frequency bands and all conditions, the prominent connections were evenly distributed throughout all channels and densely clustered over the midline channels.

(iii) *Baseline vs BE* and *Baseline vs WO*: FC and FPo were found to have higher significant connection count during gaming in all frequency, while PoF, PoC, and PoPo were more active during Baseline.

(iv) *Baseline vs BE*: significant decreases of average DTF during BE were found in FC (alpha), FPo and CPo (all frequency bands), CC and PoC (lower beta), and PoPo (theta, alpha, and higher beta), and significant increases of average DTF

during BE were found in all zones coming to F (all frequency bands), and all zones coming to C (theta and higher beta).

Baseline vs WO: significant decreases of average DTF during WO were found in all zones coming to Po (all frequency bands) and CC (lower beta), and significant increases during WO were found in all zones coming to F (all frequency bands), FC (both beta bands),

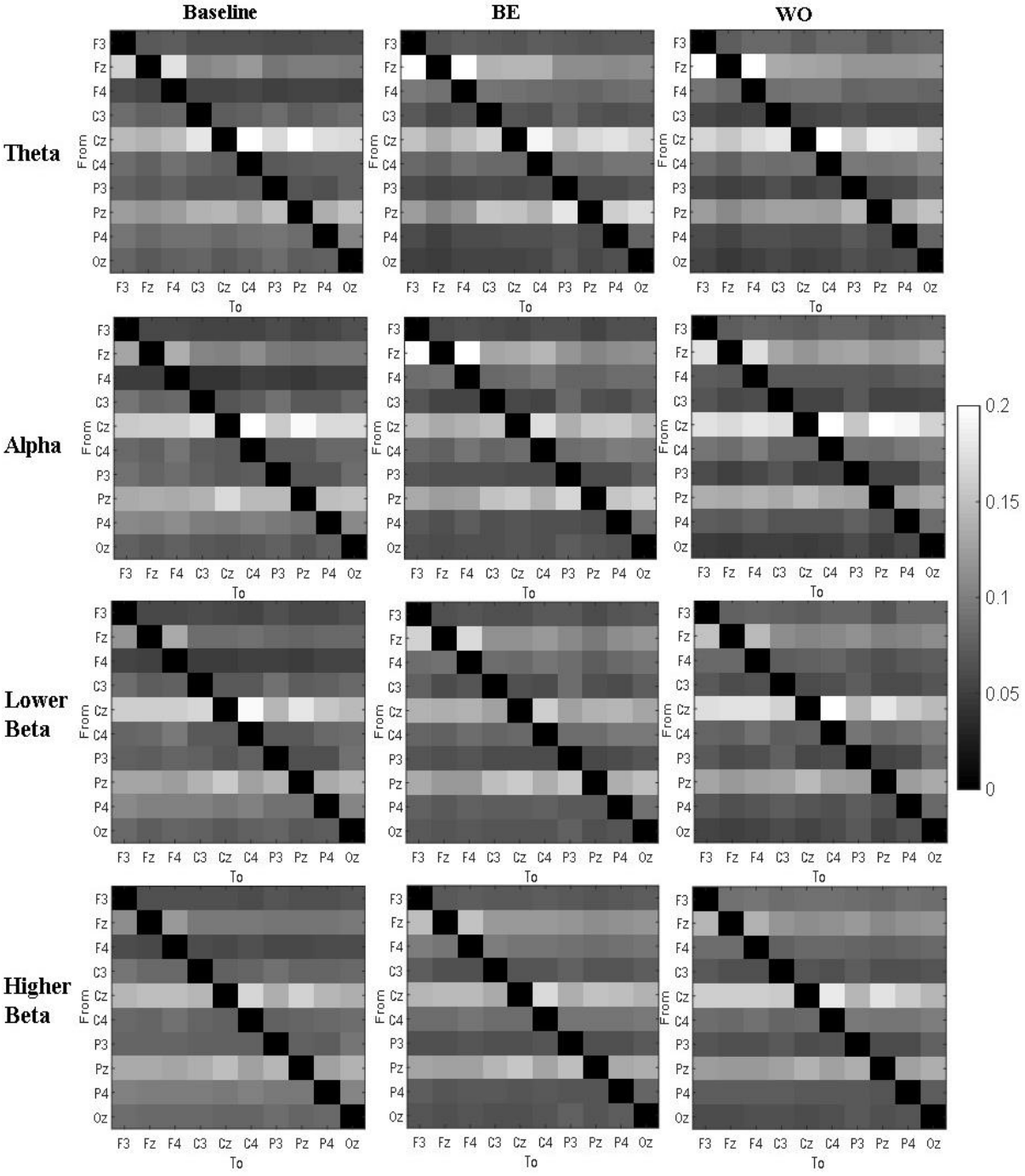

Figure 7.7 The average DTF matrices **for group D** for Baseline, BE and WO conditions, in each frequency band.

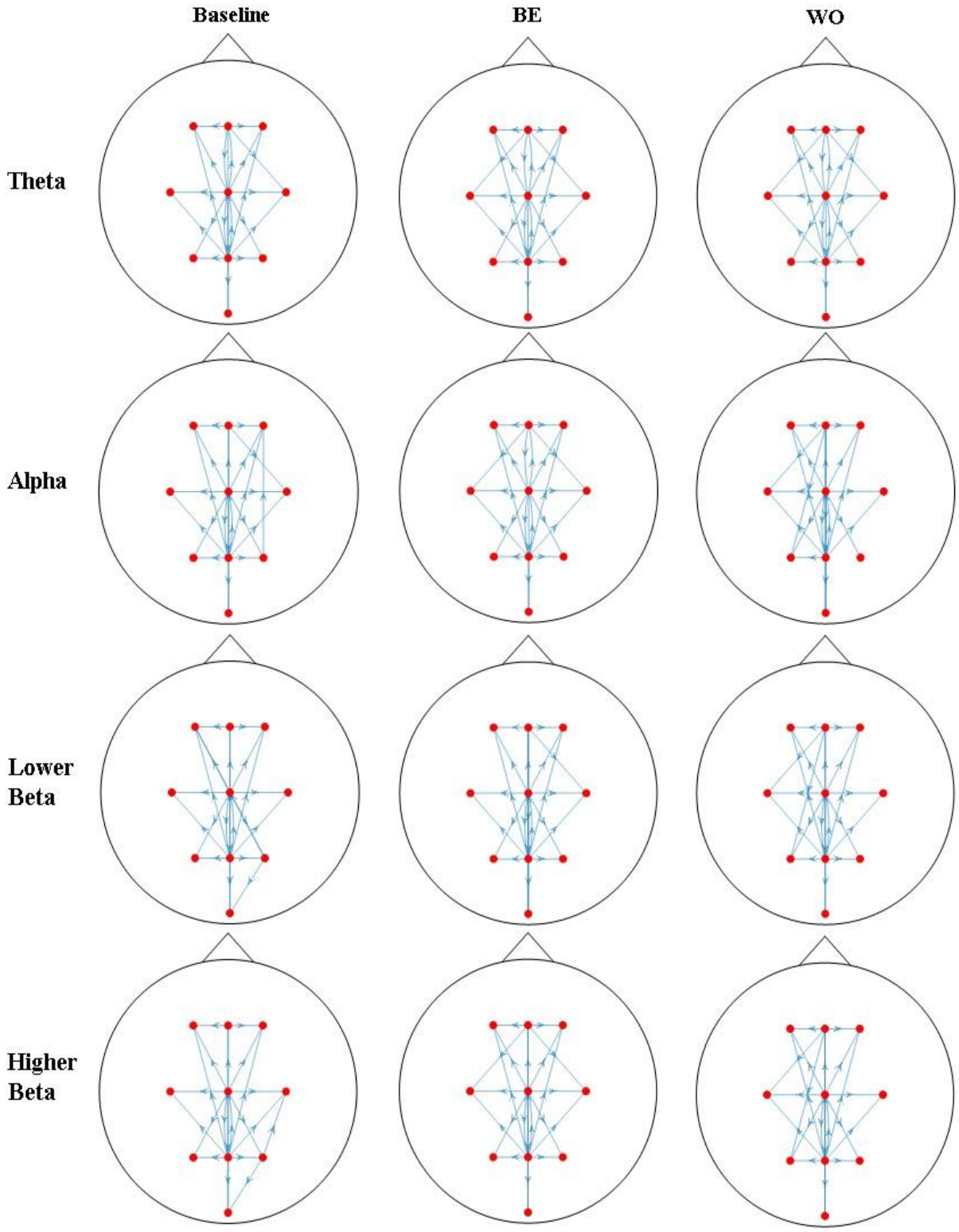

Figure 7.8 The connectivity maps display the average DTF values for group D above the 75th percentile of its corresponding matrix shown in Figure 7.7, for Baseline, BE and WO conditions, in each frequency band.

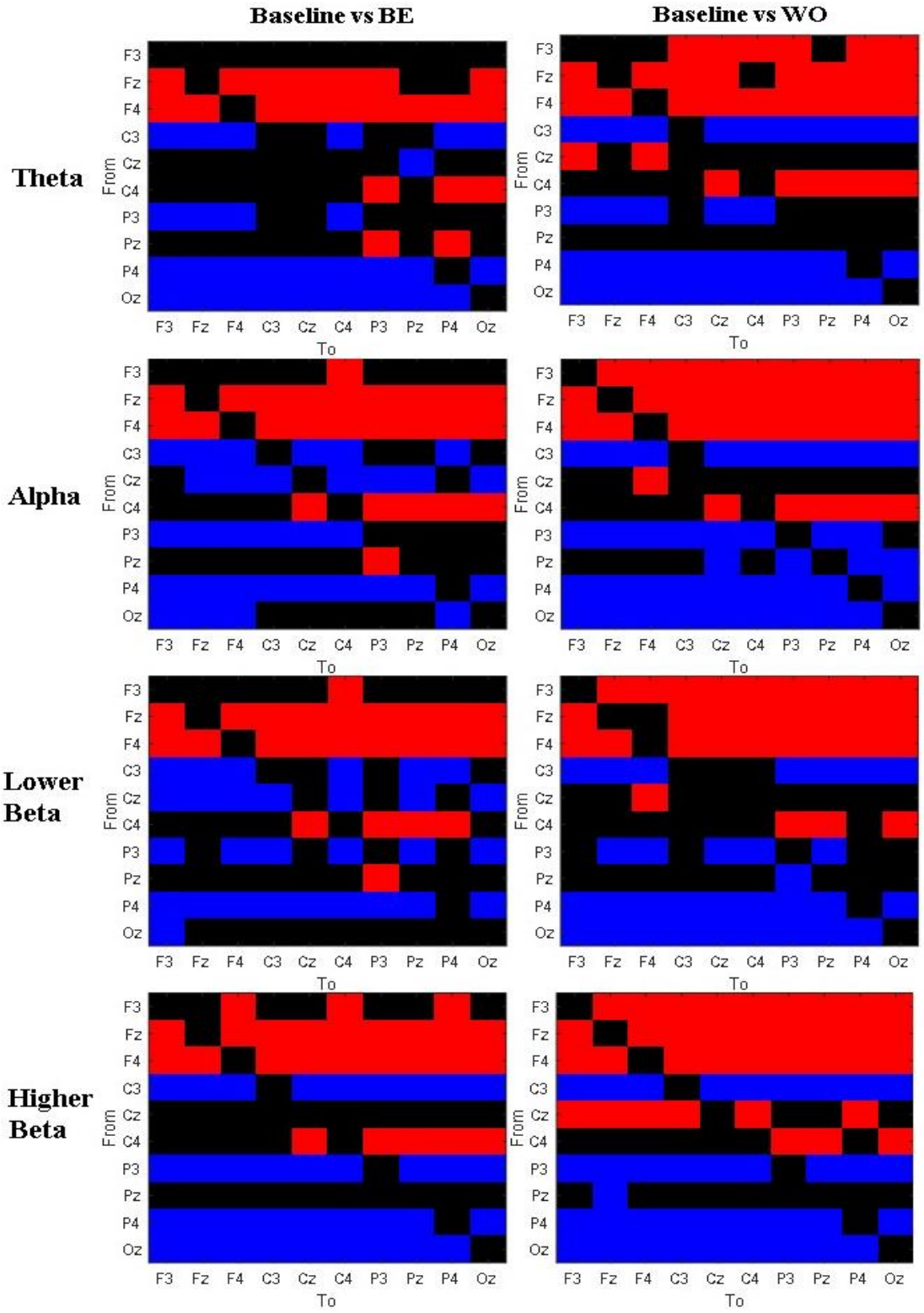

Figure 7.9 The matrices of *p*-values generated from a non-parametric paired permutation ($p<0.01$) of the DTF values from all trials **between Baseline and each gaming condition** (Baseline vs BE and Baseline vs WO) for **group D** in each frequency band with FDR correction applied. The blue and red squares indicate the significant connections, blue indicates higher average DTF value in Baseline and red indicates higher average DTF value in gaming.

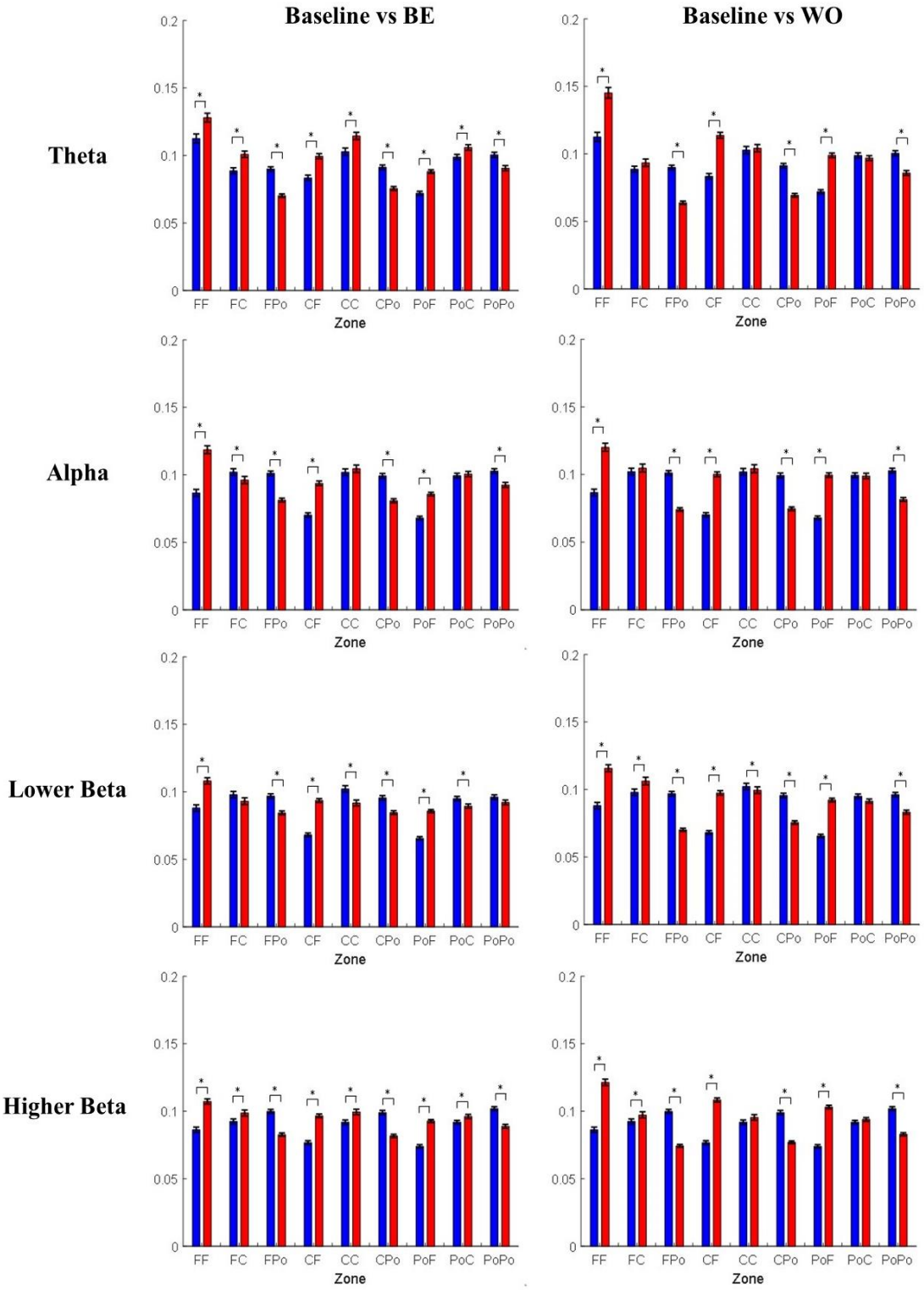

Figure 7.10 The bar graphs of the average DTF values (mean ± standard error) in each zone between Baseline and each gaming condition (Baseline vs BE, and Baseline vs WO) for group D, in each frequency band. A non-parametric paired permutation (p<0.01) was performed to compare the statistic between two conditions, with FDR correction applied. The blue bars indicate the average DTF during Baseline and the red bars indicate the average DTF during gaming experiment (BE/WO).

DTF of group ND

(i) *Baseline vs BE*: in BE, for Pz as a source, decreased connections were flowing to all channels in all frequency bands. For Pz as a sink, increased connections were flowing from F3, C3, and Cz (in all frequency bands), and from Cz (in alpha and both beta bands), C4 (in both beta bands), P3 (in higher beta band), and P4 (in alpha and both beta bands), and decreased connections were coming from Fz and F4 (in alpha and both beta bands).

Baseline vs WO: in WO, for Pz as a source, decreased connections were flowing to C3 and all parieto-occipital channels in all frequency bands and to F4 (in theta band), to Cz (in theta, alpha, and lower beta bands) and to C4 (in theta and lower beta bands). For Pz as a sink, increased connections were flowing from F3, C3, and Cz (in all frequency bands), and from C4 (in theta, alpha, and lower beta bands), and decreased connections were coming from P4 in theta band.

(ii) The prominent connections were evenly distributed throughout all channels in Baseline and WO, with a dense cluster around the midline channels. In BE, the prominent connections were found clustered in the left hemisphere and particularly denser in the left fronto-central area, in all frequency bands.

(iii) *Baseline vs BE* and *Baseline vs WO*: CPo was found to have higher significant connection count during gaming in all frequency, while FC and FPo were more active during Baseline.

(iv) *Baseline vs BE*: significant decreases of average DTF during BE were found in FPo and CPo (alpha and both beta bands), and PoPo (both beta bands), and significant increases of average DTF during BE were found in FC, PoF, and PoC (all frequency bands), CF (theta and lower beta), and CC (alpha and both beta bands).

Baseline vs WO: significant decreases of average DTF during WO were found in FF (higher beta), and all zones coming to Po (all frequency bands), and significant increases of average DTF during WO were found in all zones coming to C (all frequency bands), and PoF (theta and lower beta).

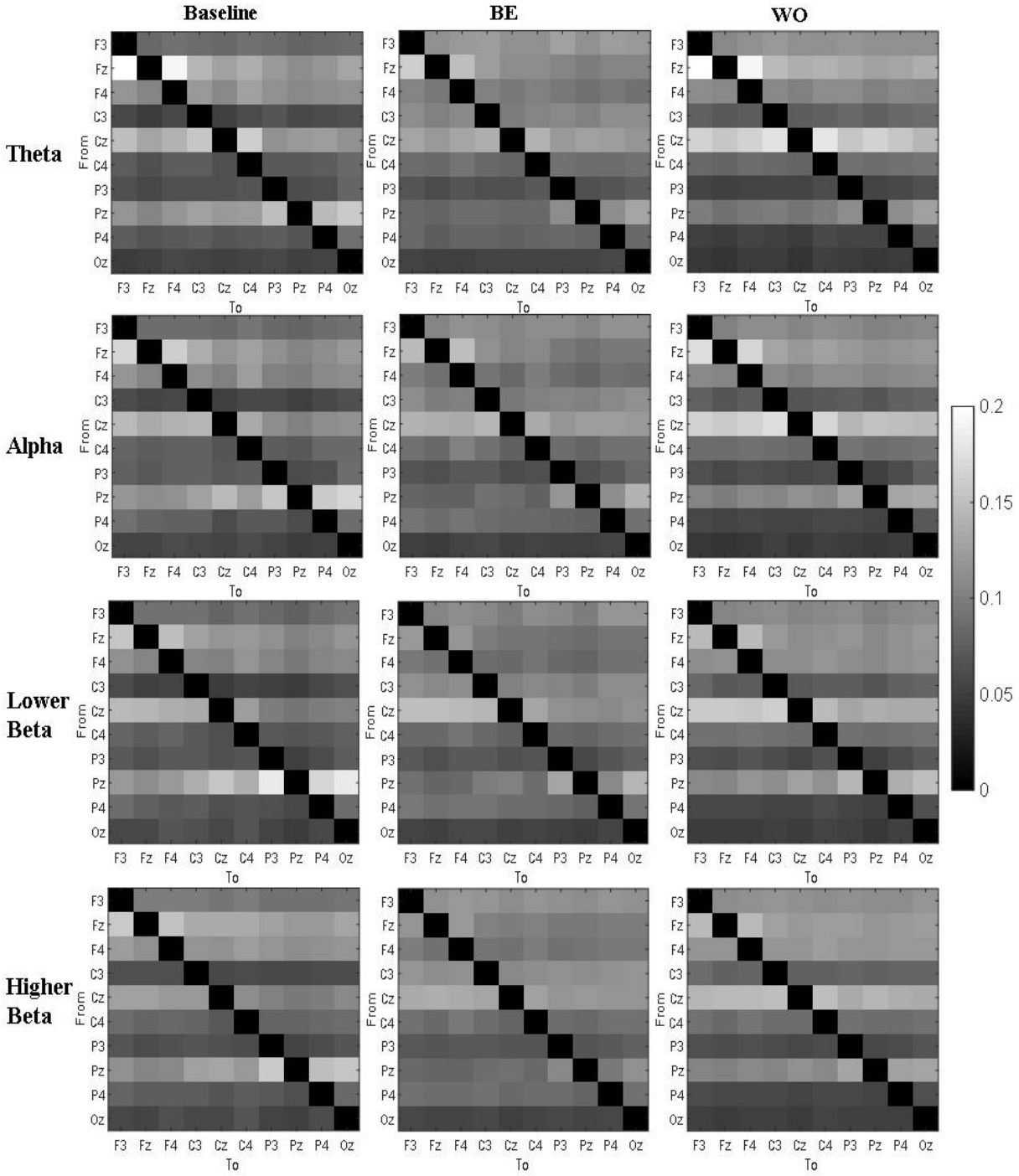

Figure 7.11 The average DTF matrices **for group ND** for Baseline, BE and WO conditions, in each frequency band.

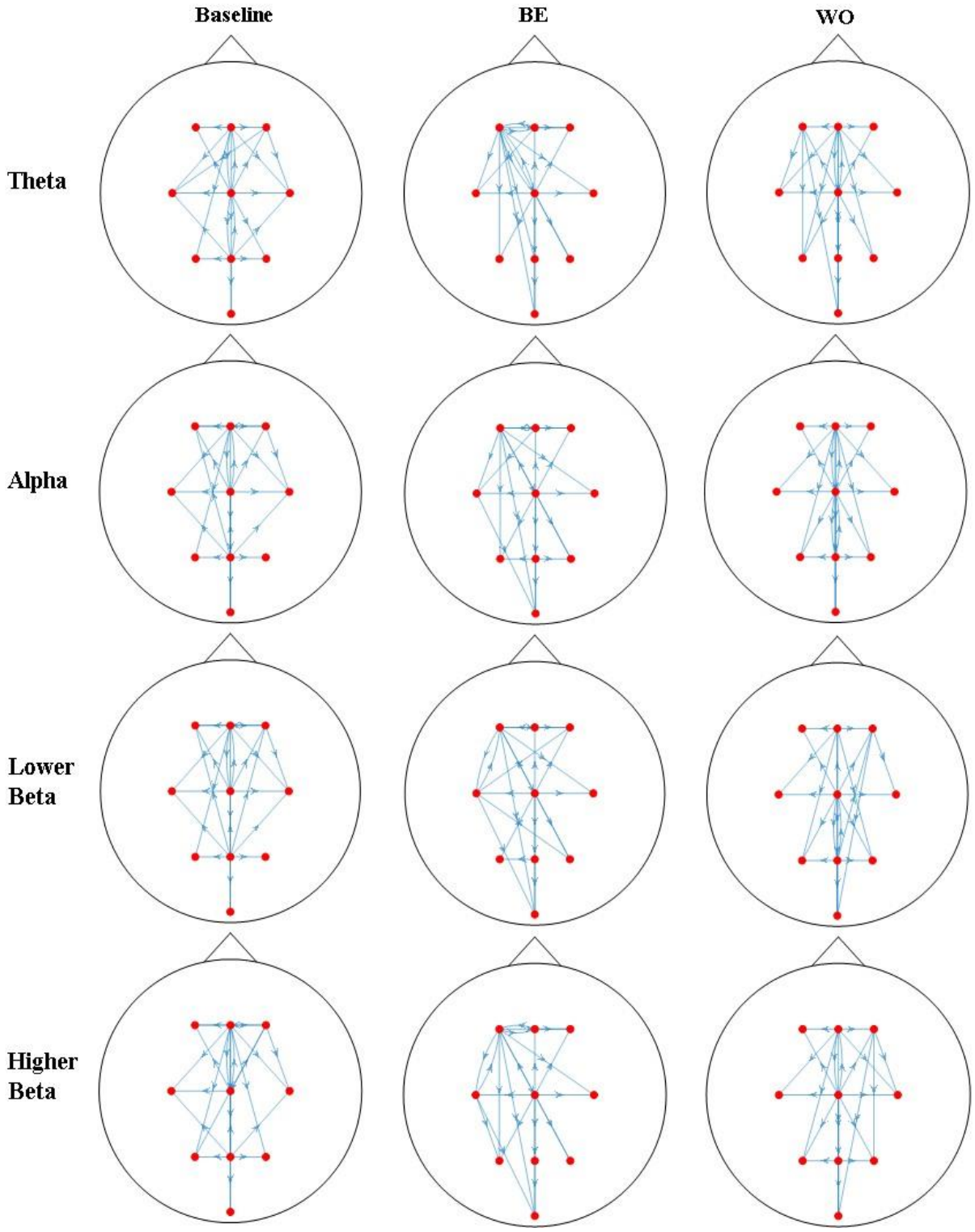

Figure 7.12 The connectivity maps display the average DTF values for group ND above the 75th percentile of its corresponding matrix shown in Figure 7.11, for Baseline, BE and WO conditions, in each frequency band.

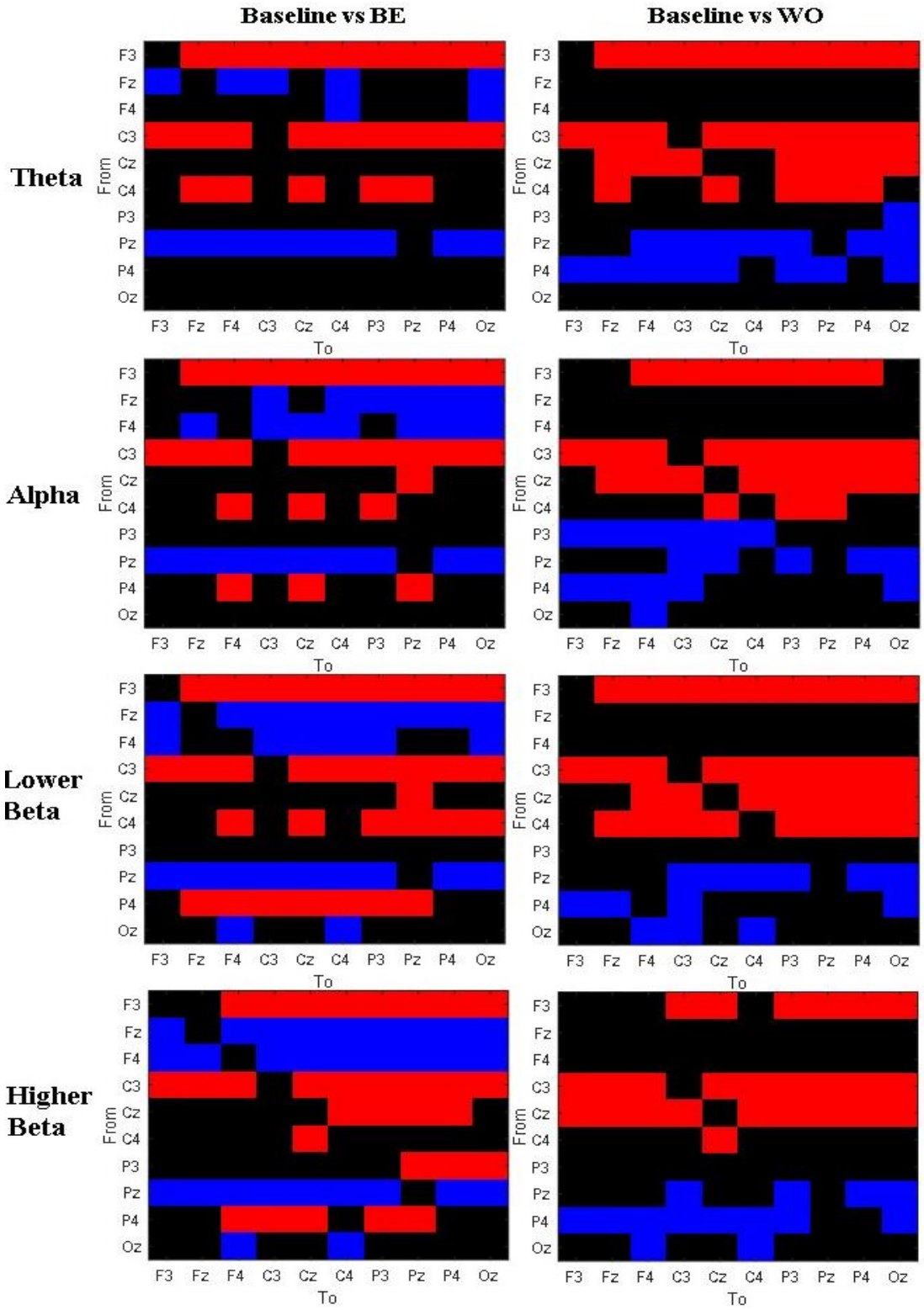

Figure 7.13 The matrices of *p*-values generated from a non-parametric paired permutation ($p<0.01$) of the DTF values from all trials **between Baseline and each gaming condition** (Baseline vs BE and Baseline vs WO) for **group ND** in each frequency band with FDR correction applied. The blue and red squares indicate the significant connections, blue indicates higher average DTF value in Baseline and red indicates higher average DTF value in gaming.

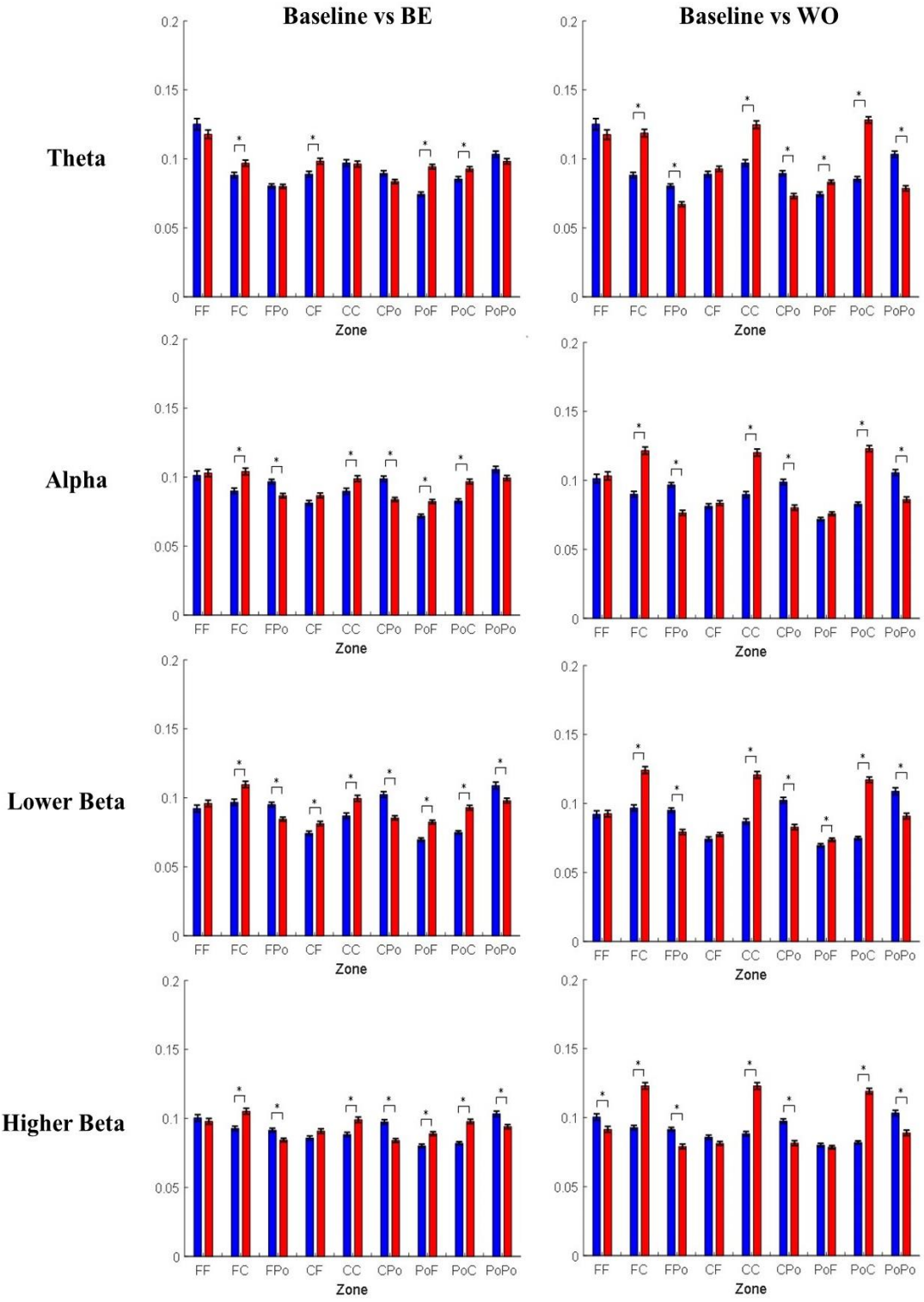

Figure 7.14 The bar graphs of the average DTF values (mean ± standard error) in each zone between Baseline and each gaming condition (Baseline vs BE, and Baseline vs WO) for group ND, in each frequency band. A non-parametric paired permutation (p<0.01) was performed to compare the statistic between two conditions, with FDR correction applied. The blue bars indicate the average DTF during Baseline and the red bars indicate the average DTF during gaming experiment (BE/WO).

Statistical comparisons between BE vs WO

(i) *Group D*: in BE, for Pz as a source, weaker connections were flowing to all frontal channels in alpha band, and stronger connections were flowing to F3 (in higher beta band), C3 (in alpha band), Cz (in alpha, and both beta bands), and Oz (in alpha band). For Pz as a sink, weaker connections were coming from P4 in alpha band, and stronger connections were coming from P3 (in theta, alpha, and lower beta bands), from C3 (in higher beta band), and from Oz (in alpha band).

Group ND: in BE, for Pz as a source, weaker connections were flowing to Fz, C3, and Cz in all frequency bands, to F4 and P4 (in alpha and both beta bands), to P3 (in alpha and higher beta bands), and stronger connections were flowing to P4 (in theta band). For Pz as a sink, weaker connections were coming from most of the fronto-central connections in alpha and both beta bands, except from F3 and C3 (in alpha band) and from P4 (in lower beta band) which indicate stronger DTF in BE.

(ii) *Group D*: the highest statistically different connectivity between BE and WO was found in alpha band. Higher connectivity during BE was found in PoC while higher connectivity during WO was found in CF and PoF.

Group ND: significantly higher connectivity was found in PoF (in both beta bands) and PoC (in all frequency bands) during BE, while significantly higher connectivity was found in FC (in theta and alpha bands) and FPo (in both beta bands) during WO.

(iii) *Group D*: significantly higher average DTF during BE compared to WO were found in FC (theta), FPo (all frequency bands), CC and PoC (theta), and PoPo (alpha and both beta bands), and significantly lower average DTF during BE compared to WO were found in FF (theta and higher beta), FC (alpha and lower beta), CF (theta, alpha, and higher beta), and PoF (all frequency bands).

Group ND: significantly higher average DTF during BE compared to WO were found in FF and CF (higher beta), FPo (theta and alpha), CPo (theta), PoF (all frequency bands), and PoPo (theta, alpha, and lower beta), and significantly lower average DTF during BE compared to WO were found in FC, CC, and PoC (all frequency bands).

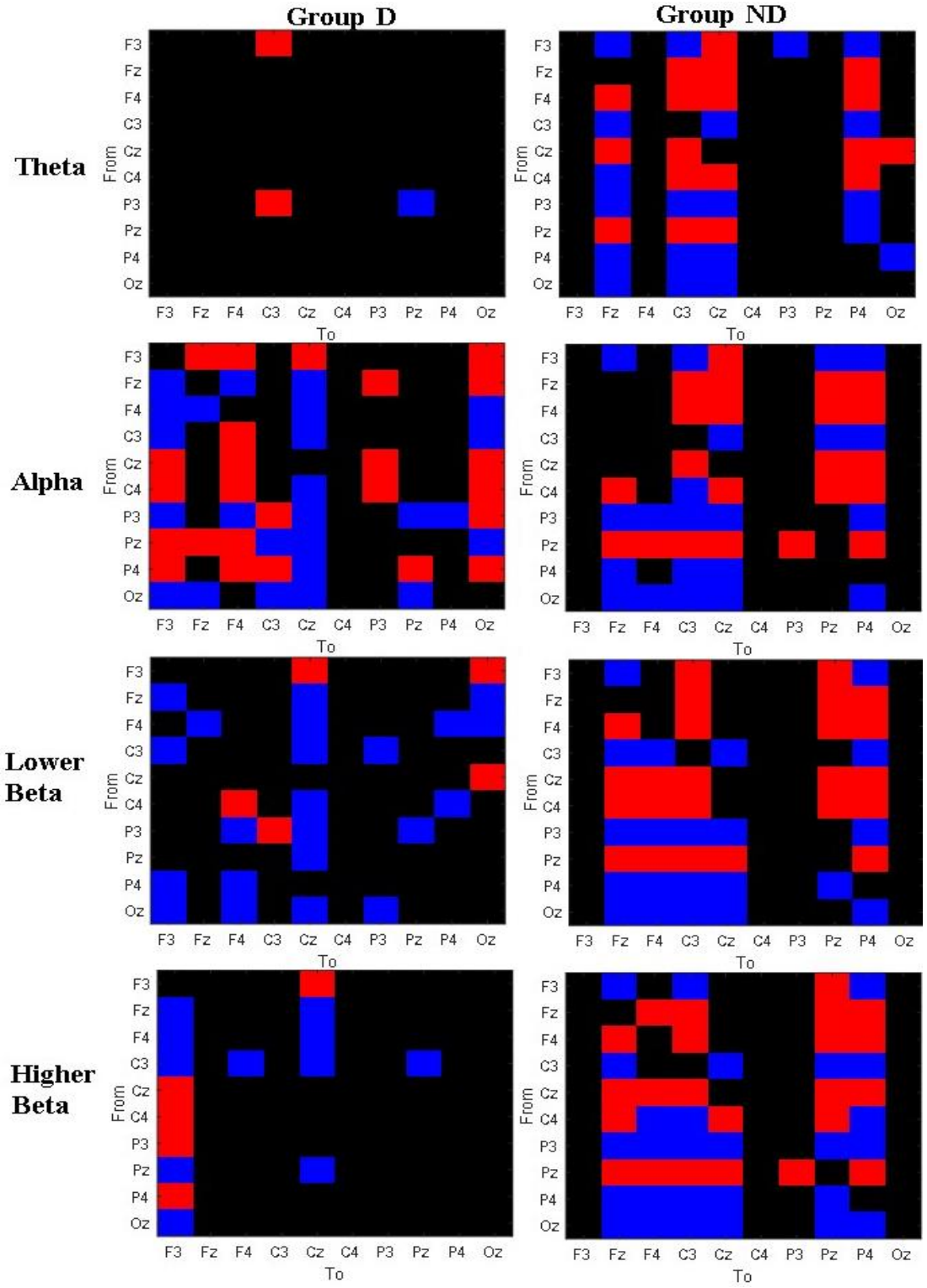

Figure 7.15 The matrices of *p*-values generated from a non-parametric paired permutation ($p<0.01$) of the DTF values from all trials **between BE and WO for each group,** in each frequency with FDR correction applied. The blue and red squares indicate the significant connections, blue indicates higher average DTF value in BE and red indicates higher average DTF value in WO.

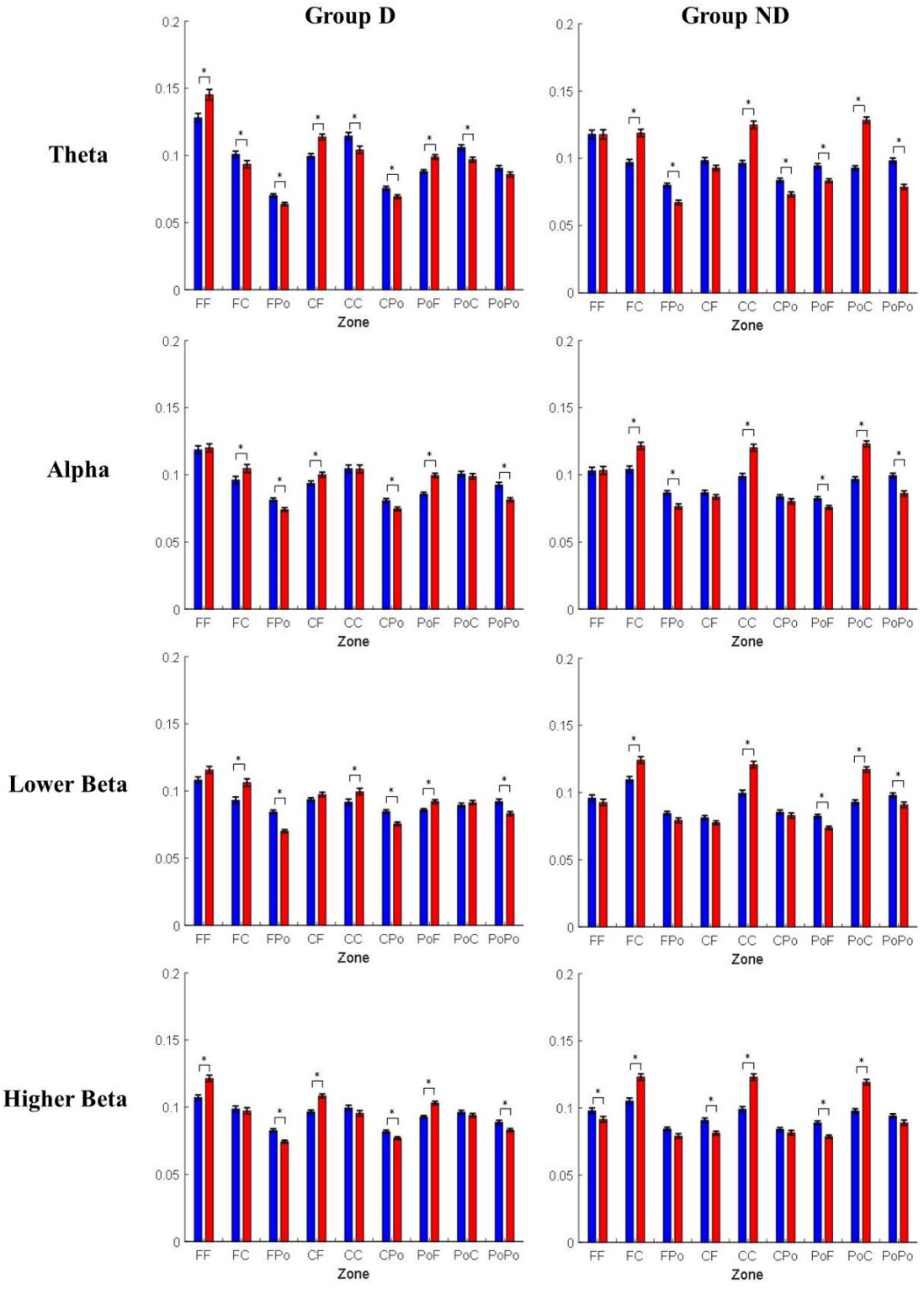

Figure 7.16 The bar graphs of the average DTF values (mean ± standard error) in each zone between BE and WO for both groups, in each frequency band. A non-parametric paired permutation (p<0.01) was performed to compare the statistic between two conditions, with FDR correction applied. The blue bars indicate the average DTF during BE and the red bars indicate the average DTF during WO.

Statistical comparisons between group D and group ND

(i) *Baseline*: for Pz as a source, group D shows stronger connections to Fz (in alpha and both beta bands), F4, Cz (both in alpha and higher beta bands), C4 (in alpha band), P3 (in lower beta band), P4 (in both beta bands), and Oz (in lower beta band). For Pz as a sink, group D shows stronger connections from C3, Cz, P4, and Oz (in all frequency bands), and from P3 (in both beta bands), and weaker connections from all frontal channels (in all frequency bands).

BE: for Pz as a source, group D shows stronger connections to all fronto-central channels and to some parieto-occipital channels in all frequency bands. For Pz as a sink, group D shows stronger connections from Fz (in alpha and higher beta bands) and Cz (in all frequency bands.), and weaker connections from F3 and C3 (in all frequency bands).

WO: for Pz as a source, group D shows stronger connections to most fronto-central channels (in theta, alpha, and higher beta bands), and to P4 and Oz (in theta band). For Pz as a sink, group D shows stronger connections from Cz (in alpha and both beta bands) and from P4 and Oz (in higher beta band), and weaker connections from F3 and F4 (in all frequency bands) and from C3 (in theta, alpha, and higher beta bands).

(ii) *Baseline*: Higher connectivity in group D was found in CPo (in alpha, theta, and lower beta bands), PoF (in theta and higher beta bands), and PoPo (in lower beta band), and higher connectivity in group ND was found in FPo in all frequency bands.

BE: Higher connectivity in group D was found in PoF (in alpha and both beta bands), PoPo (in theta, alpha, and higher beta bands), CPo (in theta band), and PoC (in lower beta band), and higher connectivity in group ND was found in FPo in all frequency bands.

WO: Higher connectivity in group D was found in PoF (in alpha and higher beta bands), PoPo (in theta and lower beta bands), PoC (in alpha band), and CPo (in theta band), and higher connectivity in group ND was found in FPo in all frequency bands.

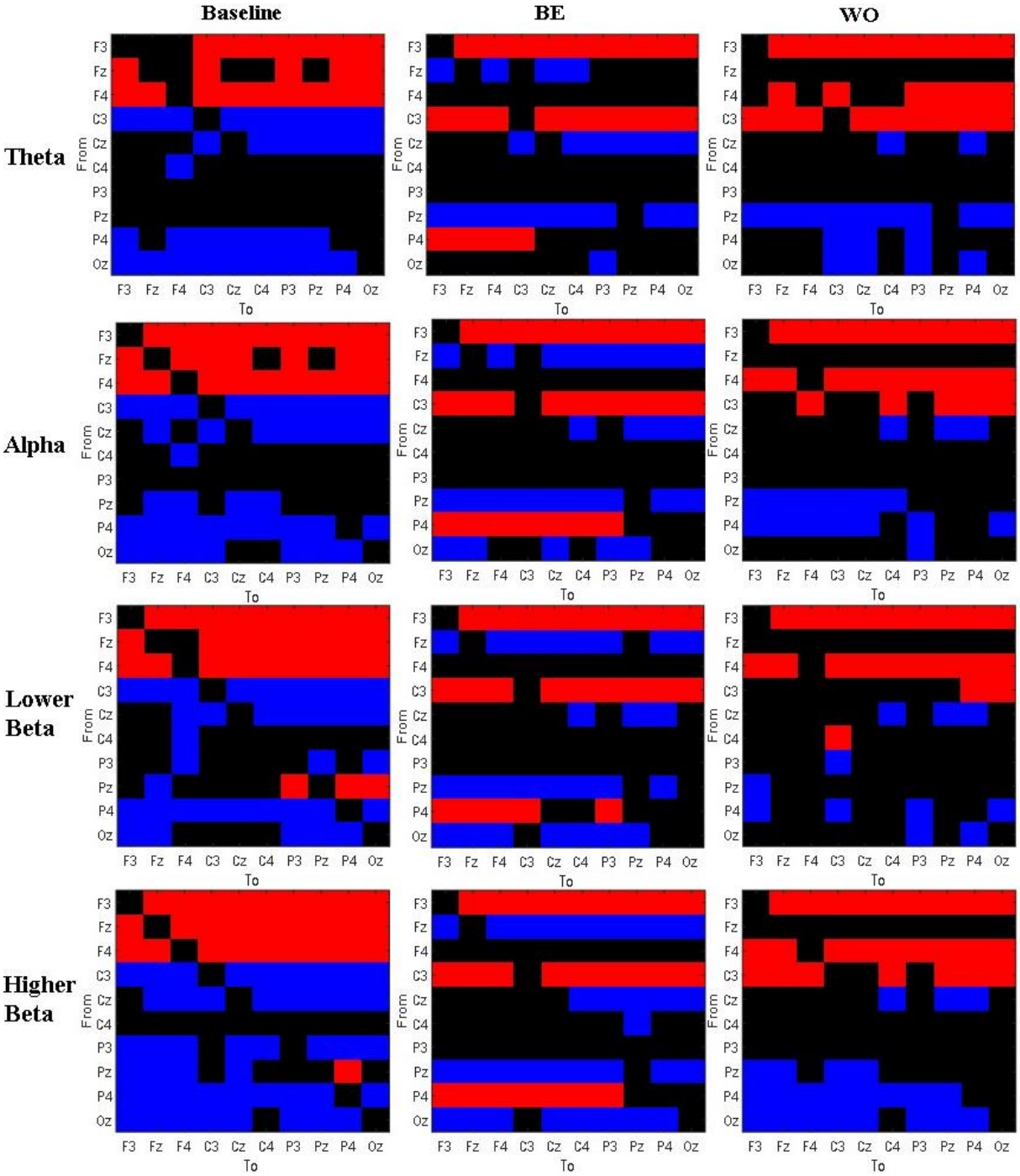

Figure 7.17 The matrices of *p*-values generated from a non-parametric paired permutation ($p<0.01$) of DTF values from all trials **between groups** (D and ND) for Baseline and each gaming condition (BE and WO), in each frequency with FDR correction applied. The blue and red squares indicate the significant connections, blue indicates higher average DTF value in group D and red indicates higher average DTF value in group ND.

7.3.3. Inter-brain Granger Causality

Inter-brain GC results are presented in two ways: as matrices presenting the grand average of GC values of all epochs from all pairs in each direction (i.e. from group D to group ND will be called 'direction I' and from group ND to group D will be called 'direction II') (Fig. 7.18), as a set of *p-values* matrices displaying the significant connections, as a result of a non-parametric single-sample permutation test (Fig. 7.19), and as inter-brain connectivity maps displaying the significant connections obtained from the *p-values* matrices (Fig. 7.20).

The significant connections found in the inter-brain GC showed that significant connections were found only in direction I during both BE and WO (Fig. 7.19 and 7.20), while there was no significant connection found in the opposite direction. This condition indicates that group D was more actively engaged to the social aspect of the game- to adjust their intra-brain activity to the same level as their partner's. On the other hand, the lack of significant connections in direction II showed that group ND did not contribute enough to increase their brain activity to match their partner. These results indicate that collaborative scores were achieved due to the active effort of brain activity adjustment by group D.

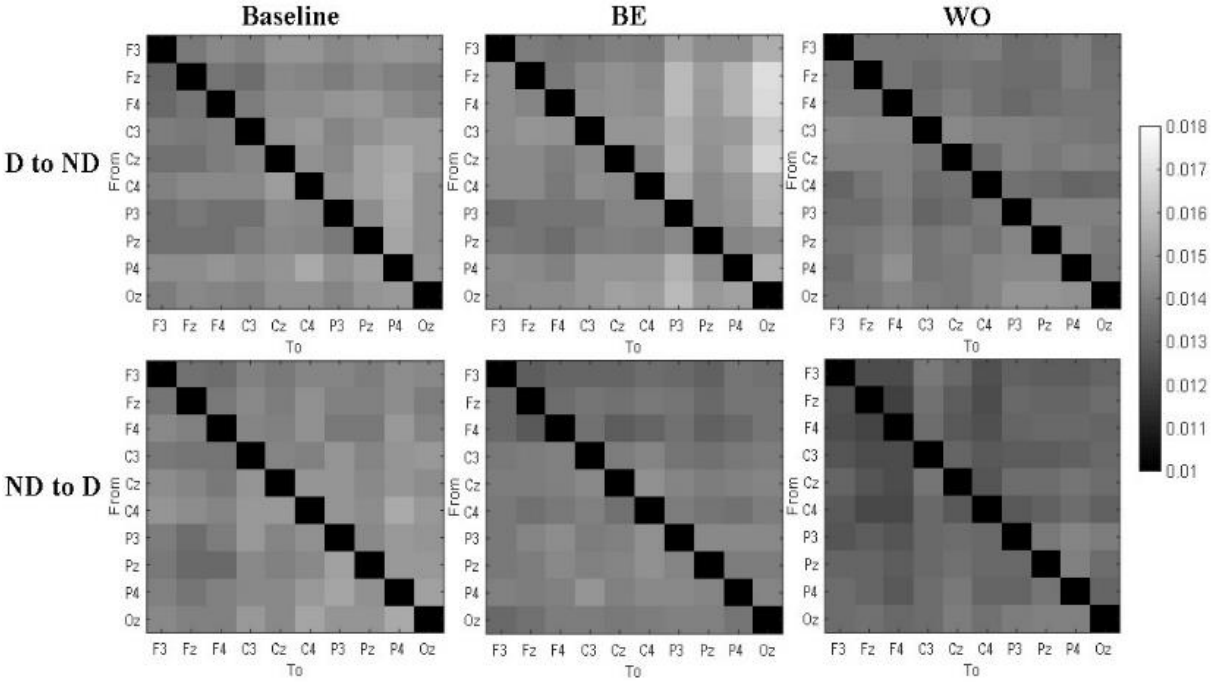

Figure 7.18 The matrices of the average inter-brain GC for each condition, i.e. Baseline, BE, and WO for each direction.

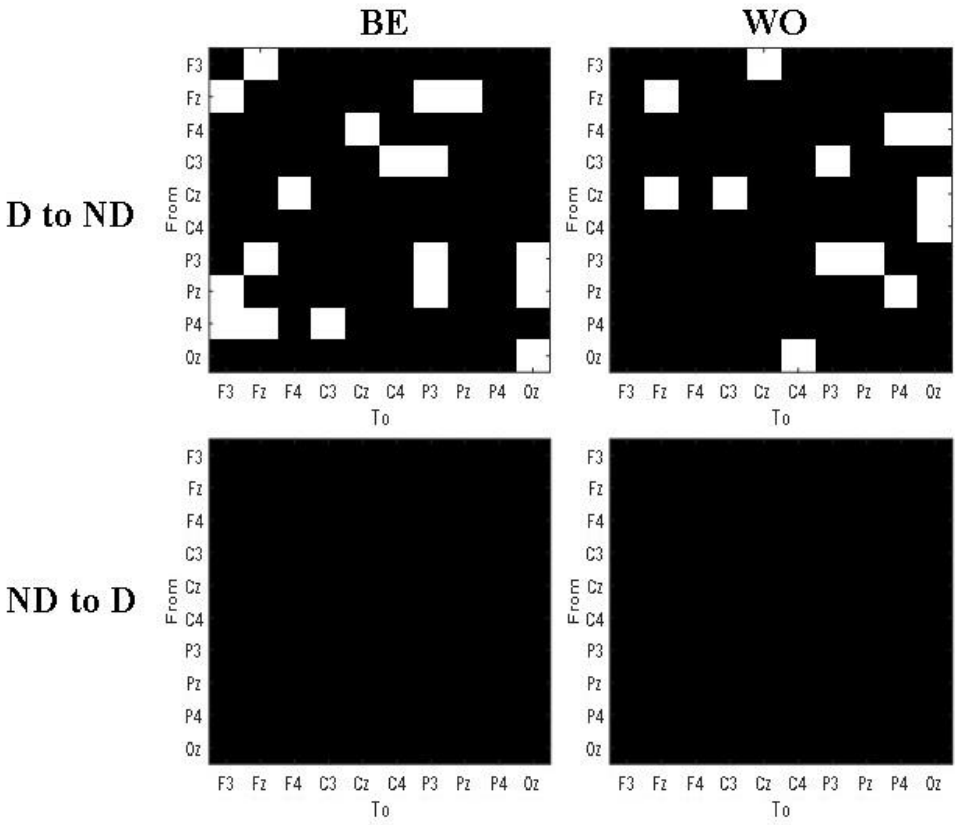

Figure 7.19 The matrices of *p*-values generated from a non-parametric single-sample permutation ($p<0.001$) with FDR correction applied, of the inter-brain GC of all pairs for both gaming conditions. The white boxes represent the significant connections.

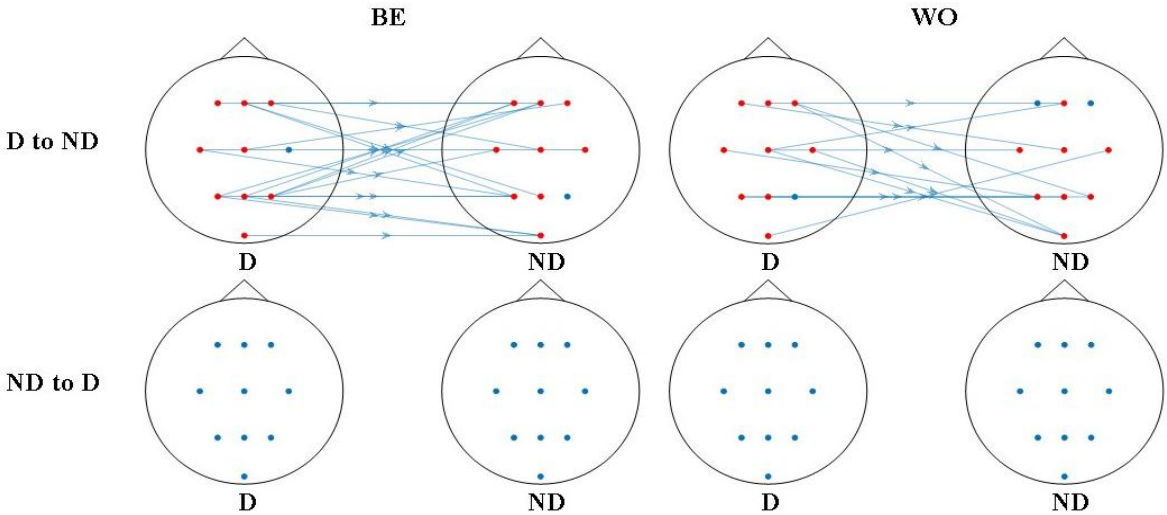

Figure 7.20 The significant inter-brain connectivity map based on the significant connections found in Figure 7.19, for both gaming conditions (BE and WO), in both directions.

7.4 Discussions

Multi-user BCI collaborative gaming has been previously studied [62, 63], however, the information regarding the cortical activation within and between the interacting brain are still relatively limited. In this study, we performed intra-brain and inter-brain connectivity analysis in order to explore the impact of collaborative BCI gaming that is based on alpha band operant conditioning, to the brain cortical activity. Three different conditions were measured such as pre-gaming Baseline, BE, and WO, with the group of players divided into group D and group ND. Connectivity analysis were divided into intra-brain GC, DTF, and inter-brain GC, with a non-parametric statistical analysis to compare the results based on the types of condition (i.e. Baseline vs BE and Baseline vs WO), based on BE vs WO, and based on the groups (i.e. between group D and group ND). Intra-brain connectivity (both GC and DTF) detected the fluctuation of connections coming from Pz in group D during gaming, indicating the flexibility to adjust alpha power to the similar level to group ND. Inter-brain connectivity during collaboration only found significant inter-brain connections from group D during BE and WO, indicating the higher effort to engage in collaborative interaction was mainly coming from group D regardless the gaming condition.

Intra-brain GC

Intra-brain GC results detected Pz activity during gaming in group D shows more fluctuation (increased connectivity to frontal channels and decreased connectivity to central and parietal channels) compared to in group ND, which only shows a decreased connections during BE and no changes during WO. This result is consistent with the previous finding s in Chapter VI, that group D has the better ability to regulate their brain activity at Pz.

Midline connectivity revealed that group D shows a significant decrease in the connections between Pz and Cz bidirectionally, and from Fz to Pz.in both gaming conditions. The decreasing trend the midline area might indicate the activity of the cingulate cortex, which is divided into anterior (ACC) and posterior cingulate cortex (PCC) [185, 238]. PCC is a part of the default mode network (DMN) along with medial prefrontal cortex (mPFC) and temporoparietal junction (TPJ) [184] ACC is a part of salience network (SN), along with ventrolateral prefrontal cortex (vlPFC), anterior insula [13, 192]. DMN is a network that is more active during resting and less active during

cognitive control and SN detects stimuli and mediates the switching between DMN and central executive network [13, 239]. Decreasing activity in the midline area might reflect the process of network switching as a response of a cognitive task. Moreover, we also found an increase in the bilateral fronto-parietal connection during BE (from F4 to P4 and from Pz to F3), which indicate the activation of the fronto-parietal attention network [180].

In contrast, the brain networks in group ND tend to decrease during both gaming conditions, showing that there was a decrease in the midline area, however there was no increase in any network. However, during the best collaborative performance (BE) both players decreased the connections coming from the left frontal channels (F3) towards all the other channels. In group D, this reduced GC originated from the left frontal area was accompanied by a fluctuation in Pz activity, while in group D network connectivity reduction occurred more globally. This suggest that the reduction of GC may not necessarily reflect a task-specific brain response to collaborative interaction performed by the players.

Intra-brain GC comparison between groups show that, even during Baseline, the two groups displayed statistically different connectivity pattern, showing higher GC from the fronto-central to the parieto-occipital areas in group D. Based on our results, the connectivity difference during resting period between the groups may allow the prediction of a gaming/training outcome, as previously studied with the functional resting connectivity and its ability to predict task performance [45, 183].

Directed Transfer Function

DTF analysis at channel Pz revealed that group D shows more connectivity fluctuation. During BE, Pz shows an increase of towards the parietal cortex in theta, alpha, and lower beta bands. While during WO, Pz shows a decrease of connections in alpha and lower beta bands towards the central and parietal cortex and towards Fz in higher beta band. In contrast, Pz activation in group ND mainly shows decreased connections to different cortical areas during both gaming condition, and these changes are less frequency-specific compared to group D. These results, once again reflect the effort of the players to regulate Pz activity within alpha frequency band, which was successfully done by group D.

DTF results in group D shows frequency-specific dynamic changes involving Cz, i.e. different gaming conditions were marked by different connectivity patterns coming

from Cz. Decreased connections was found from Cz to all cortical areas in alpha and lower beta bands during BE, and increased connections from Cz to frontal channels (in theta, alpha, and lower beta bands) and to central and parietal channels in higher beta band, during WO. The fluctuation of midline activity can be associated to the activity of cingulate cortex, in which divided into ACC and PCC, and each section of the cingulate cortex has been linked to social behaviour [240, 241]. Non-frequency specific increase of network connections were found coming from frontal area to all channels and from C4 to parietal area, in both gaming conditions compared to Baseline, while non-frequency specific decreased were found from C3 and the parietal channels to fronto-central areas. Results in group D suggest that the frequency specific changes were facilitated by the midline area, while the constant changes in all frequency were facilitated by the bilateral channels over the cortical area. However, the lateralization trend in DTF is different than the results in GC. This difference will be discussed later in the chapter.

DTF results in group ND show that non-frequency-specific increased connectivity was found from the left fronto-central area to all cortical areas in both gaming conditions, and from the midline central channel to all cortical areas only during WO. The activity around the left fronto-central area might reflect the activation of the left prefrontal gyrus, that is associated with various functions, including verbal processing as well as self-related processing [242, 243] and long term memory retrieval [244].

Furthermore, the frequency specific increase of connection in group D in the localised parietal area during BE, suggest that a successful collaborative gaming only increase the short distance/localised connectivity closer to the targeted area (Pz). In addition, taken from the source activation results in alpha band presented in Chapter VI, the highest increase of source activation was found in the left inferior parietal lobule (IPL), which might explain the increased connection from Pz to P3 in alpha band (as well as in the frequency which might overlap with alpha, i.e. theta and lower beta band).

Similar to intra-brain GC, DTF comparison between groups show that, in Baseline condition, the two groups displayed statistically different connectivity pattern in (despite being relatively non-frequency specific). The connections from frontal area to all cortical areas during Baseline in group ND were higher compared to group D (which is consistent with the results in competitive gaming), which remained high during gaming, consequently caused them to perform poorly. **These dynamical differences during**

resting might be the useful to predict a successful/non-successful gaming performance [45, 183].

Inter-brain GC

Inter-brain GC analysis revealed that the significant inter-brain connections were only appeared in the direction from group D to group ND. This result indicates the majority of the collaborative effort were mainly done by group D, which is in line with the single-brain EEG analysis results of group D. Compared to the results during competition, collaborative gaming showed larger number of inter-brain connections from group D to group ND, and the opposite condition for group ND (larger number of connections were found in competitive instead). These trends show the tendency of each different group (D/ND) to engage only to a certain type of social interaction, i.e. group D was more challenged in collaboration and group ND was more challenged in competition, suggesting that having different social interaction options in the game can be useful for different types of players. Moreover, the inter-connectivity results done by Astolfi et al. [84], during the Prisoner's Dilemma game showed that the inter-brain connection's density were higher when the subjects decided to cooperate, than when they decided to defect the other player. Their results show different trend than the ones in this chapter, however the difference suggests that the inter-connectivity density are not mainly influenced by the types of interaction (cooperation/defective) but also by the manner of how the interaction was performed (for example: in a decision-based/turn-taking manner or in a simultaneous manner).

Notable findings

Our study analysed the brain intra- and inter- connectivity as a response to collaborative interaction in an alpha operant-conditioning training paradigm. We found that different method of multivariate connectivity analyses, i.e. GC and DTF, might show different results, particularly evident after the statistical analysis comparing gaming condition with Baseline. It has been proposed that, despite the similar concept of GC and DTF in estimating directed connectivity, DTF estimates the total information affecting one time series on another, while GC mainly estimates the direct effect that one series can give to another [195]. Moreover, GC can have the tendency to promote type I spurious causality, which likely to cause a false detection of a direct effect between two time series [195],

while DTF detects not only a direct effect but also a cascade effect [196]. Different connectivity detection during Baseline and gaming by these two methods, consequently, resulted different trend of brain activation pattern after statistical analysis. However, both approaches are equally needed in our study to provide connectivity information in both time and frequency domain.

Moreover, we found that intra-brain connectivity results in this study to some extent, complement the single-brain analysis electrophysiological signatures, performed in the previous chapter (Chapter VI). Our results revealed that significant connectivity changes in a specific frequency band might appear, despite the power spectral density results did not find any significant activation in the localised area. These significant connections displayed the brain activity as multiple separate networks and depicted their influences on each other during resting and active states. In addition, we found that individual intra-brain connectivity during resting is potentially useful in predicting gaming performance. Lastly, the inter-brain connectivity analysis revealed that the significant connections were only found from group D to group ND in BE and WO, suggesting that group D had higher level of engagement to the social aspect of gaming, and produced higher effort to achieve the mutual scores.

Limitations

The limitations of this study including small number of channels as well as the shorter time-series length that were used in connectivity analysis. A larger number of channels that evenly distributed over all cortical areas will provide a better connectivity resolution. Faster computational facility was also required in order to perform connectivity analysis efficiently. Inter-brain synchrony analysis could be added for future direction to validate the inter-personal brain synchrony that might occur during collaborative task [245, 246]. An extensive questionnaire for quantitative measures of user experience is also required in order to design a more user-friendly collaborative BCI in the future. Lastly, there is always a room to increase the number of players in order to get better and more precise group statistical results.

7.5 Conclusions

The study performed intra- and inter- brain connectivity analysis of the data obtained by multi-user collaborative BCI game that is based on alpha band operant conditioning. Our

results suggest that group D have the better ability in adjusting their Pz activity to a similar level as their partner's. Intra-brain connectivity results also highlighted the dynamics of midline areas during Baseline and during gaming and revealed a higher activation of fronto-parietal control network in group D during gaming compared to group ND. These results indicate that they are capable of both levelling their Pz activity similar to their partner's, while at the same time being engaged to the interactive task. This ability might be predictable based on their intra-brain baseline connectivity. Intra-brain connectivity in group ND suggests that they did not show any meaningful frequency-specific dynamic in the connections that involve Pz, and they were likely to have lower task-engagement level. Finally, our inter-brain connectivity results found significant connections only in the direction from group D to group ND in both gaming conditions (most successful and least successful conditions), which show that group D had higher engagement level to the collaborative gaming.

Chapter VIII

General Discussion

The aim of this thesis is to investigate the electrophysiological changes that occur in the brain, due to the multi-user BCI gaming, by performing EEG signal processing techniques i.e. power spectral analysis, signal complexity analysis, source localisation analysis, and brain connectivity analysis, where the BCI paradigm used is based on the alpha band non-verbalised operant conditioning at channel Pz. In order achieve this aim, two main experiments have been performed to address the objectives, and they are organised as the following:

- Chapter IV presented the main finding of the EEG power spectral and source localisation analysis from the multi-user competitive BCI gaming performance.
- Chapter V presented the main finding of the (intra- and inter-) brain connectivity analysis from the multi-user competitive BCI gaming performance.
- Chapter VI presented the main finding of the EEG power spectral and source localisation analysis from the multi-user collaborative BCI gaming performance.
- Chapter VII presented the main finding of the (intra- and inter-) brain connectivity analysis from the multi-user collaborative BCI gaming performance.

8.1 Discussions of the main findings

1) *What are the strategies applied by the players when they were engaged to the different social interactions applied in the game, judging by the changes of their brainwaves?*

- *Competitive interaction*

Chapter IV showed that both players maintained Pz alpha power to a close level as in Baseline, during successful competitive gaming conditions. The instruction given to the players was for them to upregulate their alpha power at Pz to be higher than their opponent, thus required them to play based on their own feedback and based on their opponent's feedback. The maintenance of Pz alpha similar to Baseline was the consequence of the given instruction. Since alpha activity is higher during resting and lower in the presence of visual stimulation and cognitive task [20], the maintenance of alpha power to the similar level at Baseline reflects the control to upregulate alpha activity even when the power never exceed the level in Baseline. The trend of the averaged absolute alpha power at Pz during successful competitive gaming in both groups are depicted in Figure 8.1, where the difference level of gaming alpha in each group are very distinctive. Moreover, the source localisation analysis in group D during a successful competition revealed that the brain area with the highest increase of source activity in alpha band was found in the precuneus, which is located in the parietal cortex closer to the midline channel. This result was later confirmed by the frequency specific connectivity increase found by DTF analysis, from Pz to Cz, which are closely located to the precuneus area.

- *Collaborative interaction*

Chapter VI showed that group D the flexibility to adjust Pz alpha activity to a close level to group ND, as shown during the most successful collaboration where group D decreased alpha power at Pz, while group ND maintained the same alpha level to Baseline. In this interaction, the flexibility to adjust alpha level is important, and the results indicate that only group D showed a significant activity changes, although maintenance of alpha by ND might also indicate their effort to adjust to group D's level. The trend of the averaged absolute alpha power at Pz during successful collaborative gaming in both groups are depicted in Figure 8.1, where the similarity of gaming alpha in each group are very distinctive. Moreover, the source localisation analysis in group D during a successful

collaboration revealed that the brain area with the highest increase of source activity in alpha band was found in the left hemisphere of the inferior parietal lobule (IPL). This result was later confirmed by the frequency specific connectivity increase found by DTF analysis, from Pz to P3., which are closely located to the IPL area.

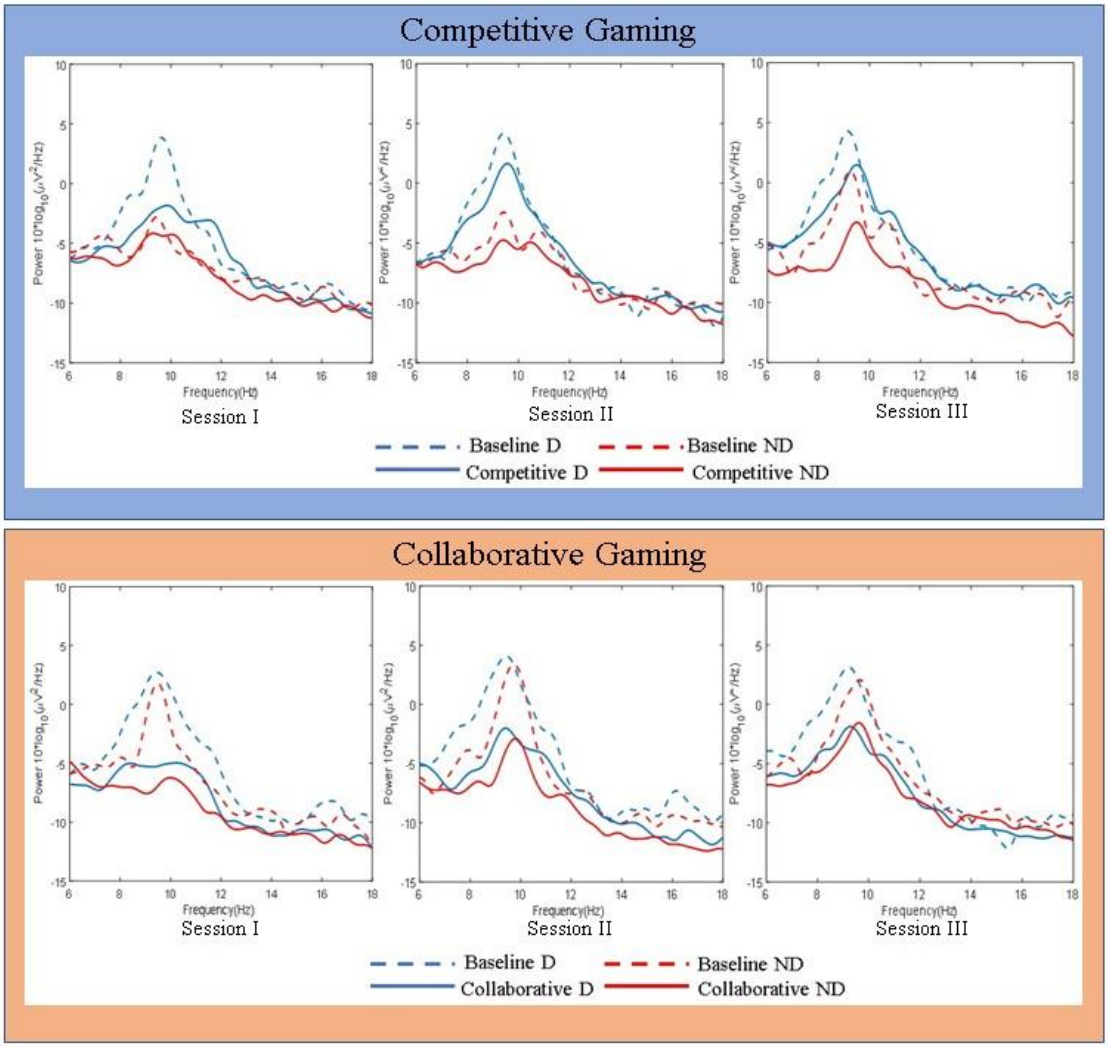

Figure 8.1 The averaged absolute alpha power at Pz from all players in each group, in each session, for competitive gaming (blue box), and collaborative gaming (orange box) and for their respective baselines.

2) How relevant is EEG neurofeedback strategy for the multi-user BCI gaming?

The exact neurofeedback rule is not entirely relevant, as unlike in the typical single-user EEG alpha neurofeedback, where the subject maintains their brain activity based on their own feedback. In our multi-user BCI gaming, the goal is to get higher score. Scores can be achieved by attending both personal feedback and the feedback of others, thus adjusting alpha power level based on the opponent's/partner's is much more relevant than

following the neurofeedback instruction to upregulate alpha. While upregulating alpha power could be clearly related to the winning strategy in competition, in collaboration upregulating alpha power would be irrelevant, as the strategy for collaboration is to maintain alpha power to the close level to the other player, which could be either upregulation or downregulation of alpha power.

3) What are the differences between competing players in competitive gaming?

Due to the difference of Pz behaviour in modulating alpha activity, different the intra-brain connectivity patterns were also found between the groups. Intra-GC brain connectivity showed that during both competitive gaming conditions, group D had more significantly increased connections compared to group ND, with most connections coming from the parietal channels towards the fronto-central channels, while group ND only maintained a very few increased connections, mostly coming from the right fronto-central channels towards the midline and right parieto-occipital channels. DTF analysis also found that group D showed frequency specific connections that are coming from Pz, particularly stronger during BSD, meanwhile group ND did not show any increased connections coming from Pz in any frequency in any gaming condition. In both gaming conditions, group ND showed a significantly decreased connections coming from the parietal channels towards fronto-central channels in all frequency bands. These intra-brain connectivity results indicate that group D modulated their parietal cortex activity where the control channel (Pz) is located, which did not occur in group ND. In addition, in SSD, group D did not show any increased connections from Pz while in group ND the same connections remained low, this condition suggest that group ND's best gaming performance (SSD) might not be entirely due to their better performance, but more likely due to the poor performance of group D.

4) Is there any consistency or differences found in the inter-brain connectivity between competition and collaboration?

Chapter V and Chapter VII found that different gaming interactions resulted in different inter-brain connectivity for each group of players (Fig. 8.2). In competition, higher number of significant inter-brain connections were found in the direction from group ND to group D in both BSD and SSD gaming conditions, while in the opposite direction, group D only showed significant inter-brain connections during BSD. These results

indicate that: 1) group D achieved their best gaming performance when they actively engaged to the social aspect of the game (in addition to their intra-brain activity modulation), 2) group ND was more engaged to the social aspect of the game regardless their gaming condition – suggesting that the key success of the game is to be engaged in both individual (as intra-brain activity modulation) and social aspects, 3) group ND showed higher number of channels that are actively sending out significant connections to group D during their best gaming condition (SSD), suggesting that larger brain activation area combined with the lack of social engagement by group D allow them to reach their best gaming performance.

In collaboration, significant inter-brain connections were found only in the direction from group D to group ND, in both BE and WO gaming conditions. Unlike the results from competitive gaming, during collaborative gaming, only group D that was actively engaged to the social aspect of the game, regardless the gaming condition. This result indicates that the gaming scores were mainly achieved due to the higher effort done by group D to adjust their intra-brain activity level to the same level as their partner.

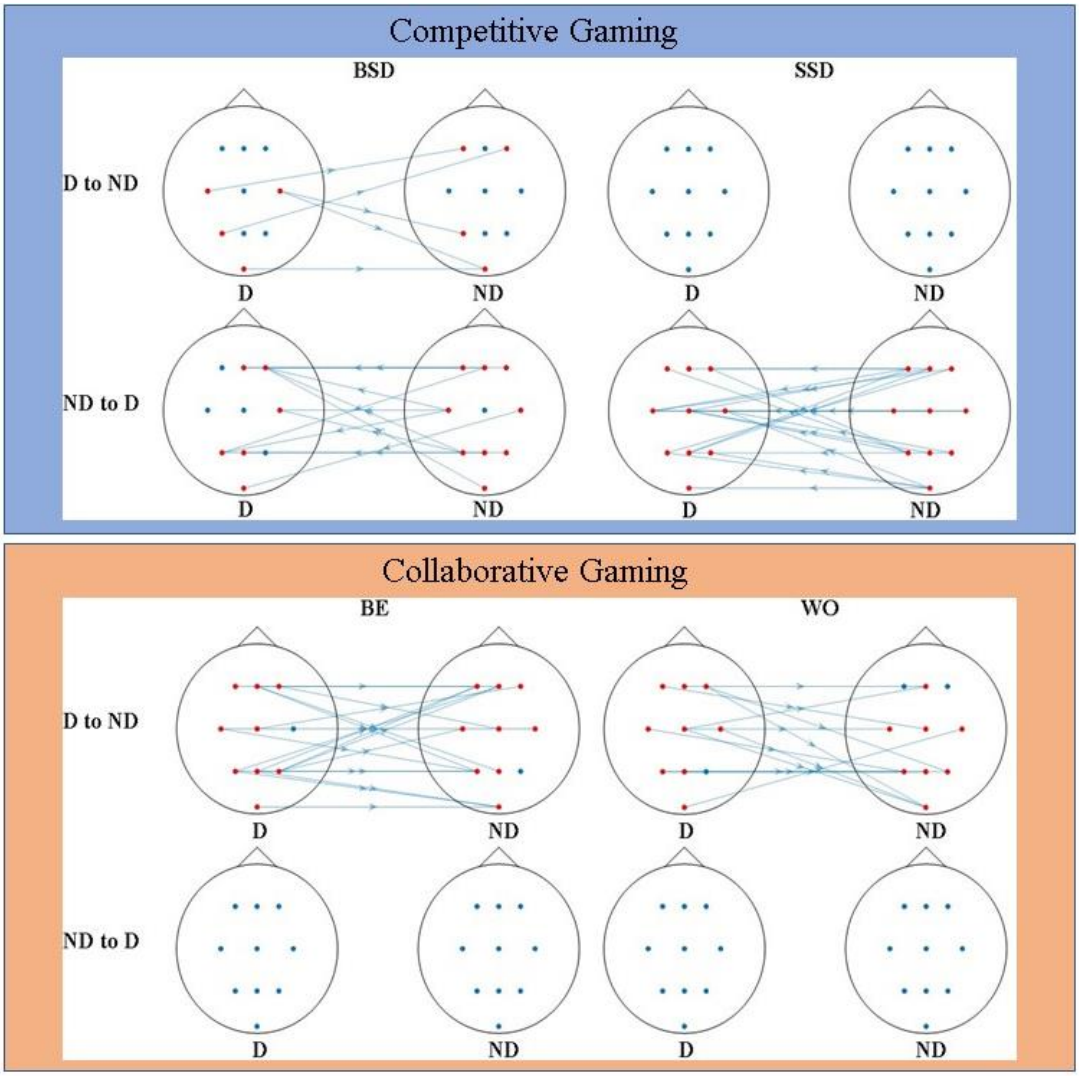

Figure 8.2 The significant inter-brain connectivity map based on the significant connections generated by a non-parametric single-sample permutation ($p < 0{,}001$) with FDR correction applied, for competitive (blue box) and collaborative (orange box) gaming, in both directions (group D to group ND, and group ND to group D).

5) Is there any resting state prognostic brain marker to characterise the players gaming performance?

Both studies showed that both groups had different level of occipital alpha power during resting as well as a different intra-brain connectivity pattern between the two groups. These results support the idea of using resting alpha power and resting connectivity as a predictor of gaming performance [42, 45, 183]. The dominant players were shown to have higher occipital alpha power and stronger intra-brain connections, particularly the

connections that involved the parieto-occipital channels, compared to the non-dominant players.

6) *What are the differences in terms of the brain activities between multi-user interactive BCI gaming and conventional physically controlled video gaming?*

The multi-user BCI interactive gaming in our study found that the main changes of brain activity in both studies occurred around/involving the parietal area specifically around the frequency of alpha band and the other frequency band that might overlap with alpha band i.e. theta and lower beta bands, which are evident in group D during competition. These posterior activities mainly occurred due to the game experimental design which required the control over the parietal cortex of the players. However, despite being non-statistically significant, we also found a wider activation site around the frontal cortex, particularly in the middle frontal gyrus, in group D during both gaming interactions. Frontal cortex has been reported to be activated during non-BCI gaming, in both single-user and hyperscanning studies. [78, 79, 247, 248].

The brain's frontal cortex, particularly the prefrontal cortex, has been associated with various cognitive functions, e.g. in decision making and social comparison [144, 193], emotional processing [249, 250], memory processing [251], moral judgement [252], planning [194], and motivation to approach or to withdraw [229]. Any of these functions can be easily triggered during a very stimulating, multi-sensory activity e.g. interactive gaming. Some studies have reported the long-term effect of video gaming in structural and functional alteration of the brain, including the frontal cortex [253-256], suggesting that the influence of gaming to the frontal cortex activity is more inclined to the tendency of gaming in stimulating complex cognitive processes, regardless the type of gaming control (BCI/non-BCI). Apart from the specificity of the game control (i.e. alpha activity at Pz), our gaming experiments were performed in a non-verbal and non-physical manner, therefore the activation of such brain areas responsible for speech processing and motor control, e.g. temporal and motor cortex [91, 247], were not highlighted in this study.

7) *Is the mental strategy applied during multi-user BCI gaming similar to during single-user neurofeedback BCI gaming?*

While certain areas of the brain related to the responses of arousal and dominance are active in both conditions [257], a success of the multiuser game is not necessarily related

to the single-user neurofeedback BCI strategy, which in this case was to increase the alpha band power at Pz. The main difference is that during single user BCI, a player is trying to control EEG power with respect to their own baseline level while in multiuser BCI the "baseline" is dynamic and affected by an external factor, i.e. performance of the other player. As a consequence, multiuser BCI might not necessarily serve the same purpose as single user BCI. For example, single user BCI can be used for therapeutic purpose where a player is consistently upregulating brain activity, while in multiuser BCI this consistency is lost even when a player is winning the game.

8.2 Limitations

For the EEG experiments, a higher number of channels that are evenly distributed throughout the cortical areas should be used, as higher number of channels can provide better spatial resolution and minimise the effect of volume conduction from the sparse electrodes distribution, thus, producing better accuracy, particularly in connectivity and source localisation analyses. Equal number of EEG channels should be used by both players regardless their dominance level.

For connectivity analysis, a higher number of channels and longer data length should be used, as higher number of EEG channels may allow more precise representation of the brain connectivity in a specific or in a larger area, while longer data length would increase the number of epochs/trials, thus producing more precise connectivity results. Faster computational power is also required, as a faster computational facility is beneficial to perform connectivity analysis efficiently, allowing the use of higher number of channels and longer data length.

For experimental designs, a higher number and more frequent training sessions should be added to provide players with more time to learn and to eventually gain better performance. Larger number of participants should be recruited, as it can give more precise and powerful statistical results.

8.3 Suggestion for future work

A post-experimental questionnaire for quantitative behavioural measures and/or for user experience measures, would be useful to assess the players perception of the game and

the user-friendliness of the BCI paradigm, which will be beneficial for the future improvement of the game.

Inter-brain synchronization analysis would be useful to provide more accurate information related to inter-brain connectivity and coupling during different social interaction tasks.

Prior the first gaming session, classifying the players based on their resting state alpha power/intra-brain connectivity to make sure each player in a pair is closely matched, would be useful to avoid extreme outperformance that might affect confidence level and motivation of the players.

Performing/providing data from the single-user gaming BCI experiment with the similar interface would provide comparable information that can be useful to study the efficiency of the same interface with/without social interaction.

8.4 Conclusion

This thesis studied the brain activity changes as a response to an EEG-based multi-user BCI gaming that incorporated different social interaction types (i.e. competitive and collaborative interaction), with the BCI paradigm that is based on alpha non-verbalised operant conditioning. Extensive analyses of the electrophysiological signatures and brain connectivity were performed to the EEG data, in order to explore the brain cortical changes during gaming experiments. The results of the analyses were compared between competition and collaboration., and it was revealed that different types of interaction produced different kind of response in the brain activity of the players. These responses including the fluctuation and the spatial distribution of alpha power, the changing brain source localisation pattern, and the changes in of intra- and inter-brain connectivity. It was found that the level of dominance between players produced different response in brain activity, in both gaming interactions. Additionally, it was revealed that the level of alpha power and intra-brain connectivity during resting state can be used to predict the gaming performance. Overall, the thesis has contributed in providing the information regarding the brain's cortical activity changes during different kinds of multi-user BCI gaming interaction, which is expected to benefit for the development of multi-user BCI games and for other methodological considerations in designing multi-user BCI application.

References

1. Reece, J.B., Taylor, M. R., Simon, E. J., Dickey, J. L., & Cummings, B., *Nervous Systems*, in *Biology: concepts & connections*. 2012, Pearson Benjamin Cummings: San Francisco, CA. p. 562-585.
2. *Studying the Nervous Systems of Human and Other Animals*, in *Neuroscience*, D. Purves, Augustine, G. J., Fitzpatrick, D., Hall, W. C., LaMantia, A.-S., McNamara, J. O., & Williams, S. M., Editor. 2004, Sinauer Associates: Sunderland, MA, US. p. 1-27.
3. Kandel, E. and A. Hudspeth, *The Brain and Behavior*, in *Principles of Neural Science*. 2013, McGraw-Hill Medical. p. 5-19.
4. Brodmann, K., *The Basic Laminar Pattern of the Cerebral Cortex*, in *Brodmann's: Localisation in the Cerebral Cortex*. 2006, Springer Science & Business Media. p. 13-30.
5. *The Association Cortices*, in *Neuroscience*, D. Purves, Augustine, G. J., Fitzpatrick, D., Hall, W. C., LaMantia, A.-S., McNamara, J. O., & Williams, S. M., Editor. 2004, Sinauer Associates: Sunderland, MA, US. p. 613-635.
6. Jann, K., et al., *Topographic electrophysiological signatures of fMRI resting state networks.* PloS one, 2010. **5**(9): p. e12945.
7. Raichle, M.E., et al., *A default mode of brain function.* Proc Natl Acad Sci U S A, 2001. **98**(2): p. 676-82.
8. Seeley, W.W., et al., *Dissociable intrinsic connectivity networks for salience processing and executive control.* J Neurosci, 2007. **27**(9): p. 2349-56.
9. Fox, M.D., et al., *Spontaneous neuronal activity distinguishes human dorsal and ventral attention systems.* Proc Natl Acad Sci U S A, 2006. **103**(26): p. 10046-51.
10. Drysdale, A.T., et al., *Resting-state connectivity biomarkers define neurophysiological subtypes of depression.* Nature medicine, 2017. **23**(1): p. 28.
11. Damoiseaux, J.S., *Resting-state fMRI as a biomarker for Alzheimer's disease?* Alzheimer's research & therapy, 2012. **4**(2): p. 8.
12. Buckner, R.L., J.R. Andrews-Hanna, and D.L. Schacter, *The brain's default network: anatomy, function, and relevance to disease.* Ann N Y Acad Sci, 2008. **1124**: p. 1-38.
13. Fox, M.D., et al., *The human brain is intrinsically organized into dynamic, anticorrelated functional networks.* Proceedings of the National Academy of Sciences, 2005. **102**(27): p. 9673-9678.
14. Uddin, L.Q., et al., *Functional connectivity of default mode network components: correlation, anticorrelation, and causality.* Human brain mapping, 2009. **30**(2): p. 625-637.
15. Sridharan, D., D.J. Levitin, and V. Menon, *A critical role for the right fronto-insular cortex in switching between central-executive and default-mode networks.* Proc Natl Acad Sci U S A, 2008. **105**(34): p. 12569-74.
16. Goulden, N., et al., *The salience network is responsible for switching between the default mode network and the central executive network: replication from DCM.* Neuroimage, 2014. **99**: p. 180-90.
17. Da Silva, F.L., *EEG: origin and measurement*, in *EEG-fMRI*, C. Mulert, Lemieux, Louis Editor. 2009, Springer. p. 19-38.
18. Sanei, S. and J.A. Chambers, *Introduction to EEG*, in *EEG signal processing*. 2007, John Wiley & Sons, Ltd: West Sussex, England. p. 1-31.
19. Nunez, P.L.S., R., *The physics-EEG interface*, in *Electrical Fields of the Brain: The Neurophysics of EEG*. 2006, Oxford University Press. p. 3-52.
20. Niedermeyer, E., *The Normal EEG of the Waking Adult*, in *Electroencephalography: Basic Principles, Clinical Applications, and Related Fields*, E. Niedermeyer and F.L. Da Silva, Editors. 1999, Lippincott Williams & Wilkins: Philadelphia. p. 149-173.
21. Marcuse, L.V., M.C. Fields, and J.J. Yoo, *The Normal Adult EEG*, in *Rowan's Primer of EEG*. 2016, Elsevier Health Sciences. p. 39-66.
22. Jensen, O. and C.D. Tesche, *Frontal theta activity in humans increases with memory load in a working memory task.* Eur J Neurosci, 2002. **15**(8): p. 1395-9.
23. Gärtner, M., S. Grimm, and M. Bajbouj, *Frontal midline theta oscillations during mental arithmetic: effects of stress.* Front Behav Neurosci, 2015. **9**: p. 96.
24. Klimesch, W., *EEG alpha and theta oscillations reflect cognitive and memory performance: a review and analysis.* Brain Res Brain Res Rev, 1999. **29**(2-3): p. 169-95.

25. Pfurtscheller, G., et al., *Foot and hand area mu rhythms.* Int J Psychophysiol, 1997. **26**(1-3): p. 121-35.
26. Sitaram, R., et al., *Closed-loop brain training: the science of neurofeedback.* Nature Reviews Neuroscience, 2017. **18**(2): p. 86.
27. Kropotov, J.D., *Neurofeedback*, in *Functional neuromarkers for psychiatry: Applications for diagnosis and treatment*. 2016, Academic Press. p. 247-266.
28. Sherlin, L.H., et al., *Neurofeedback and basic learning theory: implications for research and practice.* Journal of Neurotherapy, 2011. **15**(4): p. 292-304.
29. Enriquez-Geppert, S., R.J. Huster, and C.S. Herrmann, *EEG-Neurofeedback as a Tool to Modulate Cognition and Behavior: A Review Tutorial.* Front Hum Neurosci, 2017. **11**: p. 51.
30. Marzbani, H., H.R. Marateb, and M. Mansourian, *Neurofeedback: a comprehensive review on system design, methodology and clinical applications.* Basic and clinical neuroscience, 2016. **7**(2): p. 143.
31. Vuckovic, A., et al., *A pilot study on clinical and neurological effects of neurofeedback training for treatment of central neuropathic pain*, in *Replace, Repair, Restore, Relieve–Bridging Clinical and Engineering Solutions in Neurorehabilitation*. 2014, Springer. p. 823-831.
32. Lansbergen, M.M., et al., *ADHD and EEG-neurofeedback: a double-blind randomized placebo-controlled feasibility study.* Journal of neural transmission, 2011. **118**(2): p. 275-284.
33. Bazanova, O.M., T. Auer, and E.A. Sapina, *On the efficiency of individualized theta/beta ratio neurofeedback combined with forehead EMG training in ADHD children.* Frontiers in human neuroscience, 2018. **12**: p. 3.
34. Gruzelier, J.H., *EEG-neurofeedback for optimising performance. I: a review of cognitive and affective outcome in healthy participants.* Neurosci Biobehav Rev, 2014. **44**: p. 124-41.
35. Gruzelier, J.H., *EEG-neurofeedback for optimising performance. III: a review of methodological and theoretical considerations.* Neurosci Biobehav Rev, 2014. **44**: p. 159-82.
36. Alkoby, O., et al., *Can we predict who will respond to neurofeedback? A review of the inefficacy problem and existing predictors for successful EEG neurofeedback learning.* Neuroscience, 2018. **378**: p. 155-164.
37. Witte, M., et al., *Control beliefs can predict the ability to up-regulate sensorimotor rhythm during neurofeedback training.* Frontiers in human neuroscience, 2013. **7**: p. 478.
38. Kober, S.E., et al., *Learning to modulate one's own brain activity: the effect of spontaneous mental strategies.* Frontiers in human neuroscience, 2013. **7**: p. 695.
39. Nan, W., et al., *Individual alpha neurofeedback training effect on short term memory.* International journal of psychophysiology, 2012. **86**(1): p. 83-87.
40. Nijboer, F., N. Birbaumer, and A. Kubler, *The influence of psychological state and motivation on brain–computer interface performance in patients with amyotrophic lateral sclerosis–a longitudinal study.* Frontiers in neuroscience, 2010. **4**: p. 55.
41. Blankertz, B., et al., *Neurophysiological predictor of SMR-based BCI performance.* Neuroimage, 2010. **51**(4): p. 1303-1309.
42. Wan, F., et al., *Resting alpha activity predicts learning ability in alpha neurofeedback.* Frontiers in human neuroscience, 2014. **8**: p. 500.
43. Neumann, N. and N. Birbaumer, *Predictors of successful self control during brain-computer communication.* Journal of Neurology, Neurosurgery & Psychiatry, 2003. **74**(8): p. 1117-1121.
44. Weber, E., et al., *Predicting successful learning of SMR neurofeedback in healthy participants: methodological considerations.* Applied Psychophysiology and Biofeedback, 2011. **36**(1): p. 37-45.
45. Scheinost, D., et al., *Resting state functional connectivity predicts neurofeedback response.* Frontiers in Behavioral Neuroscience, 2014. **8**: p. 338.
46. Enriquez-Geppert, S., et al., *The morphology of midcingulate cortex predicts frontal-midline theta neurofeedback success.* Frontiers in human neuroscience, 2013. **7**: p. 453.
47. Wolpaw, J.R., et al., *Brain-computer interfaces for communication and control.* Clin Neurophysiol, 2002. **113**(6): p. 767-91.
48. Graimann, B., B. Allison, and G. Pfurtscheller, *Brain–computer interfaces: A gentle introduction*, in *Brain-Computer Interfaces*. 2009, Springer. p. 1-27.
49. Nicolas-Alonso, L.F. and J. Gomez-Gil, *Brain computer interfaces, a review.* sensors, 2012. **12**(2): p. 1211-1279.
50. Zander, T.O., et al., *Enhancing human-computer interaction with input from active and passive brain-computer interfaces*, in *Brain-computer interfaces*. 2010, Springer. p. 181-199.

51. Ahn, M., et al., *A review of brain-computer interface games and an opinion survey from researchers, developers and users.* Sensors, 2014. **14**(8): p. 14601-14633.
52. Bos, D.P.-O., et al., *Brain-computer interfacing and games*, in *Brain-Computer Interfaces*. 2010, Springer. p. 149-178.
53. Brunner, C., et al. *BNCI horizon 2020–towards a roadmap for brain/neural computer interaction*. in *International Conference on Universal Access in Human-Computer Interaction*. 2014. Springer.
54. Nijholt, A., D.P.-O. Bos, and B. Reuderink, *Turning shortcomings into challenges: Brain–computer interfaces for games.* Entertainment computing, 2009. **1**(2): p. 85-94.
55. Järvelä, S., et al., *Stimulus games*, in *Game Research Methods*, Lankoski P and B. S, Editors. 2015, ETC Press. p. 193-205.
56. Nijholt, A., *Competing and collaborating brains: multi-brain computer interfacing*, in *Brain-Computer Interfaces*. 2015, Springer. p. 313-335.
57. Nijholt, A. and M. Poel. *Multi-brain BCI: Characteristics and social interactions*. in *International Conference on Augmented Cognition*. 2016. Springer.
58. Gurkok, H., A. Nijholt, and M. Poel, *Brain-computer interface games: Towards a framework*, in *Entertainment Computing - ICEC 2012*, M. Herrlich, R. Malaka, and M. Masuch, Editors. 2012, Springer: Berlin/Heidelberg, Germany. p. 373-380.
59. R., G., et al., *BOLD brain pong: self-regulation of local brain activity during synchronously scanned, interacting subjects*, in *Presented at the 34th Annual Meeting of the Society for Neuroscience*. 2004: San Diego.
60. Duan, L., et al., *Cross-brain neurofeedback: scientific concept and experimental platform.* PloS one, 2013. **8**(5): p. e64590.
61. Obbink, M., et al. *Social interaction in a cooperative brain-computer interface game*. in *International Conference on Intelligent Technologies for Interactive Entertainment*. 2011. Springer.
62. Gürkök, H., et al., *Evaluating a multi-player brain–computer interface game: Challenge versus co-experience.* Entertainment Computing. 2013. **4**(3): p. 195-203.
63. Cruz, I., et al. *Kessel Run-A Cooperative Multiplayer SSVEP BCI Game*. in *International Conference on Intelligent Technologies for Interactive Entertainment*. 2017. Springer.
64. Korczowski, L., et al. *" Brain Invaders 2": an open source Plug & Play multi-user BCI videogame*. in *6th International Brain-Computer Interface Meeting (BCI Meeting 2016)*. 2016.
65. Maby, E., et al., *BCI could make old two-player games even more fun: a proof of concept with connect four.* Advances in Human-Computer Interaction, 2012. **2012**: p. 1.
66. Bonnet, L., F. Lotte, and A. Lécuyer, *Two brains, one game: design and evaluation of a multiuser BCI video game based on motor imagery.* IEEE Transactions on Computational Intelligence, 2013. **5**(2): p. 185-198.
67. Mühl, C., et al. *Bacteria Hunt: A multimodal, multiparadigm BCI game*. in *Fifth International Summer Workshop on Multimodal Interfaces*. 2009.
68. Frith, C.D., *The social brain?* Philosophical Transactions of the Royal Society B: Biological Sciences, 2007. **362**(1480): p. 671-678.
69. Amodio, D.M. and C.D. Frith, *(2006) Meeting of minds: the medial frontal cortex and social cognition*, in *Discovering the Social Mind*. 2016, Psychology Press. p. 183-207.
70. Montague, P.R., et al., *Hyperscanning: simultaneous fMRI during linked social interactions*. 2002, Academic Press.
71. Hjelm, S.I. and C. Browall. *Brainball-using brain activity for cool competition*. in *Proceedings of NordiCHI*. 2000.
72. van Almkerk, M., et al., *BrainSnake: Exploring Mode of Interaction in a Cooperative Multi-brain BCI Game Based on Alpha Activity.*
73. Poli, R., D. Valeriani, and C. Cinel, *Collaborative brain-computer interface for aiding decision-making.* PloS one, 2014. **9**(7).
74. Yuan, P., et al. *A collaborative brain-computer interface for accelerating human decision making*. in *International Conference on Universal Access in Human-Computer Interaction*. 2013. Springer.
75. Poli, R., et al. *Towards cooperative brain-computer interfaces for space navigation*. in *Proceedings of the 2013 international conference on Intelligent user interfaces*. 2013.
76. Li, Y. and C.S. Nam, *Collaborative brain-computer interface for people with motor disabilities [Research Frontier].* IEEE Computational Intelligence Magazine, 2016. **11**(3): p. 56-66.
77. Kovacevic, N., et al., *'My virtual dream': Collective neurofeedback in an immersive art environment.* PloS one, 2015. **10**(7).

78. Decety, J., et al., *The neural bases of cooperation and competition: an fMRI investigation.* Neuroimage, 2004. **23**(2): p. 744-751.
79. Liu, T., H. Saito, and M. Oi, *Role of the right inferior frontal gyrus in turn-based cooperation and competition: a near-infrared spectroscopy study.* Brain and cognition, 2015. **99**: p. 17-23.
80. Astolfi, L., et al. *Estimation of the cortical activity from simultaneous multi-subject recordings during the prisoner's dilemma*. in *2009 annual international conference of the ieee engineering in medicine and biology society*. 2009. IEEE.
81. Balconi, M. and M.E. Vanutelli, *Competition in the Brain. The Contribution of EEG and fNIRS Modulation and Personality Effects in Social Ranking.* Front Psychol, 2016. **7**: p. 1587.
82. Tognoli, E. and J. Kelso, *The coordination dynamics of social neuromarkers.* Frontiers in Human Neuroscience, 2015. **9**: p. 563.
83. Babiloni, F., et al. *Cortical activity and connectivity of human brain during the prisoner's dilemma: an EEG hyperscanning study*. in *2007 29th Annual International Conference of the IEEE Engineering in Medicine and Biology Society*. 2007. IEEE.
84. Astolfi, L., et al., *Imaging the Social Brain by Simultaneous Hyperscanning During Subject Interaction.* IEEE Intell Syst, 2011. **26**(5): p. 38-45.
85. Fallani, F.D.V., et al., *Defecting or not defecting: how to "read" human behavior during cooperative games by EEG measurements.* PloS one, 2010. **5**(12).
86. Balconi, M. and M.E. Vanutelli, *Functional EEG connectivity during competition.* BMC neuroscience, 2018. **19**(1): p. 63.
87. Balconi, M., et al., *Two is better than one: The effects of strategic cooperation on intra-and inter-brain connectivity by fNIRS.* PloS one, 2017. **12**(11).
88. Balconi, M., M.E. Vanutelli, and L. Gatti, *Functional brain connectivity when cooperation fails.* Brain and cognition, 2018. **123**: p. 65-73.
89. Toppi, J., et al., *Investigating cooperative behavior in ecological settings: an EEG hyperscanning study.* PloS one, 2016. **11**(4): p. e0154236.
90. Suda, M., et al., *Frontopolar activation during face-to-face conversation: an in situ study using near-infrared spectroscopy.* Neuropsychologia, 2010. **48**(2): p. 441-447.
91. Kinreich, S., et al., *Brain-to-brain synchrony during naturalistic social interactions.* Scientific Reports, 2017. **7**(1): p. 1-12.
92. Nozawa, T., et al., *Interpersonal frontopolar neural synchronization in group communication: an exploration toward fNIRS hyperscanning of natural interactions.* Neuroimage, 2016. **133**: p. 484-497.
93. Pedro, J.A.G., *EEG-based Joint BCI: Competitive and Collaborative Tasks Between Two Subjects*, in *Neuroscience and Psychology*. 2014, University of Glasgow: Glasgow, United Kingdom.
94. Ling, P. and A. Vučković. *Competitive and collaborative multiuser BCI*. in *Proceedings of the 6th International Brain–Computer Interface Meeting*. 2016.
95. Cryer, J.D. and K.-S. Chan, *Introduction to Spectral Analysis*, in *Time Series Analysis With Applications in R*. 2008, Springer Science + Business Media: New York, USA. p. 319-350.
96. Stoica, P. and R.L. Moses, *Basic Concept*, in *Spectral Analysis of Signals*. 2005, Prentice Hall: New Jersey, USA. p. 1-14.
97. Hasan, M.A., et al., *Reversed cortical over-activity during movement imagination following neurofeedback treatment for central neuropathic pain.* Clinical Neurophysiology, 2016. **127**(9): p. 3118-3127.
98. Hassan, M.A., et al., *The mechanism of neurofeedback training for treatment of central neuropathic pain in paraplegia: a pilot study.* BMC neurology, 2015. **15**(1): p. 200.
99. Haegens, S., et al., *Inter- and intra-individual variability in alpha peak frequency.* Neuroimage, 2014. **92**: p. 46-55.
100. Gonçalves, S.I., et al., *Correlating the alpha rhythm to BOLD using simultaneous EEG/fMRI: inter-subject variability.* Neuroimage, 2006. **30**(1): p. 203-213.
101. Homan, R.W., J. Herman, and P. Purdy, *Cerebral location of international 10-20 system electrode placement.* Electroencephalogr Clin Neurophysiol, 1987. **66**(4): p. 376-82.
102. Butterworth, S., *On the theory of filter amplifiers.* Wireless Engineer, 1930. **7**(6): p. 536-541.
103. Makeig, S., et al. *Independent component analysis of electroencephalographic data*. in *Advances in neural information processing systems*. 1996.
104. Langlois, D., S. Chartier, and D. Gosselin, *An introduction to independent component analysis: InfoMax and FastICA algorithms.* Tutorials in Quantitative Methods for Psychology, 2010. **6**(1): p. 31-38.

105. Welch, P., *The use of fast Fourier transform for the estimation of power spectra: A method based on time averaging over short, modified periodograms.* IEEE Transactions on Audio and Electroacoustics, 1967. **15**(2): p. 70-73.
106. Higuchi, T., *Approach to an irregular time series on the basis of the fractal theory.* Physica D: Nonlinear Phenomena, 1988. **31**(2): p. 277-283.
107. Accardo, A., et al., *Use of the fractal dimension for the analysis of electroencephalographic time series.* Biological cybernetics, 1997. **77**(5): p. 339-350.
108. Kesić, S. and S.Z. Spasić, *Application of Higuchi's fractal dimension from basic to clinical neurophysiology: a review.* Computer methods and programs in biomedicine, 2016. **133**: p. 55-70.
109. Bojić, T., A. Vuckovic, and A. Kalauzi, *Modeling EEG fractal dimension changes in wake and drowsy states in humans—a preliminary study.* Journal of theoretical biology, 2010. **262**(2): p. 214-222.
110. Hadjidimitriou, S.K., et al., *Revealing action representation processes in audio perception using fractal EEG analysis.* IEEE Transactions on Biomedical Engineering, 2010. **58**(4): p. 1120-1129.
111. Klonowski, W., E. Olejarczyk, and R. Stepien. *Sleep-EEG analysis using Higuchi's fractal dimension*. in *International Symposium on Nonlinear Theory and its Applications*. 2005.
112. Weiss, B., et al., *Comparison of fractal and power spectral EEG features: Effects of topography and sleep stages.* Brain Research Bulletin, 2011. **84**(6): p. 359-375.
113. Carrozzi, M., A. Accardo, and F. Bouquet, *Analysis of sleep-stage characteristics in full-term newborns by means of spectral and fractal parameters.* Sleep, 2004. **27**(7): p. 1384-1393.
114. Lutzenberger, W., et al., *Dimensional analysis of the human EEG and intelligence.* Neuroscience Letters, 1992. **143**(1-2): p. 10-14.
115. Smits, F.M., et al., *Electroencephalographic fractal dimension in healthy ageing and Alzheimer's disease.* PloS one, 2016. **11**(2): p. e0149587.
116. Zappasodi, F., et al., *Fractal dimension of EEG activity senses neuronal impairment in acute stroke.* PLoS One, 2014. **9**(6): p. e100199.
117. Raghavendra, B., et al., *Complexity analysis of EEG in patients with schizophrenia using fractal dimension.* Physiological measurement, 2009. **30**(8): p. 795.
118. Khoa, T.Q.D., V.Q. Ha, and V.V. Toi, *Higuchi fractal properties of onset epilepsy electroencephalogram.* Computational and mathematical methods in medicine, 2012. **2012**.
119. Bachmann, M., et al., *Spectral asymmetry and Higuchi's fractal dimension measures of depression electroencephalogram.* Computational and mathematical methods in medicine, 2013. **2013**.
120. Michel, C.M., et al., *EEG source imaging.* Clin Neurophysiol, 2004. **115**(10): p. 2195-222.
121. Grech, R., et al., *Review on solving the inverse problem in EEG source analysis.* J Neuroeng Rehabil, 2008. **5**: p. 25.
122. Jatoi, M.A., et al., *EEG based brain source localization comparison of sLORETA and eLORETA.* Australasian physical & engineering sciences in medicine, 2014. **37**(4): p. 713-721.
123. Becker, H., et al., *Brain-source imaging: From sparse to tensor models.* IEEE Signal Processing Magazine, 2015. **32**(6): p. 100-112.
124. Baillet, S., J.C. Mosher, and R.M. Leahy, *Electromagnetic brain mapping.* IEEE Signal processing magazine, 2001. **18**(6): p. 14-30.
125. Song, J., et al., *EEG source localization: sensor density and head surface coverage.* Journal of neuroscience methods, 2015. **256**: p. 9-21.
126. Pascual-Marqui, R.D., *Standardized low-resolution brain electromagnetic tomography (sLORETA): technical details.* Methods Find Exp Clin Pharmacol, 2002. **24**: p. 5-12.
127. Talairach, J., *Co-planar stereotaxic atlas of the human brain-3-dimensional proportional system.* An approach to cerebral imaging, 1988.
128. Pascual-Marqui, R.D., *Instantaneous and lagged measurements of linear and nonlinear dependence between groups of multivariate time series: frequency decomposition.* arXiv preprint arXiv:0711.1455, 2007.
129. Kaminski, M. and K. Blinowska, *Directed transfer function: A pioneering concept in connectivity analysis*, in *Methods in Brain Connectivity Inference through Multivariate Time Series Analysis, K. Sameshima and LA Baccalá*. 2014, CRC Press. p. 13-34.
130. Blinowska, K.J. and M. Kamiński, *Multivariate Signal Analysis by Parametric Models*, in *Handbook of Time Series Analysis: Recent Theoretical Developments and Applications*. 2006. p. 373-406.

131. Akaike, H., *A new look at the statistical model identification*, in *Selected Papers of Hirotugu Akaike*. 1974, Springer. p. 215-222.
132. Barnett, L. and A.K. Seth, *The MVGC multivariate Granger causality toolbox: a new approach to Granger-causal inference.* Journal of neuroscience methods, 2014. **223**: p. 50-68.
133. Kaminski, M.J. and K.J. Blinowska, *A new method of the description of the information flow in the brain structures.* Biological cybernetics, 1991. **65**(3): p. 203-210.
134. Baccalá, L.A., D.Y. Takahashi, and K. Sameshima, *Consolidating a Link Centered Neural Connectivity Framework with Directed Transfer Function Asymptotics.* arXiv preprint arXiv:1501.05836, 2015.
135. Wilson, S. and R. Maclean, *Comparing Differences between Two Samples or Conditions*, in *Research Methods and Data Analysis for Psychology*. 2011, McGraw-Hill Education: United Kingdom. p. 344-378.
136. Wilson, S. and R. Maclean, *Comparing between More than Two Conditions: Part 1- One-way Designs*, in *Research Methods and Data Analysis for Psychology*. 2011, McGraw-Hill Education: United Kingdom. p. 379-414.
137. Wilson;, S. and R. Maclean, *Comparing Differences between More than Two Conditions: Part 2- Factorial Designs*, in *Research Methods and Data Analysis for Psychology*. 2011, McGraw Hill Education: United Kingdom p. 415-460.
138. Scheff, S.W., *Nonparametric Statistics*, in *Fundamental statistical principles for the neurobiologist: a survival guide*. 2016, Academic Press. p. 157-182.
139. Legendre, P. and L.F. Legendre, *Numerical ecology*. 1998, Elsevier. p. 17-26.
140. Hart, S.G. and L.E. Staveland, *Development of NASA-TLX (Task Load Index): Results of empirical and theoretical research*, in *Advances in psychology*. 1988, Elsevier. p. 139-183.
141. Polosan, M., et al., *An fMRI study of the social competition in healthy subjects.* Brain and cognition, 2011. **77**(3): p. 401-411.
142. Fehr, E. and I. Krajbich, *Chapter 11. Social Preferences and the Brain*, in *Neuroeconomics*. 2013, Elsevier Inc. Chapters.
143. Staudinger, M.R., S. Erk, and H. Walter, *Dorsolateral prefrontal cortex modulates striatal reward encoding during reappraisal of reward anticipation.* Cerebral cortex, 2011. **21**(11): p. 2578-2588.
144. Bault, N., et al., *Medial prefrontal cortex and striatum mediate the influence of social comparison on the decision process.* Proceedings of the national Academy of sciences, 2011. **108**(38): p. 16044-16049.
145. van den Bos, W., A. Talwar, and S.M. McClure, *Neural correlates of reinforcement learning and social preferences in competitive bidding.* Journal of Neuroscience, 2013. **33**(5): p. 2137-2146.
146. Fareri, D.S. and M.R. Delgado, *Differential reward responses during competition against in-and out-of-network others.* Social cognitive and affective neuroscience, 2014. **9**(4): p. 412-420.
147. Lee, D., *Game theory and neural basis of social decision making.* Nature neuroscience, 2008. **11**(4): p. 404-409.
148. Zink, C.F., et al., *Know your place: neural processing of social hierarchy in humans.* Neuron, 2008. **58**(2): p. 273-283.
149. Schmälzle, R., et al., *Brain connectivity dynamics during social interaction reflect social network structure.* Proceedings of the National Academy of Sciences, 2017. **114**(20): p. 5153-5158.
150. Assaf, M., et al., *Brain activity dissociates mentalization from motivation during an interpersonal competitive game.* Brain imaging and behavior, 2009. **3**(1): p. 24.
151. Lee, T.-W., et al., *Do resting brain dynamics predict oddball evoked-potential?* BMC neuroscience, 2011. **12**(1): p. 121.
152. Benjamini, Y. and Y. Hochberg, *Controlling the false discovery rate: a practical and powerful approach to multiple testing.* Journal of the Royal statistical society: series B (Methodological), 1995. **57**(1): p. 289-300.
153. SPASIĆ, S., et al., *Estimation of parameter kmax in fractal analysis of rat brain activity.* Annals of the New York Academy of Sciences, 2005. **1048**(1): p. 427-429.
154. Bachmann, M., et al. *Revealing small hidden changes in human EEG by Higuchi's fractal dimension*. in *International Symposium on Biomedical Engineering and Medical Physics, 10-12 October, 2012, Riga, Latvia*. 2013. Springer.
155. Kalauzi, A., T. Bojić, and A. Vuckovic, *Modeling the relationship between Higuchi's fractal dimension and Fourier spectra of physiological signals.* Medical & biological engineering & computing, 2012. **50**(7): p. 689-699.

156. Holm, S., *A simple sequentially rejective multiple test procedure.* Scandinavian journal of statistics, 1979: p. 65-70.
157. Haegens, S., et al., *Inter-and intra-individual variability in alpha peak frequency.* Neuroimage, 2014. **92**: p. 46-55.
158. Bazanova, O. and L. Aftanas, *Individual measures of electroencephalogram alpha activity and non-verbal creativity.* Neuroscience and behavioral physiology, 2008. **38**(3): p. 227-235.
159. Li, J., et al. *A competitive brain computer interface: Multi-person car racing system*. in *2013 35th Annual International Conference of the IEEE Engineering in Medicine and Biology Society (EMBC)*. 2013. IEEE.
160. Klimesch, W., H. Schimke, and G. Pfurtscheller, *Alpha frequency, cognitive load and memory performance.* Brain Topogr, 1993. **5**(3): p. 241-51.
161. Doppelmayr, M., et al., *Individual differences in brain dynamics: important implications for the calculation of event-related band power.* Biological cybernetics, 1998. **79**(1): p. 49-57.
162. Hanslmayr, S., T. Staudigl, and M.-C. Fellner, *Oscillatory power decreases and long-term memory: the information via desynchronization hypothesis.* Frontiers in human neuroscience, 2012. **6**: p. 74.
163. Aftanas, L. and S. Golocheikine, *Non-linear dynamic complexity of the human EEG during meditation.* Neuroscience letters, 2002. **330**(2): p. 143-146.
164. Díaz, M.H., et al., *Order and chaos in the brain: fractal time series analysis of the EEG activity during a cognitive problem solving task.* Procedia Computer Science, 2015. **55**: p. 1410-1419.
165. Aron, A.R., et al., *Stop-signal inhibition disrupted by damage to right inferior frontal gyrus in humans.* Nature neuroscience, 2003. **6**(2): p. 115.
166. Hampshire, A., et al., *Selective tuning of the right inferior frontal gyrus during target detection.* Cognitive, Affective, & Behavioral Neuroscience, 2009. **9**(1): p. 103-112.
167. Hampshire, A., et al., *The role of the right inferior frontal gyrus: inhibition and attentional control.* Neuroimage, 2010. **50**(3): p. 1313-1319.
168. Krall, S.C., et al., *The role of the right temporoparietal junction in attention and social interaction as revealed by ALE meta-analysis.* Brain Structure and Function, 2015. **220**(2): p. 587-604.
169. Harmon-Jones, E., et al., *The effect of personal relevance and approach-related action expectation on relative left frontal cortical activity.* Psychological Science, 2006. **17**(5): p. 434-440.
170. Cavanna, A.E. and M.R. Trimble, *The precuneus: a review of its functional anatomy and behavioural correlates.* Brain, 2006. **129**(Pt 3): p. 564-83.
171. Utevsky, A.V., D.V. Smith, and S.A. Huettel, *Precuneus is a functional core of the default-mode network.* Journal of Neuroscience, 2014. **34**(3): p. 932-940.
172. Vernon, D., et al., *Alpha neurofeedback training for performance enhancement: reviewing the methodology.* Journal of neurotherapy, 2009. **13**(4): p. 214-227.
173. Buades-Rotger, M., et al., *Winning is not enough: ventral striatum connectivity during physical aggression.* Brain imaging and behavior, 2016. **10**(1): p. 105-114.
174. Chiao, J.Y., et al., *Knowing who's boss: fMRI and ERP investigations of social dominance perception.* Group Processes & Intergroup Relations, 2008. **11**(2): p. 201-214.
175. Ullsperger, M., et al., *Conscious perception of errors and its relation to the anterior insula.* Brain Structure and Function, 2010. **214**(5-6): p. 629-643.
176. Cáceda, R., et al., *Organization of intrinsic functional brain connectivity predicts decisions to reciprocate social behavior.* Behavioural brain research, 2015. **292**: p. 478-483.
177. Camara, E., A. Rodriguez-Fornells, and T.F. Münte, *Functional connectivity of reward processing in the brain.* Frontiers in human neuroscience, 2009. **2**: p. 19.
178. Harsay, H.A., et al., *Functional connectivity of the striatum links motivation to action control in humans.* Journal of Neuroscience, 2011. **31**(29): p. 10701-10711.
179. Gao, W. and W. Lin, *Frontal parietal control network regulates the anti-correlated default and dorsal attention networks.* Human brain mapping, 2012. **33**(1): p. 192-202.
180. Marek, S. and N.U. Dosenbach, *The frontoparietal network: function, electrophysiology, and importance of individual precision mapping.* Dialogues in clinical neuroscience, 2018. **20**(2): p. 133.
181. Raemaekers, M., et al., *Knowing left from right: asymmetric functional connectivity during resting state.* Brain Structure and Function, 2018. **223**(4): p. 1909-1922.
182. Nielsen, J.A., et al., *An evaluation of the left-brain vs. right-brain hypothesis with resting state functional connectivity magnetic resonance imaging.* PloS one, 2013. **8**(8).

183. Mennes, M., et al., *Inter-individual differences in resting-state functional connectivity predict task-induced BOLD activity.* Neuroimage, 2010. **50**(4): p. 1690-1701.
184. Raichle, M.E., et al., *A default mode of brain function.* Proceedings of the National Academy of Sciences, 2001. **98**(2): p. 676-682.
185. Leech, R. and D.J. Sharp, *The role of the posterior cingulate cortex in cognition and disease.* Brain, 2014. **137**(1): p. 12-32.
186. Spreng, R.N. and J.R. Andrews-Hanna, *The default network and social cognition.* Brain mapping: An encyclopedic reference, 2015. **1316**: p. 165-169.
187. Van Overwalle, F., *Social cognition and the brain: a meta-analysis.* Human brain mapping, 2009. **30**(3): p. 829-858.
188. Kennedy, D.P., E. Redcay, and E. Courchesne, *Failing to deactivate: resting functional abnormalities in autism.* Proceedings of the National Academy of Sciences, 2006. **103**(21): p. 8275-8280.
189. Cherkassky, V.L., et al., *Functional connectivity in a baseline resting-state network in autism.* Neuroreport, 2006. **17**(16): p. 1687-1690.
190. Brewer, J., K. Garrison, and S. Whitfield-Gabrieli, *What about the "self" is processed in the posterior cingulate cortex?* Frontiers in human neuroscience, 2013. **7**: p. 647.
191. Flagan, T. and J.S. Beer, *Three ways in which midline regions contribute to self-evaluation.* Frontiers in human neuroscience, 2013. **7**: p. 450.
192. Seeley, W.W., et al., *Dissociable Intrinsic Connectivity Networks for Salience Processing and Executive Control.* Journal of Neuroscience, 2007. **27**(9): p. 2349-2356.
193. Heekeren, H.R., et al., *Involvement of human left dorsolateral prefrontal cortex in perceptual decision making is independent of response modality.* Proceedings of the National Academy of Sciences, 2006. **103**(26): p. 10023-10028.
194. Kaller, C.P., et al., *Dissociable contributions of left and right dorsolateral prefrontal cortex in planning*. Cerebral cortex, 2011. **21**(2): p. 307-317.
195. Eichler, M., *On the evaluation of information flow in multivariate systems by the directed transfer function.* Biological cybernetics, 2006. **94**(6): p. 469-482.
196. Blinowska, K.J., *Review of the methods of determination of directed connectivity from multichannel data.* Medical & biological engineering & computing, 2011. **49**(5): p. 521-529.
197. Balconi, M. and M.E. Vanutelli, *Brains in competition: Improved cognitive performance and inter-brain coupling by hyperscanning paradigm with functional Near-Infrared Spectroscopy.* Frontiers in behavioral neuroscience, 2017. **11**: p. 163.
198. Sinha, N., et al. *EEG hyperscanning study of inter-brain synchrony during cooperative and competitive interaction*. in *2016 IEEE International Conference on Systems, Man, and Cybernetics (SMC)*. 2016. IEEE.
199. Boucher, D.H., S. James, and K.H. Keeler, *The ecology of mutualism.* Annual Review of Ecology and Systematics, 1982. **13**(1): p. 315-347.
200. Kapeller, C., et al. *Toward multi-brain communication: collaborative spelling with a P300 BCI*. in *International Conference on Augmented Cognition*. 2014. Springer.
201. Boisgueheneuc, F.d., et al., *Functions of the left superior frontal gyrus in humans: a lesion study.* Brain, 2006. **129**(12): p. 3315-3328.
202. Rypma, B., et al., *Load-dependent roles of frontal brain regions in the maintenance of working memory.* Neuroimage, 1999. **9**(2): p. 216-226.
203. Li, W., et al., *Subregions of the human superior frontal gyrus and their connections.* Neuroimage, 2013. **78**: p. 46-58.
204. Behrmann, M., J.J. Geng, and S. Shomstein, *Parietal cortex and attention.* Current opinion in neurobiology, 2004. **14**(2): p. 212-217.
205. Coull, J. and C. Frith, *Differential activation of right superior parietal cortex and intraparietal sulcus by spatial and nonspatial attention.* Neuroimage, 1998. **8**(2): p. 176-187.
206. Vandenberghe, R., et al., *Functional specificity of superior parietal mediation of spatial shifting.* Neuroimage, 2001. **14**(3): p. 661-673.
207. Koenigs, M., et al., *Superior parietal cortex is critical for the manipulation of information in working memory.* Journal of Neuroscience, 2009. **29**(47): p. 14980-14986.
208. Jäncke, L., et al., *The role of the inferior parietal cortex in linking the tactile perception and manual construction of object shapes.* Cerebral Cortex, 2001. **11**(2): p. 114-121.

209. Craig, A., *Emotional moments across time: a possible neural basis for time perception in the anterior insula.* Philosophical Transactions of the Royal Society B: Biological Sciences, 2009. **364**(1525): p. 1933-1942.
210. Craig, A.D. and A. Craig, *How do you feel--now? The anterior insula and human awareness.* Nature reviews neuroscience, 2009. **10**(1).
211. Gu, X., et al., *Anterior insular cortex and emotional awareness.* Journal of Comparative Neurology, 2013. **521**(15): p. 3371-3388.
212. Wiech, K., et al., *Anterior insula integrates information about salience into perceptual decisions about pain.* Journal of Neuroscience, 2010. **30**(48): p. 16324-16331.
213. Wróbel, A., *Beta activity: a carrier for visual attention.* Acta neurobiologiae experimentalis, 2000. **60**(2): p. 247-260.
214. Gola, M., et al., *EEG beta band activity is related to attention and attentional deficits in the visual performance of elderly subjects.* International Journal of Psychophysiology, 2013. **89**(3): p. 334-341.
215. Poli, R., et al. *Improving decision-making based on visual perception via a collaborative brain-computer interface*. in *2013 IEEE International Multi-Disciplinary Conference on Cognitive Methods in Situation Awareness and Decision Support (CogSIMA)*. 2013. IEEE.
216. Dimpfel, W., F. Schober, and M. Spüler, *The influence of caffeine on human EEG under resting condition and during mental loads.* The clinical investigator, 1993. **71**(3): p. 197-207.
217. Barry, R.J., et al., *Caffeine effects on resting-state arousal.* Clinical Neurophysiology, 2005. **116**(11): p. 2693-2700.
218. Higuchi, S., et al., *Diurnal variations in alpha power density and subjective sleepiness while performing repeated vigilance tasks.* Clinical neurophysiology, 2001. **112**(6): p. 997-1000.
219. Shigihara, Y., et al., *Two types of mental fatigue affect spontaneous oscillatory brain activities in different ways.* Behavioral and Brain Functions, 2013. **9**(1): p. 2.
220. Bornas, X., et al., *Self-focused cognitive emotion regulation style as associated with widespread diminished EEG fractal dimension.* International Journal of Psychology, 2013. **48**(4): p. 695-703.
221. Mölle, M., et al., *EEG complexity and performance measures of creative thinking.* Psychophysiology, 1999. **36**(1): p. 95-104.
222. Rolls, E.T., *The orbitofrontal cortex and reward.* Cerebral cortex, 2000. **10**(3): p. 284-294.
223. Womelsdorf, T., et al., *Theta-activity in anterior cingulate cortex predicts task rules and their adjustments following errors.* Proceedings of the National Academy of Sciences, 2010. **107**(11): p. 5248-5253.
224. Atzil, S., T. Hendler, and R. Feldman, *The brain basis of social synchrony.* Social cognitive and affective neuroscience, 2014. **9**(8): p. 1193-1202.
225. Ward, A.M., et al., *The parahippocampal gyrus links the default-mode cortical network with the medial temporal lobe memory system.* Human brain mapping, 2014. **35**(3): p. 1061-1073.
226. Cavanagh, J.F. and M.J. Frank, *Frontal theta as a mechanism for cognitive control.* Trends in cognitive sciences, 2014. **18**(8): p. 414-421.
227. Scheeringa, R., et al., *Frontal theta EEG activity correlates negatively with the default mode network in resting state.* International journal of psychophysiology, 2008. **67**(3): p. 242-251.
228. Bell, A.J. and T.J. Sejnowski, *An information-maximization approach to blind separation and blind deconvolution.* Neural computation, 1995. **7**(6): p. 1129-1159.
229. Spielberg, J.M., et al., *Prefrontal Cortex, Emotion, and Approach/Withdrawal Motivation.* Soc Personal Psychol Compass, 2008. **2**(1): p. 135-153.
230. Frith, C.D. and U. Frith, *Interacting minds--a biological basis.* Science, 1999. **286**(5445): p. 1692-5.
231. Frith, C.D., *The social brain?* Philos Trans R Soc Lond B Biol Sci, 2007. **362**(1480): p. 671-8.
232. Decety, J. and C. Lamm, *The role of the right temporoparietal junction in social interaction: how low-level computational processes contribute to meta-cognition.* The Neuroscientist, 2007. **13**(6): p. 580-593.
233. Santiesteban, I., et al., *Enhancing social ability by stimulating right temporoparietal junction.* Current Biology, 2012. **22**(23): p. 2274-2277.
234. Arora, A., et al., *Left inferior-parietal lobe activity in perspective tasks: identity statements.* Frontiers in human neuroscience, 2015. **9**: p. 360.
235. Mevorach, C., G.W. Humphreys, and L. Shalev, *Opposite biases in salience-based selection for the left and right posterior parietal cortex.* Nature neuroscience, 2006. **9**(6): p. 740-742.

236. Sänger, J., V. Müller, and U. Lindenberger, *Intra-and interbrain synchronization and network properties when playing guitar in duets.* Frontiers in human neuroscience, 2012. **6**: p. 312.
237. Cui, X., D.M. Bryant, and A.L. Reiss, *NIRS-based hyperscanning reveals increased interpersonal coherence in superior frontal cortex during cooperation.* Neuroimage, 2012. **59**(3): p. 2430-2437.
238. Kennerley, S.W., et al., *Optimal decision making and the anterior cingulate cortex.* Nature neuroscience, 2006. **9**(7): p. 940-947.
239. Goulden, N., et al., *The salience network is responsible for switching between the default mode network and the central executive network: replication from DCM.* Neuroimage, 2014. **99**: p. 180-190.
240. Rudebeck, P.H., et al., *A role for the macaque anterior cingulate gyrus in social valuation.* Science, 2006. **313**(5791): p. 1310-1312.
241. Li, W., X. Mai, and C. Liu, *The default mode network and social understanding of others: what do brain connectivity studies tell us.* Frontiers in human neuroscience, 2014. **8**: p. 74.
242. Costafreda, S.G., et al., *A systematic review and quantitative appraisal of fMRI studies of verbal fluency: role of the left inferior frontal gyrus.* Human brain mapping, 2006. **27**(10): p. 799-810.
243. Morin, A. and J. Michaud, *Self-awareness and the left inferior frontal gyrus: inner speech use during self-related processing.* Brain research bulletin, 2007. **74**(6): p. 387-396.
244. Wagner, A.D., et al., *Recovering meaning: left prefrontal cortex guides controlled semantic retrieval.* Neuron, 2001. **31**(2): p. 329-338.
245. Zhang, Y., et al., *Interpersonal brain synchronization associated with working alliance during psychological counseling.* Psychiatry Research: Neuroimaging, 2018. **282**: p. 103-109.
246. Hu, Y., et al., *Inter-brain synchrony and cooperation context in interactive decision making.* Biological psychology, 2018. **133**: p. 54-62.
247. Nagamitsu, S., et al., *Prefrontal cerebral blood volume patterns while playing video games—a near-infrared spectroscopy study.* Brain and Development, 2006. **28**(5): p. 315-321.
248. Russoniello, C.V., K. O'Brien, and J.M. Parks, *The effectiveness of casual video games in improving mood and decreasing stress.* Journal of CyberTherapy & Rehabilitation, 2009. **2**(1): p. 53-66.
249. Etkin, A., T. Egner, and R. Kalisch, *Emotional processing in anterior cingulate and medial prefrontal cortex.* Trends in cognitive sciences, 2011. **15**(2): p. 85-93.
250. Herrington, J.D., et al., *Emotion-modulated performance and activity in left dorsolateral prefrontal cortex.* Emotion, 2005. **5**(2): p. 200.
251. Euston, D.R., A.J. Gruber, and B.L. McNaughton, *The role of medial prefrontal cortex in memory and decision making.* Neuron, 2012. **76**(6): p. 1057-1070.
252. Kuehne, M., et al., *Transcranial direct current stimulation of the left dorsolateral prefrontal cortex shifts preference of moral judgments.* PloS one, 2015. **10**(5).
253. Wang, Y., et al., *Decreased prefrontal lobe interhemispheric functional connectivity in adolescents with internet gaming disorder: a primary study using resting-state fMRI.* PloS one, 2015. **10**(3).
254. Kühn, S., et al., *Playing Super Mario induces structural brain plasticity: gray matter changes resulting from training with a commercial video game.* Molecular psychiatry, 2014. **19**(2): p. 265-271.
255. Gong, D., et al., *A reduction in video gaming time produced a decrease in brain activity.* Frontiers in human neuroscience, 2019. **13**: p. 134.
256. Kühn, S., et al., *Positive association of video game playing with left frontal cortical thickness in adolescents.* PloS one, 2014. **9**(3).
257. Reuderink, B., C. Mühl, and M. Poel, *Valence, arousal and dominance in the EEG during game play.* International journal of autonomous and adaptive communications systems, 2013. **6**(1): p. 45-62.

Appendix I

Appendix 1.1 Table of *p*-values and H scores from Kruskal-Wallis H test ($p<0.05$) of Higuchi Fractal Dimension from Baseline, BSD, and WO, for each group.

Channel	Group D		Group ND	
	p-value	H-statistic	*p*-value	H-statistic
AF3	0.818	0.403	0.393	1.866
AF4	0.801	0.444	0.572	1.117
F3	0.940	0.124	0.265	2.655
Fz	0.966	0.070	0.598	1.03
F4	0.708	0.692	0.566	1.138
FC3	0.951	0.101	0.418	1.745
FC4	0.826	0.382	0.737	0.612
C3	0.983	0.034	0.689	0.746
Cz	0.991	0.018	0.59	1.055
C4	0.996	0.008	0.842	0.343
P3	0.983	0.034	0.917	0.173
Pz	0.991	0.018	0.876	0.266
P4	0.988	0.023	0.855	0.312
O1	0.991	0.018	0.532	1.262
Oz	0.961	0.080	0.517	1.319
O2	0.996	0.008	0.665	0.815

Appendix 1.2 Table of *p*-values and Z scores from Wilcoxon signed rank test ($p<0.05$) of Higuchi Fractal Dimension between Baseline and competitive gaming (BSD/SSD) in group D.

Condition	Channel	*p*-value	Z score
Baseline vs BSD	AF3	0.878	-0.153
	AF4	0.241	-1.172
	F3	0.445	-0.764
	Fz	0.878	-0.153
	F4	0.074	-1.784
	FC3	0.646	-0.459
	FC4	0.169	-1.376
	C3	0.799	-0.255
	Cz	0.878	-0.153
	C4	0.959	-0.051
	P3	0.646	-0.459
	Pz	0.721	-0.357
	P4	0.959	-0.051
	O1	0.878	-0.153
	Oz	0.878	-0.153
	O2	0.508	-0.663
Baseline vs SSD	AF3	0.445	-0.764
	AF4	0.386	-0.866
	F3	0.575	-0.561
	Fz	0.445	-0.764
	F4	0.333	-0.968
	FC3	0.386	-0.866
	FC4	0.285	-1.070
	C3	0.799	-0.255
	Cz	0.285	-1.070
	C4	0.959	-0.051
	P3	0.959	-0.051
	Pz	0.575	-0.561
	P4	0.721	-0.357
	O1	0.646	-0.459
	Oz	0.721	-0.357
	O2	0.646	-0.459

Appendix 1.3 Table of *p*-values and Z scores from Wilcoxon signed rank test ($p<0.05$) of Higuchi Fractal Dimension between Baseline and competitive gaming (BSD/SSD) in group ND.

Condition	Channel	*p*-value	Z score
Baseline vs BSD	AF3	0.241	-1.172
	AF4	0.241	-1.172
	F3	0.139	-1.478
	Fz	0.799	-0.255
	F4	0.203	-1.274
	FC3	0.169	-1.376
	FC4	0.203	-1.274
	C3	0.575	-0.561
	Cz	0.139	-1.478
	C4	0.333	-0.968
	P3	0.799	-0.255
	Pz	0.878	-0.153
	P4	0.878	-0.153
	O1	0.646	-0.459
	Oz	0.959	-0.051
	O2	0.508	-0.663
Baseline vs SSD	AF3	0.059	-1.886
	AF4	0.139	-1.478
	***F3**	**0.037**	**-2.090**
	Fz	0.285	-1.070
	F4	0.169	-1.376
	***FC3**	**0.017**	**-2.395**
	FC4	0.139	-1.478
	***C3**	**0.047**	**-1.988**
	Cz	0.074	-1.784
	C4	0.646	-0.459
	P3	0.285	-1.070
	Pz	0.575	-0.561
	P4	0.646	-0.459
	O1	0.093	-1.682
	Oz	0.074	-1.784
	O2	0.169	-1.376

*) Channels with significant *p*-value (before Holm-Bonferroni correction).

Appendix 1.4 Table of *p*-values and Z scores from Wilcoxon signed rank test ($p<0.05$) of Higuchi Fractal Dimension between groups (group D and group ND)

	Baseline		**BE**		**WO**	
Channel	*p*-value	Z score	*p*-value	Z score	*p*-value	Z score
AF3	0.721	-0.357	0.386	-0.866	0.139	-1.478
AF4	0.508	-0.663	0.386	-0.866	0.139	-1.478
F3	0.721	-0.357	0.386	-0.866	0.241	-1.172
Fz	0.646	-0.459	0.959	-0.051	0.508	-0.663
F4	0.386	-0.866	0.169	-1.376	0.285	-1.070
FC3	0.203	-1.274	0.575	-0.561	0.285	-1.070
FC4	0.285	-1.070	0.386	-0.866	0.508	-0.663
C3	0.203	-1.274	0.959	-0.051	0.445	-0.764
Cz	0.445	-0.764	0.646	-0.459	0.203	-1.274
C4	0.646	-0.459	0.959	-0.051	0.959	-0.051
P3	0.646	-0.459	0.445	-0.764	0.799	-0.255
Pz	0.575	-0.561	0.333	-0.968	0.959	-0.051
P4	0.959	-0.051	0.799	-0.255	0.799	-0.255
O1	0.333	-0.968	0.386	-0.866	0.333	-0.968
Oz	0.575	-0.561	0.445	-0.764	0.169	-1.376
O2	0.333	-0.968	0.285	-1.070	0.646	-0.459

Appendix II

Appendix 2.1 Table of *p*-values and H scores from Kruskal-Wallis H test ($p<0.05$) of Higuchi Fractal Dimension from Baseline, BE, and WO, for each group.

Channel	Group D		Group ND	
	p-value	H-statistic	*p*-value	H-statistic
AF3	0.985	0.031	0.922	0.163
AF4	0.951	0.101	0.756	0.560
F3	0.973	0.054	0.801	0.444
Fz	0.939	0.126	0.922	0.163
F4	0.879	0.258	0.75	0.575
FC3	0.903	0.204	0.924	0.157
FC4	0.966	0.070	0.91	0.188
C3	0.827	0.379	0.953	0.095
Cz	0.983	0.034	0.924	0.157
C4	0.953	0.095	0.897	0.217
P3	0.790	0.472	0.921	0.165
Pz	0.842	0.343	0.784	0.488
P4	0.689	0.746	0.636	0.906
O1	0.652	0.854	0.679	0.774
Oz	0.842	0.343	0.606	1.001
O2	0.727	0.637	0.374	1.969

Appendix 2.2 Table of *p*-values and Z scores from Wilcoxon signed rank test ($p<0.05$) of Higuchi Fractal Dimension between Baseline and collaborative gaming (BE: best gaming condition; WO: worst gaming condition) in group D.

Condition	Channel	*p*-value	Z score
Baseline vs BE	AF3	0.959	-0.051
	AF4	0.285	-1.07
	F3	0.386	-0.866
	Fz	0.721	-0.357
	F4	0.285	-1.07
	FC3	0.508	-0.663
	FC4	0.959	-0.051
	C3	0.203	-1.274
	Cz	0.241	-1.172
	C4	0.575	-0.561
	***P3**	**0.028**	**-2.191**
	Pz	0.203	-1.274
	P4	0.114	-1.58
	***O1**	**0.017**	**-2.395**
	Oz	0.074	-1.784
	O2	0.114	-1.58
Baseline vs WO	AF3	0.575	-0.561
	AF4	0.878	-0.153
	F3	0.721	-0.357
	Fz	0.878	-0.153
	F4	0.445	-0.764
	FC3	0.959	-0.051
	FC4	0.799	-0.255
	C3	0.508	-0.663
	Cz	0.445	-0.764
	C4	0.799	-0.255
	P3	0.203	-1.274
	Pz	0.575	-0.561
	P4	0.285	-1.07
	O1	0.074	-1.784
	Oz	0.386	-0.866
	O2	0.203	-1.274

*) Channels with significant *p*-value (before Holm-Bonferroni correction).

Appendix 2.3 Table of *p*-values and Z scores from Wilcoxon signed rank test ($p<0.05$) of Higuchi Fractal Dimension between Baseline and collaborative gaming (BE: best gaming condition; WO: worst gaming condition) in group ND.

Condition	Channel	*p*-value	Z score
Baseline vs BE	AF3	0.878	-0.153
	AF4	0.508	-0.663
	F3	0.508	-0.663
	Fz	0.799	-0.255
	F4	0.878	-0.153
	FC3	0.386	-0.866
	FC4	0.646	-0.459
	C3	0.721	-0.357
	Cz	0.878	-0.153
	C4	0.721	-0.357
	P3	0.721	-0.357
	Pz	0.333	-0.968
	P4	0.878	-0.153
	O1	0.878	-0.153
	Oz	0.878	-0.153
	O2	0.721	-0.357
Baseline vs WO	AF3	0.445	-0.764
	AF4	0.203	-1.274
	F3	0.508	-0.663
	Fz	0.959	-0.051
	F4	0.575	-0.561
	FC3	0.878	-0.153
	FC4	0.799	-0.255
	C3	0.799	-0.255
	Cz	0.959	-0.051
	C4	0.959	-0.051
	P3	0.508	-0.663
	Pz	0.203	-1.274
	P4	0.508	-0.663
	O1	0.445	-0.764
	Oz	0.333	-0.968
	O2	0.139	-1.478

Appendix 2.4 Table of *p*-values and Z scores from Wilcoxon signed rank test ($p<0.05$) of Higuchi Fractal Dimension between groups (group D and group ND)

	Baseline		**BE**		**WO**	
Channel	*p*-value	Z score	*p*-value	Z score	*p*-value	Z score
AF3	0.959	-0.051	0.799	-0.255	0.575	-0.561
AF4	0.575	-0.561	0.721	-0.357	0.203	-1.274
F3	0.799	-0.255	0.721	-0.357	0.878	-0.153
Fz	0.508	-0.663	0.959	-0.051	0.721	-0.357
F4	0.878	-0.153	0.799	-0.255	0.878	-0.153
FC3	0.508	-0.663	0.721	-0.357	0.646	-0.459
FC4	0.386	-0.866	0.721	-0.357	0.508	-0.663
C3	0.203	-1.274	0.646	-0.459	0.203	-1.274
Cz	0.241	-1.172	0.646	-0.459	0.508	-0.663
C4	0.445	-0.764	0.646	-0.459	0.575	-0.561
P3	0.203	-1.274	0.959	-0.051	0.721	-0.357
Pz	0.285	-1.07	0.799	-0.255	0.285	-1.07
P4	0.333	-0.968	0.646	-0.459	0.721	-0.357
O1	0.139	-1.478	0.799	-0.255	0.646	-0.459
Oz	0.386	-0.866	0.575	-0.561	0.508	-0.663
O2	0.241	-1.172	0.959	-0.051	0.203	-1.274

Appendix 2.5 Significantly increased voxel ($p<0.05$) found after paired t-test analysis in higher beta frequency between Baseline and BE gaming condition

Brain lobe	**BA**	**Structure**	**Voxel value**	**MNI coordinate (x,y,z)**
Occipital	19	Cuneus	7.34	-25,-95,20
Occipital	19	Middle Occipital Gyrus	7.19	-30,-95,15
Occipital	19	Cuneus	7.14	-30,-90,25
Occipital	19	Superior Occipital Gyrus	6.96	-30,-90,20
Occipital	18	Middle Occipital Gyrus	6.94	-25,-95,15

Appendix 2.6 Significantly increased voxel (p<0.05) found after paired t-test analysis in lower beta frequency between Baseline and WO gaming condition

Brain lobe	BA	Structure	Voxel value	MNI coordinate (x,y,z)
Parietal	19	Precuneus	7.36	-25,-85,40
Parietal	19	Precuneus	7.35	-25,-85,35
Parietal	19	Precuneus	7.23	-30,-85,35
Occipital	19	Cuneus	7.16	-30,-85,30
Parietal	19	Precuneus	7.15	-20,-85,40
Parietal	19	Precuneus	7.07	-25,-80,40
Occipital	19	Cuneus	7.04	-25,-85,30
Parietal	19	Precuneus	7.03	-25,-80,35
Parietal	19	Precuneus	6.99	-30,-85,40
Occipital	19	Superior Occipital Gyrus	6.95	-35,-85,30
Parietal	7	Precuneus	6.93	-20,-80,45
Parietal	7	Superior Parietal Lobule	6.90	-25,-80,45
Parietal	19	Precuneus	6.87	-20,-85,35
Parietal	19	Precuneus	6.79	-35,-85,35
Occipital	19	Cuneus	6.77	-25,-90,35
Occipital	19	Superior Occipital Gyrus	6.77	-30,-85,25
Occipital	19	Cuneus	6.66	-30,-90,30
Parietal	19	Precuneus	6.66	-30,-80,40
Parietal	19	Precuneus	6.59	-20,-80,35
Occipital	19	Cuneus	6.58	-25,-90,30
Temporal	39	Angular Gyrus	6.57	-35,-80,30
Occipital	19	Superior Occipital Gyrus	6.54	-35,-80,25
Occipital	19	Cuneus	6.51	-25,-85,25
Occipital	19	Superior Occipital Gyrus	6.50	-40,-85,30
Occipital	19	Superior Occipital Gyrus	6.49	-40,-85,25
Occipital	19	Cuneus	6.44	-20,-90,35
Parietal	7	Superior Parietal Lobule	6.41	-30,-80,45
Occipital	19	Cuneus	6.40	-20,-85,30
Temporal	19	Middle Temporal Gyrus	6.39	-35-85,20
Occipital	19	Cuneus	6.37	-30,-90,25
Parietal	19	Precuneus	6.36	-35,-80,35
Parietal	7	Precuneus	6.33	-25,-75,40

Parietal	19	Precuneus	6.31	-25,-75,35
Temporal	19	Middle Temporal Gyrus	6.29	-40,-85,20
Parietal	7	Precuneus	6.29	-20,-75,50
Occipital	19	Middle Occipital Gyrus	6.28	-30,-80,20
Parietal	7	Superior Parietal Lobule	6.28	-25,-75,45
Parietal	7	Precuneus	6.27	-20,-75,45
Parietal	7	Precuneus	6.25	-15,-80,45
Parietal	19	Precuneus	6.24	-15,-85,40
Occipital	19	Superior Occipital Gyrus	6.24	-40,-80,25
Occipital	7	Cuneus	6.20	-20,-80,30
Parietal	19	Precuneus	6.20	-30,-75,35
Temporal	39	Middle Temporal Gyrus	6.19	-35,-75,25
Parietal	7	Precuneus	6.18	-25,-75,50
Parietal	7	Precuneus	6.17	-20,-75,40